

---

**Spatio-temporal and structural analysis of  
vegetation dynamics of Lowveld Savanna in South  
Africa**

**Dissertation**

Zur Erlangung des akademischen Grades doctor rerum naturalium

(Dr. rer. nat)

Vorgelegt dem Rat der Chemisch-Geowissenschaftlichen Fakultät der  
Friedrich-Schiller-Universität Jena

von Odipo, Victor Onyango (MSc.)

geboren am 08.04.1982 in Bondo, Kenia.

---

Zugl.: Dissertation, Friedrich-Schiller-Universität Jena, 2019

Gutachter:

1. Prof. Dr. Christiane Schmallius (FSU Jena)
2. Prof. Dr. Alexander Brenning (FSU Jena)
3. Dr. Habil. Christian Thiel (DLR Jena)

Tag der öffentlichen Verteidigung: 06.02.2019

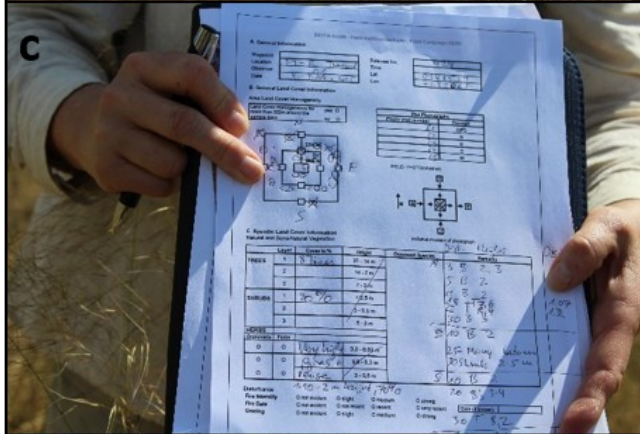
*“A man who calls his kinsmen to a feast does not do so to save them from starving. They all have food in their own homes. When we gather together in the moonlit village ground it is not because of the moon. Every man can see it in his own compound. We come together because it is good for kinsmen to do so.”*

— Chinua Achebe, *Things Fall Apart* (1994)

*Next page (photos):*

*The Lowveld savanna in Skukuza around the Eddy Covariance Flux Tower (a - f). The continuous grass cover with scattered trees; Tree variable inventory in the field in March 2015; Bush encroachment in some sections of the biome; Bare ground patches in the sodic lowlands, with mainly medium tree coverage; Effects of mega herbivore in modification of savanna vegetation structure as can be seen in large trees fell by elephants. Photos courtesy of Victor Odipo (Skukuza- South Africa, March 2015).*





## **Acknowledgements**

I would like to begin by thanking God for giving me the breath of life and guiding me in my everyday path towards finishing this task. Second, this work would not have been possible without significant inputs from several persons and institutions. Foremost, I would like to express my gratitude to the German Academic Exchange Service (DAAD) for the financial support in the form of scholarship for the past three years without which, my doctorate studies at the Friedrich-Schiller University of Jena would not have been possible. I wish to convey my heartfelt appreciation to Prof. Dr Christiane Schmullius, my supervisor and Head of the Department of Earth Observation at the Friedrich-Schiller University of Jena, for supervising my Doctorate thesis. The academic support and guidance provided towards the achievement of my professional goals are invaluable.

I warmly thank Dr Christian Thiel for his reviews and comments on drafting this dissertation, Dr Christian Hüttich, Dr Christian Berger, Michael Urbazaev and Felix Cremer for your contributions towards this dissertation, especially giving insights and reviews on the manuscripts. I am indebted to Dr Jussi Baade for the acquisition of terrestrial laser scanning (TLS) data and allowing me to use this dataset for my dissertation. I am grateful to all of those with whom I have had the pleasure to work in the ARS AfricaE Project at the Department of Earth Observation. Much appreciation to the MSc students at the Department who assisted with data analysis during their engagement within the project, particularly Mr Harry Luck and Christian Walther.

A special gratitude goes out to all the faculty members, doctorate and postdoctoral students at the Department of Earth Observation at Friedrich-Schiller-University for the fun and study times shared. Much appreciation goes to Ms Alicia Nickless from the University of Oxford for her scientific insights on carbon stock error estimations within savannas. I would also like to make a special mention to South African National Parks (SANPARKS), specifically the Scientific Services Department at Skukuza for facilitating field data collection at the Kruger National Park through provision of game wardens and assisting with data and information. I am very grateful to Mr Wolfgang Luke for allowing me to work at Forest Sense in Tshwane during my exchange visit in South Africa. I am indebted to Johann Heinrich von Thünen Institute in Braunschweig, especially the Institute for Climate-smart Agriculture for hosting me for my

four-month practicum prior to doctorate studies – Dr Werner Kutsch, Dr Christian Brümmer, Dr Eva Falge and Kanisios Mukwashi am very grateful for your kind gesture.

Finally, none has been more important to me pursuing this project than my family. I warmly thank the Odipos for their unwavering interest, encouragement and enthusiasm throughout the period of my studies. To my little princess Florence, you are the best study partner, and you who made it appear like I was undertaking two doctorate studies – this is for you! Always keen to know what I was doing, although it is unlikely that she grasped what it was all about! I am also grateful to my parents, Mr and Mrs Odipo the moral and emotional support. Your belief in me kept my hopes up.

## Foreword

I base this dissertation on the work spanning three years, with an initial intention of making three publications. However, because of time constraints, only one peer reviewed publication was feasible by the time of this write up. This dissertation therefore borrows a lot of its contents from the work of this publication:

Odipo VO, Nickless A, Berger C, Baade J, Urbazaev M, Walther C and Schullius C (2016) Assessment of Aboveground Woody Biomass Dynamics Using Terrestrial Laser Scanner and L-Band ALOS PALSAR Data in South African Savanna. *Forests* 7 (12), 294. Doi: 10.3390/f7120294.

## **Deutsche Kurzfassung der Arbeit**

### Wissenschaftlicher Hintergrund:

Parameter zur Beschreibung der Struktur der Savannenvegetation sind bei der Beurteilung der Fähigkeit des Bioms, Ökosystemleistungen unter verschiedenen Störungsszenarien zu erbringen, von besonderer Bedeutung. Studien, die auf eine Strukturkartierung auf der Skale einzelner Bäume abzielen, eröffnen die Möglichkeit, geringfügige Änderungen zu detektieren. Zur Durchführung solcher Studien werden räumlich und zeitlich mittel- bis hochauflösende Daten benötigt, die eine Operationalisierung von Initiativen zur Vegetationsüberwachung ermöglichen. Trotz des über viele Anbieter kostenfreien und somit einfachen Zugangs zu optischen Fernerkundungsdaten hat die auf diesen Daten basierende Kartierung der Vegetationsstruktur von Savannen den Nachteil, dass die spärliche und heterogene Verteilung der Vegetation zu ähnlichen spektralen Signaturen für verschiedene Lebensformen sowohl innerhalb als auch zwischen den Jahreszeiten führt. Darüber hinaus führen Beeinträchtigungen der Fernerkundungsdaten durch Wolken und Aerosolverunreinigungen zu Lücken in den Datenzeitreihen, die für eine kontinuierliche Überwachung der Vegetation, insbesondere in den Tropen, notwendig sind. Lang- und mittelwellige Mikrowellendaten wie sie durch das Radar mit synthetischer Apertur (SAR) erhoben werden, bieten aufgrund ihrer geringen Sensitivität gegenüber Wolken und ihrer hohen zeitlichen und räumlichen Auflösung Lösungsansätze zu einigen dieser Probleme an. Dennoch sind viele der Studien, die satellitengestützt erhobenen Fernerkundungsdaten zur Überwachung der Vegetation nutzen, durch die geringe Qualität der verfügbaren Referenzdaten von Strukturparametern, limitiert. Mittels terrestrischem Laserscanning (TLS) abgeleitete vertikale und horizontale biophysikalische Parameter, wie die auf Plot-Skale erhobenen Maßzahlen des Bedeckungsgrads (CC) und der Höhe des Kronendaches (CH); und die auf der Skale einzelner Bäume erhobener Parameter, wie der Basisdurchmesser und die Baumhöhe, können zur Verbesserung der SAR-basierten Schätzungen zur Vegetationsstruktur sowohl auf der Plot- als auch der Landschafts-Skale und der Separation von Lebensformen in der Savanne beitragen. Vor diesem Hintergrund ist es für diese Arbeit von zentraler Bedeutung, das Potenzial multi-temporaler C- und L-Band-SAR-Datensätze auf verschiedenen räumlichen und zeitlichen Skalen zur Überwachung der Struktur der Savannenvegetation zu untersuchen, wobei die als Referenz für die Lowveld-Savanne um Skukuza, Südafrika, eingesetzten Felddaten durch hochauflösende TLS-Daten ergänzt werden.

## Forschungsziele

Das übergeordnete Ziel dieser Arbeit ist es, das Potenzial hochauflösender, aus TLS-Daten abgeleiteter Strukturvariablen der Vegetation als Referenz für SAR-Datensätze zur Überwachung der Savannenvegetation innerhalb eines typischen Savannenökosystems zu untersuchen. Die bei der Untersuchung eingesetzten SAR-Datensätze wurden von unterschiedlichen Sensoren akquiriert und sind durch unterschiedliche temporale und räumliche Auflösungen gekennzeichnet. Das Gesamtziel dieser Arbeit umfasst daher folgende Forschungsziele:

1. Evaluierung des Potenzials von hochauflösenden TLS-Daten zur Extraktion von Strukturvariablen der Savannenvegetation;
2. Schätzung der AGB für das Untersuchungsgebiet und Bestimmung der Veränderungen in der AGB auf der Basis multi-temporalen L-Band-SAR-Daten für einen Zeitraum von vier Jahren in einem Areal der Lowveld-Savanne im Krüger-Nationalpark;
3. Betrachtungen zu Wechselwirkungen zwischen C-Band-SAR und verschiedenen Strukturvariablen der Savannenvegetation.

## Methoden

Bisher wurden in wenigen Studien die Stärken von TLS zur Kartierung von Vegetationsstrukturen in Savannen untersucht. Im Rahmen dieser Arbeit wird das Potential des Bedeckungsgrades sowie von Höhenmetriken und baumbezogenen biophysikalischen Parametern, die aus hochauflösenden TLS-Daten abgeleitet wurden, evaluiert, um die oberirdische Biomasse auf der Plot-Skala zu schätzen und um diese für eine Biomasseabschätzung der Savannenvegetation mittels multi-temporalem Radar mit SAR im L-Band innerhalb des 9 km<sup>2</sup> großen Untersuchungsgebiets im Krüger Nationalpark (KNP) zu extrapolieren. Darüber hinaus werden in dieser Arbeit multi-temporale C-Band-SAR-Daten verwertet, um die TLS abgeleiteten Metriken zu kartieren, zusätzlich zur Separation der mittels TLS abgeleiteten pflanzlichen Savannenlebensformen. In der Regenzeit 2015 wurde der Baumbestand auf 42 Plots inventarisiert und zur Berechnung der AGB auf der Skala einzelner Bäume herangezogen. Dabei fanden standortspezifische allometrische Gleichungen Verwendung. Darauf aufbauend wurden mittlere AGB-Werte für jeden Plot berechnet. Das aus TLS-Daten abgeleitete Vegetationshöhenmodell (CHM) wurde zur Berechnung von CC, CH sowie den daraus generierten Produkten verwendet. Für den Bereich des TLS-Footprints

wurden die Parameter mittels Regression mit der plotweise gemittelten AGB in Beziehung gesetzt. Im Untersuchungsgebiet wurde indes für die Jahre 2007, 2008, 2009 und 2010 die L-Band-SAR-Rückstreuung zur Modellierung der jährlich in der Trockenzeit anfallenden Biomasse innerhalb der 30 m-Plots verwendet. Darüber hinaus wurden TLS-Punktwolken verwendet, um die Höhe einzelner Bäume und deren Durchmesser 1 m oberhalb des Bodens für die TLS-basierte Baumbiomasseabschätzung über C-Band-SAR-Pixel mit einer räumlichen Auflösung von 20 m zu extrahieren. Letztlich wurde das CHM verwendet, um die fünf Hauptvegetationsklassen in der Savanne bezüglich ihrer Wuchshöhe zu kategorisieren. Innerhalb des Untersuchungsgebietes wurde dabei zwischen Hintergrund, Sträuchern, kleinen, mittleren und großen Bäumen unterschieden. Um die Varianz in der untersuchten Vegetationsstruktur zu reduzieren, wurden die Pixel in Häufigkeitsklassen eingeteilt: hoch, mittel und niedrig für AGB und CC und große Bäume, mittlere Bäume und kleine Bäume für Vegetationslebensklassen. Die Auswirkungen der hochauflösenden hyper-temporalen Sentinel-1-Polarisation im C-Band und der Saisonalität, sowie die Auswirkungen der Fenstergröße des Specklefilters auf die Nachweisbarkeit der vertikalen (AGB, H) und horizontalen (CC und Klassen der Lebensformen) Strukturparameter der Savannenvegetation wurden auf Pixelebene über die Dauer des Untersuchungszeitraums, der die Regenzeit 2015/2016 und die Trockenzeit 2016 umfasst, untersucht.

### Hauptergebnisse

Die Ergebnisse der Validierung der AGB-Modellierung zeigen einen signifikanten linearen Zusammenhang ( $p < 0,05$ ) zwischen den aus TLS-Daten abgeleiteten Prädiktoren und der Feldbiomasse und das korrigierte  $R^2$  umfasst Werte zwischen 0,56 für den aus SAR-Daten abgeleiteten und 0,93 für den aus TLS-Daten abgeleiteten Bedeckungsgrad beziehungsweise die Höhe. Die Ableitung der logarithmisch transformierten AGB aus den TLS-Metriken ergab im Vergleich zur Ableitung der nicht transformierten AGB geringere Fehler. Die Untersuchung der Rückstreuung mit Hilfe des RMSE ergab eine höhere Vorhersagegenauigkeit für die aus kreuzpolarisierten Daten abgeleitete AGB (RMSE = 6,1 t/ha) gegenüber der aus co-polarisierten Daten abgeleiteten AGB (RMSE = 6,7 t/ha), was auf die Volumenstreuung der verholzten Vegetation entlang von Flusstälern und Wasserläufen zurückzuführen ist. Die Veränderungsanalyse bezüglich der AGB ergab, dass auf 32 ha der untersuchten Fläche von 900 ha (entspricht 3,5%) eine Reduktion der AGB von durchschnittlich  $>5$  t/ha pro Jahr stattfindet, was im Wesentlichen auf das Fällen von Bäumen durch Megaherbivoren wie Elefanten zurückzuführen ist. Die VH-Polarisation berücksichtigt die volumetrische Streuung,



die von der Struktur der Baumkronen in der Savanne ausgeht und die in der Regenzeit aufgrund der höheren Verfügbarkeit von Feuchtigkeit, durch die für die Regenzeit typischen Niederschlagsperioden, stärker ausgeprägt ist. Klassen, die mit geringer Häufigkeit auftreten, sind im Gegensatz zu Klassen, die mit großer Häufigkeit auftreten, durch geringe Rückstreuintensitäten des SAR im C-Band gekennzeichnet, obgleich in beiden Fällen nur geringe Anteile an strukturellen Vegetationskomponenten vorhanden sind, die mit dem eingehenden Signal interagieren. Zusätzlich wird die Rückstreuintensität der Pixel, die zu den Klassen gehören, die mit einer geringen Häufigkeit auftreten, durch die Phasendifferenz, die aufgrund von Mehrfachstreuungen entsteht (beispielsweise an Sträuchern bzw. in der Krautschicht), beeinflusst, was zu einem hohen Speckle-Rauschen beiträgt. Die Auswirkungen von Speckle bezüglich der Reduzierung von Varianz und Standardabweichung spiegeln sich in der Reduktion der Rückstreuintensität der Vegetationsklassen mit geringer Wuchshöhe, wie etwa Sträuchern, wieder. Gleichzeitig führt eine Vergrößerung der Fenstergröße des Speckle-Filters proportional zu einem Verlust an Sensitivität gegenüber nicht-dominanten Strukturklassen.

#### Wichtigste Schlussfolgerungen

Hochauflösende TLS-Daten eignen sich nicht nur als Referenzdaten, sondern können auch zur Extraktion biophysikalischer Parameter mit Genauigkeiten genutzt werden, wie sie durch herkömmliche Feldkampagnen aufgrund des benötigten Zeitaufwandes, der Kosten und der räumlichen Abdeckung, nicht zu erheben wären. Lang- und mittelwellige SAR-Daten des C- bzw. L-Bands, können zur Detektion geringfügiger Veränderungen in der Vegetationsstruktur und zur Trennung von verschiedenen Klassen von Lebensformen innerhalb eines Savannenökosystems verwendet werden, wenn diese für diverse Aufnahmezeitpunkte im Jahr vorliegen.

Diese Arbeit zeigt das Potenzial von lang- als auch mittelwelligen SAR-Datensätzen zur Überwachung von Veränderungen bezüglich des Baumniveaus auf und trägt zu einer Aufwertung des Potenzials von C-Band-SAR-Daten im Bereich der Vegetationsüberwachung bei, ohne die räumliche Auflösung zu verschlechtern. Die Methodik ist daher für die Überwachung der Entwaldung und Waldschädigung von entscheidender Bedeutung und eröffnet vielversprechende Perspektiven auf ein operationell einsetzbares Monitoring bei mittlerer bis hoher räumlicher Auflösung. Großes Potenzial zur kontinuierlichen Überwachung der Vegetation und damit zur Erfassung der möglichen Veränderungen innerhalb und zwischen



den Jahreszeiten bergen aufgrund ihrer hohen zeitlichen und räumlichen Auflösung die frei zugänglichen Daten die von Sentinel-1 im C-Band aufgenommen werden.

## **Executive summary**

### Scientific background

Savanna vegetation structure parameters are important for assessing the biome's ability to provide ecosystem services under various disturbance scenarios. Studies aimed at tree-level structure mapping provide a way to detect forest changes due to degradation and assists in vegetation monitoring initiatives that would otherwise be impossible at coarse spatial and temporal resolutions. Despite availability and open-access of remote sensing data because of de-commercialisation, the use of optical remote sensing data for savanna vegetation structure mapping is limited by sparse and heterogeneous distribution of vegetation canopy, leading to near-similar spectral signatures among cover classes both within and between seasons. Cloud and aerosol contamination lead to inconsistency in the availability of time series data necessary for continuous vegetation monitoring, especially in the tropics. Long- and medium wavelength microwave data such as synthetic aperture radar (SAR), with their low sensitivity to clouds and atmospheric aerosols, high temporal and spatial resolution addresses some of these problems. However, many such studies utilising space-borne remote sensing data for vegetation monitoring lack quality structural reference data. Conventional sources of validation data through field inventory are expensive in terms of both time and labour. Terrestrial laser scanning (TLS) derived vertical and horizontal vegetation biophysical parameters, both plot-level such as canopy cover (CC) and canopy height (CH) metrics; and tree-level parameters like tree height and basal diameter can improve remote sensing-based vegetation structure modelling at both plot and landscape level scales. It is against this background that this study finds it of critical importance to assess the potential of multi-temporal C- and L-band SAR datasets at different spatial and temporal scales in savanna vegetation structure monitoring by complementing field data with high resolution TLS data as a reference within a Lowveld savanna in Skukuza, South Africa.

### Research Objectives

The general objective of this study is to explore the potential of high-resolution TLS-derived vegetation structure variables as a reference to multi-temporal, -spatial and -sensor SAR datasets in savanna vegetation monitoring within a typical savanna ecosystem. The overall objective of this study therefore comprises the following research objectives:

1. To evaluate the potential of high-resolution TLS-data in extraction of savanna vegetation structure variables;
2. To estimate landscape-wide AGB and assess AGB changes over four years using multi-temporal L-band SAR within a Lowveld savanna in Kruger National Park;
3. To assess interactions between C-band SAR with various savanna vegetation structure variables.

## Methods

To date, few studies have explored the strength of TLS for vegetation structural mapping, with few focusing on savannas. In this study, the potential of high-resolution TLS-derived canopy cover - height metrics and tree biophysical parameters are evaluated to estimate plot-level aboveground biomass, and to extrapolate to a landscape-wide biomass estimation using multi-temporal L-band SAR within a 9 km<sup>2</sup> area savanna in Kruger National Park (KNP) in South Africa. Further, the study exploits multi-temporal C-band SAR data in mapping these TLS-derived metrics besides separation of TLS-derived savanna vegetation cover classes. Trees were inventoried within 42 field plots in the wet season in March 2015 and used to compute tree-level aboveground biomass (AGB) using site-specific allometry and later averaged for each plot biomass estimates. TLS-derived canopy height model (CHM) is used to compute CC, CH and their product (CC x CH) which were then regressed with plot-level AGB over the TLS-footprint. The L-band SAR backscatter was used to model inter-annual dry season biomass within 30 m plots for the years 2007, 2008, 2009, and 2010 over the study area. The study further used TLS point clouds to extract individual tree height and basal diameter at 1 m tree height for TLS-based tree biomass estimation over 20 m C-band SAR pixels. Finally, height thresholding of CHM enabled classification of background and four major savanna vegetation cover classes within the study area: shrubs, small trees, medium trees and large trees. To reduce variance in the sampled vegetation structure, this study classified pixels into three abundance classes; high, moderate and low for AGB and CC and large trees, medium trees and small trees classes for vegetation cover classes. The effects of high resolution hyper-temporal C-band Sentinel-1 polarisation, seasonality and the effects of application of multi-temporal speckle filter with varying window sizes on detectability of vertical savanna vegetation structure parameters are investigated at pixel-level, over the length of the study period spanning wet season of 2015/2016 and dry season of 2016.

## Main results

The results from AGB model validation showed a significant linear relationship between TLS-derived predictors with field biomass,  $p < 0.05$  and adjusted  $R^2$  ranging between 0.56 for SAR to 0.93 for the TLS -derived canopy cover and height. Log-transformed AGB yielded lower errors with TLS metrics compared with non-transformed AGB. An assessment of the backscatter based on RMSE showed better AGB prediction with cross-polarised (RMSE = 6.1 t/ha) as opposed to co-polarised data (RMSE = 6.7 t/ha), attributed to volume scattering of the woody vegetation canopy along river valleys and streams. The AGB change analysis showed 32 ha (3.5%) of the 900-ha experienced AGB losses above an average of 5 t/ha per annum, which can mainly be attributed to falling of trees by mega herbivores such as elephants. VH polarisation's account for volumetric scattering emanating from SAR interactions with the savanna canopy structure (leaves and branches) in the wet season resulting from elevated moisture availability from rainfall events typical of the wet season. Low abundance classes showed a low response to C-band SAR backscatter compared to high abundance classes since in the former case there is less in proportion of the structure components exposed to interact with the incoming signal. SAR backscatter response is high for both polarisations and seasons, since soil - low vegetation interactions attenuates backscatter response from vegetation, attributed to open canopy allowing SAR signals to penetrate to the ground. The effect is more pronounced after rainfall events, leading to elevated soil moisture. The study sees the effects of speckle filter window in reducing the backscatter response in lower vegetation cover classes like shrub; increasing speckle window size led to a proportionate loss of sensitivity to non-dominant structure classes.

## Main conclusions

This study uses high resolution TLS data not only as reference data in most remote sensing studies but also useful in extraction of vegetation biophysical parameters with accuracies that would otherwise be infeasible through field inventories because of time, labour and geographical coverage constraints. Long and medium wavelength SAR data, particularly L- and C-band respectively, can be used in detection of small vegetation structural changes and separation of vegetation classes within a savanna ecosystem. This study points to the potential of both L- and C-band SAR datasets in monitoring tree level changes and puts more premium on the potential of C-band SAR in vegetation monitoring without degrading the spatial resolution. The method adopted is therefore critical in deforestation and forest degradation monitoring, with a promise of operational monitoring from medium to high resolution. There

is a high potential in the freely available C-band Sentinel-1 A data because of high temporal and spatial resolution, in continuous monitoring of vegetation capturing the changes within and between seasons.

## Table of Contents

Acknowledgements .....	VI
Foreword .....	VIII
Deutsche Kurzfassung der Arbeit.....	IX
Executive summary .....	XIV
Table of Contents .....	XVIII
Figures.....	XX
Tables .....	XXIV
Abbreviations .....	XXV
<b>CHAPTER 1 .....</b>	<b>1</b>
1. Literature Review.....	1
<b>1.1. Background to savanna ecosystem.....</b>	<b>1</b>
<b>1.2. Savanna heterogeneity and heterogeneity drivers.....</b>	<b>3</b>
<b>1.3. Remote sensing in Savanna vegetation structure mapping .....</b>	<b>19</b>
<b>1.4. Study motivation.....</b>	<b>22</b>
<b>1.5. Research objectives and questions .....</b>	<b>27</b>
<b>CHAPTER 2 .....</b>	<b>30</b>
2. Theoretical background and techniques .....	30
<b>2.1. Basic principles of SAR systems.....</b>	<b>30</b>
<b>2.2. Vegetation structure mapping using SAR data .....</b>	<b>41</b>
<b>2.3. Reference data for validation of remote sensing vegetation products .....</b>	<b>45</b>
<b>CHAPTER 3 .....</b>	<b>58</b>
3. Methodology .....	58
<b>3.1. Summary on methodology .....</b>	<b>58</b>
<b>3.2. Study Area.....</b>	<b>60</b>
<b>3.3. Data Acquisition and Processing.....</b>	<b>65</b>
<b>3.4. Aboveground Biomass (AGB) Modelling.....</b>	<b>74</b>
<b>3.5. Savanna vegetation cover classes and canopy cover .....</b>	<b>81</b>
<b>3.6. Conclusion on methodology.....</b>	<b>84</b>
<b>CHAPTER 4 .....</b>	<b>86</b>

4. Results .....	86
<b>4.1. Field and TLS Biomass</b> .....	86
<b>4.2. SAR-TLS Biomass Prediction Models</b> .....	89
<b>4.3. Radar Sensitivity to Biomass</b> .....	92
<b>4.4. Biomass Change Detection</b> .....	94
<b>4.5. C-band SAR interactions with savanna vegetation structure components</b> .....	98
<b>4.6. Uncertainty and Error Analysis</b> .....	117
<b>CHAPTER 5</b> .....	121
5. Discussion of results.....	121
<b>5.1. Spatial distribution of savanna vegetation structure within Skukuza</b> .....	121
<b>5.2. Temporal dynamics in savanna vegetation structure</b> .....	124
<b>5.3. Uncertainties in savanna structure mapping</b> .....	137
<b>CHAPTER 6</b> .....	141
6. Summary, conclusions and outlook.....	141
<b>6.1. Summary</b> .....	141
<b>6.2. Conclusions</b> .....	144
<b>6.3. Outlook</b> .....	146
<b>References</b> .....	149
<b>Selbständigkeitserklärung</b> .....	189

## Figures

Figure 1-1. A typical savanna's vertical and horizontal structure showing continuous C4 grasses layer and a discontinuous shrub and tree cover. (Source: Charles-Dominique <i>et al.</i> , 2015).....	1
Figure 1-2. Carbon storage by biome. Savannas and grasslands are the second largest terrestrial sinks. (Source: Olson <i>et al.</i> 2001).....	2
Figure 1-3. The various triggers of savanna heterogeneity and shifts between stable to unstable conditions. (Source: Oliveras & Malhi, 2016). ....	4
Figure 1-4. Greenhouse gas emission in Gt CO <sub>2</sub> per source from 1990 to 2016. Fires constitute the highest emission source. (Source: Houghton & Nassikas, 2017). ....	8
Figure 1-5. Effects of grazing and browsing on grass biomass (fuel load). Low grass biomass leads to low fuel load, meaning less fire intensity with low damage to trees resulting in woody vegetation increase. (Source: van Langevelde <i>et al.</i> , 2003). ....	11
Figure 1-6. Current defined limits of maximum tree cover (Sankaran <i>et al.</i> 2005) shown by the blues line across a rainfall gradient. Maximum tree cover in low-rainfall savannas (MAP < 650 mm) is constrained by water availability. The red arrow: CO <sub>2</sub> fertilization is expected to lead to an increase in tree cover. ....	15
Figure 1-7. Global distribution of grass, shrub and savanna vegetation (Hansen, 2000). ....	22
Figure 1-8. Evidence of disturbance in Skukuza, Kruger National Park (KNP) by (a) fire, (b) browsers, (c) tree fall by elephants (Photos courtesy Victor Odipo, Nov. 2016) .....	24
Figure 1-9. Global cloud cover frequency between 1994-2001 (International Satellite Cloud Climatology Project-ISCCP; Wylie, 2015). ....	26
Figure 2-1. Electromagnetic spectrum showing location of the various electromagnetic radiation wavelengths (Source: Liew, 2001).....	30
Figure 2-2. Radar geometry showing the flight direction A, Nadir point directly below the radar platform B, the swath of the radar beam C, and both range – and azimuth directions as D and E respectively (Source: CCRS, 2019).....	32
Figure 2-3. Aperture synthesis by radar platform, with the virtual aperture length (B) after complete illumination of ground target (A) (Source: CCRS, 2019) .....	33
Figure 2-4. SAR data processing workflow: raw data pre-processing, Doppler centroid estimation, SAR focusing and decompression, and post-processing (Credit: ESA, 2019).....	35
Figure 2-5. SAR backscatter interactions with vegetation components at different wavelengths, a) L-band and b) C-band SAR. (Source: Evans <i>et al.</i> , 2013). ....	42



Figure 2-6. SAR backscatter interactions with vegetation components at different wavelengths, a) L-band and b) C-band SAR. (Source: Evans <i>et al.</i> , 2013). .....	49
Figure 3-1. Methodology adopted in AGB modelling and change analysis using L-band ALOS PALSAR with field inventory and TLS as reference datasets (Odipo <i>et al.</i> , 2016; TLS data by Dr. J. Baade).....	59
Figure 3-2. Methodology adopted in assessment of C-band Sentinel 1A SAR interactions with TLS-derived savanna vegetation structure.....	59
Figure 3-3. Map showing the biomes of South Africa, with savanna biome divided into bioregions A to F (source: Mucina & Rutherford, 2006).....	61
Figure 3-4. Imagery showing location of the study site in Skukuza, showing the terrestrial laser scanner (TLS) footprint. The study is centred on the Skukuza eddy covariance tower (EC Tower) as shown in the map. (Imagery source: Google Earth/Digital Globe). .....	62
Figure 3-5. Average monthly rainfall (mm) for the period 1912 to 2001 (Kruger <i>et al.</i> , 2002). .....	63
Figure 3-6. Decadal rainfall statistics for Skukuza region for the year 2015. Dark blue bars are rainfall values for 2015 while light blue shows 20-year averages (1994-2013). Source: FAO VAM.....	63
Figure 3-7. Plot layout, tree identification and measurement adopted in plot sampling for individual tree mensuration. ....	66
Figure 3-8. Individual tree parameter measurement from TLS point clouds: a) noise-reduced point clouds showing individual trees within the study area, b) tree DBH measurement at 1 m height, c) tree height measurement as the distance between the lowest surface-level. ....	69
Figure 3-9. TLS-derived (a) digital surface model; (b) digital terrain model; and (c) canopy height model. (Data acquired by J. Baade).....	70
Figure 3-10. C-band Sentinel-1A time series data showing the dates of acquisition used in this study, as a response to precipitation and soil moisture content. Soil moisture data was derived from flux data in Skukuza. ....	71
Figure 3-11. L- and C-band SAR processing workflow in GAMMA as used in this study. The blue boxes are more relevant for GRD C-band data which does not require multi-looking. ....	72
Figure 3-12. Plot-level aboveground woody biomass distribution from a) field inventory and b) TLS tree measured datasets. ....	76
Figure 3-13. Sampled 20 m plots for assessment of C-band SAR backscatter metrics response to a) AGB plots and b) CC plots.....	77

Figure 3-14. TLS-derived (a) Percentage canopy cover (CC) and (b) canopy height (CH) for 30 m plots around Skukuza flux tower site. ....	78
Figure 3-15. Validation results of field measured height and TLS canopy height.....	80
Figure 3-16. A photo showing savanna vegetation cover classes in Skukuza, Kruger National Park in March 2015. (Photo courtesy: Victor Odipo).....	82
Figure 3-17. Cumulative bar graphs showing proportion of class distribution within each of the 60 sampled 20 m grids.....	83
Figure 4-1. Distribution of 30 m field inventoried plots around Skukuza eddy covariance (EC) flux tower, and the extent of TLS data footprint (Background imagery source: Google Earth). ....	86
Figure 4-2. Tree height, diameter, and the resultant AGB per inventoried tree within the study area..	87
Figure 4-3. Map showing biomass distribution within 445 reference plots derived from TLS point cloud tree measurement within the study area. (Background imagery source: Google Earth). ....	88
Figure 4-4. Biomass estimates for each of the 42 sampled plots in kg. The red line shows the mean AGB in kg while the bars are 95% confidence intervals for AGB. Each plot is 0.09 ha in size.....	89
Figure 4-5. Correlation between TLS canopy cover height metrics and AGB and log (AGB).....	91
Figure 4-6. Regression and residual plots between TLS metrics derived AGB and field. CC denotes canopy cover, CH denotes canopy height, and RMSE denotes root mean square error .....	92
Figure 4-7. Correlation between L-band SAR-derived biomass and reference TLS-metrics derived biomass. The graphs show co- and cross polarised L-band ALOS derived AGB responses .....	93
Figure 4-8. Predicted woody biomass from L-band SAR backscatter intensity (HH and HV) for the years 2007, 2008, 2009, and 2010.....	95
Figure 4-9. Biomass change results over the study period 2007–2010, with six change combinations with (a) 2007–2008; (b) 2008–2009; and (c) 2009–2010.....	98
Figure 4-10. Five vegetation cover classes obtained from OBIA height thresholding the TLS CHM. Inset is the grid partition and dominant class selection. ....	99
Figure 4-11. Temporal changes in C-band SAR backscatter response to the various vegetation cover classes for (a) VV - and (b) VH polarisation.....	102
Figure 4-12. Effects of Quegan multi-temporal speckle filter on a 3 by 3 window, on the seasonal changes in C-band SAR backscatter response to the various vegetation cover classes for (a) VV - and (b) VH polarisation.....	104

Figure 4-13. Effects of Quegan multi-temporal speckle filter on a 5 by 5 window, on the seasonal changes in C-band SAR backscatter response to the various vegetation cover classes for (a) VV - and (b) VH polarisation.....	105
Figure 4-14. Map showing canopy cover (CC) distribution within 1206 reference plots derived from TLS CHM within the study area. ....	106
Figure 4-15. Seasonal changes in C-band SAR backscatter response to CC abundance classes for (a) VV - and (b) VH polarisation.....	108
Figure 4-16. Effects of Quegan multi-temporal filter on a 3 by 3 window on the seasonal changes in C-band SAR backscatter response to CC abundance classes for (a) VV - and (b) VH polarisation.....	110
Figure 4-17. Effects of Quegan multi-temporal filter on a 5 by 5 window on the seasonal changes in C-band SAR backscatter response to CC abundance classes.....	111
Figure 4-18. Seasonal changes in C-band SAR backscatter response to AGB abundance classes. ....	113
Figure 4-19. Effects of Quegan multi-temporal filter on a 3 by 3 window on the seasonal changes in C-band SAR backscatter response to AGB abundance classes.....	114
Figure 4-20. Effects of Quegan multi-temporal filter on a 5 by 5 window on the seasonal changes in C-band SAR backscatter response to AGB abundance classes.....	115
Figure 4-21. Trunk diameter measurement from TLS PCs. Reconstruction of the DBH is dependent on availability of enough points.....	119
Figure 4-22. Multi-stem tree within the study area. Depending the height at which the trunks split, all must be measured, averaged and assigned to the common tree.....	120
Figure 5-1. Tree-level height, diameter, and the computed AGB derived from TLS point clouds within the study area.....	122

## Tables

Table 1-1. Mean seasonal fire intensity classification in Kruger National Park. (Source: Govender <i>et al.</i> , 2006). .....	6
Table 2-1. Commonly used SAR frequency bands with corresponding wavelengths .....	31
Table 3-1. Riegl VZ-1000 specification (RIEGL, 2015).....	67
Table 3-2. Characteristics of the L-band Advanced Land Observation Satellite (ALOS) Phased Array L-band Synthetic Aperture Radar (PALSAR) and C-band Sentinel-1 A datasets used in the study area. (Source: JAXA) .....	71
Table 3-3. Summary statistics of the field inventoried and TL-measured trees. DBH = diameter at breast height (basal diameter); H= tree height; AGB = aboveground biomass.....	75
Table 3-4. Summary statistics of the sampled vegetation cover classes based on dominant class (%) per grid. ....	84
Table 4-1. TLS and microwave AGB predictor variables and associated error and coefficient of determination ( $R^2$ ). .....	90
Table 4-2. Relative change in AGB in Skukuza between 2007 and 2010.....	96
Table 4-3. Summary statistics of the TLS CHM derived canopy cover within 20 m plots in Skukuza. ....	106
Table 5-1. Mean biomass values from various studies within and around Skukuza. *TLS ref= TLS reference tree dataset over 20 m plots; **Published and part of this dissertation. ....	122

## Abbreviations

AGB	Aboveground biomass
ALOS PALSAR	Advanced Land Observation Satellite Phased Array L-band SAR
ARS AfricaE	Adaptive Resilience of Southern African Ecosystems
ASPRS	American Society of Photogrammetry and Remote Sensing
BEF	Biomass Expansion Factor
CHM	Canopy Height Model
CSIR	South Africa's Council for Scientific and Industrial Research
DAAD	Deutscher Akademischer Austauschdienst
DBH	Diameter at breast-height
DTM	Digital Terrain Model
ENL	Equivalent number of looks
ENVISAT	Environmental Satellite
ESA	European Space Agency
ESRI	Environmental Systems Research Institute
FBD	Full-beam dual
GHG	Green House Gas
GLAS	Geosciences Laser Altimeter
GPS	Global Positioning System
GRD	ground range detected
HV	Horizontal-Vertical
ICE Sat	Ice, Cloud and land Elevation Satellite
IPCC	International Panel on Climate Change

JAXA	Japan Aerospace Agency
JERS-1	Japanese Earth Resources Satellite-1
KNP	Kruger National Park
LiDAR	Light Detection and Ranging
ML	Multi-looking
NDVI	Normalized Difference Vegetation Index
NPP	Net Primary Productivity
RTK-GNSS	Real-Time Kinematic Global Navigation Satellite System
SAFARI	South African Regional Science Initiative
SANPARKS	South Africa National Parks
SANSA	South Africa National Space Agency
SAR	Synthetic Aperture Radar
SRTM	Shuttle Radar Topographic Mission
TIN	Triangulated Irregular Network
TLS	Terrestrial Laser Scanner
UN-REDD (+)	United Nations Reducing Emissions from Deforestation and Degradation
UNFCCC	United Nations Framework Convention on Climate Change

# CHAPTER 1

## 1. Literature Review

### 1.1. Background to savanna ecosystem

Savanna landscapes make up one of the largest natural resource bases in the world (van Wilgen, 2009), covering about twenty percent of the earth's land surface (Campbell, 2013). On a global scale, the African continent records the highest number of the total land area characterised by savanna ecosystems as sixty-five percent of land surface is typically comprised of spatially heterogeneous savanna ecologies (Shirima *et al.*, 2011) mainly characterised by codominance of expansive unbroken herbaceous layer of perennial grassland and varying densities of discontinuous tree canopies (Figure 1-1, Charles-Dominique *et al.*, 2015; Mermoz *et al.*, 2014). East Africa maintains the largest savanna in the world; the Miombo woodlands in Tanzania, which supports over 100 million livelihoods (Carreiras *et al.*, 2012). Among other African countries with expansive savanna biomes is Botswana, whose most land area is characterised by semi-arid savanna ecosystems that act as habitats for the largest populations of world's remaining wildlife (Mishra *et al.*, 2015).



Figure 1-1. A typical savanna's vertical and horizontal structure showing continuous C4 grasses layer and a discontinuous shrub and tree cover. (Source: Charles-Dominique *et al.*, 2015).

Savannas are prominently common in tropical and subtropical regions with highly contrasting dry and wet seasons. Savanna ecosystem is only second to tropical forests in terms of global net primary productivity (NPP), apart from being a substantive terrestrial carbon pool (Figure

1-2, Olson *et al.*, 2001; Scholes & Walker, 1993). Savanna ecosystem covers some two-thirds of sub-Saharan Africa and is a source of livelihood to some eight percent of African rural livelihoods since they form a profound resource to a larger fraction of rural communities as they derive their livelihood from them. These ecosystems are also substantive components to the world's carbon balance and hence a climate modifier.

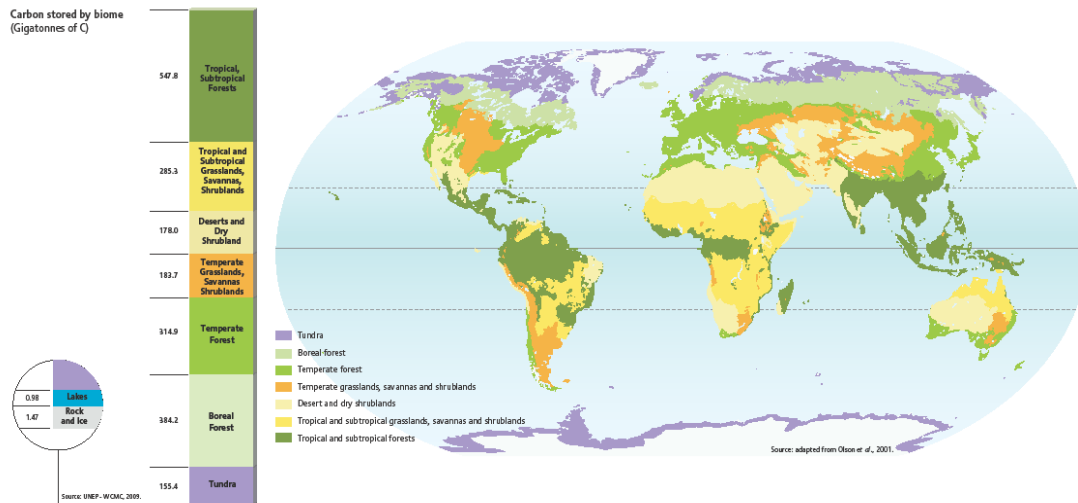


Figure 1-2. Carbon storage by biome. Savannas and grasslands are the second largest terrestrial sinks. (Source: Olson *et al.* 2001).

Sub-Saharan Africa alone accounts for twenty-five percent of the global 193 Gigaton carbon stock (Saatchi *et al.*, 2011), with uncertainty in quantification within the tropics (Baccini *et al.*, 2008) because of direct threats by constant direct disturbances, in the form of woody biomass harvesting, herbivory, changes in land use in the form of agricultural expansion, settlements, urbanization, wild fires; and indirect disturbances from climate change caused by rising concentrations of atmospheric carbon dioxide (CO<sub>2</sub>) in the atmosphere (Kutsch *et al.*, 2012; Asner *et al.*, 2010). With rising concerns in global climate change primarily emanating from observable modifications of the structure and functioning of the disturbance-driven ecosystems, there is an equal growing initiative in estimating forest parameters such as above and belowground biomass in these ecosystems to gauge the extent to which these disturbances scenarios have compromised the global roles of these ecosystems as carbon sinks. This, and woody cover, helps in understanding the vegetation community assemblages and the distributions, frequencies and characteristics of their driver variables. Information about forest carbon stock estimates and the spatial extent of vegetation classes are key to intergovernmental stakeholders, research communities, conservationists and scientists. The information helps to monitor and re-evaluate the management policy options and adaptive strategies aimed at



addressing international framework conventions on climate change mitigation policies (Carreiras *et al.*, 2012; Saatchi *et al.*, 2011) and to implement the United Nation's Reducing Emissions from Deforestation and Degradation (UN-REDD+) programme (Cutler, 2012).

## **1.2. Savanna heterogeneity and heterogeneity drivers**

Savannas make up the largest natural resource base, particularly in the sub-Saharan Africa (Gosling, 2014). The classical description of savannas broadly identifies them as disturbance-driven (disequilibrium) systems (Sankaran *et al.*, 2004), exhibiting enormous disparities in their structural complexities, functioning and life-form compositions at both ecosystem and global scales (Levick & Rogers, 2006). The structural type, disparity and balance of especially the woody vegetation cover play an integral role in determining savanna heterogeneity and functional dynamism (Kiker *et al.*, 2014).

Studies to monitor savanna ecosystems have affirmed analogy that most savannas of the world appear to have transformed from their 'natural states' since their establishments (Sankaran & Anderson, 2009). The spatiotemporal dynamism in savannas is a function of the changing regimes in the general factors that shape all vegetation kinds, the drives of an ecosystem (Sankaran & Anderson, 2009). These change variables typically alter resource availability within an ecosystem (Scholtz *et al.*, 2014). The transition could be a product of competition-based or anthropogenic processes or an interplay of most of these parameters. In this context, studies mainly consider water and nutrients as the primary determinants, while fire and herbivory are the modifiers (Sankaran *et al.*, 2004). Diversity is an enormous and long term when the level of competition lies between the extremes of availability or lack of disturbance (Carlsson, 2005).

The system responses to these drivers are either structural - changes in vegetation type, coverage and community composition; or functional - changes in hydrological processes, nutrient cycling, and primary productivity (van Wilgen, 2009; Winnie *et al.*, 2008). The change variables can significantly maintain or devastate the ecosystem integrity (Scholes & Archer, 1997), and have become a global phenomenon and hence potential centres of many studies (Scholtz *et al.*, 2014).

The classical perception of savanna heterogeneity also explains these dynamisms in the context of equilibrium and non-equilibrium states. Equilibrium represents a scenario whereby an ecosystem maintains tree – grass ratio (implying less competition for resources) coexistence for a very long time without expressing no remarkable fluctuations in their tree population structures, spatial patterns, and species composition, irrespective of the active driver variables (Sankaran *et al.*, 2004). This concept has essentially been used to explain the long-term existence of pure grasslands or woodlands in other parts of the world. Non-equilibria perception contravenes this model and brings dynamism in the tree - grass ratio coexistence and emphasises that the varying ratios are a function of prevailing driver variables. Generally, at low rainfall levels, savannas with low woody cover dominate, grasses produce a high fuel that enhances the probability of fire episodes and/or herbivory, leading to juvenile woody vegetation. High rainfall on the other hand leads to closed woody canopy, shading off light from grass understory, leading to fire suppression. With moderate rainfall, if fire/herbivore disturbances are suppressed, the tree canopy will eventually be closed enough as to suppress the herbaceous layer and therefore fire. Heavy fire and herbivory triggers lead to an open environment, resulting from continuously preventing tree saplings from escaping the fire or herbivore. The presence of these two positive feedbacks acting in different directions results in a tendency for relatively abrupt changes in the tree and grass cover (Figure 1-3, Oliveras & Malhi, 2016).

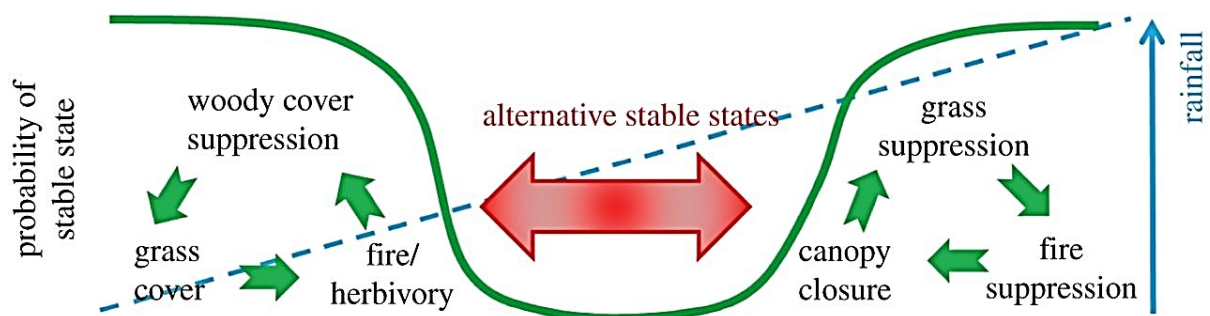


Figure 1-3. The various triggers of savanna heterogeneity and shifts between stable to unstable conditions. (Source: Oliveras & Malhi, 2016).

Regime shifts and system variability in savannas are direct feedback from complex interactions of different variables operating at varied spatial and temporal scales (Sankaran & Anderson, 2009). These variables could be the climatic conditions and geological substrates properties (Scholes & Walker, 1993) of an area, or disturbances such as prevalent wildfire outbreaks,

human manipulations and effects of wildlife inhabiting an ecosystem. Climate and soil are distinctively considered as exogenous drivers and unaffected by internal dynamics, whereas fires and herbivory are regarded as endogenous factors and are influenced by external forces. However, the variability and interdependence of these components, and challenges in quantifying the intensities of their impacts sometimes make it uneasy to determine the main mechanism that defines the state of an ecosystem (Scholes & Archer, 1997).

The rate and scale of savanna succession depend on the sequence, the frequency and magnitude of the disturbance variables and this also varies between regions and within ecosystems (Scholes & Archer, 1997). In some parts of Africa, climatic changes (mainly drought and high seasonal rainfall variability) have been identified as the core regulator of the balance between woody and herbaceous vegetation covers (Sankaran *et al.*, 2008), while interruptions such as those resulting from severe fires and anthropogenic factors (Levick & Rogers, 2006) have formed the basis of change (Sankaran & Anderson, 2009). Within the KNP in South Africa for instance, the natural variables such as rainfall and geology were found to have more effects on woody structural diversity and composition than the disturbance from fire and wildlife (Scholtz *et al.*, 2014).

The response pattern of savanna vegetation parameters depicts varied reactions to different or similar predictive variables (Scholtz *et al.*, 2014). For instance, terrestrial fires are known to influence woody vegetation structure and have less effect on woody vegetation composition and species. A review of previous studies conducted in Kenyan savannas also established that rainfall mainly influences woody canopy cover whereas drainage mainly influences tree height only at certain elevations (Colgan *et al.*, 2012). Soil properties mainly regulate species composition. The following is a highlight of the major drivers of savanna heterogeneity and details about the triggers influencing these drivers.

### *Biomass Burning*

Forest fires have been traced from prehistoric human activities spanning several decades back and have been cited as one of the major perturbations of savanna biomes especially in the African continent (Walker, 1985). Savanna ecosystems are the most susceptible to fires, especially in the tropical regions (Andersen *et al.*, 2012). Depending on the type, frequency, seasonal occurrence, and their intensity, fires can lead to detrimental loss of large proportions

of tree and grass species at various spatial scales such as the scenarios in KNP which has had a long fire history of fire occurrence studies (Table 1-1, Govender *et al.*, 2006). This is because they can indiscriminately consume nearly all materials of any structural type hence destroying soil biota and damaging exposed living tissues (Govender, 2003). From Table 1-1, it is evident that fire intensities  $> 2000 \text{ kW m}^{-1}$  are experienced in seasons with high fuel loads of  $> 2000 \text{ kg ha}^{-1}$  typical of autumn, winter and spring seasons.

Table 0-1. Mean seasonal fire intensity classification in Kruger National Park. (Source: Govender *et al.*, 2006).

<i>Season of burn</i>	<b>Descriptor</b>	<i>Fuel loads (kg ha<sup>-1</sup>)</i>				
		<b>&lt;1000</b>	<b>1000-2000</b>	<b>2000-4000</b>	<b>4000-6000</b>	<b>&gt;6000</b>
<i>Summer</i> (1 December-31)	Fire intensity class	Very low	Low	Moderate	Moderate	Moderate
	Mean fire intensity (kW m <sup>-1</sup> )	287	578	1031	1432	1650
	Number of fires	1	17	95	83	31
<i>Autumn</i> (1 April-30)	Fire intensity class	Very low	Low	Moderate	High	High
	Mean fire intensity (kW m <sup>-1</sup> )	No data	7328	1455	2106	1900
	Number of fires	0	19	62	79	23
<i>Winter</i> (1 June-31)	Fire intensity class	Very low	Low	High	High	Very high
	Mean fire intensity (kW m <sup>-1</sup> )	194	835	2082	3625	4385
	Number of fires	4	65	187	83	19
<i>Spring</i> (1 September-30)	Fire intensity class	Very low	Low	Moderate	High	Very high
	Mean fire intensity (kW m <sup>-1</sup> )	No data	712	1570	3066	5253
	Number of fires	0	15	103	55	16

Plants have different tolerance levels to fire. Some plants can recover after a fire incidence while others completely die. Persistent fires can therefore lead to complete extinction of fire-intolerant species (Carlsson, 2005) and sometimes lead to invasion of alien species (Kontoes *et al.*, 2013). In fire-prone areas, the landscapes are dominated by homogenous savanna tree species (van Wilgen *et al.*, 2000) which can resist effects of severe burning (Kontoes *et al.*, 2013). Such vegetation owes their existence from developing mechanisms such as extreme heights and enough bark thickness (Furley *et al.*, 2008). Hoffmann *et al.*, (2012) coined this state of an ecosystem as having reached a fire-resistance threshold. This however depends on the interval between disturbance occurrences; long intervals allow enough time for saplings to undergo this process. In most cases, however, this time is interrupted by other factors such as levels of resource availability (Hoffmann *et al.*, 2012). A shift in the savanna regime is typical if this threshold has been crossed.

Biomass burning modifies the spatial distribution of savanna ecosystems by affecting the structural elements and species composition (Reis *et al.*, 2015) through complex interactions involving climate, resources and species traits (Govender *et al.*, 2006; Hoffmann *et al.*, 2012). The magnitude of the impact of biomass burning also depends on the time interval between the disaster and the occurrence of subsequent agents such as precipitation and herbivory (Walker, 1985). Terrestrial fires also change the energy and soil mineralisation- nitrogen, carbon and sulphur, and phosphorus and potassium to a lesser extent (Sankaran & Anderson, 2009). They also have effects on the hydrological cycle (water fluxes), the soil chemistry and other physical characteristics (Thonicke *et al.*, 2001) hence affecting the atmospheric, morphological and physiological characteristics of savanna ecosystems (Walker, 1985). Some of these mineral elements are volatile and hence easily lost to the atmosphere. Higher soil temperatures reduce the reflection coefficient (albedo) of the soil surface, and this allows for higher absorption of solar radiation which directly devastates belowground biomass (Walker, 1985). Fires also reduces the soil surface stability, hence exposing it to harsh environmental conditions, making them susceptible to extensive erosion and reduced water holding capacity.

Severe recurrent fire regimes also lead to destruction of grass-lads and shrubs. This eventually leads to woody dominance in an ecosystem (Sankaran & Anderson, 2009). However, with relative minimum resources such as precipitation, savannas can experience high growth rates and a rapid increase in the total biomass. This rapid growth is accelerated by increased levels of nutrients in the soils (mainly Nitrogen and Phosphorous) resulting from biomass burning and decomposition of inorganic matter (Gosling, 2014). Destruction of woody vegetation and tall grass also enhances plants' (especially understory) exposure to sunlight hence favouring fast growth of grass. Like trees, grasses come in various species classes, and some grass varieties have also developed mechanisms that can support their existence by responding quickly after an event of fire. Most previously disturbed patches within savanna ecosystems are now colonised by stoloniferous grass forms like the lawns and coppices (bunch grasses), which can resist fires and replenish their root reserves relatively faster (Gosling, 2014).

Repeated and large scale burning in the tropics has been cited as one of the major causal agents for greenhouse gas concentrations (Figure 1-4, Houghton & Nassikas, 2017; Maraseni *et al.*, 2016; Andersen *et al.*, 2012), hence exacerbating the process of climate change (Thonicke *et al.*, 2001). In northern Australia, fires account for an average of 3% of Australia's greenhouse gas emissions (Andersen *et al.*, 2012). Fires can also burst open the vulnerable woody fruits

hence help in dispersing tree seeds for germination (Sodhi & Ehrlich, 2010). Fires commonly occur over two seasons, the dry season (Walker, 1985) and at the onset of a rainy season (Sankaran *et al.*, 2008). Because of low densities of highly flammable biomass load characteristic of long droughts, arid savannas experience longer fire return periods than the frequencies observed in wet savanna regions (van Wilgen *et al.*, 2000). Contrary, rains in mesic savannas facilitate high production and accumulation of grass, which form fuel environment that supports fires of higher intensities (Sankaran *et al.*, 2008). Dry season fires are mainly induced by man to pave way for land use activities. Analysis of fires that occurred between 1980 and 1993 in the Kruger National Park showed that 90 percent of fire was caused by man (van Wilgen *et al.*, 2000). Lightening only accounted for 10 percent. Fires occurring at the beginning of a rainy season are mainly caused by frequent lightning, which characterise most tropical rains.

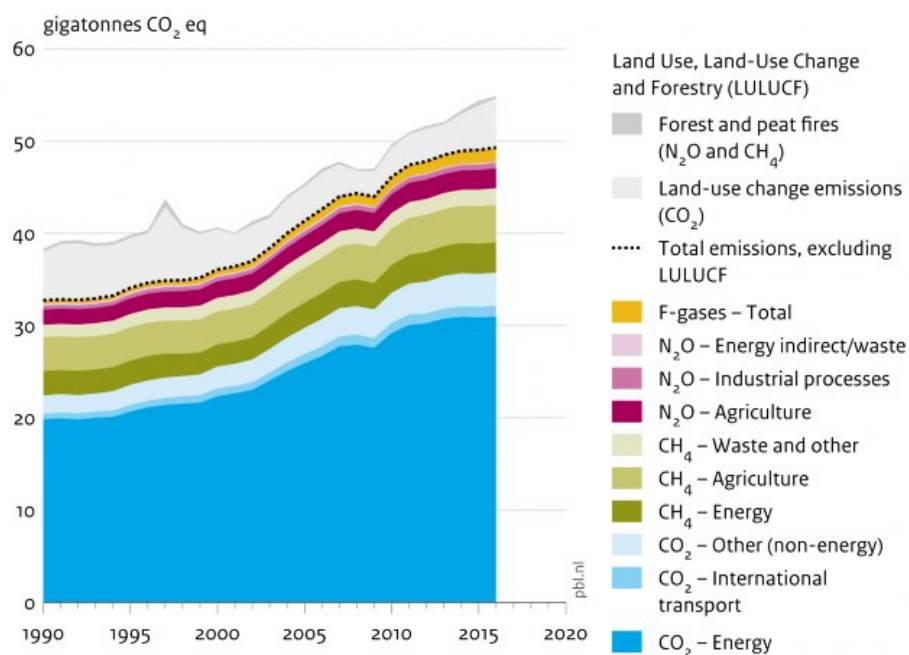


Figure 1-4. Greenhouse gas emission in Gt CO<sub>2</sub> per source from 1990 to 2016. Fires constitute the highest emission source. (Source: Houghton & Nassikas, 2017).

The role of fire as a change agent in savanna ecosystems depends mainly on the mean fire return period. Despite their tremendous effect on savanna landscapes, fires have also been perceived as maintainers of species balance and coexistence. Fire regimes are a significant variable that needs to be incorporated in the models designed to evaluate the changing regimes in savanna ecosystems. Interestingly, most forest fires experienced today are ignited by man to derive their livelihoods from these ecosystems. Such human manipulations can be regulated. Recent global

concerns and approaches on fire management have had a marked impact on the recurrence patterns (Sankaran & Anderson, 2009). Fire management goals have saved savanna vegetation from the adverse effects of massive burning and constant pressures. Prescribed periodic burning has been implemented in various savanna regions and this has helped stabilise savannas.

### *Herbivory*

Savanna ecosystems are ideal habitats for the largest proportion of animal communities (Gosling, 2014). Unlike other continents that experienced massive herbivore extinction during Pleistocene, African continent has the largest and diverse extant mega fauna like elephants, buffalos and white rhinos, and browsers such as antelopes and other mixed feeders. These animals depend on savanna growth forms for foraging (Gosling, 2014; Bond & Archibald, 2003).

Elephants are the leading drivers for the extinction of woody plants and modification of woody community composition (Wigley *et al.*, 2014). Structural variation is the primary ecological response to the effects of ungulate wildlife such as elephants and buffalos (Landman *et al.*, 2014). Enormous-bodied herbivores reduce biomass concentrations, and this maintains vegetation at a low standing, hence reducing competition for light among plants. This further influences the coexistence of different plant forms. Asner *et al.*, (2008) establish the impact of elephants in Kruger National Park and found huge differences in tree heights and herbaceous biomass densities between areas where herbivory was excluded and areas open to herbivore communities.

Wildlife distribution pattern is determined by the system variability in terms of the availability, quality, quantity and the structure of the plant communities that characterise an ecosystem. Grazers, browsers, and mixed feeders have different nutritional needs and hence different feeding behaviour. This creates feedback cycles within an ecosystem (Gosling, 2014). Many herbivores opt for annual over perennial vegetation. Short and stoloniferous herbaceous plants are also vulnerable (suitable for herbivores) compared to tall plants or plants with tussock design (Wigley *et al.*, 2014). Native ungulate browsers are associated with shrub dynamics in east African savannas (Wigley *et al.*, 2014). Increase in the number of large mega fauna is also responsible for the high rates of tree falls at ecosystem scales (Asner *et al.*, 2016; Odipo *et al.*, 2016). Selective feeding creates heterogeneity by modifying the balance between cover classes

in an ecosystem (Hoffmann *et al.*, 2012). Increased pressures beyond the site's carrying capacity could explain disparities within savannas ecosystems (Sankaran *et al.*, 2008).

Other factors affecting wildlife distribution and population levels include predation. Herbivores are risk-sensitive and therefore avoid the zones they perceive to be dangerous such as the dense vegetation patches. They mostly occupy and forage in higher visibility surroundings like the hill crests or short grass patches (Gosling, 2014) where they can easily detect the threat. Predation also increases the survival opportunity of plant varieties and creates bare patches at an ecosystem scale (Carlsson, 2005).

Through foraging, herbivores influence the occurrence probability and frequency of fires at various spatial scales (Winnie *et al.*, 2008) by either reducing or increasing grass dominance and resource competition in an ecosystem (Gosling, 2014). Herbivory influences plant-to-plant interaction which plays an essential role in sustaining species functional diversity and richness. In his study to assess the interaction between herbivory and fire occurrences, Carlsson (2005) pointed out that browsers and grazers influence fires differently by potentially shifting competition among species (Figure 1-5, van Langevelde *et al.*, 2003). He found that grazers exacerbates woody biomass production and growth while browsing decreases it. This is because grazing reduces herbaceous heterogeneity and the probabilities of fire occurrences thus enhancing the survival of woody growth forms. This coincides with other models which add that removal of grass declines intra-life form competition and enhances availability of moisture suitable for woody plants (Scholes & Archer 1997).

Browsing modifies the existence of shrubs and woody vegetation because most of their species are more nutritious and palatable than grass species. This provides a niche for grasses, which attracts fires that eventually damage trees (Carlsson 2005). Through urine and dung deposition, wildlife also influences the rates of nutrient cycling and hence helps in regulating nutrient status in tissues (Sankaran & Anderson, 2009). Like fires, wildlife also promotes the establishment of woody vegetation through seed dispersal and long-term grazing pressures. Herbivory and fires are interdependent; herbivores alone have less effect on vegetation in the absence of fire, but a combination of these two creates higher species diversity in an ecosystem (Carlsson, 2005).



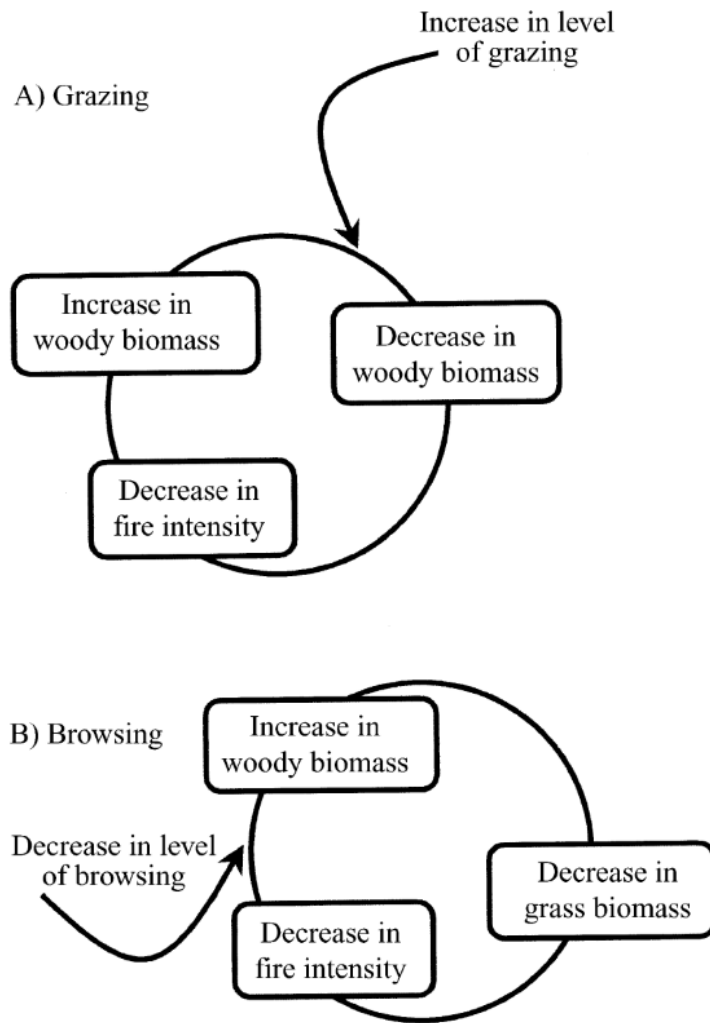


Figure 1-5. Effects of grazing and browsing on grass biomass (fuel load). Low grass biomass leads to low fuel load, meaning less fire intensity with low damage to trees resulting in woody vegetation increase. (Source: van Langevelde *et al.*, 2003).

Much as herbivory leads to ecosystem destruction, their exclusion can also cause ecosystem stress. Reduced wildlife activity in savannas is also associated with coppice encroachments and woody dominance (Sankaran & Anderson, 2009), as in the vast tracts of unused ranches which were once economically viable in South Africa. However, bush encroachment has also been attributed to large-scale environmental factors such as climate change which causes a gradual and continuous drift as opposed to regime shifts resulting from other triggers. Herbivore exclusion induces growth of poor grazing lawns characterised by grass heights that are of low quality and inefficient for both small and large-bodied wildlife. Herbivory can be used to explain the biomass states that have transformed from high to low grass dominances in Ngorongoro crater in Tanzania (Sankaran & Anderson, 2009).

Herbivory is one of the key drivers of vegetation dynamics in most savanna ecosystems. Even though they disturb their habitats, forest fires mostly work in favour of wildlife since, given suitable rainfall conditions, lead to sprouting of young and succulent vegetation.

#### *Pests and Insects: Termites*

Apart from the mammalian herbivores, invertebrate herbivores such as termites, ants, grasshoppers, and tsetse flies play a key role in establishing habitat diversity within an ecosystem (Sileshi *et al.*, 2010). Pests and insects are mainly seasonal and may be a great competitor to the mega mammalian herbivore especially during the dry seasons when the ecosystem is experiencing low rates of vegetation production (Gosling, 2014). Termites are highly abundant (diverse genera) and mobile social insects living mostly in colonies (Gosling, 2014), and can modify the geological makeup of an ecosystem through their activities such as tunnelling, mound formation, nesting and foraging (Sileshi *et al.*, 2010). Their interaction with plant life starts at a very tender age of the plant and they also consume on dry woody trees. Termites are active across all savanna ranges - the wet, semi-arid and in the arid ecosystems (Davies *et al.*, 2016). Their interactions with the soil induce spatial dynamism in terms of water and plant diversity within the ecosystem (Sileshi *et al.*, 2010).

Unlike other microbial organisms, termites are greater decomposers because they work at a range of environmental gradients and non-selectively feed on both live and dead wood and other litter. This speeds up humus accumulation in the soil, leading to rapid nutrient cycling, especially through nitrogen fixation and other mineral elements such as calcium, potassium, magnesium and sodium. Some termite species that consume dung and soil deposits also help in nutrient recycling. Decomposition of the dead termite remains also adds nutritional value to the soils. Africa's tropical ecosystems are the most prone to termite colonies. In Kenyan savannas, 90 percent of annual dead and fallen wood biomass is consumed by termites (Sileshi *et al.*, 2010). Such cases are also prominent in West Africa, where it is estimated at 60 percent. In Namibia and Serengeti National Park, termites were established to be responsible for the varied vegetation types. The mineralisation and decomposition processes help in subsidising the soil's organic matter and improving soil moisture retention capacity, hence improving its fertility (Gosling, 2014).

Through direct foraging and nesting, some termite species can lead to denudation of massive quantities of grass, seedling and more vulnerable plant materials hence creating bare patches within an ecosystem (Sileshi *et al.*, 2010). This could lead to the discriminate invasion of only alien species that can resist termite attack. Loss of biodiversity gradually modifies the coexistence of animal and plant forms. Vegetation suppression and mound formation are also known to play a role in the reduction of fire regimes and fire intensity in savannas. Mounds influence the vegetation structural type that grows around them (Gosling, 2014). Davies *et al.*, (2016), in his review of the impact of termites in KNP, observed resemblances between vegetation formed near termite mounds with lowland vegetation. Tree assemblages differed from those found in the surrounding more than approximately 10 metres away from the mounds. The same study also revealed a reduction in tree densities within a 10 metre distance range from the mounds. Tree species resistant to termite attacks however, increased in densities around mound centres. More tree destruction occurred in wetter parts of the park while drier parts of the park suffered landscape deformation due to higher mound densities.

Termites also create bands that form long and high ridges (up to 2 metres above the ground) that act as grounds for coexistence of contrasting vegetation species. The vegetated bands serve as natural bench structures that reduce soil erosion within an ecosystem. The plants on the bands are normally very nutritious and therefore form foraging sites for many herbivores. Alternating ridges lead to creation of troughs which form drainage channels during rainy seasons. The entire process creates heterogeneity and dynamism in an ecosystem. This scenario is commonly found in South Africa.

Through tunnelling, termites deposit rich red clay subsoil to the surface of the earth. The clay content in the soil alters the soil texture and other physical properties of the substrate, such as porosity, hence improving water percolation (Sileshi *et al.*, 2010). Erosion of the Above-ground nests also speeds up the mobilisation of huge densities of thick fine clay sediments over the surface. Clayey soils favour growth of grass. The downslope transportation of water also leads to deposition of mineral elements at the foot slope, hence supporting vegetation growth. Sometimes, this movement can lead to seasonal waterlogging hence creating an environment that can sustain only plants that are adapted for such conditions. On the other hand, fine clay particles tend to tightly bind during dry seasons (Colgan *et al.*, 2012). This renders them impervious, hence reducing water infiltration to soil depths during light downpour (Sankaran *et al.*, 2008). Porous soils however, allow downslope flow and vertical penetration of water

during rainy seasons, which forms good reservoirs of moisture across different soil profiles especially suitable for deep-rooted savanna vegetation during drought seasons.

### *Climate*

Climate is a primary determinant of savanna ecosystems (van Wilgen, 2009) and a key predictor of savanna heterogeneity and ecosystem productivity (Carlsson, 2005; Gosling, 2014). Other forces like fire, which also help in the structuring of savanna woody cover, vary across various precipitation gradients (Sankaran *et al.*, 2008). Climate change has a direct influence on global savanna distribution and dynamics (Scholtz *et al.*, 2014). Savannas are classified based on different climatic zones characterised by inter-annual variations in total rainfall; the arid (0 - 450 mm), semi-arid (450 - 700 mm) and the mesic savannas (700+ mm) - (Brown, 2002). Mean annual precipitation beyond 800 mm may lead to the formation of canopy covers enough to suppress grass coexistence.

Mean annual precipitation (MAP) is a driving factor for potential tree cover (structure) and canopy photosynthetic capacity (Figure 1-6; Sankaran *et al.*, 2005; Merbold *et al.*, 2009; Higgins *et al.*, 2010). There is a clear gradient in the woody plant biomass in KNP from south to north direction, attributed to changes in precipitation amounts. Above the minimum level of 200 mm MAP, the woody basal area increases at a rate of about 2.5 m<sup>2</sup>ha<sup>-1</sup> per 100 mm MAP. Mean maximum tree height also increases along the gradient, reaching 20 m at about 800 mm MAP (Scholes *et al.*, 2002). In the same view, different vegetation is supported at different MAP, with members of *Acacia* dominating the tree layer up to 400 mm MAP. Between 400 and 600 mm MAP, the *Acacia* are replaced by *Cambretum* or *Terminalia* (or *Colophospermum mopane*), and above 600 mm MAP, the representatives of *Caesalpinaceae* dominate. The vegetation between 600 to 1000 mm MAP is deciduous.

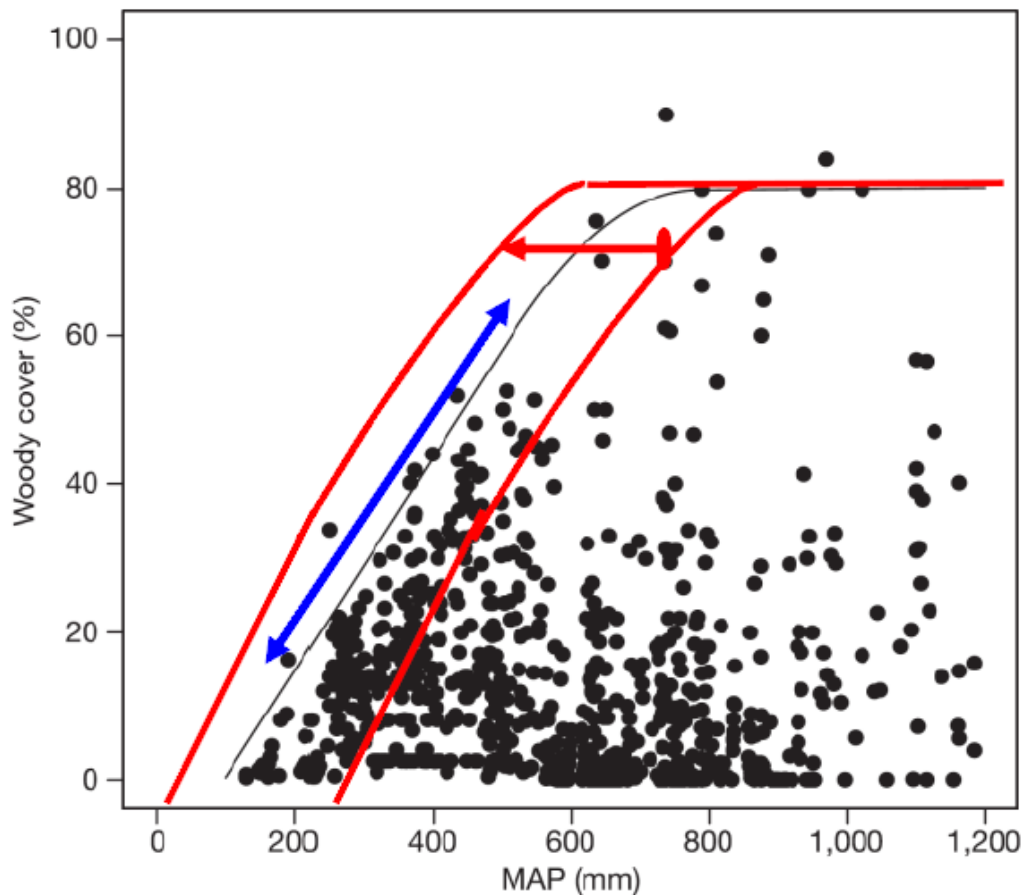


Figure 1-6. Current defined limits of maximum tree cover (Sankaran *et al.* 2005) shown by the blue line across a rainfall gradient. Maximum tree cover in low-rainfall savannahs (MAP < 650 mm) is constrained by water availability. The red arrow: CO<sub>2</sub> fertilization is expected to lead to an increase in tree cover.

While the internal drivers such as fire and herbivory modify the state of biomes (Winnie *et al.*, 2008), spatial-temporal variability of mean annual rainfall plays a pivotal role in modulating the population structure, distribution and functioning of those savanna biomes. Regardless of the nutrient content levels within the soils, savanna vegetation in regions experiencing reliable annual precipitation thrive very well compared to regions characterised by higher nutrient concentrations with erratic rainfall patterns (Colgan *et al.*, 2012). This could be used to explain the higher wood biomass on KNP's granitic sandy soils than in areas covered by basaltic substrates. However, low woody coverage could also be attributed to frequent fires eminent in areas covered with basaltic soils (Asner *et al.*, 2008) supporting heavy grass fuel loads (Colgan *et al.*, 2012; Scholes & Walker, 1993).

Savanna growth forms are continuously competing for scanty resources from germination stage all the way until stress-tolerant colonies escape to maturity classes (Sankaran *et al.*, 2004). Trees and shrubs have different inter-seasonal variations (Carlsson, 2005) and they are defined by

intra-annual and intra-seasonal rainfall fluctuations. Even at a very tender age, grasses and shrubs portray spatial root niche partitioning. In extreme arid environments experiencing sharp precipitation gradients, grasses compete for water more efficiently than deep-rooted trees. This is because their rooting system allows them to draw the limited water from the upper layers of the soil profile (Sankaran *et al.*, 2004). However, if there is variation in water distribution across the soil profile, coexistence is possible even if the rooting systems overlap or where plants have relatively different water use efficiencies. This hypothesis can be used to explain cover classes' coexistence in tropical savannas. Deep-rooted trees can, however, meet their water demands below grass rooting profiles during dry seasons. At this stage, grasses dry up quickly because the top soils are dried up by excessive evapotranspiration. Competitive displacement occurs at the established stage, since different plants show different response patterns to soil water availability (Carlsson, 2005). Savanna woody vegetation shows dependence on precipitation up to certain thresholds, normally between 200 mm and 700 mm. There is normally little or no dependence beyond this threshold (Sankaran *et al.*, 2008).

Different plant forms are also simulated to thrive under wider temperature ranges; C3 grasses can flourish in areas with minimum temperatures less than 15° C whereas C4 grasses can only flourish at minimum temperatures that exceed 20° C (Woodward *et al.*, 2004). Unlike tropical savannas characterised by long dry spells, regions receiving a mean annual rainfall greater than 650 mm (unstable savannas) are likely to be dominated by closed canopy woody cover (Sankaran *et al.*, 2005), unless constrained to reach these heights by other internal drivers (van Wilgen, 2009). The coexistence of grass in this case would highly depend on woody disturbances such as fire (Furley, 2007). Woody dominance leads to a rapid build-up of heavy fuel loads enough for massive fires that cause detrimental damages when they occur during drought seasons (Sodhi & Ehrlich, 2010).

Rainfall also influences the fire return intervals. In KNP for example, fire recurrence in areas that received higher MAP is minimal (3.5 years interval period) compared to areas that receive low mean annual rainfall (about 5.2 years interval period) - (van Wilgen *et al.*, 2000).

## *Geology*

The heterogeneous nature of savannas makes them resilient to geological properties. Soil texture (moisture and nutrient retention capabilities) and fertility are important components of savanna dynamism (Sankaran & Anderson, 2009). The geological substrate and its relationship to vegetation can help explain variations in tree-grass codominance because vegetation responds differently to soil mineralisation. Grasses, for instance, respond positively to high Nitrogen depositions in the soil, while the same has little effect on woody cover (Sankaran *et al.*, 2008). Therefore, Nitrogen enrichment in soils may alter the tree-grass balance by shifting the ecosystem towards a grassy vegetative state. Again, this can explain the differences in vegetation dominance between the less fertile granitic soils (sandy) with lower nutrient turnover, and the fertile basalt soils (clay) with high nitrogen levels in KNP. This is also consistent with the findings of Sankaran *et al.*, (2008) on a swift decline of woody cover with increasing soil Nitrogen mineralisation in Miombo of Zimbabwe.

The through-flows and overland-flows determine water availability in the soils and this varies between geologic substrate types. Hydrologically, sandy soils can sustain vegetation under prolonged dry conditions and lower rainfall range than fine-particle clayey soil (Colgan *et al.*, 2012). This is because sandy soils are more permeable and allow maximum infiltration. The topographic position and geologic substrate make up some factors that determine the scale of herbivore impact on biodiversity (Asner *et al.*, 2008). Vegetation flourishes under soils rich in nutrients, therefore attracting herbivory. Lowlands form better grazing grounds because of overhead flows that enhance nutrient and moisture availability, forming better conditions for forage growth. This is useful in understanding varied height distributions and rapid introduction of bare patches across various ecological zones (Asner *et al.*, 2008).

## *Land-use changes due to human activities*

The nature and dynamism of savannas has been defined by prehistoric, historic and recent human activities. Savannas are of great importance to human economies and have formed the primary sources of rural livelihood in most parts of the world (Sankaran *et al.*, 2004). Expanding human population rates has created an equal demand and extensive use of land to keep pace with the emerging pressures. Among the land use practices include agriculture, logging, and human settlements (Gosling, 2014). Human practices manipulate the natural state of an

ecosystem (Sankaran *et al.*, 2004), and can shift its ecological and socio-economic functioning over time (Cai *et al.*, 2012).

Savanna ecosystems are mainly defined by woody cover dominance. However, wood is the major source of energy among the world's rural and semirural populations, even in relatively developed nations which have alternative sources of energy (von Maltitz & Scholes, 1995). In South Africa, about 93 percent of the rural population relies on fresh wood harvesting for firewood and charcoal production in the Lowveld savanna (Mograbi *et al.*, 2015), and this has been outlined as one of the major causes of forest degradation and fragmentation (Duadze, 2004) and species depletion (Naidoo *et al.*, 2015).

Wood harvesting reduces biodiversity complexities and modifies the vertical stratification of vegetation, which reduces biomass productivity leading to structural heterogeneity (Mograbi *et al.*, 2015). Logging also reduces canopy cover; trees become easily desiccated, and this allows for undergrowth which exposes an ecosystem to fire susceptibility (Sodhi & Ehrlich, 2010). Continuous tree harvesting can change the species composition to multi-stemmed thickets (Campbell, 2013). Vegetation exploitation also exposes land to some natural phenomena like soil erosion and the potential of flooding. All these ecological processes, such as hydrology, nutrient cycling and primary production, have adverse effects on the habitat (Duadze, 2004; Scholes & Walker, 1993).

Tree harvesting turns a vegetative ecosystem to bare patches, hence speeding up runoff and lessening capillary movement. Erosion loses soil's nutrients and modifies the vegetation cover. Logging also reduces plant biomass, leading to desertification. All these processes have global climatic implications; they modify the temperature and precipitation, which are core drivers of a savanna ecosystem (Sankaran & Anderson, 2009).

Biomass burning has been a common phenomenon, especially in sub – Saharan Africa (Walker, 1985). Man has intentionally ignited fires to pave way for extensive crop production on one hand, and to allow for regrowth of fresh and succulent grass suitable for their livestock (Govender, 2003). Constant fire disturbances modify the structural composition of an ecosystem (Sodhi & Ehrlich, 2010). Grazing pressures can also surpass threshold levels required to support vegetation regrowth under constrained resources, especially in the rangeland (Sankaran *et al.*, 2008; Sankaran & Anderson, 2009). Extensive farming can form a gradual



transitional process in an ecosystem through suppression of woody dominance and allowing grounds for emergence of bushes and more open grasslands (Sankaran & Anderson, 2009).

#### *Conclusion:*

The drivers of savanna ecosystem cannot be perceived in isolation (Sankaran *et al.*, 2004). In changing regimes, the changes should be viewed as a response to stress and disturbance resulting from interactive effects of multiple competitive and demographic processes embedded across environmental gradients (Woodward *et al.*, 2004). For instance, invoking climate as the dominant determinant would have tropical environments supporting ecosystem productivity much more than temperate environments (Carlsson, 2005), because woody vegetation shows subtle changes to inter-annual variations in total rainfall. Regime shifts resulting from climatic changes can only be observed after long-term rainfall regimes. Assessing the manipulative effects of change variables needs a clear understanding of ecological niche of the various organisms under study (Fidelis, 2008), and a comprehensive model that can incorporate all parameters that regulate recruitment of various growth forms within a savanna landscape.

### **1.3. Remote sensing in Savanna vegetation structure mapping**

#### ***1.3.1. Basis for savanna vegetation structure mapping***

Vegetation structure components such as above- and below-ground biomass, woody cover, tree height, and basal volume, among others help with carbon stock estimation. According to the International Panel on Climate Change (IPCC), aboveground biomass (AGB) makes up “all living biomass above the soil including the stem, stump, branches, bark, seeds and foliage” (IPCC, 2003; Chave *et al.*, 2005). Valuation of these structural variables assists with the assessment of an ecosystem’s capacity in terms of carbon storage, fuelwood consumption relied upon by some 80% of sub-Saharan Africa, besides other ecological roles. Anthropogenic induced deforestation and natural forest degradation has led to the release of some 1-2 billion tons of carbon into the atmosphere, accounting for approximately 15-20% of the global greenhouse gas (GHG) emissions (Gibbs *et al.*, 2007).

By quantifying AGB through forest inventories, it is possible to understand the changes in the carbon pool and productivity of tropical forests (Roy & Ravan, 1996; Esser, 1984). Reliable

AGB reporting depends on accurate field inventory, with regular updates, which is usually unavailable in most developing countries. Reliable allometric equations for AGB estimation in this region are few or poorly documented. This is partly attributed to the tedious work involved in harvesting and weighing tree species within an ecosystem, with large financial and time costs (Chave *et al.*, 2004; Nickless *et al.*, 2011). Hence, most allometric equations do not take into consideration the differences in tree species associated with variations in ecological regions. Allometric models are developed based on relationships between biomass and tree characteristics such as height and basal diameter (Clark *et al.*, 2001). Such relationships are therefore prone to errors associated with models used in their development (Chave *et al.*, 2004; 2005). Forest impenetrability, time and financial constraints, have led to localised field inventories with few tree species (Jenkins *et al.*, 2003), which are not representative over large areas (Roy & Ravan, 1996; Brown, 2002). Remotely sensed data are more suitable for biomass assessments over wider spatial coverages. However, the associated errors, mainly emanating from sampling procedures and errors associated with the allometric models, need to be taken into consideration. Until 2005, most allometries considered only the relationship between biomass, plant diameter and wood specific density (Chave *et al.*, 2004; 2005; Nickless *et al.*, 2011), leaving out the height variable. Examples of such allometries are presented in Nickless *et al.*, (2011) where a linear relationship between AGB and log-transformed trees with D above 33 cm in KNP was derived, with 16% and 12% errors for woody and leaf biomass, respectively.

Many studies have developed empirical models to assess vegetation spectral response to biomass, with results showing significant relationships between the two. Studies by Roy & Ravan (1996) attributed these relationships to seasonal variations in phenological conditions, seen in visible and infrared bands of optical remote sensing datasets. Airborne laser scanners (ALS), Lidar – (Saatchi *et al.*, 2011; Baccini *et al.*, 2008) and TLS can solve not only the problems associated with cloud contamination in imagery but also provide the best alternative reference data for forest inventory. Combining spectral reflectance with 3-dimensional (3-D) capability facilitates canopy height estimations such as shown in the works of Lefsky *et al.*, (2005), where Geosciences Laser Altimeter (GLAS) Lidar onboard Ice, Cloud and land Elevation Satellite (ICESat) was combined with Shuttle Radar Topographic Mission (SRTM) to estimate forest heights in Brazil. Similar studies by Nickless *et al.*, (2011) and Colgan *et al.*, (2012) found a linear relationship between Lidar derived canopy cover and height metrics with AGB. Error identification and correction in AGB estimation is a major problem, and averaging canopy metrics at plot scale is a major source of error in Lidar to field data correlation (Colgan *et al.*, 2013). The potential of TLS in vegetation structural mapping are covered in the works

by Korpella (2004); Abraham & Adolt (2006); Browning *et al.*, (2009); Raunonen *et al.*, (2015) and Odipo *et al.*, (2016). Despite being a relatively new field, TLS allows a rapid acquisition of 3-D data with various applications (Tilly, 2015; Stanley, 2013; Resop & Hession, 2010; Kandrot, 2008). Unlike Lidar which cover large areas, TLS data capture is restricted to few meters, and non-destructive method of obtaining biomass estimates (Calders *et al.*, 2015; Hackenberg *et al.*, 2015). Given its ability to acquire data on the ground, TLS data can be used for validation of other remote sensing datasets (Abraham & Adolt, 2006; Browning *et al.*, 2009; Raunonen *et al.*, 2015). However, large number of point clouds (PCs) are generated which require sophisticated hardware and software for processing the data (Li *et al.*, 2016; Liu *et al.*, 2016; Warmink, 2012). New methodological workflows like those adopted by Raunonen *et al.*, (2015) can extract individual trees from TLS point clouds by splitting trees into individual cylinders.

## 1.4. Study motivation

Savanna biomes cover 20% of the earth's land surface (Campbell, 2013), mainly in tropical and subtropical regions, which typically experience contrasting wet and dry seasons. In sub-Saharan Africa (SSA), 65% of land surface displays characteristic heterogeneity in terms of both vertical and spatial vegetation composition (Figure 1.7, Hansen, 2000; Shirima *et al.*, 2011). The savanna biomes are only second to tropical forests in terms of Net Primary Productivity (Hansen, 2000), very important as carbon pools, with the African sub-continent acting as a sink to 25% of the global C-stock. Savannas are a source of livelihood to some 80% of rural population in SSA who rely on the biome as a source of timber for fuelwood and construction, hunting and gathering for food and fibre, pasture for animals, clearing for settlement and agriculture. Ecologically, savannas are important habitat for vast species of flora and fauna (Mishra *et al.*, 2015). Apart for Carbon, the biome is important in Nitrogen cycling through frequent forest fires.

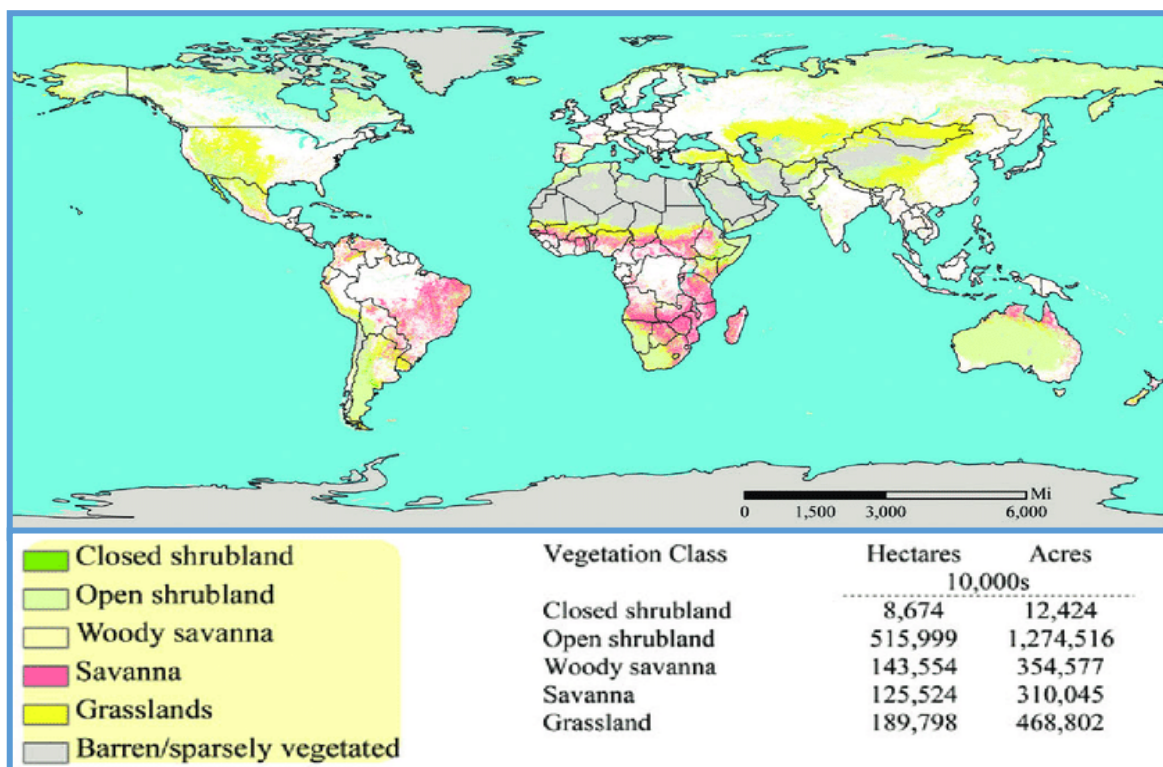


Figure 1-7. Global distribution of grass, shrub and savanna vegetation (Hansen, 2000).

Despite such importance, savanna biome can be described as a disturbance-driven, emanating directly from deriving livelihood in terms of extraction of woody products and changes in land use, and indirectly from high GHG emissions in the form of rising atmospheric carbon dioxide

(CO<sub>2</sub>). These disturbance scenarios lead to shifts in resource availability resulting in heterogeneity both in space and time (Sankrana *et al.*, 2005; Oliveras & Malhi, 2016). In KNP within which this study is conducted, mean annual precipitation (MAP) and nutrient availability are the main heterogeneity determinants, while herbivory and fire episodes are heterogeneity modifiers (Sankaran *et al.*, 2005; Levick *et al.*, 2006). Figure 1-8 below evidences the effects of fire episodes, herbivory in the form of browsers and tree fall by mega-herbivores like elephants within Skukuza study site. Low MAP leads to low woody cover dominance which allows light penetration to the understory which promotes dominance of herbaceous vegetation. The result is a high fuel load which leads to frequent fire episodes and increased herbivory. On the contrary, high MAP promotes closed canopy growth which shields sunlight penetration to the understory leading to suppression of herbaceous layer. With low herbaceous layer, there is a corresponding decrease in fuel load, fire is suppressed, and herbivory minimised.

Most of the disturbance scenarios compromises the biome's ability to provide its roles optimally, leading to forest degradation and deforestation, which results in increased atmospheric carbon emission (Simula & Mansur, 2011). Forest degradation and deforestation ranks second to fossil fuel burning in terms of atmospheric C-emission (Pistorious, 2012). To conserve the forest biomes, developing countries under United Nations Framework Convention on Climate Change (UNFCCC) enacted an incentive-based initiative aimed at adoption of sustainable forest management strategies aimed at enhancing C-stock through Reduced Emission from Deforestation and forest Degradation (REDD). Under REDD, signatories are required to detect, map and verify changes in C-stock resulting from the various disturbance scenarios, and the extent to which the adopted conservation initiatives are reducing atmospheric greenhouse gas (GHG) emissions. Changes in C-stock can be estimated through mapping changes in CC and quantification of gains and losses in AGB.



Figure 1-8. Evidence of disturbance in Skukuza, Kruger National Park (KNP) by (a) fire, (b) browsers, (c) tree fall by elephants (Photos courtesy Victor Odipo, Nov. 2016)

Using remote sensing in mapping vegetation structure changes provide the basis for detection and verification of forest degradation and deforestation. Many studies have shown a relationship between remote sensing data, both optical and microwave, and vegetation structure especially CC and AGB (Colgan *et al.*, 2013, Treuhaft *et al.*, 2009; Mitchard *et al.*, 2009; Carreiras *et al.*, 2012; Wijawa *et al.*, 2011). Most vegetation products from these studies are coarse resolution and limited in monitoring tree-level forest degradation initiatives. Despite free access and non-commercialisation of many remote sensing datasets by providers, the use of optical remote sensing data for vegetation mapping is met with a lot of challenges, especially

in the tropics. There is an inconsistency in optical data availability resulting from cloud and atmospheric aerosol contamination. The International Satellite Cloud Climatology Project (ISCCP) in Figure 1-9 estimates that at least 40% of the tropics is covered in cloud at any one given time (Wylie, 2005). This limit operationalisation of vegetation monitoring initiatives which requires consistency in time series data availability. In heterogeneous biomes like savannas, the tree-grass coexistence gives a near-similar spectral reflectance between the various life forms within and between seasons (Hansen, 2000).

Remote sensing in savanna vegetation mapping requires a reliable reference data which can be used in modelling and validation of remote sensing vegetation structure products. Conventionally used field inventory data is costly in terms of both time and labour. Such field inventories are non-representative due to their localised geographic coverage apart from differences in sampling procedures which making integration for large scale structural modelling a problem. Field inventories are error prone either resulting from instrument fault or unintentional inventor introduced biases. Most studies undertaken in KNP to map vegetation structure variables and especially around Skukuza have used Carnegie Airborne Observatory (CAO) Lidar data (Smit *et al.*, 2010; Myburgh *et al.*, 2011; Cho *et al.*, 2012; Colgan *et al.*, 2012, Colgan *et al.*, 2013; Naidoo *et al.*, 2015; Mograbi *et al.*, 2015; Urbazaev *et al.*, 2015). The costs involved in acquiring airborne Lidar data is expensive, and the acquired data has no free-access policy making its use for research a problem.



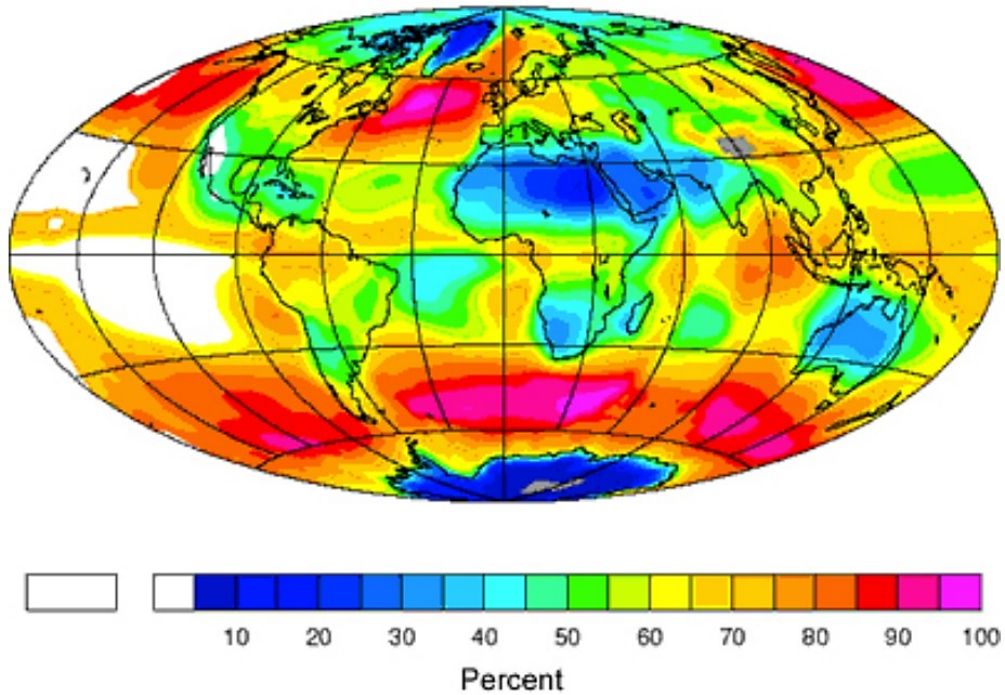


Figure 1-9. Global cloud cover frequency between 1994-2001 (International Satellite Cloud Climatology Project-ISCCP; Wylie, 2015).

The current study, based on the aforementioned problems encountered in mapping savanna vegetation structure, aims to provide a solution thus;

- Use microwave remote sensing data, especially L- and C-band SAR data with the ability to acquire data in all-weather day-and-night at regular intervals thereby eliminating the problems of inconsistency in data availability experienced with optical data due to cloud and atmospheric aerosol contamination. C-band data is freely availed by ESA under Copernicus program, making it easy for developing countries who are interested in a regular update on the status of carbon stock;
- Use high resolution TLS data as reference data in validation of remote sensing (SAR) modelled savanna vegetation products, especially canopy cover, aboveground biomass and savanna vegetation cover classes.



## **1.5. Research objectives and questions**

The general objective of this thesis is to add into our understanding of the spatial distribution of vegetation structure components and their dynamics within a protected Lowveld savanna biome using innovative remote sensing data sources which solves the problems encountered in using optical data in monitoring this ecosystem. To address research gaps especially touching on reliable reference data and ability to acquire multi-temporal data for continuous monitoring of savanna ecosystem, these objectives can be divided into the following research objectives:

- I. To evaluate the potential of high-resolution terrestrial laser scanner (TLS) in extraction of savanna vegetation structure variables;

Technological advancements in remote sensing data acquisition has seen an emergence of free to low cost medium to high spatial and temporal resolution space-borne datasets. However, studies aimed at vegetation monitoring are still limited by low quality to unavailability of reference data. Most such studies rely on sparse and patchy field inventory exercises, which are in most cases costly in terms of time, labour and with limited non-representative spatial coverage. More so, apart from foreseen commission and emission errors during such exercises, field inventories for carbon stock estimations are reliant on destructive sampling for allometric development. TLS data, with its accuracy and ability to capture both 2- and 3-D vegetation information, provides the best alternative to field-based forest inventories especially where continuous monitoring is necessary. To date, few studies have explored the strength of TLS for vegetation structural mapping, with few focusing on savannas. This study aims at assessing the potential of TLS point clouds in tree variables mapping, especially tree height and diameter at breast height (DBH) and how these can be used to compute AGB within a Lowveld savanna in South Africa. Further, TLS canopy height model (CHM) is computed and from which canopy cover, canopy height and savanna vegetation cover classes are derived through CHM height thresholding. These methodologies and the resultant variables can improve vegetation monitoring and forest inventory updates for developing countries where this information would otherwise be costly in the long run.

## II. To estimate landscape-wide AGB and assess AGB changes over four years using multi-temporal L-band SAR within a Lowveld savanna in Kruger National Park

Information on forest biomass is important in assessing a biome's ability in sequestering atmospheric carbon dioxide, stored within the trees as carbon stock. Most developing nations are signatories to United Nations' Reduced emissions from deforestation and forest degradation (REDD), requiring them to carry out regular inventories of their carbon stocks through updating their forest biomass status. It is therefore important that methodologies are developed which can assist with monitoring at regular intervals. This study based on the results from objective I above, evaluates the potential of high-resolution TLS-derived canopy cover and height metrics to estimate plot-level aboveground biomass, to extrapolate to a landscape-wide biomass estimation using multi-temporal L-band SAR within a 9 km<sup>2</sup> area savanna in KNP. For this, 42 field plots were inventoried in the wet season and AGB computed for each plot using site-specific allometry. Canopy cover, canopy height and their product will be regressed with plot-level AGB over the TLS-footprint, while SAR backscatter used to model dry season biomass for the four years under investigation; 2007, 2008, 2009 and 2010 for the study area.

## III. To assess interactions between C-band synthetic aperture radar with various savanna vegetation structure variables

Savanna vegetation structure parameters are important for assessment of the biome's ability to provide ecosystem services under various disturbance scenarios. Studies aimed at tree-level structure mapping provides the best way to monitor intrinsic changes when performed at local scales to enable forest degradation monitoring. ESA's contribution to Copernicus has seen free availability of high-resolution C-band Sentinel-1 A at high temporal resolution which when used without pixel degradation, has the potential of capturing tree-level dynamics within mixed vegetation biomes typical of savannas. This study aims at assessing the response of hyper-temporal C-band SAR with changes in savanna vegetation structural parameters over two seasons. TLS data will be used to extract individual tree height and basal diameter for tree biomass estimation, and further TLS CHM generation for computing of vegetation CC. The effects of SAR polarisation, speckle filter and seasonality on detectability of savanna structure parameters are investigated. This study will further attempt to investigate the potential of medium wave SAR datasets in monitoring tree level changes with original resolution. It is envisaged that this methodology will form a basis for deforestation and forest degradation monitoring, with a promise of operational monitoring at high resolution.

The methodological concept aimed at achieving the objectives of this thesis as outlined above, is visualised in Figure 1-9. These formulated objectives aim at answering the central research questions of this dissertation, including;

- 1) Does high resolution TLS provide a supplementary accurate data that can be used as a reference for savanna vegetation structure monitoring?
- 2) What is the potential of SAR data, especially ALOS L-band SAR in monitoring changes in savanna vegetation structure?
- 3) Does freely available high resolution and multi-temporal Sentinel 1-A C-band SAR data show promise in mapping both vertical and horizontal structural variables within a Lowveld savanna?

The questions are investigated within the following three chapters. Chapter 5 looks at the implications of the results so obtained from Chapters 2 to 4 in the context of the reviewed literature, the results and discussions thereafter, with an outlook for future improvements on the methodologies adopted in this study given in Chapter 5. Chapter 6 looks at the major results from the foregoing study, to answer the three questions above.

# CHAPTER 2

## 2. Theoretical background and techniques

### 2.1. Basic principles of SAR systems

#### 2.1.1. Electromagnetic radiation

Remote sensing is the art and science of acquisition of information about the earth’s surface without being in physical contact with the features under investigation (Rees, 2011, Woodhouse, 2006). Sensors on-board remote sensing platforms record energy transmitted as electromagnetic radiation with wavelengths ranging between radio waves ( $\lambda > 1 \text{ m}$ ) to gamma rays ( $\lambda < 10^{-12} \text{ m}$ ). The most important sections of the electromagnetic spectrum for remote sensing are the passive sensors (optical) in the visible light range ( $\lambda = 400 - 700 \text{ nm}$ ) and active sensor combining Near Infrared region ( $\lambda = 0.7 - 1.5 \mu\text{m}$ ) and microwave ( $\lambda = 1 \text{ mm} - 1\text{m}$ ) wavelengths (Chuvieco & Heute, 2010; Liew, 2001; Figure 2-1).

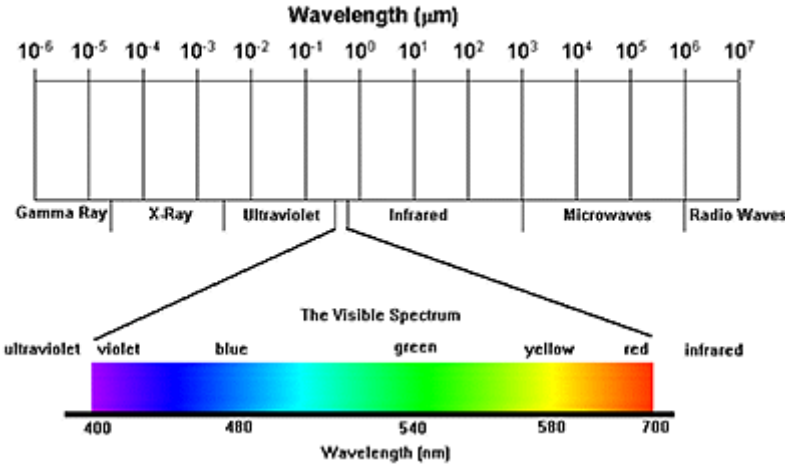


Figure 2-1. Electromagnetic spectrum showing location of the various electromagnetic radiation wavelengths (Source: Liew, 2001)

Unlike passive sensors which rely on solar radiation to image earth’s surface features and hence limited by daytime solar insolation, active sensors emit their own electromagnetic energy to illuminate surface features which enables them to acquire information during both day and night

(Tempfli *et al.*, 2009; Campbell, 2007). Examples of active sensors are ranging systems like Lidar and radio detection and ranging (Radar).

SAR is a microwave imaging radar which acquires information on the earth’s surface by estimating the time delay in the backscattered signal to the sensor. A SAR sensor consists of a transmitter which generates short pulses as the platform moves, a receiver which detects the return signal from the illuminated ground features in the azimuth (parallel to flight direction) and range directions (orthogonal to flight direction), an antenna and an electronic system to process and store the acquired data (Moreira, 2013). Table 2-1 shows the most commonly used SAR frequencies in remote sensing literature with accompanying wavelength ranges for P-, L-, S-, C- and X- bands.

Table 0-1. Commonly used SAR frequency bands with corresponding wavelengths

<b>Frequency band</b>	<b>X</b>	<b>C</b>	<b>S</b>	<b>L</b>	<b>P</b>
<b>Frequency (GHz)</b>	12-7.5	7.5-3.75	3.75-2	2-1	0.5-0.25
<b>Wavelength, <math>\lambda</math> (cm)</b>	2.5-4	4-8	8-15	15-30	60-120

**2.1.2. SAR geometry and resolution**

Figure 2-2 below shows a typical radar slant geometry (CCRS, 2019), with the platform flight direction shown by A and nadir at B. The radar beam is transmitted orthogonally to the direction of flight, illuminating a swath C determined by an incident angle ( $\theta$ ).  $\theta$  is the angle between the horizontal plane and the radar line of sight (Ackermann, 2015). The range D is the cross-track direction perpendicular to the flight direction, also known as the range direction or slant range geometry (Woodhouse, 2006), while azimuth is the along-track direction parallel to the flight direction denoted by E (Moreira *et al.*, 2013, Elachi & van Zyl, 2006).

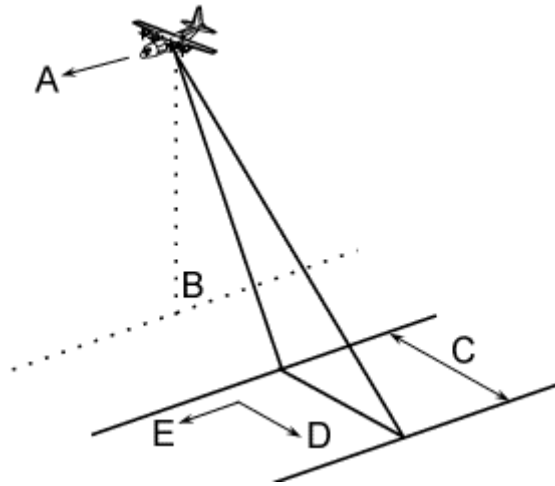


Figure 2-2. Radar geometry showing the flight direction A, Nadir point directly below the radar platform B, the swath of the radar beam C, and both range – and azimuth directions as D and E respectively (Source: CCRS, 2019).

The portion of the swath closer the nadir track is called near range while that furthest to the nadir is called the far range and are determined by the  $\theta$ . The radial line-of-sight distance between the radar platform and the earth surface features is called the slant range distance while the true horizontal distance along the ground corresponding to each point measured in slant range is the ground range distance. The ground resolution of the acquired image depends on the size of the microwave beam emitted by the antenna, with narrow beams giving finer details of the earth's surface features. Consequently, longer antennas result in a narrower beam footprint, meaning that the beam width is inversely proportional to the length of the antenna (Brown & Porcelo, 1969; Tomiyasu, 1978; Mätzler, 2008; Rees, 2006). Since the spacecraft cannot carry longer antennas required to attain a higher resolution, the platform motion is used to simulate larger antenna (synthetic aperture) with a continued view of a single location (Moreira *et al.*, 2013). Synthesised antenna length is used to increase the azimuth resolution, as shown in Figure 2-3. The SAR processor stores signals from the surface object A for the entire time the object is within the beam,  $t$ . The length of the synthesised antenna B can therefore be expressed as 2-1;

$$B = t.v \quad (2-1)$$

where  $v$  is the speed of the platform in the azimuth direction.

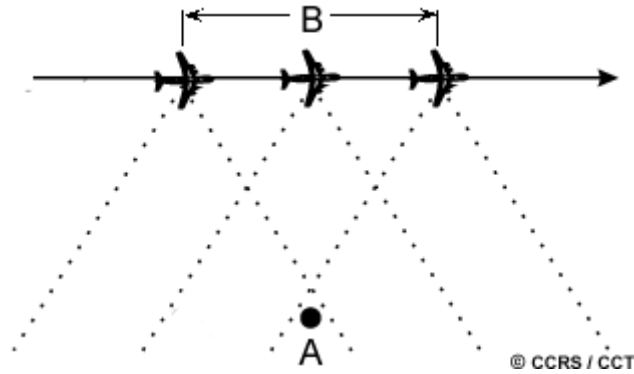


Figure 2-3. Aperture synthesis by radar platform, with the virtual aperture length (B) after complete illumination of ground target (A) (Source: CCRS, 2019)

The ground range resolution describes the ability to discriminate objects that are situated on the ground and is calculated from  $R$  via the local incidence angle  $\theta$ . Based on the radar geometry therefore, Massonnet & Souyris (2008) derived the ground range resolution using relationship in 2-2;

$$R = \frac{c\tau}{2 \sin(\theta)} \quad (2-2)$$

where  $c$  is the speed of light ( $c = 3 \times 10^8 \text{ ms}^{-1}$ ),  $\tau$  is the pulse duration ( $\mu\text{s}$ ) and  $\theta$  is the incidence angle. The factor 2 shows the length of the pulse since it travels from the antenna to the object and back to the antenna. The sine of the incidence angle is used to project the slant-range resolution onto the ground-range resolution (Ackermann, 2015). It is worth noting that the ground range resolution is proportional to the length of the pulses with the possibility of achieving finer range resolution with a shorter pulse rate. The azimuth resolution is approximately one-half length of the actual (real) aperture (antenna) describes the ability of an imaging radar system to separate two closely spaced scatterers in the direction parallel to the motion vector of the sensor (Woodhouse 2005). The azimuth resolution is independent of the platform altitude (distance from target), but rather dependent on (i) a stable, full-coherent transmitter, (ii) an efficient and powerful SAR processor, and (iii) the exact knowledge of the exact flight path and velocity of the platform (Wolff, 2009). SAR azimuth resolution can be calculated using Equation 2-3 by Massonnet & Souyris (2008) thus:

$$A = \frac{L}{2} \quad (2-3)$$

Where  $L$  is the antenna length.

### 2.1.3. SAR signal processing

Received signal from the scatterer by the antenna makes up a two-dimensional data matrix of complex samples with a real and imaginary parts representing amplitude (magnitude) and phase value respectively (Moreira *et al.*, 2013; Ackermann, 2015). The image plane is defined by the radar platform velocity vector and the radar antenna beam axis. The two orthogonal axes of the processed image are range and cross-range (azimuth). The position along the range axis is determined by a time delay in the received pulse, and the position along the cross-range axis is determined by range rate of the target distance or the Doppler frequency of the return signal from the target (Tomiyasu, 1978). Phase is denoted by a two-way distance between the sensor and the target, expressed as in Equation 2-4 (Ackermann, 2015):

$$P = - \left( \frac{4\pi}{\lambda} \right) R + \varphi_{scatterer} + \varphi_{delay} \quad (2-4)$$

Where  $R$  is the slant-range distance,  $\varphi_{scatterer}$  is the scattering effects introduced by the target and  $\varphi_{delay}$  refers to atmospheric or ionospheric effects on the signal. The proportion of energy backscattered by the target to the sensor is expressed as the backscatter coefficient,  $\sigma^0$  for distribute targets (2-5);

$$\sigma^0 = \frac{\sigma}{A_{\sigma}}. \quad (2-5)$$

where  $\sigma$  is the radar cross-section. The  $\sigma^0$  is inversely proportional to the effective area of the antenna,  $A$  and normal expressed in decibel (dB) units with a range between -30 dB to 5 dB.

Figure 2-4 is a graphical representation of SAR data processing flow (ESA, 2019). Scene information from a raw SAR data (Level-0) is meaningless and signal processing is needed to get an image (Moreira *et al.*, 2013). The conversion of Level-0 raw data to Level-1 image include pre-processing, Doppler centroid estimation, a single look complex image focusing and post-processing. To achieve this, two filter operations are performed along the range and azimuth dimensions:

- a) Range compression - the transmitted chirp signals are first compressed to a short pulse using range reference function (amplitude, range). The process involves multiplication in the frequency domain, where each range line is multiplied in the frequency domain by the complex conjugate of the spectrum of the transmitted chirp. The result is a range



compressed image, which reveals only information about the relative distance between the radar and any point on the ground.

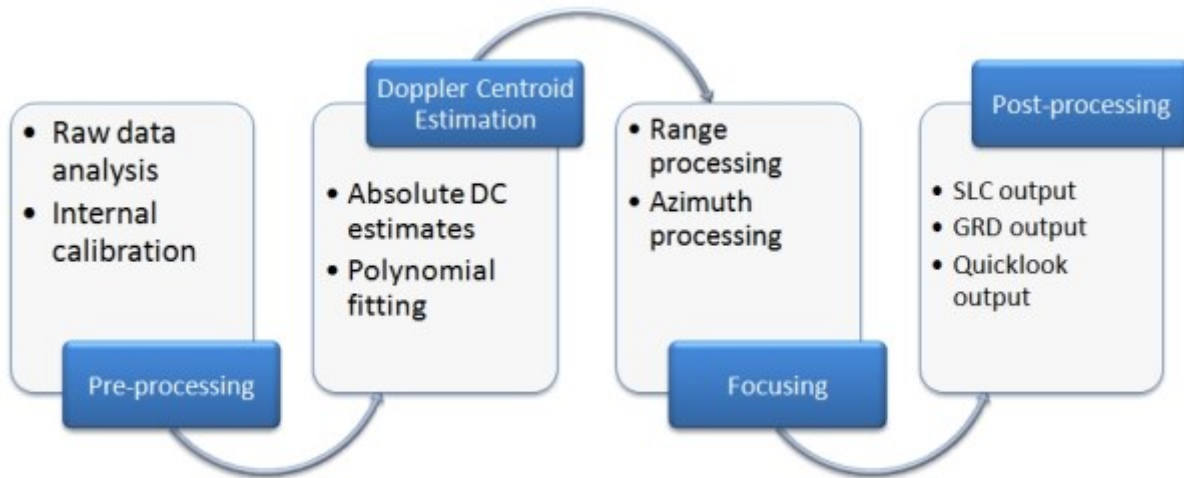


Figure 2-4. SAR data processing workflow: raw data pre-processing, Doppler centroid estimation, SAR focusing and decompression, and post-processing (Credit: ESA, 2019)

- b) Azimuth compression - the signal is convolved where azimuth reference function (azimuth, amplitude) is used to convert the range compressed data into an image data, which is the complex conjugate of the response expected from a point target on the ground.

#### 2.1.4. Speckle in SAR images

The presence of many elemental scatterers with a random distribution within a resolution cell leads to formation of speckle within SAR images (Moreira *et al.*, 2013) and produces a “salt and pepper” effect on a SAR image. Speckle is a signal dependent granular noise inherent in all active coherent imaging systems that visually degrades the appearance of images. The effects of speckle can be seen in a diminished performance of automated scene analysis and information extraction techniques, besides problems in applications requiring multiple SAR observations, like automatic multi-temporal change detection (Argenti *et al.*, 2013). The coherent sum of amplitudes and phases of different scatterers results in strong fluctuations of the backscattering from a resolution cell to another. The intensity and the phase in the final image are no longer deterministic but follow an exponential and uniform distribution, respectively (Oliver & Quegan, 2004). The effects of speckle on an image can be constructive or destructive. Constructive interference results in high-intensity return signals, while destructive interference yields weak return signals (Ackermann, 2015). A signal-to-noise ratio

(SNR) is used to quantify speckle noise within a SAR image using the equation by Kim (2009) thus;

$$\text{SNR} = \frac{S}{N} = \frac{\sigma_0}{\delta_0} \quad (2-6)$$

Where  $\sigma_0$  is the backscatter coefficient (dB) and  $\delta_0$  is the noise equivalent sigma zero, a system's sensitivity to areas of low backscatter and is given by 2-7;

$$\delta_0 = \frac{(4\pi)^3 \cdot R^3 \cdot k \cdot T_0 \cdot NF \cdot W \cdot L_{tot} \cdot 4 \cdot V_s \cdot \sin(\theta - \alpha)}{P_t \cdot G_t \cdot G_r \cdot \lambda^3 \cdot c \cdot \tau \cdot PRF} \quad (2-7)$$

where;

$k$  = Boltzmann constant,  $T_0$  = the equivalent noise temperature,  $NF$  = system noise figure,  $W$  = bandwidth,  $L_{tot}$  = total loss,  $V_s$  = velocity of the SAR platform,  $G_r$  = antenna gain at the receiver, and  $PRF$  = pulse repetitive frequency.

The conceptual framework of an ideal speckle filter is based on its ability to substantially reduce the speckle contamination in SAR imagery while effectively preserving the structural properties of the scene backscatter like the radiometric level and spatial resolution; the values of backscattering coefficient, spatial signal variability, and the edges between different geographic feature boundaries (Gagnon & Jouan, 1997), and its adaptability to the use of local rather than derived speckle and scene statistics in determining speckle noise (Qiu et al., 2004). In most cases however, speckle suppression leads to loss of subtle feature details (Sarker et al., 2013), leading to resolution degradation and indiscriminately smears homogeneous low-variance areas (Gagnon & Jouan, 1997) because it is performed within moving windows. For this case, Walker, 2000 and Sarker *et al.*, 2013 suggests performing texture measurements before applying the filtering model during forest biomass estimation.

The level of speckle noise regarding the signal intensity and noise reduction is estimated by determining similarities between independent intensity values used in pixels (Gagnon & Jouan, 1997), and the number of radar image azimuth spectral bandwidth (signal-to-noise) segment of the same point of scene (multiple-look processing). When the equivalent number of looks (ENL) across the pixels is higher, it implies a stronger speckle reduction and further shows that an appropriate filter model should be used (Amini & Sumantyo, 2009). Other statistical filtering criteria that can be employed to evaluate a filter performance include Speckle Suppression Index (ratio of the variance between the speckled and the original image), Speckle Image

Statistical Analysis (Qiu *et al.*, 2004), Edge-Enhancing Index (EEI), Feature-Preserving Index (especially linear features and other subtle structures) and Speckle Suppression and Mean Preservation Index (Wang *et al.*, 2012).

### ***SAR speckle suppression***

Despite the documented advantages of microwave over optical remote sensing data, signal dependent granular noise and the associated visual degradation of image appearance remains a problem limiting its use in scene analysis and information extraction (Qiu *et al.*, 2004). It is therefore important to reduce this noise to permit better scene target discrimination and further automated image segmentation in radar images. Erroneous variations in backscatter from inhomogeneous cells increase SAR image variances (Mansourpour *et al.*, 2006), obscure image clarity, and act as a barrier for texture-based analysis. To reduce speckle, spatial, frequency, and temporal filters can be used (Argenti *et al.*, 2013; Dasari *et al.*, 2015). One common way of reducing noise and improving the estimates of backscatter intensity is to incoherently evaluate the average intensity of a collection of  $L$  pixels through multi-looking (ML) (Ackermann, 2015). During SAR image pre-processing, ML incoherently averages the independent number of looks (ENL), resulting in an  $L$ -look intensity image. The ENL is used in testing the performance of ML and application of a speckle filter on a SAR image, and is statistically expressed by equation 2-8 (Oliver & Quegan, 2004);

$$\text{ENL} = \frac{\text{Mean}^2}{\text{Variance}} \quad (2-8)$$

The level of speckle noise regarding the signal intensity and noise reduction can be estimated by determining similarities between independent intensity values used in the pixels (Gagnon & Jouan, 1997), and the number of radar image azimuth spectral bandwidth (signal-to-noise) segment of the same point of scene (multiple-look processing). When the ENL across the pixels is higher, it implies a stronger speckle reduction and further shows that an appropriate filter model should be used (Jaybhay & Shastri, 2015). Speckle filtering significantly optimises the ability to exploit the texture variance between neighbouring pixels in SAR imagery, and to discern spatial information of the ground scene target and land use types in forested areas, and thus enhance data interpretability and efficient image classification (Amini & Sumantyo, 2009). Speckle filters are applied on moving windows to average the noises from adjacent pixels, and

Kupidura, (2016) notes that there is a steady improvement in the performance and efficiency of a filter with increasing window size, when the same is applied for a homogeneous study area. Conversely, besides much computational performance needed for larger window sizes (for example  $11 \times 11$ ), there is too much smoothing of the textural variation leading to distortion of texture information (Sarker *et al.*, 2013). A very small window, such as  $3 \times 3$  exaggerates variations within the moving windows, hence creating more noise on the SAR texture image (Amini & Sumantyo, 2009).

Spatial filters are principally grouped into adaptive and non-adaptive filters. Over the last decade, several studies have concentrated in developing appropriate speckle filters, each concentrating in addressing a difficulty in SAR image interpretation attributed to speckle (e.g. Bruniquel & Lopes 1997; Ferretti *et al.* 2011, Huang *et al.*, 2009; Lee *et al.*, 1991; Lee *et al.*, 1994; Lopez-Martinez & Pottier, 2007; Novak & Burl, 1990; Sveinsson & Benediktsson, 2003). Quegan & Yu, (2001) developed a change-preserving multi-temporal filter which can filter multi-temporal SAR image stacks with the ability to reduce speckle while preserving changes inherent in a time series. This is necessary for forest degradation and deforestation monitoring initiatives that require observation of backscatter changes within an area over an extended period. Lee Filter (Lee, 1980) is a standard deviation-based ( $\sigma$ ) speckle filter that suppresses noise while preserving image sharpness and detail. By placing each SAR pixel into three surface target types – homogeneous, heterogeneous and point target, Lopez *et al.*, (1990) adopted the Lee filter thereby creating Enhanced Lee Filter. For homogeneous targets, the pixel values are replaced with the average of the filter window, while for heterogeneous targets the pixel values are replaced with a weighted average. To resolve speckle for point targets, the pixel values are not changed. The Frost filter is an exponentially damped circularly symmetric filter that uses local statistics (Frost *et al.*, 1982). The Enhanced Frost filter is an adaptation of the Frost filter which classifies and filters pixels according to the three target types as in Enhanced Lee Filter (Lopez *et al.*, 1990). Another spatial filter, a non-local means filter, provides an estimate of the clean image via a proper averaging of similar pixels or patches, found in the image. Essentially, the algorithm searches for image patches that resemble the area around the pixel to be filtered. Using some similarity criterion, these patches are found and averaged together to de-noise the image without losing resolution (Buades *et al.*, 2005; Chen *et al.*, 2014; Di Martino *et al.*, 2016; Martino *et al.*, 2015).

An ideal speckle filter is characterised by its distinctive ability to reduce the speckle contamination in SAR imagery while effectively preserving the intrinsic structural properties

of the scene backscatter like the radiometric level and spatial resolution; the values of backscattering coefficient, spatial signal variability, and the edges between different geographic feature boundaries (Gagnon & Jouan, 1997), and its adaptability to the use of local rather than derived speckle and scene statistics in determining speckle noise (Qiu *et al.*, 2004). In most cases however, speckle suppression leads to loss of subtle feature details (Sarker *et al.*, 2013), leading to resolution degradation and indiscriminately smears homogeneous low-variance areas (Gagnon & Jouan, 1997) because it is performed within moving windows. For this case, Walker, (2000) and Sarker *et al.*, (2013) suggests performing texture measurements if any, before applying the filtering model during forest biomass estimation.

### ***2.1.5. SAR Polarimetry***

SAR polarisation points to the orientation of the field of electromagnetic energy emitted and received by the antenna (Campbell & Wynne, 2011), in a plane perpendicular to the direction of wave propagation. Most of today's SAR sensors are linearly polarised and transmit horizontally and/or vertically polarised wave forms, denoted by H and V respectively (Flores-Anderson *et al.*, 2019). SAR polarimetric system works in the linear H-V basis, where the antenna transmits a H-polarised wave and receiving H wave measured in  $S_{hh}$  and  $S_{hv}$  elements. For the  $S_{vv}$  and  $S_{vh}$  elements, a V-polarised wave is transmitted by the sensor and receiving in H and V (Moreira *et al.*, 2013). Like polarisation occurs when the antenna receives similar wave orientation as it emits, e.g. HH or VV for transmit H receive H, and transmit V receive V respectively. Cross-polarisation occurs when the antenna receives a different polarisation to the one emitted, e.g. VH or HV. These HH or VV or VH or HV examples above are single polarisations. Radar systems can also possess dual polarisations, where an antenna emits and receives two different combinations, e.g. HH and HV, VV and VH or HH and VV. Such systems produce two images of the same landscape (Campbell & Wynne, 2011). A quadrature (quad-pol) radar uses four polarisations, and measures phase difference between the channels and the magnitudes (CCRS, 2019). These takes the four possible polarisations, HH, VV, HV and VH. In some radar systems, the antenna can transmit and receive waves at more than one polarisation. The polarisation information in backscattered waves gives more information about the target on the earth's surface, and is related to the target's geometric structure, reflectivity, shape and orientation and its geophysical properties such as humidity, roughness, among others. Areas and features on the landscape that depolarise the SAR signal can be identified by comparing two images, i.e. the co- and cross-pol images. Such scatterers change the orientation

of the incident microwave energy since they reflect the incident H signal back to the antenna as a V polarised energy. A visual comparison between the HV and HH shows that bright regions in the former as depolarizing scatterers, and dark or dark grey regions in the latter - the polarisation of the energy that would have contributed to the brightness of the HH image has been changed, so it creates instead a bright area on the HV image (Campbell & Wynne, 2011). Polarimetric radar can be used to measure the scattering properties of surface features. As the radar system illuminates the target at an incident angle, the target scatters the wave in all directions. The system only records part of the waves that are redirected back to the antenna, known as backscatter,  $\sigma^0$ .

#### ***2.1.6. Effects of target dielectric constant on SAR backscatter***

Dielectric constant is a measure of the electric properties of surface features and comprise two parts – permittivity and conductivity. Material permittivity and conductivity are affected by the moisture content of the surface target under investigation. A change in moisture content of surface material therefore leads to a significant change in the dielectric properties of the material (ESA, 2019; Picard *et al.*, 2003). Moisture content or availability of it dictates how much of the incoming SAR signal scatters at the surface, how much signal penetrates the medium, and how much of the energy gets lost to the medium through absorption. The magnitude of these processes on the incoming and outgoing signal is however dictated by the SAR sensor wavelength. The wavelength results in differences in the appearance of image datasets acquired by different SAR sensors.

SAR signal penetration into vegetation depth depends on moisture, canopy density and geometric properties of the vegetation in the form of leaves, branch and trunk orientation. Wang *et al.*, 1993 assessed variations in soil moisture on observed ERS C-band backscatter for loblolly pine in North Carolina. The study attributed a rise in biomass backscatter intensity (from 2 to 3 dB) to a corresponding increase in surface soil moisture and leaf moisture. The availability of moisture in the soil in turn affects moisture availability to the plants since this water is available to the plant through absorption by the plant roots, hence greening. Moisture availability increases with rainfall availability and reduced with onset of prolonged dry conditions. Whenever such moisture is not available to the plants, then it means the dominant backscatter intensity is attributed to surface scattering, and not canopy volume scattering (Wang *et al.*, 1993).

Vegetation canopy density affects the backscatter response. Backscatter intensity from a closed canopy differs from that in an open canopy because the former only allows signal penetration from long-wave SAR to penetrate deeper. Open canopy allows signal penetration between canopy gaps and in the case of short to medium wavelength SAR, the signal not only interact with the sub-canopy, but can penetrate to the surface through the gaps within the canopy. Wang *et al.*, (1994 b) observed that surface scattering was important for stands with low standing biomass. Dobson *et al.*, (1992) observed that where the canopy is sparse and moisture increases, surface backscatter becomes the major contributor. Temporal changes in moisture availability through alternating dry and wet conditions not only affect vegetation canopy but also canopy moisture availability. During rainfall, water remains on the canopy through interception by leaves and branches. Besides water that reaches the soil surface, wet seasons are characterised with high moisture availability, while dry seasons experience low moisture availability both on plant canopy and in the soil. However, volumetric soil moisture has a high overall effect on the backscattered signal than leaf moisture through interception. A study by Griffiths & Wooding (1996) on the effects of temporal dynamics of soil moisture on C-band ERS-1 SAR data found a high positive correlation between volumetric soil moistures for bare soil fields with a much weaker positive relationship for grassland fields.

## **2.2. Vegetation structure mapping using SAR data**

As earlier noted in section 2.1 above, the microwave portion of the electromagnetic spectrum (EMS) covers the range from approximately 1cm to 1m in wavelength (Woodhouse, 2006; Oliver & Quegan, 2004). Because of their long wavelengths compared to the visible and infrared range, microwaves have special properties important for remote sensing. Active microwave sensors such SAR provide their own source of microwave radiation to illuminate the target under investigation. SAR is an active all-weather sensor operating by sending a microwave radiation to targets and detecting the intensity of radiation scattered back to the sensor by the target, backscatter ( $\sigma^0$ ). The  $\sigma^0$  is a function of the incident angle  $\theta$ , frequency and polarisation and is affected by the dielectric properties of the target and the surface geometry (Rees, 2001). The wavelength ( $\lambda$ ), relative to the size of the scatterer affects interactions between the two. Longer wavelengths such as P-, L- and S- bands are more relevant for detection of vegetation geometry because of their penetrative effects, resulting in volume scattering (Mitchard *et al.*, 2009; Woodhouse, 2006). The wavelength interaction with canopy elements results in diffuse scattering, hence more energy returning to the sensor (Ryan *et al.*,

2012). Longer wavelength SAR systems like L-band sensors penetrate the canopy (Figure 2-5, Evans *et al.*, 2013; Rees, 2001; Mitchard *et al.*, 2009; Woodhouse, 2006; Ryan *et al.*, 2012; Le Toan *et al.*, 1992).

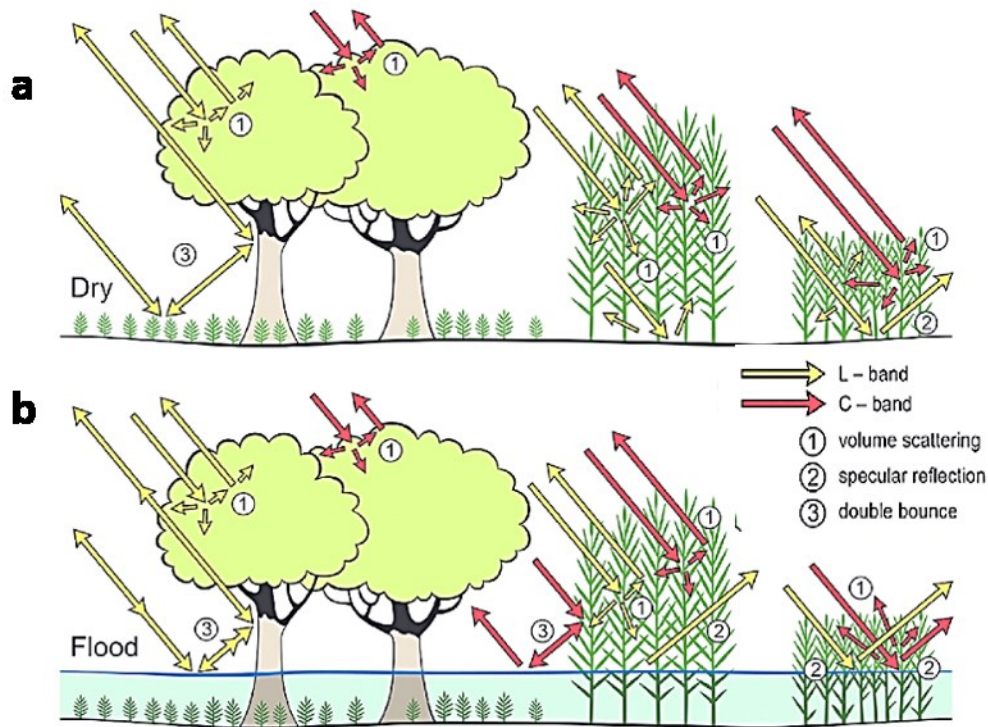


Figure 2-5. SAR backscatter interactions with vegetation components at different wavelengths, a) L-band and b) C-band SAR. (Source: Evans *et al.*, 2013).

Cross-polarised measurements (HV, VH) works better than co-polarised (HH or VV) in correlating  $\sigma^0$  to AGB since the former accounts for canopy as opposed to ground components. By using dualpol SAR (both HH, HV), Mitchard *et al.*, (2009) found a relationship between AGB and  $\sigma^0$ . Additional studies by Antonarakis *et al.*, (2011) and Treuhaft *et al.*, (2009) combined SAR and Lidar to improve AGB models by eliminating bias from too many large trees. By using different polarisations of SAR with Landsat Enhanced Thematic Mapper (ETM) data, Wijaya *et al.*, (2011) developed empirical models to estimate how forest parameters responded to  $\sigma^0$  in Sumatra, while Carreiras *et al.*, (2012) assessed the relationship between dualpol  $\sigma^0$  and AGB using models after Adler & Synnott (1992). Relevant studies by Urbazaev *et al.*, (2015) and Hamdan *et al.*, (2014) both used multi-temporal and dual-pol SAR in assessing vegetation structure components, AGB and woody cover respectively. The capability of L-band SAR backscatter intensity in quantifying small-scale forest degradation in the



Miombo woodlands of Mozambique over a three-year period was demonstrated in Ryan *et al.*, (2012).

### ***2.2.1. Rationale for microwave over optical data***

Characterisation of vegetation seasonal dynamics is a very important process in understanding both endogenous and exogenous processes responsible for the state of a biome. Using remote sensing in vegetation assessment has been dominated by optical remote sensing data for surface phenology analysis (Verbesselt *et al.*, 2010). Despite ease of access because of non-commercialisation by most providers to leverage on the potential of this technology in developing nations towards achieving the REDD objectives, the use of optical remote sensing data for savanna vegetation structure mapping is limited by sparse and heterogeneous distribution of vegetation canopy, leading to near-similar spectral signatures among vegetation cover classes. Cloud and aerosol contamination leads to inconsistency in availability of time series data necessary for continuous vegetation monitoring, especially in the tropics. Wang *et al.*, (1999) and Wang *et al.*, (2009) estimates that two-thirds of the earth's surface is covered by clouds throughout the year, while Esche, (2002) states that fifty percent of the earth is covered with clouds at any given time. However, recent technological advancements in remote sensing data acquisition and processing has seen an emergence of high temporal resolution SAR, with several studies gaining interest in its applications in time-series analysis of vegetation (Schlaffer *et al.*, 2016; Nguyen *et al.*, 2016; Martini & Rieke, 2015; Torbick *et al.*, 2017), with some focussing on its synergy with optical data (Saatchi, 1996; White *et al.*, 2015; Joshi *et al.*, 2016). Long- and medium wavelength microwave SAR, with their low sensitivity to clouds, high temporal and spatial resolution addresses optical remote sensing challenges. SAR, also referred simply as Radar sensors, detects backscattered energy by emitting their energy on surface features, making them able to illuminate the earth under a wide range of atmospheric conditions regardless of light availability (Brown, 1991), thereby reducing the previous limitations and challenges faced in using optical sensors (Amini & Sumantyo, 2009). The backscattered energy, which is the response from the ground target, is dependent on different parameters including polarisation, frequency, sensor resolution and the incidence angle. These parameters influence the information content of the SAR imagery (Walker, 2016), while the properties of the elements that comprise the ground target such as size of the surface target (McNeill & Belliss, 2002), its orientation, density and distribution pattern of scatterer, target surface texture relative to wavelength and the dielectric constant, are also important determinants of the strength and characteristics of the backscattered signal (Sandberg *et al.*,

2014). SAR remote sensing has been used in mapping different vegetation parameters including aboveground biomass (Odipo *et al.*, 2016), woody cover (Urbazaev *et al.*, 2015; Naido *et al.*, 2015; Main *et al.*, 2016), and therefore suitable for monitoring vegetation changes in relation to disturbance regimes and seasonal photosynthetic processes of many forest types (Viergever *et al.*, 2007).

Studies have pointed ways of enhancing vegetation mapping based on the prevailing influences of incoming SAR signal orientation – polarisation, and forest features. Sarkar *et al.*, (2013) looked at how biomass estimation can be improved using dual-polarimetric C-band SAR backscatter data, by combining high resolution SAR texture parameters with intensity and texture parameter ratios. Consistent to previous research findings, texture parameters of the raw HH polarisation data gave poor relationships to biomass estimation.

### ***2.2.2. SAR backscatter and vegetation phenology***

The temporal variations of backscattered intensity within vegetated areas is a function of the dielectric properties and structure of vegetation, the conditions of sub-canopy surface and the size and orientation of the target feature in relation to the SAR system (Salas *et al.*, 2002). Seasonal variations in SAR backscatter are also influenced by the climatic characteristics typical of an area. In wetter and waterlogged areas, there is little variance in vegetation structural properties, with the amount of water in the ground target and the soil determining the backscattering characteristics. Moisture content of the scatterer reduces penetration of the emitted energy and thus increases the backscattered energy while in contrast, backscatter reduces during the dry season when vegetation's absorption rate increases. The dielectric constant changes with the amount of water contained in vegetation parameters such as leaves, stems, and branches. Studies by Salas *et al.*, (2002) and Magagi *et al.*, (2002) in their assessment of variations in plants' ability to absorb and propagate SAR signals in both wet and dry climatic conditions, notes that SAR backscatter coefficient from canopy and ground potentially changes with changes in seasons. Wang *et al.*, (2012) studied the relationship between Normalised Difference Vegetation index (NDVI) time series with corresponding C-band "Environmental Satellite" (ENVISAT) SAR and Advanced Land Observation Satellite Phased-array L-band SAR (ALOS PALSAR) datasets, with respect to pasture biomass. The findings revealed a more significant correlation between NDVI with the SAR backscatter sensitivity coefficients (HV+HH and VV+VH) at HH and VV polarisations in L-band particularly during the growing season, with wet season NDVI showing no significant relationship to L-band backscatter. The

findings resonate with those of Salas *et al.*, (2002) and Sano *et al.*, (2005) who also studied the spatial-temporal variability of HH polarisation using Japanese Earth Resources Satellite-1 (JERS-1) SAR data for secondary vegetation succession stands and soil resulting from land-use changes in Rondonia. By assessing the scattering properties of plant regrowth at various stages of their growing phase, the studies found a stable increase in soil and vegetation backscatter during the late dry season/early wet season, with the trend growing steadily with an increase in soil moisture content thereby posing difficulties in discriminating pasture and forests because of decreased image contrast across the landscape. Longer wavelength SAR such as P- and L-band with cross polarisation (HV or VH) are more sensitive to different vegetation parameters and hence suitable for discerning different vegetation types (Sarker *et al.*, 2013). Greater sensitivity is attributed to the vertical structure of the ground target in a vegetated environment and requires greater stand height variations to delineate roughness.

### **2.3. Reference data for validation of remote sensing vegetation products**

Regional and global periodic forest biomass estimation is paramount, especially in tropical regions experiencing adverse ecological destabilisations. This information provides a platform for evaluating, modelling and quantifying the structural and functional dimensions and the productivity of the forest ecosystem (Sawadogo *et al.*, 2010). Vegetation structure attributes, such as AGB estimates helps in understanding the spatiotemporal variation in the atmospheric carbon emission factors (Colgan *et al.*, 2014), and tracking any changes that occur in an ecosystem. Studies have identified two principal approaches for estimating forest biomass: the direct and the indirect methods. Direct methods entail felling trees and taking measurements of the predictor variables. Over 80 percent of the total forest biomass is found in the aboveground constituent of a tree, mainly the stem and the branches that meet the 10-cm perimeter cut-off, with the remaining 20 percent of the tree biomass in the underground, and the deviation is very minimal between species (Malimbwi *et al.*, 1994).

#### **2.3.1. Field Surveys**

The exercise of AGB estimation involves placing a systematic or strictly random sampling method to the study area using predetermined coordinates. Depending on the size, density and structure variations of the sample region under study, a robust scientific methodology is used to place the plots for both vegetative and non-forested areas. The approach could involve the

use of random placement or stratified random sampling (Condit, 2008). The site is sub-divided into standard and corresponding fixed-area plots scaled mainly for 1 hectare (for heavily vegetated portions), and 0.04 hectares for sparsely vegetative forest portions, tree plantations and forests remnants (Condit, 2008). According to the sampling protocol (Woodward *et al.*, 2009), a minimum of six plots each measuring at least 0.25 hectares (Maniatis, 2010) is required for any study. The sampling unit can assume a square (mostly used), rectangular, circular or triangular shapes, and can also be dimensionless like with point sampling. Researchers however reinforce the use of plots for sampling and further show that the accuracy of AGB estimates is improved by large plot size and an appropriate plot design (Malimbwi *et al.*, 1994; Maniatis, 2010).

The tree variable measurements are taken, and the trees are felled for further statistical processes. The tree stumps are then tagged numerically according to the sequence of the work for easier relocation during data re-evaluation. Using precise published correlation formulae, the measured attributes are then used to compute AGB. Dead wood biomass is obtained from counting and taking measurements of both fallen and standing dry wood following the same procedure. This is duly important because it has been proved that fallen and dead trees can also store enormous volumes of carbon in some parts of the world, and even more than living trees in other parts. In tropical forests, a percentage of 10 - 15 is normally assigned to this vegetation category since these regions experience less existing fallen wood because of accelerated decaying processes. In other regions like the North America, sampling of dry trunks is substantial since their contribution to the forest biomass is tremendously more than the stipulated 15 percent (Condit, 2008). For bare land, ground cover is weighed. The direct method of predicting forest biomass is suitable for relatively smaller tree covers with fewer species counts. For enormous and spatially heterogeneous forest covers, the indirect methods of biomass estimation are used to estimate biomass. This involves the use of disparate generic allometric regression equations, combined with a non-destructive measure of tree attributes to estimate the overall forest biomass.

Nearly all developed countries have a scheduled system of executing their forest inventories on both private and public lands, and to conduct project-scale exercises that form the basis of biomass estimations across all forest types. For over seventy years for instance, the United States (US) has maintained an immense network of sample plots that act as a source of plot-level information such as the standard measurements of individual tree diameter, forest species

composition and forest health and the aggregate population of trees that make up a forest location (Brown, 2002). This information can be analysed and routinely used to generate annual data for general forest monitoring programs (Jenkins *et al.*, 2003). There are well established and proven methods for developing a statistical sampling design, and it involves estimating the number of field plots, field plot size, and distribution of permanent plots for varied precision levels (Brown, 2002). The methods also involve substantiating and analysing information about the forest parameters such as tree volume, which is transformed to forest biomass by applying a Biomass Expansion Factor (BEF) and significant tree allometric regression models (Baccini, 2004) such as the power function model with multiplicative error, a power function model with additive error, a polynomial model, combined variable model, and a square root transformed model (Samalca, 2007).

Using SAR data in vegetation mapping requires updated ground validation data to assess the results obtained from using backscatter intensities in modelling vegetation structure. Traditionally, tree inventory for ground verification has involved the physical measurement of various vegetation parameter variables, such as tree height and DBH using specialised tools. This method has proved expensive in terms of logistics and geographical coverage and is prone to instrument and introduced inventor errors which in most cases involve destructive sampling where trees must be felled and both wet and dry weight measured for allometric development (Yu *et al.*, 2010; van Laar & Akca, 2007). However, the last two decades have seen a rise in using Lidar in forest parameter retrieval because of its ability to capture both 2- and 3-D vegetation attributes (Streutker & Glenn, 2006; Yang & Lin, 2009; Ehinger, 2010; Glenn *et al.*, 2010; Spaete *et al.*, 2010; Berni *et al.*, 2011; Tinkham *et al.*, 2011; Holopainen *et al.*, 2011; Bright *et al.*, 2012; Magarick, 2012; Colgan *et al.*, 2012; Colgan *et al.*, 2013; Heritage & Large, 2009). However, the high costs of airborne Lidar acquisitions and technological advancements in remote sensing has seen development in ground-based TLS with the ability of 3-D data acquisition with diverse applications in seafloor, coastal and geomorphology (Fairly *et al.*, 2016, Williams *et al.*, 2011, Reinwarth *et al.*, 2017), vegetation (Richardson *et al.*, 2014; Pirotti *et al.*, 2013), and cadastral applications (Moskal & Zheng, 2012). Studies on application of TLS data in forest inventory are documented in the works of Simonse *et al.*, (2003) and Bienert *et al.*, (2006). The former determined tree stem coordinates using fitted circles to the digital terrain model (DTM) derived tree DBH (at 1.3 m). Thies *et al.*, (2004) accurately modelled tree stems by fitting cylinders to TLS-derived PCs, with the results showing a slight deviation with field reference DBH of -1.3 cm and 0.6 cm for beech and cherry trees respectively, and an

RMSE of 1.7 in fitting cylinders to the PCs. Hackenberg *et al.*, (2015) used TLS to predict AGB for three tree species - evergreen coniferous, evergreen broadleaved and a leafless deciduous, and concluded that tree diameters larger than 10 cm can be modelled more accurately than smaller ones, which are overestimated.

### **2.3.2. Terrestrial Laser Scanning**

Terrestrial Laser Scanning (TLS) technology is a ground-based data capture method using light detection and ranging (LiDAR), introduced towards the end of the 20th century (Calders *et al.*, 2015; Puttonen *et al.*, 2013; Xiao *et al.*, 2007). TLS is an active sensor and emits its own source of target illumination to capture information about a target (Hudak *et al.*, 2009). The sensor continuously emits coherent and monochromatic laser beam towards the objects under investigation, and receives the returned beam by the object to the sensor which it uses to estimate the distance to an object (Lefsky *et al.*, 2002). The beam is directed by rotating or oscillating mirrors (Lemmens, 2011; Kankare, 2015). The object information is collected in the form of dense point-clouds, which after processing is each assigned with X, Y, Z coordinates, colour for intensity and reflectance values. These characteristics make it possible to create 3D models of objects of a wide range of sizes and shapes (Colombo & Marana, 2010; Doneus *et al.*, 2009; Lemens, 2010).

#### **Data acquisition principles**

There are two main laser principles of terrestrial laser sensor scanning that guide distance measurements regarding forestry and other outdoor applications: the time-of-flight ranging principle and, second, the phase-shift based ranging principle (Calders *et al.*, 2015; Kankare, 2015). Time-of-flight instruments determines the range based on the precise travel time that the scanner pulses take to travel back and forth between the sensor and the object (Kankare, 2015; Liang *et al.*, 2016) and the speed of the energy. For the phase-shift based ranging instruments, the distance measurements are calculated by determining the difference in the phase of the reflected energy and that of the emitted energy based on the time when a pulse with a specific phase was emitted. Unlike single scans in time-of-flight instruments, phase-shift based ranging take continuous modulated pulses or waves - modulated in width and frequency - and the phase of the returning pulse is measured to determine the range. This principle is effectively used in both TLS and ALS.

TLS laser beams are configured to take regular scans over a pre-defined angle between the scan and the object (Holopainen *et al.*, 2011). The density of the point clouds produced depends on the number of returns, with multiple returns producing dense point clouds. The point clouds are a mass of three-dimensional points recorded by the laser scanner, and are a 3D reconstruction of an object geometry (Xiao *et al.*, 2007). Current TLS systems are capable of capturing up to millions of points per second. Figure 2-6 shows a graphic representation of a TLS system with the resultant tree objects reconstructed from point clouds. During data capture, the TLS instrument is mounted on a static tripod. The scanner in the TLS instrument scans the surrounding using a vertical rotating mirror while the TLS instrument makes slow horizontal rotation. TLS scans objects from different positions to enable true 3-D modelling of objects of interest (Tempfli *et al.*, 2009)

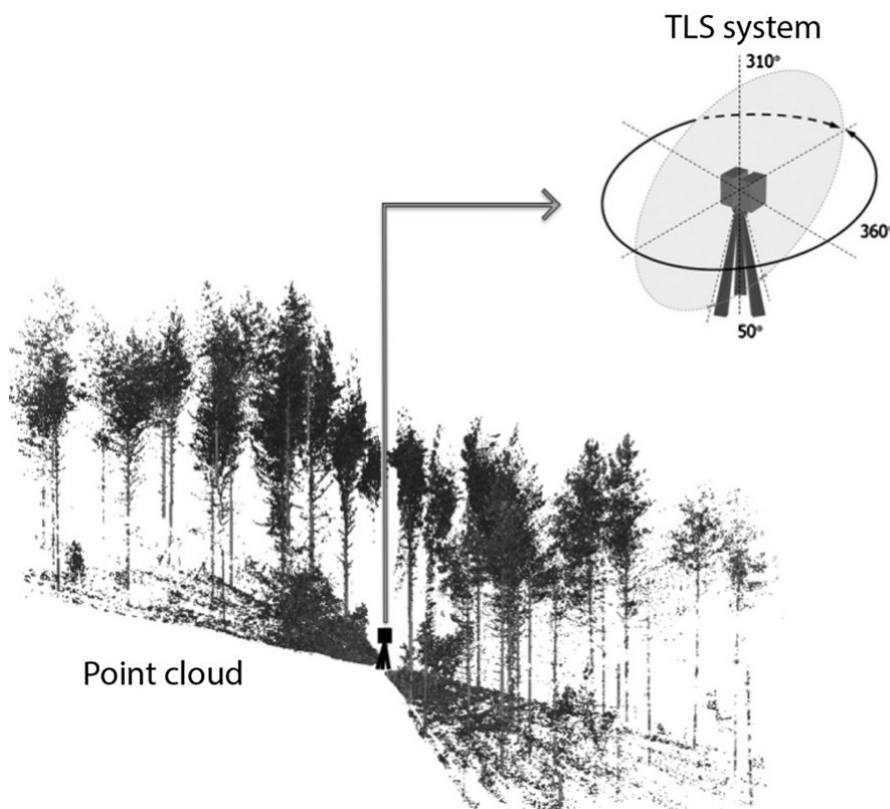


Figure 2-6. SAR backscatter interactions with vegetation components at different wavelengths, a) L-band and b) C-band SAR. (Source: Evans *et al.*, 2013).

To obtain the point cloud of 3D coordinates, the range or distance between the scanner and the object, the time of flight of the laser beam, the scanner position and sampling interval, and the angle at which laser signal hits the target object, are the measurement components that guide

the process. The TLS system has three times of ranges: the short range is up to 25m, the midrange is up to 250m and the long range is more than 250m. The range determines the application based on the scan rate, beam width, and spatial resolution (Lemmens, 2011; Kankare *et al.*, 2013; Holopainen *et al.*, 2011). TLS instruments with a shorter maximum range (e.g. phase-shift-based ranging instruments) have higher precision because of a higher point density recording. Laser scanners are optimized for automatic extreme high speed and precise scene scanning at over 1,000 point clouds per second (Xiao *et al.*, 2007; Lemmens, 2011; Kankare *et al.*, 2013), giving datasets with a high point density, high coordinate precision ( $\pm 6\text{mm}$ ) and an overall improved accuracy of 2-5mm. Slight variations in accuracy result from differences in the accuracy of each scanned point and the structure of the surface object. Besides, TLS provides dense point-cloud object surface measurements at varying resolutions. The information captured can be integrated with digital imagery during image reconstruction, coloring and texturing of objects surveyed. Terrestrial scanners measure range, the geometric information and the intensity value of terrain points recorded by the laser beams (Kankare, 2015), which is also stored as x, y, z coordinate together with intensity information.

Point clouds are represented as color-coded features based on the intensity value as recorded on the freely selectable point grid. Trees are represented as hierarchical collections of preferably circular cylinders or other building blocks, thus forming discontinuous models. TLS is versatile in that it provides surface measurement at independently varying standoff distance (BÖHM & Stuttgart, 2005) thus recording data about a specific object from multiple stations. Using data from multiple scan locations significantly reduces the effects of occlusion, common in a single scan mode. It achieves this through a process called co-registration or point cloud registrations of the scans using suitable overlap areas, identifying the tie-points of dissimilar scan stations (Kankare *et al.*, 2013) or through a transformation during post processing. As a result, co-registration increases the capability of a detailed reconstruction of tree parameters that would otherwise be lower with single scans.

### **TLS in forest inventories**

Direct field inventory has been used for decades to obtain tree variable data for the validation of remote sensing products (FAO, 1981). These methods have, however proved to be inefficient both in time and space; non-representative geographical coverage and a high possibility of omission and commission errors in such data acquisition. Where such data is to be used in developing allometries for carbon stock estimation, destructive sampling harms the biome in the long run. However, by assessing the dependence between such field inventories and TLS



metrics, it is possible to predict forest structure (Niemi *et al.*, 2015; Calders *et al.*, 2015). TLS has also been used to validate individual tree variables like height (Holopainen *et al.*, 2011). TLS technology provides a high precision of up to millimeter-level details of the objects being mapped (Kankare *et al.*, 2013), and the ability to measure and create 3D models for single-tree attributes. The structure models developed can then periodically update the existing allometric model.

Since its introduction, there has been a progressive development and widespread use of the TLS (Calders *et al.*, 2015). The 3D point cloud has been used to examine and reconstruct ecosystem structural properties of a plot at increasingly high spatial and temporal scales for both structurally continuous and fragmented surfaces (Orwig *et al.*, 2018). There has also been potential advancement in the validation of TLS techniques to support its application in forest inventory (Calders *et al.*, 2015). TLS has been exploited to offer robust survey and mapping solutions in diverse fields including but not limited to archaeology, architecture, engineering, geology, mineral and petrochemical exploration, seafloor, geomorphology (Fairly *et al.*, 2016, Williams *et al.*, 2011, Reinwarth *et al.*, 2017), vegetation (Richardson *et al.*, 2014; Pirotti *et al.*, 2013; Gruszczynski *et al.*, 2017), cadastral applications (Moskal & Zheng, 2012), forest inventory (Simonse *et al.*, 2003; Bienert *et al.*, 2006) and forest ecology applications (Puttonen *et al.*, 2013; Calders *et al.*, 2015).

TLS offers three different techniques of field data capturing based on the scanner position: in a case where the TLS sensors are mounted on a tripod fixed at a specific location on the ground to record static measurements obtained from single scans of the surface of the objects, the technology is called TLS (Calders *et al.*, 2015; Lemmens, 2011). Here, reference targets within the study are divided into constant size plots in a way that allows visibility from the center scan. Fixed-position laser scanners offer a high potential for 3D mapping of smaller areas with a greater aspect. The data captured can be integrated with existing datasets through georeferencing using 3D control points. When laser scanning instruments are mounted on any flying platform like an aircraft or helicopter, the technology is referred to as Airborne Laser Scanning (ALS). ALS is costly and is partly the reason for the development of TLS (Holopainen *et al.*, 2011). Sometimes however, the laser scanners can be mounted on such moving platform as cars, vans, vessels or boats and is referred to as Mobile Laser Scanning (MLS) or Terrestrial Mobile Mapping (Lemmens, 2011; Kankare *et al.*, 2013). MLS is popularly used in mapping features that exhibit relatively large expanses such as roads and highways to avoid road closures

and disruptions during survey, and also for high acquisition of trajectory measurements (Lemmens, 2011).

In forest inventories, TLS can be used in sample plot measurements, Stand-level forest inventories and in the development of tree allometric models. The technology can quantify individual and plot-level attributes through 3D mapping of vegetation structural metrics such as tree population (Kankare *et al.*, 2013), diameter of stem form, curve or inclination angle of the stem, branch segments, tree species, class and height, tree location and canopy layer and understory related elements such as canopy size (Saarinen *et al.*, 2017; Liang *et al.*, 2016; Liang *et al.*, 2017; Kankare *et al.*, 2013; Kankare, 2015; Holopainen *et al.*, 2011; Calders *et al.*, 2015). Such measurements are used to establish models like the stem volume models and to conduct gap probability estimates and overall forest biomass estimates. Thus, TLS is, and has been a viable alternative or additional data acquisition technique to other survey technologies such as geodetic or photogrammetry, and allometric biomass estimation novel algorithms (Sternberg *et al.*, 2004).

TLS technology has potentially revolutionized the process of forest inventory. It is possible to use a TLS point cloud-based approach to rapidly and accurately measure forest biomass at greater details without cutting down the trees (Xiao *et al.*, 2007; Liang *et al.*, 2016; Kankare, 2015).

### ***TLS data processing***

Processing of TLS data can be divided into two steps: pre-processing and post-processing (Xiao *et al.*, 2007). Pre-processing includes data re-sampling, camera calibration, image rectification, coloring the point clouds (RGB band), registration and merging of different multiple single scans to produce a single, unified point cloud from each study object. Using a geodetic reference system, each point cloud from the reference targets (raw data of the scans) is converted into a position by transforming the local scanner coordinate system into a common coordinate system, giving it 3D dimensional point clouds. Further manipulation can then be done on the data including filtering, visualization, classification, and analysis (Liang *et al.*, 2016; Lemmens, 2011). The post processing involves triangulation and interpolation of the measured points to permit registration and the 2D- and 3D data evaluation. It also involves use of models that can control the scanning parameters for the duration of data acquisition (Sternberg *et al.*, 2004), reconstruction, visualization of objects and production of ortho-images for documentation of 2D view of surface objects necessary for mapping (Xiao *et al.*, 2007).

### ***2.3.3. Allometries in biomass estimation***

Tree allometric models have profound relevance in the development of information on the approaches to sustainable AGB estimation. They can also be extrapolated to other spatially extensive ecosystems of similar disposition. The equations are of importance in very large and multi-species biomes where initial methods of inventorying the forest to get raw field data could lead to expansive destruction of sample trees and would also involve massive resources in terms of time and finances.

In the tropical regions and North American forests, studies have been conducted to develop and document different statistical generic equations - linear, logarithmic, exponential and power, to represent the circumstances characterising the entire forest range and across different landscapes (Sawadogo *et al.*, 2010). In Africa, there has been tremendous effort to develop allometric models for some regions (Malimbwi *et al.*, 1994; Sawadogo *et al.*, 2010; Mate *et al.*, 2014) which have been useful in estimating forest biomass in other regions where such a database is lacking. Tropical vegetation is majorly multi-species in nature (Hunter, 2013) and is also diverse in their form and growth characteristics across forest categories of a similar nature. Because of intensiveness in terms of resources needed to develop biomass estimation models for diverse species ecosystems at extensively varying spatial scales, there is a consistent lack of ecosystem-specific equations in most parts of Africa. Only a few such studies have been conducted in regions like West Africa for the Sudanian savanna woodlands (Sawadogo *et al.*, 2010). Most tropical regions rely on forest inventories taken some decades back, with few developing countries having recurrent field measurement inventories of their existing forest covers that can reliably be used for regional biomass and carbon predictions. By the year 2005 for example, there was no published theoretical models and field data on ground measurements in the central Africa's Congo Forest Basin, which covers more than half of Africa's flora and fauna (Maniatis, 2010).

### ***2.3.4. Sources of errors and uncertainties in aboveground biomass assessment***

An error is a statistical uncertainty insinuated at each phase in creating and applying a model, such as an allometry. Errors are potentially inherent regardless of the method or the spatial scale of the sampled area (Henry *et al.*, 2011). These errors are propagated in the ultimate results of the forest inventory (Condit, 2008), leading to misleading sets of estimates and other predictions

that rely on such data, like the carbon emission inventories (Cifuentes-Jara *et al.*, 2013). The variance can be even higher when inferring published dimensional equations developed for a different region to synthesise forest biomass of another landscape. It is stipulated that most of the existing biomass allometries were developed by foresters and ecologists. Regression errors are associated with generic or species-specific empirical models used during the conversion of tree parameters to derive the biomass (Brown, 2002). The error resulting from most of the allometric equations is an accumulation of errors incurred during field sampling, variable measurement, and the discrepancy along the allometric regression models used. These errors can contribute to about 31 percent (10 cm or more trunk diameter) and 55 percent (less than 10 cm trunk diameter) uncertainty to the AGB estimation (Maniatis, 2010).

Sampling errors emanate from deviations in sampling units such as the number and the size of plots within the study area. The size of the sampling error depends on the sampling strategy, sample size, estimation process and the underlying variables being used in the biomass calculations. Another form of sampling error is a function of improper presentation of the ecological variations of stand structure and composition as determined by the environmental gradient. The sample used in biomass estimation may not be a complete reflection of the entire site and hence there is a high possibility of obtaining different parameter estimates in the subsequent studies over the same area (Samalca, 2007).

There has also been varying debates on the need to include smaller diameter trees in the sample and their contribution to the final estimate results. According to Sawadogo *et al.*, (2010), generating species-specific equations should involve the inclusion of large tree components such as the tree trunk because these components provide concise estimates than smaller elements such as tree branches and twigs. Studies give premium to stem diameter as the main biomass indicator, especially for mixed forests whose trees grow close together with overlapping or interlocking crowns (Chave, 2005). However, studies especially in heterogenous ecosystems like savannas, small diameter trees especially shrub vegetation, contribute high to the woody vegetation component because they by large comprise the woody vegetation component. This is also true with temperate regions where their contribution highly depends on the chronological phase of the forest and ignoring small trees has been identified as a source of error leading to underestimation in AGB calculations (Brown, 2002). Difference in forest wood densities may yield different AGB stocks across different ecological stratifications (Maniatis, 2010), making it crucial to choose an appropriate model for a forest type. Regression error is

another main source of error (Colgan *et al.*, 2013) because it does not reduce with changing variables.

Measurement errors may be realised while taking the dimensions of tree attributes such as base diameter, diameter at breast height, during species identification and counting, measuring shoot height and establishing the dry weights. The erroneous estimates can be caused by poor and wrong recording (duplicated and/or mismatched field) which calls for proper screening of data after plotting (Condit 2008). Errors can also result from the error in the measuring instrument (Samalca, 2007), and nature of the object being measured, for example, presence of buttress, or irregular girth shape, and multi-stemmed trees like those in the Lowveld savanna (Scholes *et al.*, 2001).

Uncertainties and statistical variations in biomass estimate results also stem from differences in the sample size (limited samples for some cases), and the input variable measurements (e.g. trunk measurements, wood specific gravity, forest type and height measurements) that are incorporated during the development of linear functions (Sawadogo *et al.*, 2010). Some allometries may have been constructed using the trunk diameter only to predict biomass (Colgan *et al.*, 2013) or from trees whose measurements do not correspond to tree diameters of the region whose biomass is to be estimated. Previous works have proved that inclusion of height in biomass allometries improves accuracy (Hunter *et al.*, 2013). The use of diverse variables on a significantly large sample-range reduces biasness. Chave (2005) emphasises the inclusion of the stem diameter, wood specific gravity, total height, and forest type as the most important variables in AGB estimation. Working with a range of tree variables improves the accuracy of the model and its reliability for broad-scale extrapolations. Besides, wood density has also been considered as the second most crucial factor in AGB estimates (Maniatis, 2010), with Colgan *et al.*, (2014) pointing out that wood density as the key driver of variations in biomass between dominant species of the same size.

Another source of error and uncertainties is the poor choice of the allometric model. Point studies may reflect variations in terrain gradient and vegetation types, and drainage status of a forest cover. The structural parameters of the tree such as the stem measurements, the height and density of the sub-sampled trees also vary with different climatic zones (Samalca, 2007). Inference of the regression models requires a comprehensive review of various existing models based on the zone under study. Maniatis, (2010) provides an empirical evidence to this

hypothesis by using different allometric models from the sub-Saharan database to review the errors propagated by the choice of the model across three different ecological zones in Ghana and Cameroon. In his study, he found out that there is a considerable variation of AGB estimates and hence the carbon stocks between different allometric equations. His findings correspond to Jenkins (2003) who showed inconsistent results unsuitable for broad-scale applications by validating US models. Ngomanda *et al.* (2013) also reinforced this in their study to validate the applicability of six wet forest regression models developed for Madagascar to the Zadié, with results pointing to a systematic overestimation of AGB up to 47 percent.

### ***2.3.5. Error and uncertainty reduction in aboveground biomass estimation***

Most studies that have encountered errors and uncertainties have come up with different suggestions aimed at providing a framework for reducing errors in AGB and carbon stock estimations. According to Brown, (2002), forests are constantly experiencing changing regimes as a function of changing climatic conditions and other driver variables, hence a considerable change in tree allometric relationships. Repeated inference of unrevised allometric datasets produces skewed estimates at varying degrees. Apparently, there is a need to develop new standard models through fresh measurements of large diameter trees and a thorough revision of datasets especially in highly heterogeneous ecosystems where only a few trees species are represented in the generalised existing commercial forest inventory data (Brown, 2002).

The allometric relationships specific for a taxonomic category are also deficient in the tropical regions. For forest types with fewer tree species, there is a need to develop species-specific biomass regression equations to ensure complete forest representation and data agreement aimed at improving the quality and reliability of point regression models (Malimbwi *et al.*, 1994; Brown, 2002). Previous studies have revealed that species-specific models can be deduced for other sites if these forest types fall within homogenous environmental conditions within which the model was built (Sawadogo *et al.*, 2010). Original data from which the models are derived need to be published and made completely and freely accessible by other scientists or any other body which wishes to conduct periodic biomass estimates. The respective dataset should also include reports on methods and definitions. Data on global dead wood densities for different forest types (dry, moist, wet) must be accumulated by decomposition class and archived for easier access and use.

Some researchers have proposed a comprehensive review and reanalysis of the tree mensuration data and the methodologies used. This involves direct destruction of sample tree species from the respective sampling units and performing different variable measurement procedures. Most studies have had to employ efforts to test the credibility of the available equations by carrying out actual field inventory measurements (Nickless *et al.*, 2011; Henry *et al.*, 2011; Colgan *et al.*, 2012; Odipo *et al.*, 2016). An ideal approach for developing allometric equations that can produce consistent regional biomass estimates would require sampling different sizes of all tree populations from a representative sample of species for all ecosystems characterising the entire region (Brown, 2002). This is evidently impracticable since most countries have well-established laws governing their protected forest reserves.

# CHAPTER 3

## 3. Methodology

### 3.1. Summary on methodology

Figures 3-1 and 3-2 visualises the methodological concept adopted in achieving the objectives of this study – AGB modelling and change analysis using L-band SAR, and C-band SAR interactions with savanna vegetation structure, respectively. The present study, combining field inventory, high resolution TLS data, and L- and C-band SAR data each with varying spatial and temporal resolutions, assesses (i) the potential of high resolution TLS in extraction of savanna vegetation structure variables, both at individual tree-level (height, DBH and vegetation classes) and plot-level (AGB and CC); (ii) the use of sub-canopy data to estimate biomass at plot-level and the use of remote sensing datasets to upscale to the landscape level; (iii) the potential of L-band SAR in biomass change detection within a Lowveld savanna ecosystem, and (iv) assess the interactions between C-band SAR and TLS-derived vegetation structure variables in (i) above. 42 field plots were established within the study area, each measuring 30 m from which tree height and basal diameter were inventoried. The inventoried variables were later used to compute both tree- and plot-level aboveground biomass based on an allometric model specific to the Lowveld savanna. A TLS survey was carried out in the same area and provided point clouds which were used to inventory individual tree heights and reconstruct individual tree trunks. The same was used to generate CHM for estimation of vegetation canopy variables—canopy height and cover. These variables were regressed with plot-derived AGB to generate a reference biomass for subsequent SAR biomass estimation over the study area. With multi-temporal L-band SAR, an assessment of biomass changes within the study area over a four-year period between 2007 and 2010 was possible. The study assessed the errors and accuracies associated with the various biomass models (TLS and SAR metrics) used. Finally, the TLS-derived vegetation variables provided a basis on which this study assessed the interactions and C-band SAR backscatter response to the vegetation cover classes, AGB and CC within the TLS footprint.



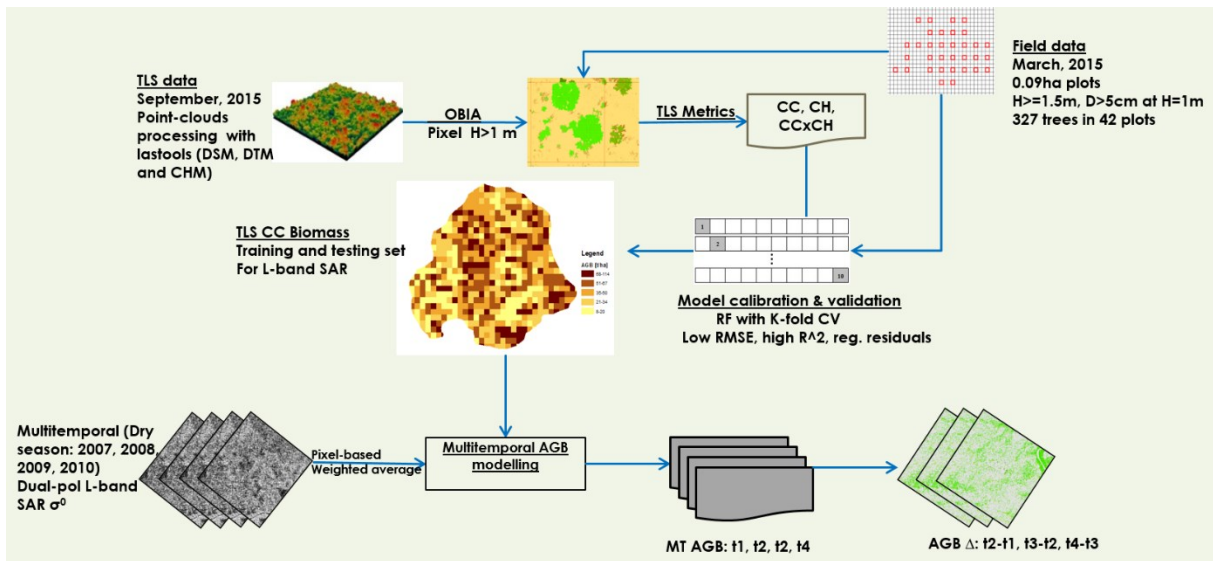


Figure 3-1. Methodology adopted in AGB modelling and change analysis using L-band ALOS PALSAR with field inventory and TLS as reference datasets (Odipo *et al.*, 2016; TLS data by Dr. J. Baade)

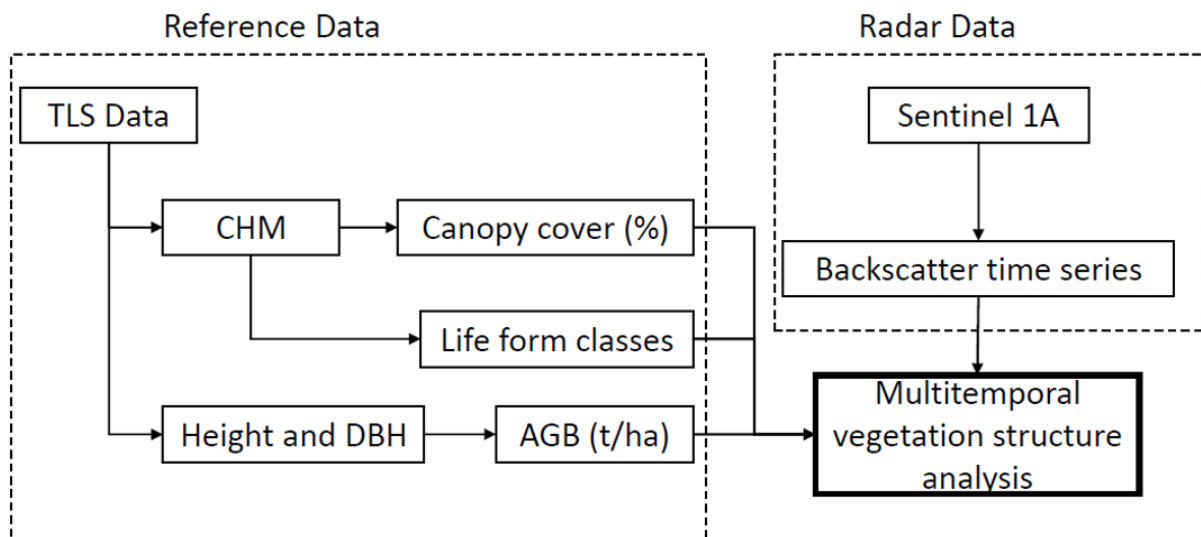


Figure 3-2. Methodology adopted in assessment of C-band Sentinel 1A SAR interactions with TLS-derived savanna vegetation structure.

## 3.2. Study Area

### 3.2.1. *Southern Africa Savanna Biome Distribution*

Statistically, over 40 percent of the African population lives in arid and semi-arid environments and derives their livelihoods from the surrounding ecosystems (Ciais *et al.*, 2011). In addition, Sub-Saharan Africa experiences a rapid population growth rate than any other part of the world. The distribution of these populations across the outskirts of savannas has seen extreme direct negative effects in areas initially under natural forest cover, reducing carbon sink while elevating the amount of terrestrial carbon emission in the atmosphere resulting from degradation and deforestation. The human population - environment interaction in the African savannas has rendered them vulnerable to change through different land use practices such as the expansion in cropland and human settlements.

In South Africa, savannas constitute between 35 to 46 percent of the terrestrial land area (Figure 3-3, Mucina & Rutherford, 2006; Steenkamp *et al.*, 2015), with KNP alone occupying almost 2.5 percent of the total land surface area (van Wilgen, 2009; Scholes & Walker, 1993). On the extraneous parts of the park, land use practices include farming, cattle ranching, private game reserves and human dwellings (Scholes *et al.*, 2001).

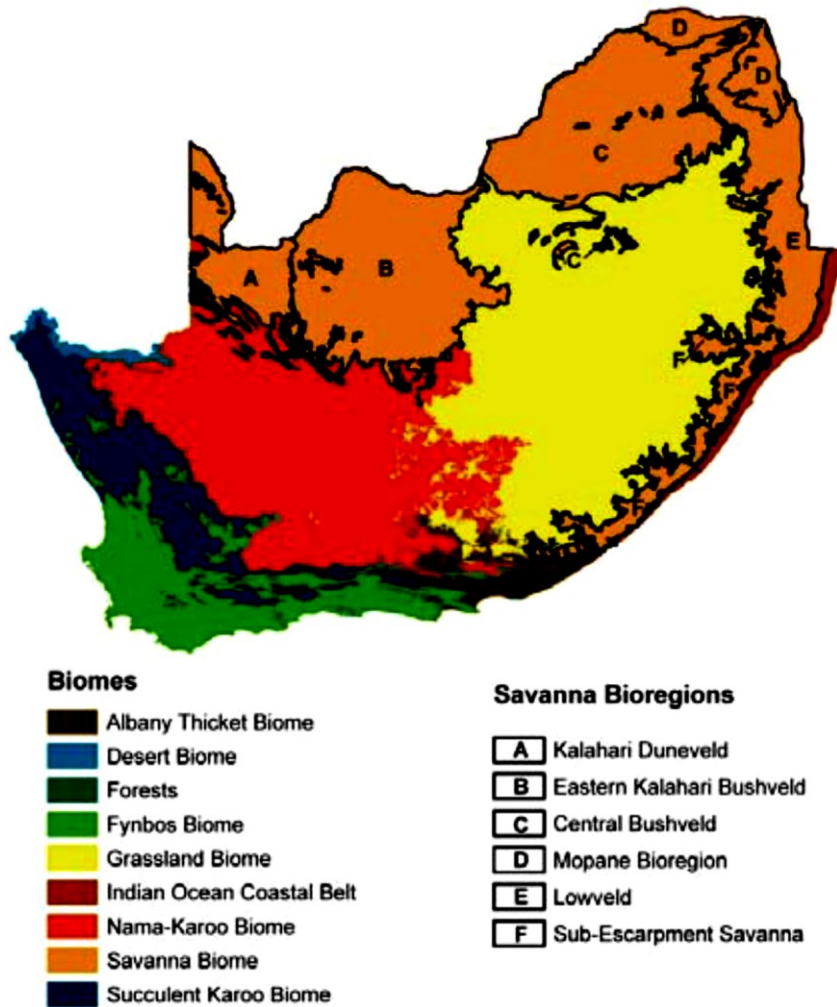


Figure 3-3. Map showing the biomes of South Africa, with savanna biome divided into bioregions A to F (source: Mucina & Rutherford, 2006)

### 3.2.2. Skukuza Site

#### *Choice and location*

The study was conducted near the Skukuza Flux Tower in the southern part of KNP (Figure 3-4) about 13 km southwest of Skukuza town in the N'waswitshaka catchment. The current study is carried out under the framework of the Adaptive Resilience of Southern African Ecosystems (ARS AfricaE) project. ARS AfricaE is implemented around Skukuza eddy covariance (EC) flux tower to assess biogeochemical interactions and their significance to the resilience of the savanna biome to climate change (Kutsch *et al.*, 2012), a factor which dictated the site apart from the fact that Skukuza area provides a typical Lowveld savanna features in terms of vegetation structure. The study area is restricted to nine square kilometres around Skukuza Flux tower site. The EC flux tower (25.0197° S, 31.4969° E) was established in early 2000 to study

carbon, water, and energy dynamics of semi-arid African savannas, as part of the South African Regional Science Initiative (SAFARI 2000) experiment to understand the interactions between the atmosphere and the land surface in southern Africa (Scholes *et al.*, 2001). The site is situated within a broad- and fine-leaved savanna biome, an ecosystem covering 32% of South Africa. The dominant tree species here are *Combretum* sp. and *Acacia* sp. and the soil type is sandy clay loam Arenosol (Kutsch *et al.*, 2008).

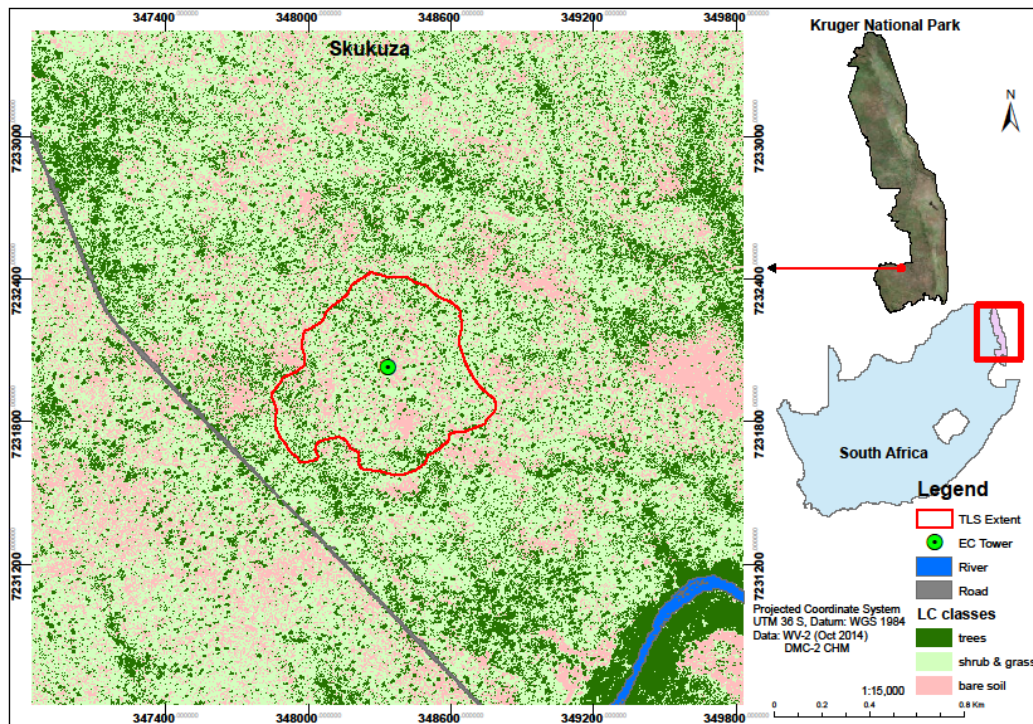


Figure 3-4. Imagery showing location of the study site in Skukuza, showing the terrestrial laser scanner (TLS) footprint. The study is centred on the Skukuza eddy covariance tower (EC Tower) as shown in the map. (Imagery source: Google Earth/Digital Globe).

### *Climate*

The climate around Skukuza is typically semi-arid subtropical with hot rainy summers and warm dry winters (Scholes *et al.*, 2001). The Skukuza EC tower site receives a mean annual precipitation (MAP) of 547 mm, while an analysis of the weather station data from 1912 shows that the area receives an annual rainfall of 500 – 700 mm per year, with maximum rainfall received in January (Kruger *et al.*, 2002). The seasonal rainfall analysis defines summer as running between the months of December to February, autumn from March to May, winter from June to August and spring from September to November. Figure 3-5 shows long-term average monthly rainfall statistics from an analysis of rainfall data within Skukuza between 1912 and 2001. Figure 3-6 shows decadal rainfall statistics for the year 2015, covering the

timeline of most of this study. The plots show rainfall amounts for the selected year (dark blue) and for the long-term average (20 years, 1994-2013) in light blue.

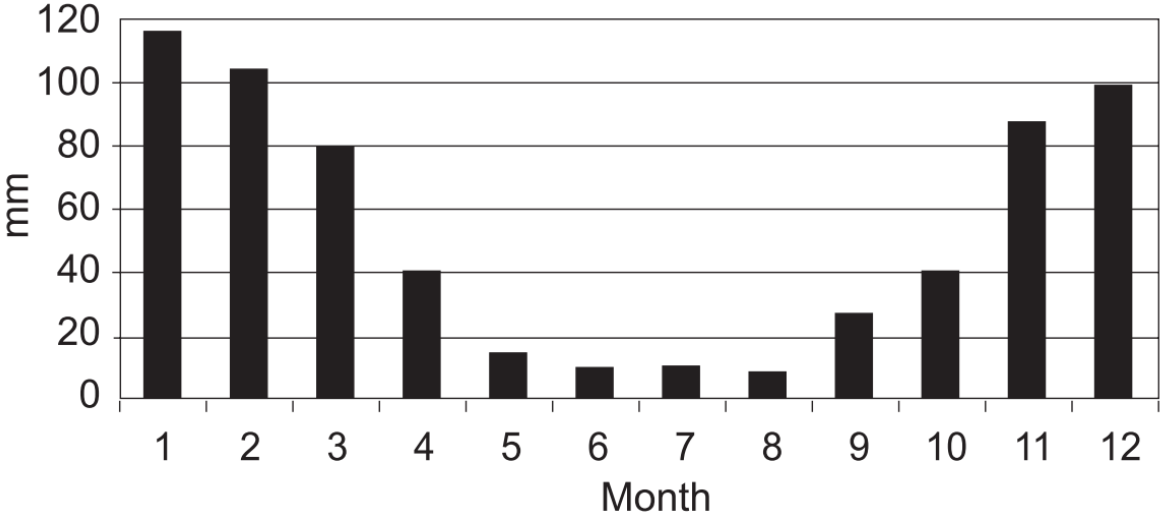


Figure 3-5. Average monthly rainfall (mm) for the period 1912 to 2001 (Kruger *et al.*, 2002).

The highest rainfall values are received between November and March, making these two months the wet season boundary, with April as a transition month, while dry season is experienced between May and September, with October as the transition month between dry and wet seasons.

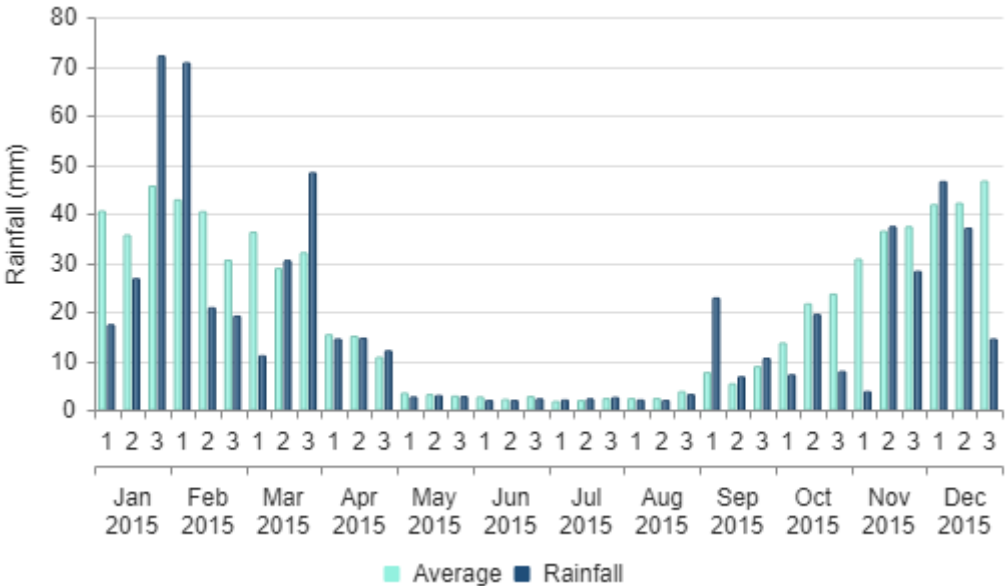


Figure 3-6. Decadal rainfall statistics for Skukuza region for the year 2015. Dark blue bars are rainfall values for 2015 while light blue shows 20-year averages (1994-2013). Source: FAO VAM.

Historical climate statistics of Skukuza between 1960 and 1999 gives a mean annual temperature range of 14.3 to 29.5 °C (Scholes *et al.*, 2001; Gartenbach, 1980). The area is underlain with granite and gneiss and characterised by very distinctive catena sequence of soils from the crest to the valley bottom (Colgan *et al.*, 2012), with reddish or yellowish-brown sand, grey hydromorphic sand, and clay (seasonal waterlogged band of soils).

The characteristic biome is subtropical savanna, where the cover is not discrete but characterised by a mixture of growth forms, primarily grasses, with shrub, and tree patches. Small patches and gradual transition between open and closed vegetation cover are typical features of these landscapes (Mistry, 2000; Scholes *et al.*, 2001; Scanlon & Albertson, 2004; Woodward *et al.*, 2004; Sankaran *et al.*, 2005; Merbold *et al.*, 2009; Hüttich *et al.*, 2011; Moses *et al.*, 2012; Gesner *et al.*, 2013). Such a characterisation has caused problems in not only differentiating between the grass, shrub, and tree vegetation cover, but also in making the use of spectral information from passive remote sensing a challenge given the inherent complexities in its structure. There is high pressure exerted by population growth and the need for people to derive their livelihoods from this ecosystem. There has been a spike in the amount of poaching in KNP, particularly in recent years, and this makes up one example of anthropogenic impacts on this supposed “closed” environment. The significance of poaching influences the savanna ecosystem stability, particularly the poaching of macro-herbivores, which is finally manifested in vegetation structure dynamics.

### *Geology*

According to Barton *et al.*, (1986), the Skukuza area is underlain by Archaean granite and gneiss. The area is characterised by very distinctive catena sequence of soils from the crest to valley bottom (Colgan *et al.*, 2013), with reddish or yellowish brown sand, grey hydromorphic sand and clay (seasonal waterlogged band of soils along the contour of the slopes called seep line), greyish brown sodic duplex soils (sand or loam abruptly overlying dispersed clay affected by the presence of the sodium), and mixed alluvial soils (Scholes *et al.*, 2001). The landscape around the flux tower is typically undulating at an altitude ranging between 355 and 378 m above sea level (a.s.l.) (Odipo *et al.*, 2016; Scholes *et al.*, 2001; Kutsch *et al.*, 2008; 2012), with the Sabie River forming the major drainage system. Venter *et al.*, (2003) describes the topography of the area as a slightly undulating plain and classifies the geology into two categories: uplands characterised with sandy soils and bottomlands with duplex sodic clays.

## *Vegetation*

Gertenbach (1983) describes the vegetation around Skukuza as the “Thickets of Sabie and Crocodile Rivers”, Low & Robelo (1996) describe it as “Mixed lowveld bushveld”, while Venter (1990) described the dominant woody vegetation within the area as moderately dense *C. apiculatum*/*G. bichor* bush savanna with *A. exuvialis* and *A. nigrescens*. The vegetation of Skukuza results from the geological catena sequence; sandy uplands, the mid-slopes with a wetter clay seep line and the foot slopes with duplex soils. The sandy (granite) uplands characterised by dense deciduous broad-leaved bushveld occurring in relatively dry infertile situations (Coetzee & Werger 1978). This area is mainly dominated by *Combretum spp* such as the red bushwillow (*C. apiculatum*), large fruited bushwillow (*C. zeyheri*), variable bushwillow (*C. collinum* subspecies *suluense*), and silver cluster-leaf *Terminalia sericea*. The mid slopes are wetter because the impervious layer created by the clay illuviation from the sandy uplands. This region is characterised by water tolerant grasses such as the gum grass (*Eragrotis gummiflua*) and sedge grass (*Cyperaceae*) (Venter *et al.*, 2003; Scholes *et al.*, 2001). The foot slopes with duplex soils are dominated by open fine-leaved bushveld with thorny woody plants, mainly red thorn (*A. gerrardi*), knob thorn (*A. nigrescens*), common false-thorn (*Albizia harveyi*), sickle bush (*Dichrostachys cinerea*) and magic guarri (*Euclea divinorum*) among others.

### **3.3. Data Acquisition and Processing**

#### ***3.3.1. Field Inventory Data***

##### ***Field sampling strategy***

First, different satellite imagery sources, including Google Earth and Landsat imageries were used to study the vegetation distribution within the study site around the Skukuza EC flux tower before the field inventory. This was purposively chosen to fit the overall objectives of the ARS AfricaE, project (Kutsch *et al.*, 2012), under which this study was based. For convenience, and a possibility of later using the results from SAR-based vegetation structure modelling to widely available optical data, the study opted to use 30 m plots, with Landsat pixels as the sampling plots. OBIA within eCognition (Trimble, 2017) was therefore used with chessboard segmentation at a scale of 1, for each 30 m pixel of Landsat TM data for the year 2015, covering



the study area. A detailed field inventory around the flux tower was carried out in March 2015. 42 field-sampling plots, each measuring 30 m × 30 m were established around the tower. The location coordinates of the centre of each plot was recorded using Trimble eTrex handheld Global Positioning System (GPS). Figure 3-7 shows the plot layout and sampling strategy used in individual tree identification and measurement.

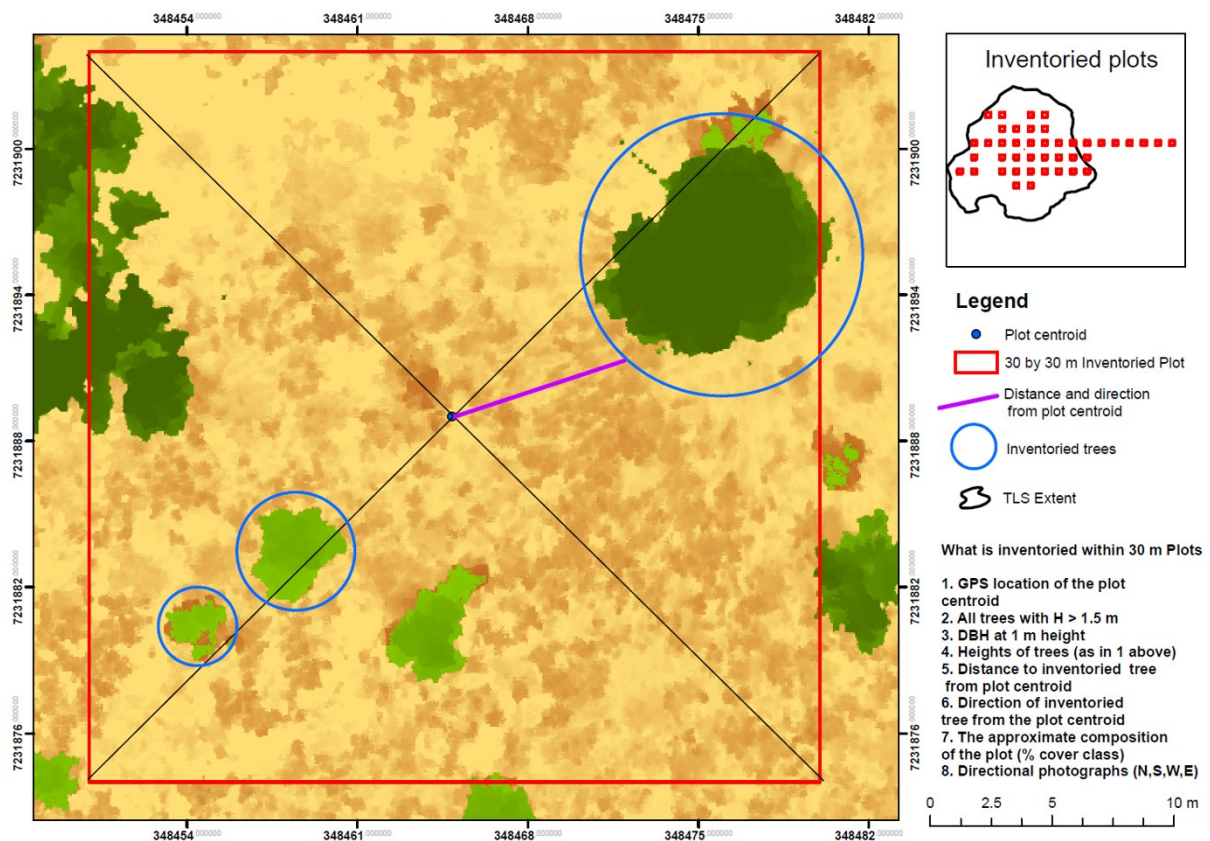


Figure 3-7. Plot layout, tree identification and measurement adopted in plot sampling for individual tree mensuration.

### *Tree inventory*

Within each 30 m plot, tree heights and basal stem diameter from stems greater than 5 cm thick were measured at 1 m height from the ground and recorded. For tree heights, Nikon Forestry Pro laser rangefinder hypsometer was used to measure heights of trees taller than 1 m within the plots. The hypsometer uses a three-point height measurement function (trigonometry) by first calculating the horizontal distance between the enumerator and the tree, then capturing two other points (location of the enumerator and tree top) to create an angle which it uses to calculate vertical height. For basal diameter, a DBH tape was used to measure the basal diameter at 1 m height. In this study, a tree and a stem are loosely defined as single- or multi-stemmed



individuals from the same rootstock and all branches from a point on the ground, respectively (Colgan *et al.*, 2012; 2013; Mograbi *et al.*, 2015). Where a tree had multiple stems, individual stems were measured, summed up and assigned to a single tree. In total 237 trees were inventoried during the field campaign.

### 3.3.2. Terrestrial Laser Scanner (TLS) data

TLS data was acquired for the study area over a 51.8 ha footprint around the flux tower in September 2015 using a RIEGL VZ-1000. The instrument uses a near infrared laser beam and is suitable for forestry research. The system provides a measurement range of up to 1400 m with 5 mm repeatability (RIEGL, 2015) (Table 3-1). Thirty scans were acquired around the flux tower at 300 kHz (limiting the range to 450 m) with an angular resolution of 0.015 degrees. Reference points determined by Real-Time Kinematic Global Navigation Satellite System (RTK-GNSS) measurements (Baade & Schnullius, 2016) were used to georeference the scans to the WGS84 ellipsoid. RiSCAN PRO software (provided by RIEGL) was used for the co-registration of the scans and point cloud generation. The point clouds were an octree data structure with a mean point density and a spacing of 286.27 points/m<sup>2</sup> and 0.05 m, respectively. To produce the pit-free CHM, the point clouds were processed using LAStools rapidlasso GmbH (Isenburg, 2016), following the method used in Khosravipour *et al.*, (2014) and substituting the platform from airborne to non-airborne to adapt the process to TLS data.

Table 0-1. Riegl VZ-1000 specification (RIEGL, 2015)<sup>1</sup>.

Laser Wavelength	Near Infrared
Scanning method	Rotating multi-facet mirror (V); rotating head (H)
Field of view	100° vertical, 360° horizontal
Laser beam divergence	0.3 mrad
Laser beam footprint	13.5 cm at 450 m, 70 cm at 1,400 m *
Laser pulse repetition rate	70–300 kHz
Measurement rate	29,000–122,000/s
Scan speed	3–120 lines/s (V); 0–60°/s (H)

---

<sup>1</sup> The entire laser beam footprint is 0.7 m at 1400 m but for this study it was restricted the footprint to 0.134 m at 450 m

For ease of manageability, the point clouds were divided into 250 Mb large tiles with a 25 m buffer. ‘*lasground.exe*’ was used to extract bare-earth by classifying ground and non-ground points. All z-values above 0.1 m were dropped. ‘*lasthin.exe*’ was further used to simulate the diameter of the laser beam at 135 mm in 450 m distance from the scan position (Lim *et al.*, 2003). To replicate each point eight times in a discrete circle, a radius of 0.075 m around every input point was used, and the spatial resolution of the point clouds was then increased two-fold to 0.03 m. Noise and unclassified points were filtered from ground points.

### ***3.3.3. Individual tree measurement from TLS point clouds***

TLS tree measurement was carried out as visualised in Figure 3-8 and was aimed at computing TLS-based AGB values around the TLS footprint. To derive individual trees from TLS point clouds (PC), QuickTerrain Reader, QTR (Applied Imagery, 2017) was used to identify and mark all visible trees from classification view using locational markers. The locational markers (with coordinates) were then exported to the Environmental Systems Research Institute’s (ESRI) shapefile format. Trimble’s RealWorks Viewer (Trimble, 2016) was further used in manual tree height and DBH measurement. Derivation of a tree DBH relied on the sufficiency in the number of point clouds required in reconstructing the circular tree trunk (circumference) at 1 m height, a decision made based on the standard deviation of the surrounding points to those used in reconstructing the circumference. Trees whose point clouds were insufficient to reconstruct the circumference at 1 m height were left out, while those with a standard deviation less than 0.03 m were inventoried. Tree heights were measured as the distance between the lowest and the highest point from the normalised point clouds. For multiple stems, both H and DBH were measured, summed-up and assigned to one tree. From the PCs, it was only possible to reconstruct tree trunks, with most shrub vegetation giving high errors and so were not used in the subsequent biomass computation.

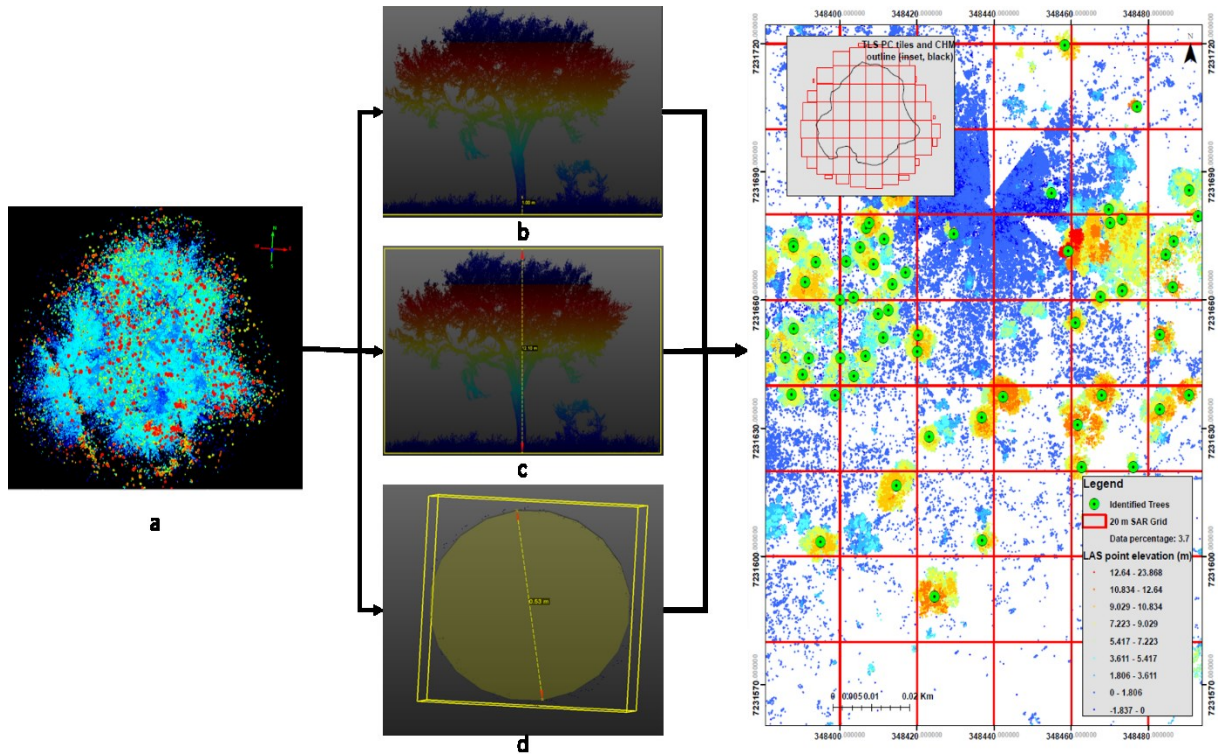


Figure 3-8. Individual tree parameter measurement from TLS point clouds: a) noise-reduced point clouds showing individual trees within the study area, b) tree DBH measurement at 1 m height, c) tree height measurement as the distance between the lowest surface-level.

### 3.3.4. TLS Canopy Height Model (CHM)

Whereas pits would be expected within TLS data just like in Lidar data, there still existed height variations within forest stands and so these were accounted for by computing CHM at different height thresholds as recommended in studies by Ben-Arie *et al.*, (2009) and Khosravipour *et al.*, (2014). The American Society of Photogrammetry and Remote Sensing (ASPRS) classification of Lidar point clouds were therefore adopted by computing CHM for every class (ASPRS, 2011) as  $<0.5$  m (bare + understory),  $0.5-<2$  m (low vegetation),  $2-<5$  m (medium vegetation), and  $\geq 5$  m (high vegetation). Following this sequence, six CHMs were derived. The consecutive 5 m interval heights help in improving the original morphological structure of tree crowns. According to Scholes *et al.*, (2001), the average tree height within the study area is 9.1 m, weighed by tree basal area and so, apart from the flux tower and riverine vegetation which stand at about 24 m and above 21 m, respectively, this study confirms that most trees are below 20 m in height (Figure 3-9 (c)).

The final step involved triangulating the four CHM height thresholds (bare + understory, low vegetation, medium vegetation, and high vegetation) using ‘*blast2dem.exe*’ to create a pit-free CHM as a GeoTiff by merging all the tiles. A kill size of 0.18 was used in triangulating Triangulated Irregular Networks (TINs), a value that is three times the step size (point resolution = 0.06 m). This would ensure that only triangles three times larger than the resolution were used for CHM generation. Figure 3-9 (a, b, c) shows the resultant digital surface model (DSM), a digital terrain model (DTM), and a CHM respectively from the outlined methods.

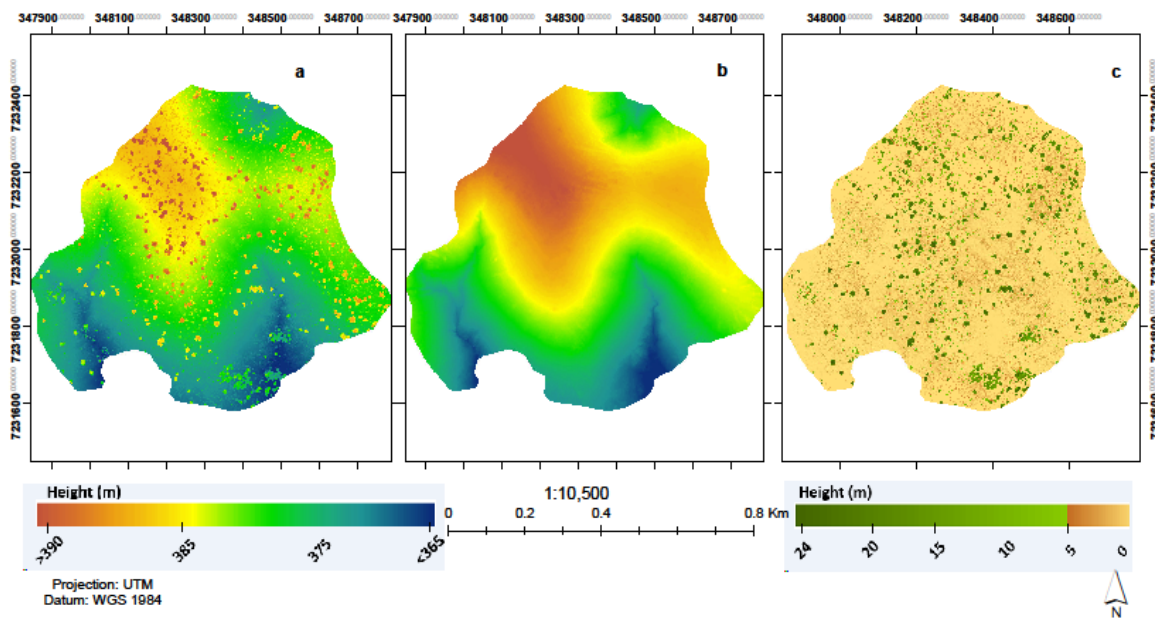


Figure 3-9. TLS-derived (a) digital surface model; (b) digital terrain model; and (c) canopy height model. (Data acquired by J. Baade).

### 3.3.5. ALOS PALSAR L-Band Data

The Japan Aerospace Agency (JAXA) launched Phased Array L-band Synthetic Aperture Radar (PALSAR), on board Advanced Land Observation Satellite (ALOS) in 2006. PALSAR is a day and night, all-weather land observation satellite and is an active microwave sensor using L-band technology to achieve this capability. ALOS acquires data in both fine beam single (FBS) and fine beam dual (FBD) polarimetric modes with a range resolution of between 0 and 60 degrees. This study used four scenes with dual (HH, HV) polarisations for the dry season, since TLS data was acquired during the dry season. Backscatter works well in the dry season because of low canopy and soil moisture (Naidoo *et al.*, 2015; Urbazaev *et al.*, 2015). Table 3-2 shows the specifications of L-band SAR datasets used in this study.

Table 0-2. Characteristics of the L-band Advanced Land Observation Satellite (ALOS) Phased Array L-band Synthetic Aperture Radar (PALSAR) and C-band Sentinel-1 A datasets used in the study area. (Source: JAXA).

Mode	Date	Polarisation	Incident Angle (°)	T	F	Season
FBD	29 September 2010	HH-HV	34.3	586	6680	DRY
FBD	11 August 2009	HH-HV	34.3	586	6680	DRY
FBD	23 September 2008	HH-HV	34.3	586	6680	DRY
FBD	6 August 2007	HH-HV	34.3	586	6680	DRY

### 3.3.6. Sentinel-1A C-Band Data

Level-1 Ground Range Detected (GRD) Sentinel-1A C-band (frequency = 5.405, wavelength = 3.8 - 7.5 cm) data was acquired in Interferometric Wide Swath (IW) mode with an Ascending pass. 29 dual-polarimetric (VV, VH) Sentinel-1 A images used in this study were acquired for the period between 3.11.2015 and 28.10.2016. Figure 3-10 shows mean backscatter values for the dates of dual polarisation C-band SAR acquisition, with soil moisture and precipitation.

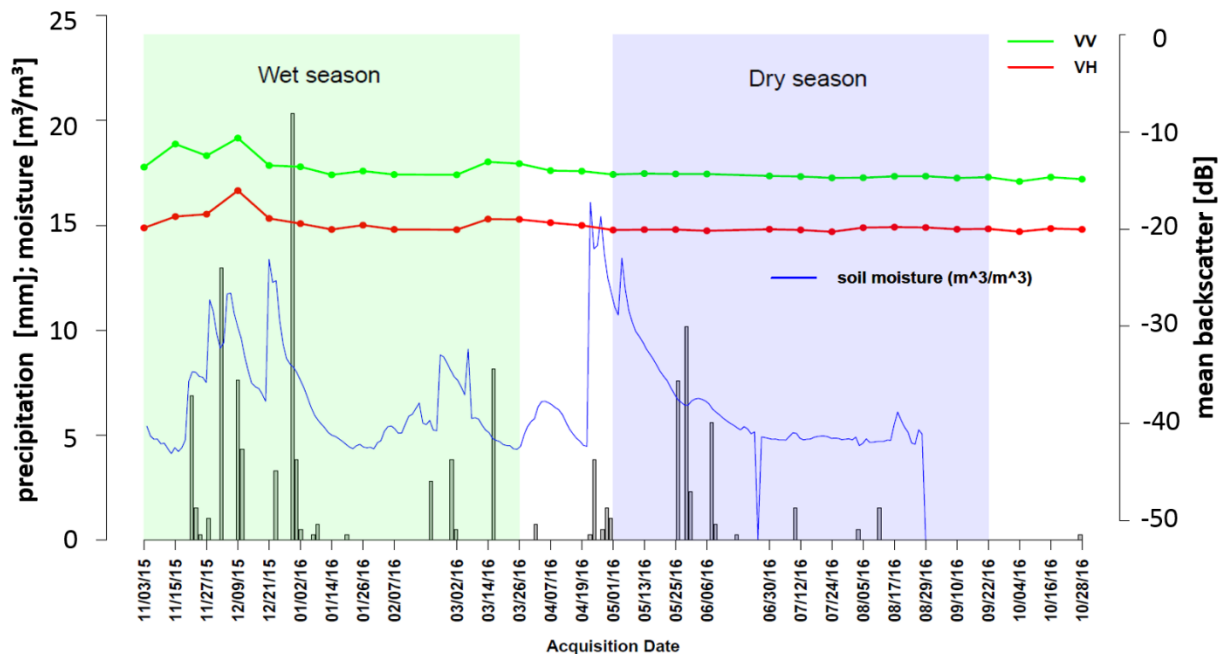


Figure 3-10. C-band Sentinel-1A time series data showing the dates of acquisition used in this study, as a response to precipitation and soil moisture content. Soil moisture data was derived from flux data in Skukuza.

### 3.3.7. SAR data processing

Both L-band ALOS PALSAR and C-band Sentinel-1A datasets were processed following methodologies adopted in Carreiras *et al.*, (2012). GAMMA Remote Sensing and Consulting AG Modular SAR Processor (MSP) was used in SAR data pre-processing (GAMMA, 2008) according to the simplified workflow in Figure 3-11. The L-band SAR datasets were acquired as level 1.1 single look complexes (SLC) with original radar geometry (range,  $R_g \times$  azimuth,  $A_z$ ) of  $9.37 \text{ m} \times 3.2$ , respectively, hence the first processing procedure was to apply multi-looking (ML) to derive backscatter intensity values. Since the C-band Sentinel-1A data was acquired in GRD, the images are already radiometrically corrected and re-sampled. The processing steps involved multi-looking (ML) to reduce speckle by averaging range and azimuth resolutions, reducing the image dimension and speeding up SAR image processing. Image calibration was performed on the ML image to convert the digital numbers (DN) to physical quantities in sigma naught ( $\sigma^0$ ) backscatter. A conversion from linear to logarithmic units in decibels (dB) enhanced image visualisations. Terrain correction was then performed to project the C-band images onto map system and correct for distortions because of terrain. For L-band SAR, a sensor specific calibration factor of  $-115 \text{ dB}$  was used to radiometrically calibrate the ML images.

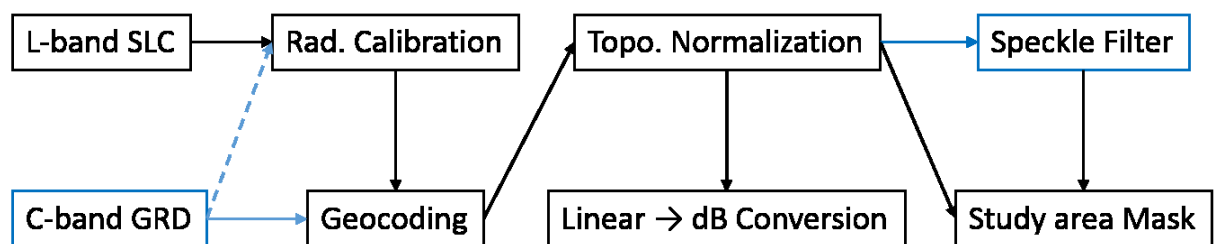


Figure 3-11. L- and C-band SAR processing workflow in GAMMA as used in this study. The blue boxes are more relevant for GRD C-band data which does not require multi-looking.

The backscatter images were then geo-coded using a 20 m digital elevation model (DEM) by first generating the positional look-up table for each pixel in the SAR Range-Doppler and DEM geometry (Carreiras *et al.*, 2012). This was followed by simulation of SAR intensity from DEM to map geometry and a further transformation to SAR geometry. The final geo-coding

procedure involved the co-registration of real and simulated SAR in SAR geometry, and the transformation of SAR Range-Doppler to map geometry.

To investigate speckle noise in the SAR datasets, the equivalent number of looks (ENL) was calculated by dividing the mean square backscatter intensity by variance (e.g.,  $ENL = \text{mean}^2/\text{variance}$ ) after studies by Oliver & Quegan (2004). The ENL was derived using a theoretical approach based on the nominal number of looks and the signal-to-noise ratio (SNR) according to Equation (3-1) because of heterogeneity of the study area.

$$ENL = \frac{N_r * N_{az}}{\left(1 + \frac{1}{SNR}\right)^2} \quad (3-1)$$

where  $N_r$  and  $N_{az}$  are the number of range and azimuth looks, respectively. An increase in the ENL significantly reduces speckle noise in the multi-looked SAR data (Urbazev *et al.*, 2015). Argenti *et al.*, (2013) suggested that no filtering should be attempted on heterogeneous (point targets) areas. This applies to the current study area, and so no speckle noise filtering was performed on the L-band ALOS PALSAR data. However, to investigate the effects of speckle filter window size for C-band SAR backscatter on savanna vegetation structure variables (AGB, CC and cover classes), multi-temporal speckle filter was applied on C- band SAR dataset. This was achieved by using Quegan multi-temporal filter (Quegan & Yu, 2001) with two different filter window sizes; 3 x 3 and 5 x 5. Topographic normalisation was then applied to the backscatter intensity images (Stussi *et al.*, 1995; Castel *et al.*, 2001). The final resultant geocoded, and terrain corrected backscatter SAR images had a ground resolution of 12.5 m and 20 m for L-band ALOS PALSAR and C-band Sentinel-1 A, respectively.

### **3.3.8. Ancillary datasets**

In this study climate data was used, mainly soil moisture and precipitation datasets obtained from Skukuza Flux tower, operated by South Africa's Council for Scientific and Industrial Research (CSIR). The soil moisture was measured using a CS-616 Soil Moisture Probe (Campbell Scientific Inc., Logan, UT, USA). This ground station comprises two soil moisture probes, which are acquiring volumetric moisture content ( $m^3/m^3$ ) at 6 cm, 13 cm, 26 cm and 59 cm depths. For this study, only moisture information from 6 cm and 13 cm probes were used. The values from both probes were averaged for each time step to one soil moisture

measurement. The 30-minute interval datasets were summarised to daily averages and matched with the dates of C-band Sentinel-1 data acquisition for the study area. Long-term precipitation records from the rain gauge mounted on the Skukuza EC flux tower were used (Figure 3-10).

### 3.4. Aboveground Biomass (AGB) Modelling

#### 3.4.1. Field Derived Biomass

Field-based AGB was computed with height and DBH datasets from field inventory in three steps. First, height and basal diameter of each tree was used to compute AGB at tree level in kilogram (kg) using Colgan allometry (Colgan *et al.*, 2013), as per Equation (3-2). This allometric equation was preferred because there is no species specific allometry derived for this region of KNP, or for many of the individual species found in the site. The Colgan allometry used in this study was derived from destructive tree samples located outside of the park, within a *Colophospermum mopane* dominated savanna north of the study site. Many of the tree species sampled are commonly found in KNP and so is within this Lowveld savanna, with a recommendation on a mean wood specific gravity ( $\rho$ ) of 0.9 (Colgan *et al.*, 2013).

$$AGB = 1.09D^{(1.39 + 0.14\ln(D))}H^{0.73}\rho^{0.80} \quad (3-2)$$

Where AGB is the aboveground biomass (kg/tree), D is the basal diameter (cm), H is tree height (m) and  $\rho$  is a unit less wood specific density (-). Second, all individual tree biomass within each plot (30 m) was summed up, resulting in AGB in kg per plot. Biomass is usually expressed per unit area and so the final biomass was reported in metric tons per hectare (t/ha) after conversion based on the plot size of 0.09 ha for 30 m plots. Table 3-3 summarises the results from inventoried tree variables from field inventory measurements, while Figure 3-12 (a) shows field plot biomass distribution within the study area, in t/ha.



Table 0-3. Summary statistics of the field inventoried and TL-measured trees. DBH = diameter at breast height (basal diameter); H= tree height; AGB = aboveground biomass.

	<b>Field tree inventory</b>			<b>TLS tree measurement</b>		
	<b>DBH (cm)</b>	<b>H (m)</b>	<b>AGB (kg/tree)</b>	<b>DBH (cm)</b>	<b>H (m)</b>	<b>AGB (kg/tree)</b>
<b>Min.</b>	6.4	1.5	2.9	11	5.3	27.4
<b>Median</b>	35	6.2	267.1	30	10.7	666.9
<b>Mean</b>	35.2	6.2	508.1	39.6	10.7	779.3
<b>Max.</b>	105	12	5825.6	70	16.1	3528.5

### 3.4.2. TLS Derived reference Biomass

A total of 757 trees were identified in the normalised TLS point clouds, of which some 565 trees had both their height and basal diameter measured because of sufficiency of PCs to reconstruct the tree circumference at 1 m height. These constituted the trees used in AGB estimation. For biomass estimation, the allometry in Equation (2-2) was used (Colgan *et al*, 2012). All measured individual tree biomass within each 0.04 Ha (20 m Sentinel-1A pixel) plot was summed up into kg per 0.04 Ha plot. These were then converted to tons per hectare using a plot conversion factor of 0.04 Ha. The results from TLS individual tree measurements are summarised in Table 2-3, while plot level averages are visualised in a histogram in Figure 3-12 (b).

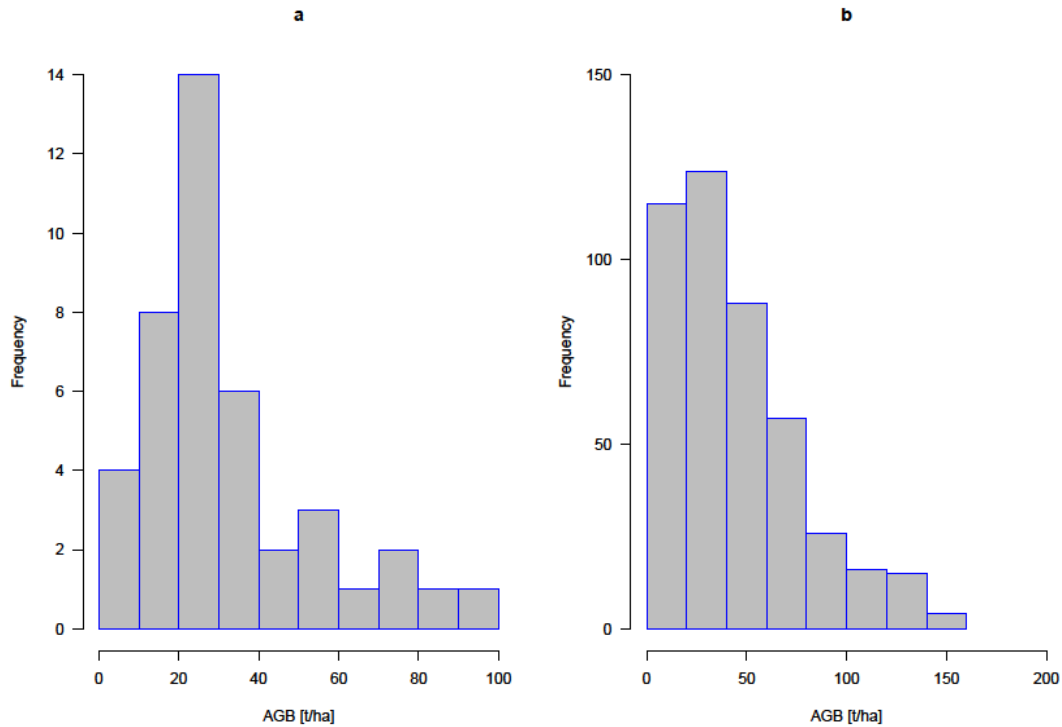


Figure 3-12. Plot-level aboveground woody biomass distribution from a) field inventory and b) TLS tree measured datasets.

To assess the effects of multi-temporal C-band SAR on AGB per SAR pixel, AGB was classified into three classes based on abundance: low biomass, as plots with AGB below 10 t/ha ( $n = 57$  plots), moderate biomass as plots with AGB between 30 – 40 t/ha in the study area ( $n = 67$  plots), and high biomass as plots with AGB values above 80 t/ha ( $n = 61$  plots) in the study area (Figure 3-13-a). These class values were plotted separately against SAR in a temporal graph. The means of each class was computed and plotted against the various multi-temporal SAR metrics – backscatter and SAR speckle filter windows 3 by 3 and 5 by 5.

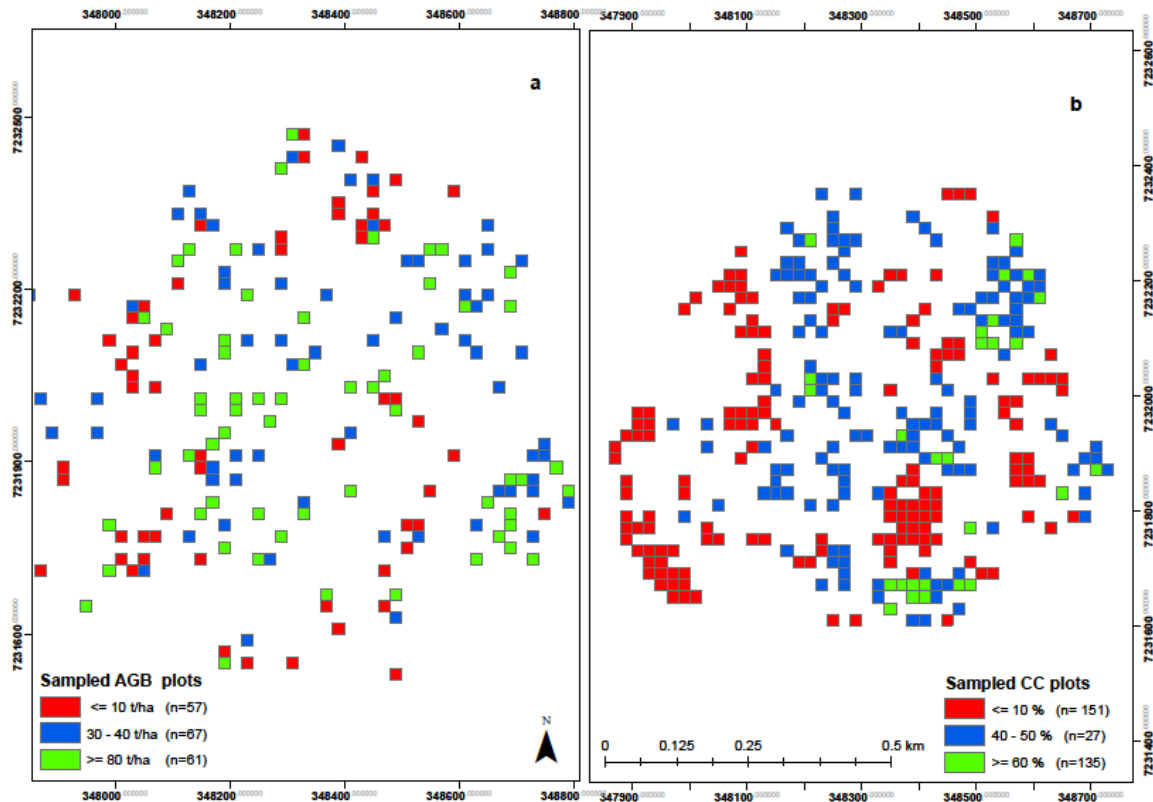


Figure 3-13. Sampled 20 m plots for assessment of C-band SAR backscatter metrics response to a) AGB plots and b) CC plots.

### 3.4.3. TLS CHM-Modelled Biomass

In this study, field inventory data were used to model AGB based on TLS CHM metrics. The 0.06 m TLS-derived CHM was used in Trimble’s eCognition 8.9 (Trimble, 2016) to delineate individual tree canopy cover and height. Pixel-based chessboard segmentation at a scale of 1 (0.06 m resolution) was performed on the CHM, with the 30 m field plots as a thematic layer to restrict cover proportions to the 30m grids. Out of the 42 field inventoried plots, only 33 full plots fell within the TLS footprint, and so these were used as reference data in deriving AGB from TLS canopy metrics. A height threshold of 1 m was used to delineate pixels for canopy cover and canopy height based on field inventory, where only trees with heights >1 m were inventoried.

The >1 m height ensured only woody vegetation contributed to biomass for the study area. CC, defined as the area of tree crowns projected onto the horizontal plane ignoring small gaps within the crown and allowing tree crown overlap (Scholes *et al.*, 2001), was computed as the area of

the 30 m grid with pixels having a height > 1 m, as a proportion of the area of the entire grid, expressed in percentage. Canopy height on the other hand, is defined as the mean height of pixels with a > 1 m height per 30 m grid. Equations 3-3 and 3-4 show simplified formulas used to derive these two metrics, as modified from Colgan *et al.*, (2012). An additional CHM metric was computed as the product of CC and CH (Figure 3-14), forming the third biomass predictor variable,  $CC \times CH$ .

$$CC = \frac{\sum \text{pixels with } H > 1 \text{ m/plot}}{\text{Total pixels/plot}} \quad (3-3)$$

$$CH = \sum \text{mean pixels } H > 1 \text{ m per plot} \quad (3-4)$$

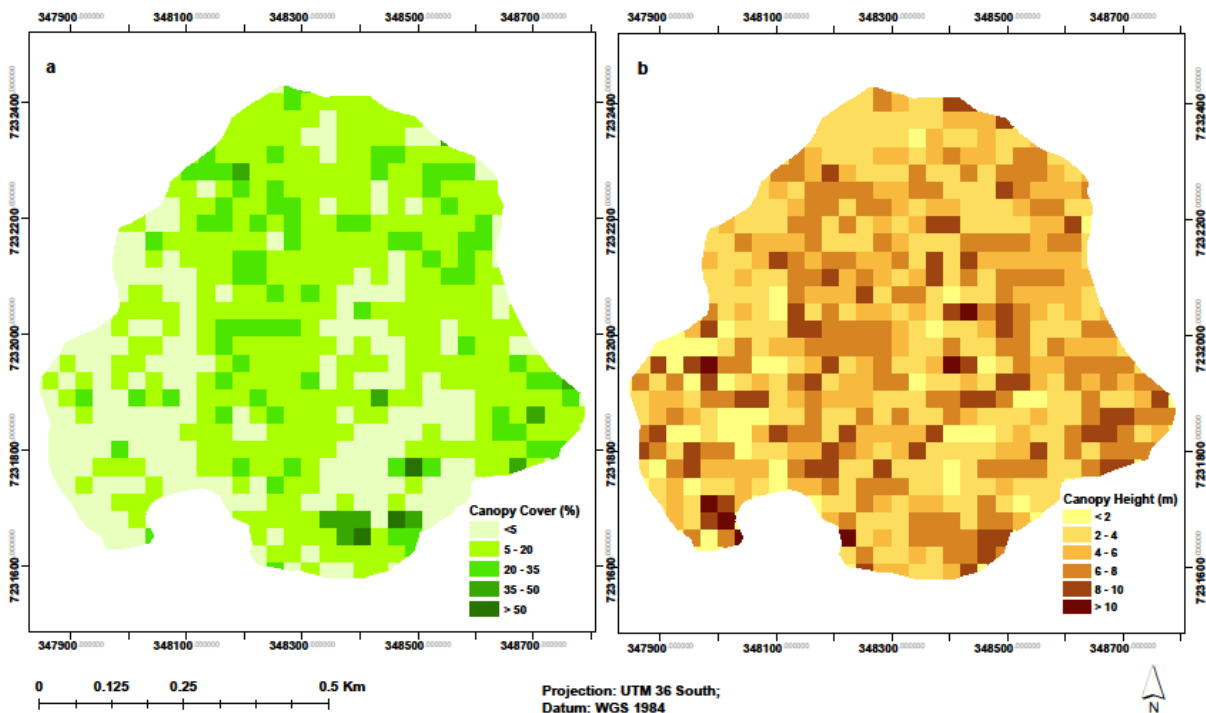


Figure 3-14. TLS-derived (a) Percentage canopy cover (CC) and (b) canopy height (CH) for 30 m plots around Skukuza flux tower site.

For assessment of multi-temporal C-band SAR response to CC, a second set of CC was computed for the 20 m SAR pixel grids within the study area. This was implemented within eCognition, using the same procedure in section 2.4.3. First, chessboard segmentation was used

to segment the 0.06 m TLS-derived CHM at a scale of 1 (each resultant pixel's grid has a dimension of the resolution similar to the CHM). All CHM pixels with height above 1 m were classified as "vegetation" and were further used in computing CC. CC was computed as the proportion of CHM pixels with height above 1 m ("vegetation") within each 20 m SAR grid, to the total number of CHM pixels within each 20 m SAR pixel grid. To assess the multi-temporal SAR response to CC, just like in the case with AGB, CC was classified into three abundance classes: low CC with those plots having CC below 10% (n = 151), moderate CC with CC between 30% and 50% (n = 135) and high CC with CC more than 60% (n = 27) per pixel/plot, totalling a sample of 313 sample plots (see Figure 3-12-b above). For class separability assessment, the means of each of the three CC classes were computed and plotted against multi-temporal C-band SAR metrics between November 2015 and October 2016 to assess the effects of SAR polarisation, speckle filter window and seasonality to these mean CC classes.

The study assessed the predictive performance of each CHM predictor (CC, CH and CC x CH) on the field AGB to select the best amongst the three metrics. A linear regression model was used to predict biomass over the TLS footprint, using field computed AGB. 60% of the field AGB dataset was used for the regression model calibration, and the remaining 40% for validation of the resulting predictions. To assess the linearity, the study looked at the model performance in terms of the resultant root mean square error (RMSE) and bias (Equations 3-5 and 3-6) from correlating the TLS metrics with both log-transformed AGB (AGB<sub>log</sub>) and normal AGB values (Chai & Draxler, 2014). To assess error distribution with AGB, residuals were computed (Equation 3-7) as the difference between observed and predicted AGB for every TLS metric.

$$\text{RMSE} = \sqrt{\frac{1}{n} \sum_{i=1}^n e_i^2} \quad (3-5)$$

$$\text{Bias} = \frac{1}{n} \sum_{i=1}^n y_i - \check{y}_i \quad (3-6)$$

$$\text{Residuals} = y_i - \check{y}_i \quad (3-7)$$

The predictors were also fitted against the log-transformed AGB ( $AGB_{log}$ ) and the resultant residuals from both the field biomass and log-normal biomass used to select the model for deriving AGB from TLS data, based on variance. Studies by Nickless *et al.*, (2011) and Colgan *et al.*, (2013) both propose modelling the logarithm of field AGB because DBH has a stronger linear relationship with  $AGB_{log}$ .

A comparison was carried out between the field measured height and the TLS-derived CH to assess the level of accuracy. Figure 3-15 shows the relationship between field-measured height and the TLS-derived CH<sup>2</sup>. The results show accuracy in field height measurement reducing with increasing height, with higher heights showing overestimation by the laser rangefinder. This is because CH is plot averaged 0.06 m pixels with > 1 m height.

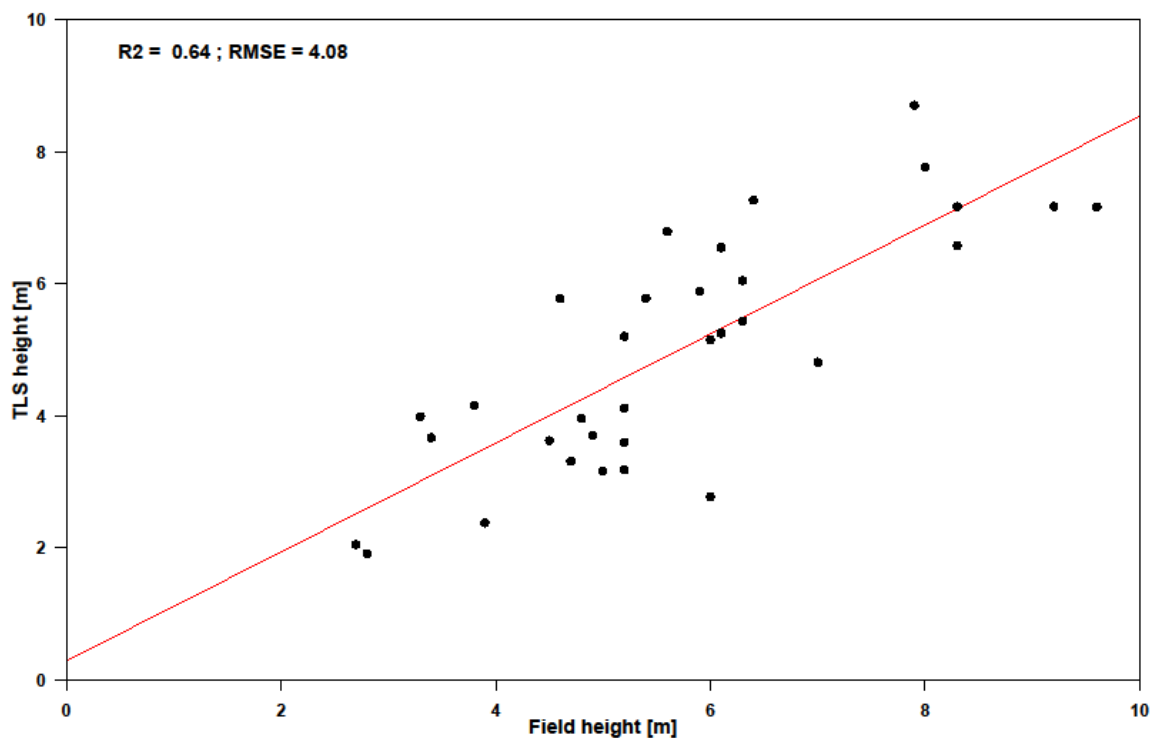


Figure 3-15. Validation results of field measured height and TLS canopy height

### 3.4.4. Estimating Aboveground Biomass from SAR

To compute AGB from L-band SAR, a weighted average of TLS AGB ( $AGB_{tls}$ ) was used, because of the difference in resolution between the reference TLS-derived AGB (30 m) and the

---

<sup>2</sup> CH is plot averaged pixels with mean height above 1 m, and is not absolute height

L-band SAR backscatter intensity (12.5 m) datasets. The contribution of field biomass to the intersecting 12.5 m SAR  $\sigma^0$  pixels were assessed by computing the area of pixels within each 30 m by 30 m field plots to get a weighted area,  $W_a$ . The AGB per intersecting object ( $AGB_{new}$ ) was computed as the product of  $AGB_{tls}$  and  $W_a$ . Chessboard segmentation was performed on the L-band SAR images in eCognition with a scale of 1 (12.5 m), and the resultant pixels were intersected with  $AGB_{tls}$ . An assessed SAR  $\sigma^0$  AGB based on polarisations (HH and HV) was performed, the years under investigation (2007–2010), and a combination of both using random forest and linear regression algorithms for polarimetric and yearly AGB estimations, respectively. Breiman *et al.*, (1984) and Breiman (2001) proposed random forest, RF as ensemble learning for regression and classification trees, with successive trees not dependent on earlier trees (bootstrapping). In bagging, the best predictors are randomly chosen to split the tree, making RF a robust classifier against over-fitting (Liaw & Wiener, 2002). A script for this analysis was written in R statistical package. The analysis involved identification of the raster pixels within each reference AGB polygon. This was run on all the pixels within all four SAR backscatter raster grids.

#### ***3.4.5. Aboveground Biomass Change Analysis***

Three image difference analyses were performed in ENVI, ArcGIS, and R statistical packages. Relative AGB changes per pixel for each of the three change combinations was investigated: 2007 to 2008, 2008 to 2009, and 2009 to 2010 for the study area. To decide whether a change was significant, R statistical package was used to reclassify both SAR backscatter predicted AGB and AGB change rasters at 5 t/ha intervals because the resultant SAR predictions had standard deviations less than 5 t/ha. The predicted biomass was then overlaid with a 2014 land cover map of the study area (Odipo *et al.*, 2016). This allowed us to assess the effects of such a change on land cover.

### **3.5. Savanna vegetation cover classes and canopy cover**

The coexistence of trees, shrubs and herbaceous vegetation within a savanna biome complicates monitoring initiatives at both localised and regional spatial scales. Separating the savanna vegetation cover classes allows an understanding of factors responsible for the typical heterogeneity within these ecosystems. Grass and herbaceous vegetation are critical for

monitoring fuel loads and how these affect fire regimes and spatial distribution of grazers. Shrub and tree vegetation are important in assessing the carbon stock and distribution of browsers and mega herbivores. In this study, TLS-derived CHM is used in the separation and classification of savanna vegetation cover classes after methodologies proposed in the works of Vaughn *et al.*, (2015) and Naidoo *et al.*, (2012). OBIA was implemented in eCognition (Trimble, 2017) to classify the 0.06 m resolution CHM into five savanna vegetation cover classes through a height thresholding, with background (< 0.5 m), shrubs (0.5 – 2.5 m), small trees (2.5 – 5 m), medium trees (5 – 10 m) and large trees (> 10 m). Figure 3-16 is a photo taken in March 2015 of Skukuza study area, a typical Lowveld savanna showing vertical vegetation stratification upon which height thresholding was based.

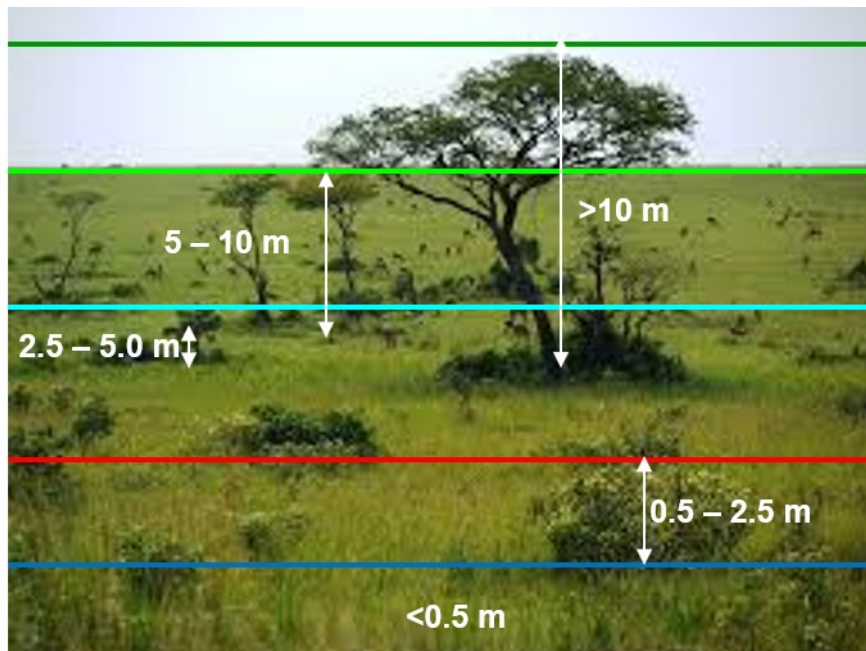


Figure 3-16. A photo showing savanna vegetation cover classes in Skukuza, Kruger National Park in March 2015. (Photo courtesy: Victor Odipo).

Chessboard segmentation was applied on the CHM, and each class was assigned based on the pixel values. The pixels with EC tower were first classified and removed based on user knowledge, visualisation and height. 20 m SAR pixel grids were created over the study area and was used to compute not only pixel-level savanna vegetation classes but also AGB and CC for the study area. The OBIA-derived classes were exported as ESRI shapefiles where these classes were intersected with 20 m SAR grids, then further dissolved based on grid/pixel IDs



to separate the classes within grids/pixels. For pixel-level analysis, proportion of each of the 5 classes was computed to allow selection of dominant classes (pure or near pure pixels) per grid/pixel. For each cover class based on proportion of cover (dominant class) per grid, 12 samples with higher proportion of cover per class were selected, making the total samples used,  $n = 60$ . Figure 3-17 below shows the proportion of class distribution within each of the 60 sampled 20 m grids, while Table 3-4 shows the range of sampled grids with pure or near pure (dominant) cover classes. First, the 12 samples per class were plotted against multi-temporal C-band backscatter values, then a mean from the 12 samples were computed per class and plotted for comparison on their separability (Chapter 4). Further, to assess the magnitude of separability in terms of backscatter intensity (dB), the difference between classes were computed, giving rise to 5 separability classes: large and medium, large and small, large and shrubs, medium and small, and medium and shrubs.

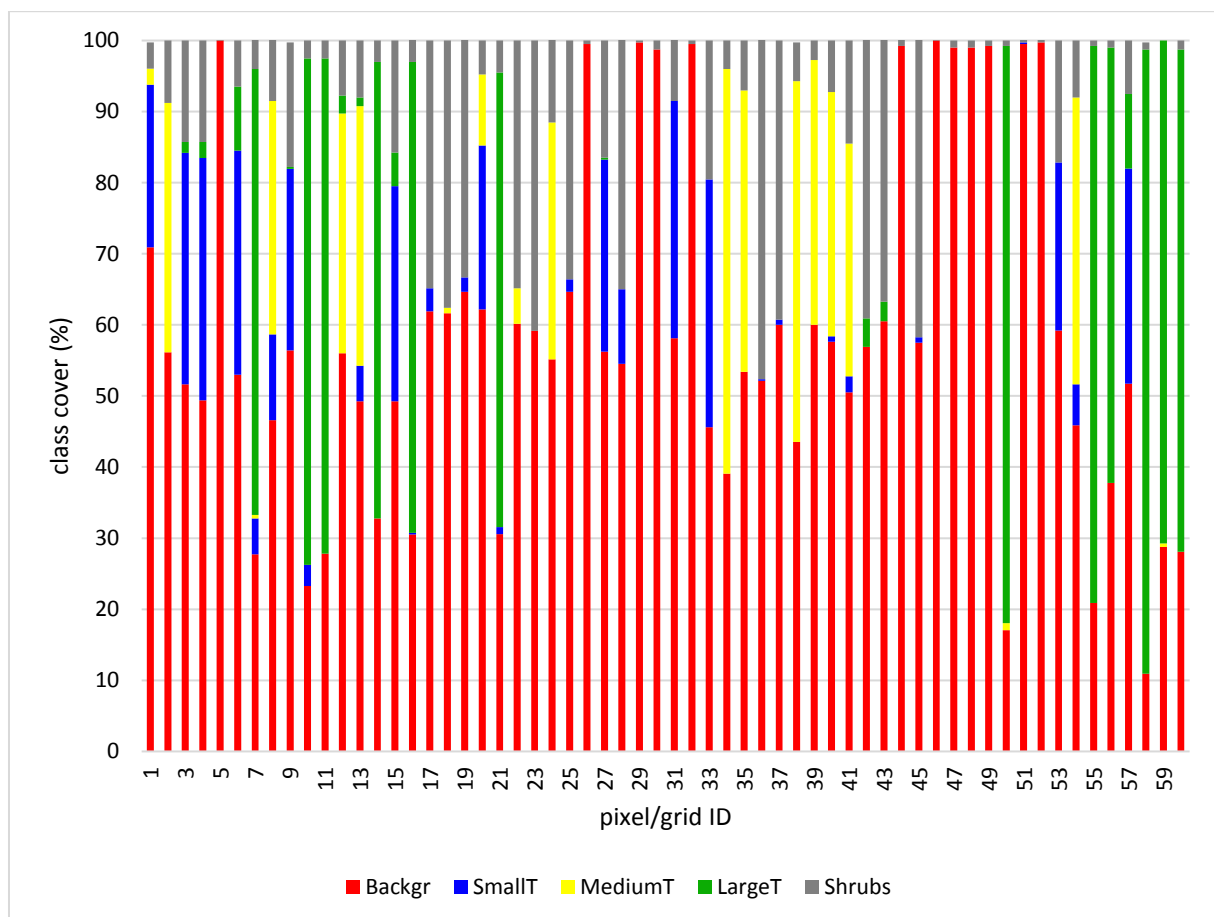


Figure 3-17. Cumulative bar graphs showing proportion of class distribution within each of the 60 sampled 20 m grids.

Table 0-4. Summary statistics of the sampled vegetation cover classes based on dominant class (%) per grid.

	<b>COVER CLASS</b>				
	<b>Grass &amp; background</b>	<b>Shrubs</b>	<b>Small trees</b>	<b>Medium trees</b>	<b>Large trees</b>
MAXIMUM	100	48	35	57	87.8
MINIMUM	11	0	0	0	0

29 C-band SAR scenes with dual polarisations (VV, VH) were used, from which the four SAR metrics were derived, with an aim of assessing their sensitivity to the vegetation structure variables within a 20 m SAR pixel. For each polarisation, multi-temporal data was subdivided into two seasons, dry (May to September) and wet (November to March) according to climate information in section 2.2.1 shown in Figures 2-1 and 2-2, leaving out transitional months (April as a transition between wet to dry season, and October as a transition between dry to wet season). Multi-temporal speckle filter was applied on the SAR backscatter datasets according to Quegan & Yu (2001) within two moving windows, 3 by 3 and 5 by 5, to assess the effects of speckle filter window size on SAR sensitivity to savanna vegetation. Savanna vegetation variables as the dependent variables were therefore computed from TLS datasets (CHM and point clouds) for each of the 20 m SAR pixels within the study area. Besides the AGB and CC abundance classes, the mean of each of the two variables was also computed. This is because the classification into abundance classes left out some data points. By computing the mean for all AGB plots and CC plots, all the range of datasets are captured in the plots.

### **3.6. Conclusion on methodology**

This section gave a description of the methods adopted in answering the research questions of this study and ultimately achieving the study objectives outlined in Section 1.5. An in-depth description of the study area has been made in Section 3.2, giving emphasis to the factors that affect vegetation dynamics within the area including but not limited to climatic conditions, soil and topography and vegetation characteristics. An overview of the microwave datasets used in modelling savanna vegetation structure within the study area, mainly L- and C-band SAR, has been presented in sections 3.3.5 and 3.3.6 respectively. For validation of SAR modelled structure variables, two reference datasets have been used, field inventory data which was

acquired in the wet season and TLS data which was acquired in the dry season. For both the SAR and reference datasets, an in-depth description of their acquisition and processing has been presented. The results from the methods adopted in this section and summarized in Section 3.1 form the basis of the next chapters.

# CHAPTER 4

## 4. Results

### 4.1. Field and TLS Biomass

Figure 3-12 (a) shows the distribution of field biomass per tree as computed from field inventory data, while Figure 4-1 is a map showing the spatial distribution of field inventoried plots within the study area. The mean AGB within the inventoried 30 m plots was  $31.9 \pm 21.3$  t/ha, with a range between 3.1 t/ha for the plot with the lowest biomass and 94.3 t/ha for the plot with the maximum biomass, consistent with estimates from similar studies carried out around KNP by Nickless *et al.*, (2011); Colgan *et al.*, (2013) and Mograbi *et al.*, (2015). The trees within the inventoried plots had basal diameter ranging between 6.4 and 105 cm, and height of between 1.5 (inventory targeted trees with  $H > 1$  m) and 12 m, with mean of 35 cm and 6.2 m for basal diameter and height, respectively. From the plot in Figure 4-2, it is evident that basal diameter has a larger impact on the estimation of AGB than does tree height. Most inventoried trees contributed biomass (modal biomass) ranging between 20 and 30 t/ha, as can be seen from the field biomass distribution in Figure 2-11 (a).

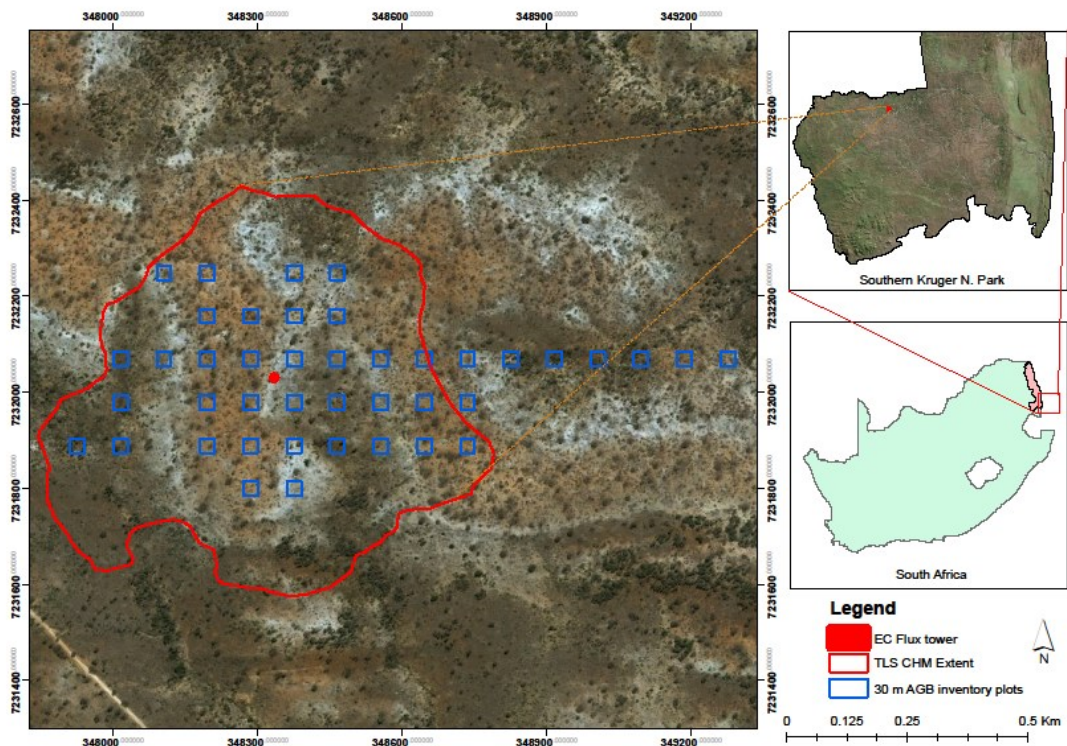


Figure 4-1. Distribution of 30 m field inventoried plots around Skukuza eddy covariance (EC) flux tower, and the extent of TLS data footprint (Background imagery source: Google Earth).

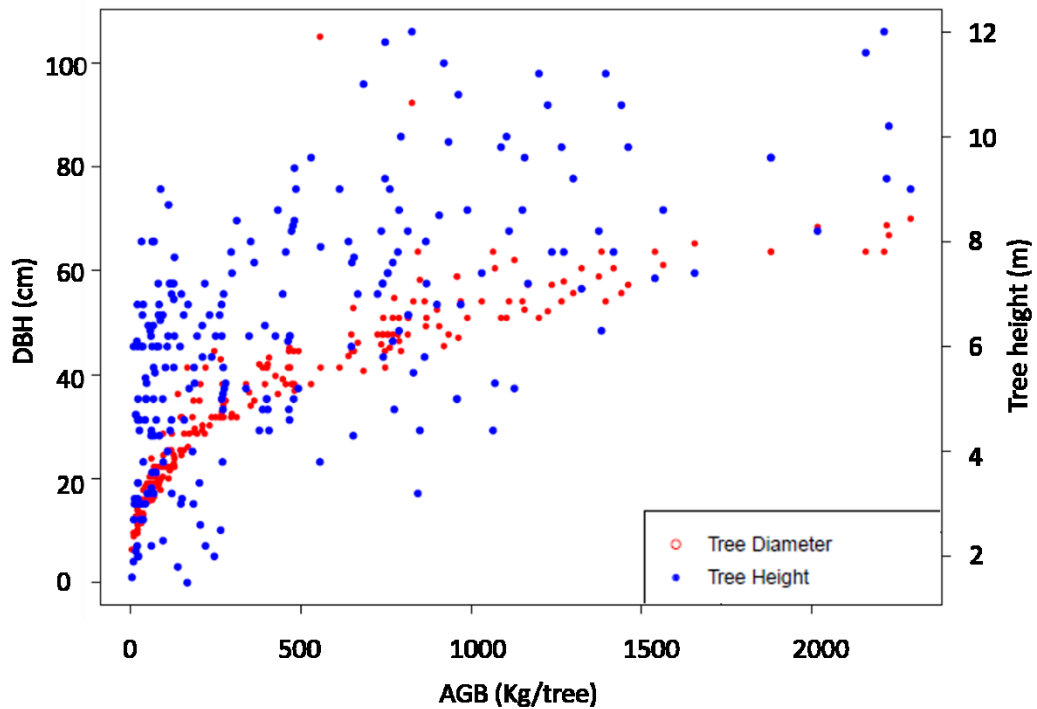


Figure 4-2. Tree height, diameter, and the resultant AGB per inventoried tree within the study area.

Figure 4-3 is a map showing spatial distribution of plot-level AGB computed from TLS data. On average, there were at least one tree or shrub within the 20 m plots, with some plots recording up to three trees, mostly multi-stemmed shrubs. Of the 674 identified trees from TLS data, only 565 had enough point clouds at 1 m height to reconstruct their circumference necessary for DBH measurement. The measured basal diameter ranges between 11 and 70 cm, with a mean of  $39.6 \pm 12.9$  cm. The individual tree heights ranged between 5.3 to 16.1 m, with a mean of  $10.7 \pm 1.7$  m. The 565 trees fell within 445 Sentinel-1 pixels around the TLS footprint, here referred to as AGB plots. The mean plot AGB from TLS measured trees is  $35.6 \pm 32.7$  t/ha, with a range of 1.2 t/ha and 145.9 t/ha within the 445 sampled plots (Figure 4-3).

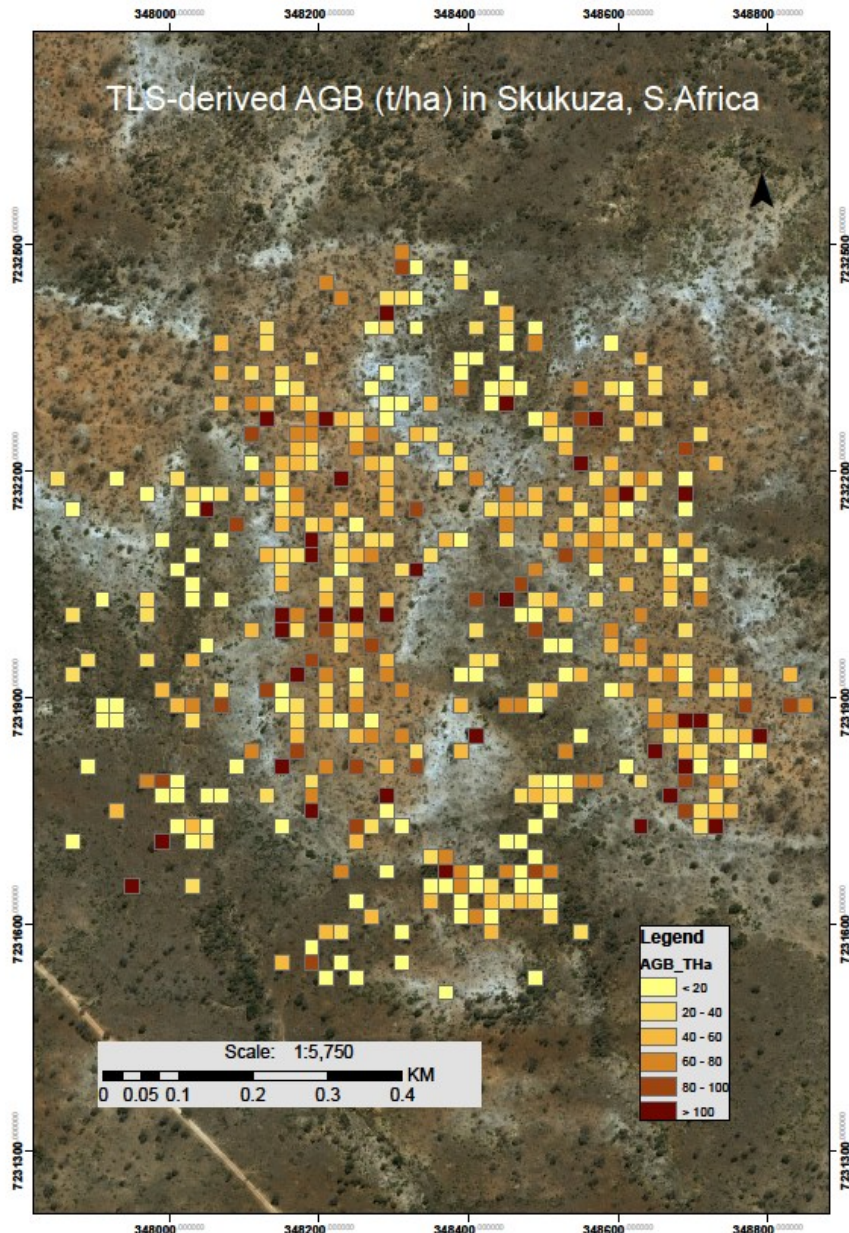


Figure 4-3. Map showing biomass distribution within 445 reference plots derived from TLS point cloud tree measurement within the study area. (Background imagery source: Google Earth).

Results from the 237 field inventoried trees show variability with regards to AGB across the plots (Figure 4-4), with a total woody biomass of 120,414 kg. The mean AGB for all field inventoried trees in the entire study site was 508.1 kg. The observed mean ( $\pm$  error margin) from all the 42 plots was estimated at  $535.9 \pm 95.1$  t/ha (at 95% confidence interval, CI: 441 to 631) as shown in the plot in Figure 4-4. Two plots (Id No. 322 and 716) recorded higher biomass values, with a total of three plots at 95% CI falling outside the overall mean plot biomass (31.9 t/ha) of the inventoried trees.



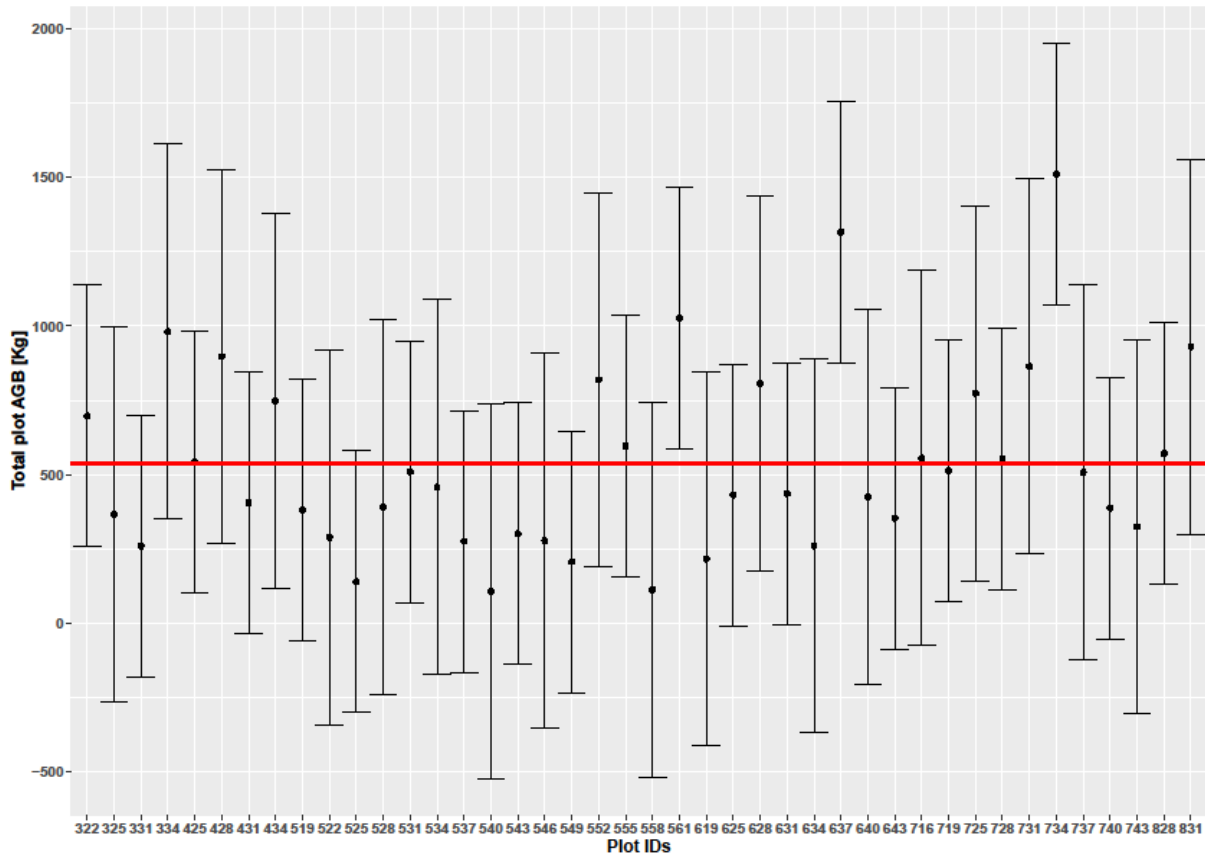


Figure 4-4. Biomass estimates for each of the 42 sampled plots in kg. The red line shows the mean AGB in kg while the bars are 95% confidence intervals for AGB. Each plot is 0.09 ha in size.

#### 4.2. SAR-TLS Biomass Prediction Models

L-band ALOS PALSAR data was used to model AGB for the study using TLS-derived CHM metrics, CC and CH. Table 4-1 summarizes field AGB performance to TLS-derived metrics and L-band SAR backscatter intensity performance to TLS-derived AGB, with correlation plots in Figure 4-5. As expected, biomass values showed correlation with all the TLS metrics and L-band SAR backscatter. Of the three TLS metrics, a product of canopy cover and canopy height (CC x CH) outperformed the individual metrics, CC or CH, with the latter two resulting in RMSE of 4.77 t/ha and 2.13 t/ha, respectively. This is in congruence with observations made by Colgan *et al.*, (2012). From these results, it is evident that variance increases with increasing AGB as evidenced by the large deviation of plot value from mean AGB value in the study area.

Table 0-1. TLS and microwave AGB predictor variables and associated error and coefficient of determination ( $R^2$ ).

<b>Predictors</b>	<b>RMSE (t/ha)</b>	<b>Mean AGB<math>\pm</math> <math>\sigma</math> (t/ha)</b>	<b>Bias</b>	<b>R<sup>2</sup></b>
CC	4.77	32.2 $\pm$ 26.73	1.27	0.91
CH	2.13	34.2 $\pm$ 24.43	-0.57	0.47
CC x CH	2.32	34.2 $\pm$ 30.78	-0.62	0.99
SAR-HH	6.7	32.2 $\pm$ 14.54	-0.21	0.63
SAR-HV	6.1	32.2 $\pm$ 14.29	-0.26	0.74
SAR-2007	9.3	19.92 $\pm$ 2.6	0.19	0.47
SAR-2008	3.9	20.07 $\pm$ 3.0	0.4	0.5
SAR-2009	4.6	20.24 $\pm$ 4.8	-0.6	0.61
SAR-2010	12.7	19.72 $\pm$ 5.2	-0.3	0.48

Studies by Nickless *et al.*, (2011) proposes log transformation of biomass to stabilize variance to achieve homoscedasticity. TLS metrics were therefore correlated with both non-transformed and log-transformed plot biomass values (Figure 4-5) and further an assessment of the resultant errors from SAR backscatter prediction using product of the two TLS metrics as reference. From these results, it is evident that variance increases with increasing AGB as evidenced by the large deviation of plot value from mean AGB value in the study area. Studies by Nickless *et al.*, (2011) proposes log transformation of biomass to stabilize variance to achieve homoscedasticity. TLS metrics were therefore correlated with both non-transformed and log-transformed plot biomass values as shown in Figure 4-5 and further an assessment of the resultant errors from SAR backscatter prediction using product of the two TLS metrics as reference.



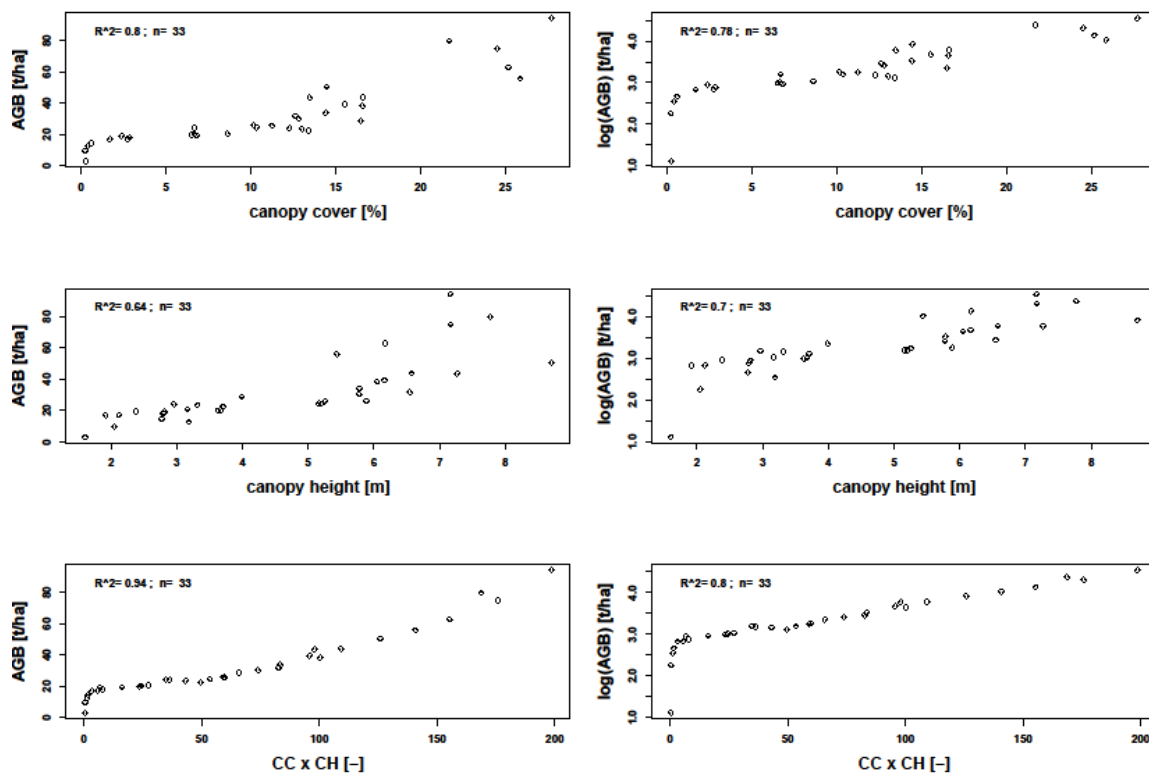


Figure 4-5. Correlation between TLS canopy cover height metrics and AGB and log (AGB).

The error distribution in L-band SAR AGB prediction by the various TLS predictor variables is shown Figure 4-6. The figure shows the regression plots for L-band SAR predicted AGB against the reference TLS-derived AGB. For the individual metrics, CC and CH, there is randomness in AGB distribution along the 0-horizontal line, while for the product of CC.CH, this is not the case, with most positive residual values. This further explains the log-transformation applied on the AGB to reduce the heteroscedasticity and variance. The residuals further show the level to which L-band SAR is sensitive to AGB within this area, beyond which there is error propagation in such prediction, here between 60 and 100 t/ha. TLS-derived biomass has RMSE lower than 5 t/ha. The error (RMSE) obtained from predicting AGB using TLS metrics as reference is higher (6.7–6.6 t/ha for HH and HV, respectively) than that derived from field inventoried biomass values (2.1–4.8 t/ha). This is due to additional error which results from step-wise prediction, where the field reference AGB was used to model TLS reference AGB for use in modelling AGB for the entire study area, and so it is assumed errors are propagated at every modelling stage.

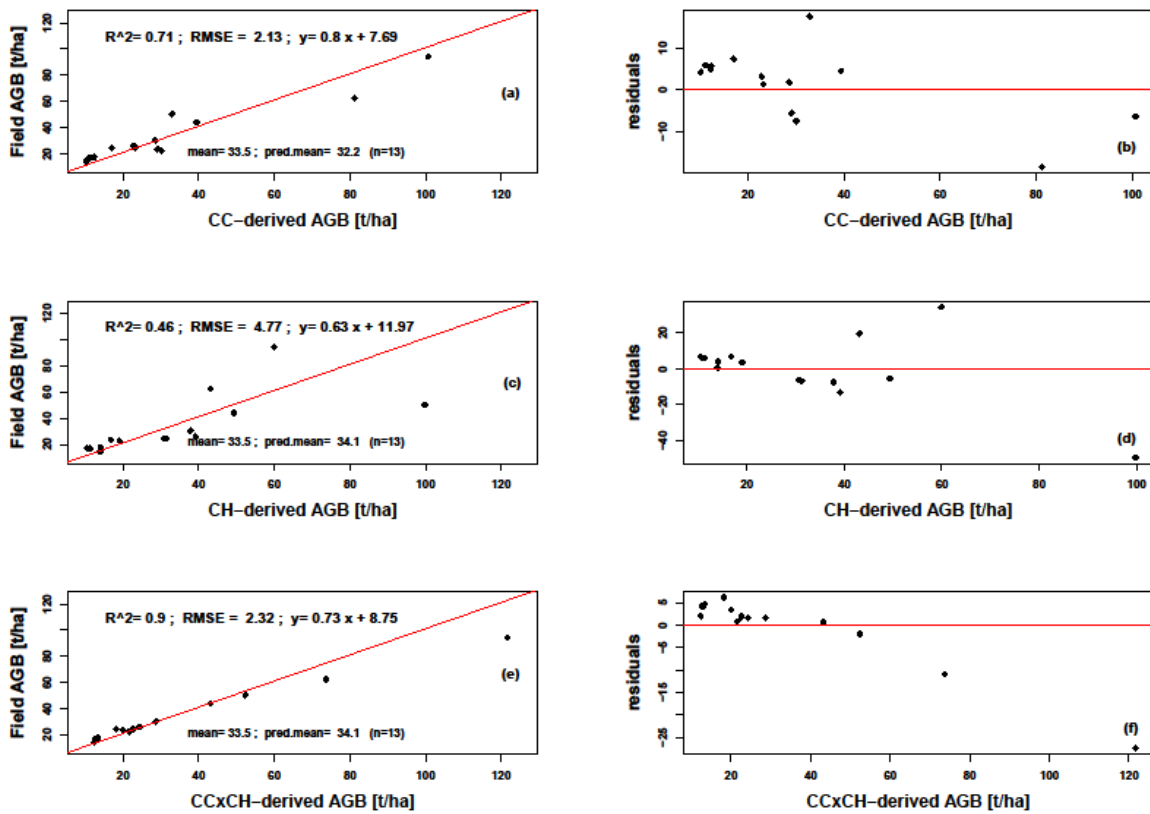


Figure 4-6. Regression and residual plots between TLS metrics derived AGB and field. CC denotes canopy cover, CH denotes canopy height, and RMSE denotes root mean square error

This is the case because the field data points derived from 33 field plots were few, and so the TLS-predicted or modelled AGB provided more reference data points necessary for landscape-wide AGB estimation. There is biomass underestimation by the SAR modelling, as can be seen in both low mean biomass and the negative bias estimates. SAR modelled AGB had a mean of 32.2 t/ha, which is lower than those from TLS metrics. All AGB predictors yielded mean biomass ranging between  $19.7 \pm 5.2$  t/ha for the 2010 SAR backscatter-based prediction, and  $34.2 \pm 30.78$  t/ha for the product of the TLS cover and height prediction. All these values are within the range of typical of biomass estimates within the Lowveld savanna as presented by previous studies within this ecosystem.

### 4.3. Radar Sensitivity to Biomass

This study evaluated the sensitivity of SAR backscatter to AGB in two ways. First, individual backscatter intensity was assessed, and then the SAR modelled biomass were assessed. Biomass

per plot was computed by weighting  $\sigma^0$  (dB) values based on area proportion intersecting the TLS-AGB pixels. A weighted biomass per intersection was then computed. A regression analysis between the  $\sigma^0$  and AGB showed that these two metrics were strongly correlated. An assessment on the response of  $\sigma^0$  to AGB was performed in three ways: first, the dual-pol multi-temporal SAR response was assessed; second, polarimetric response (HH and HV) was assessed as visualized in Figure 4-7. Lastly, yearly AGB was estimated to assess the multi-temporal, inter-annual SAR backscatter response to AGB for the four years, between 2007 and 2010.

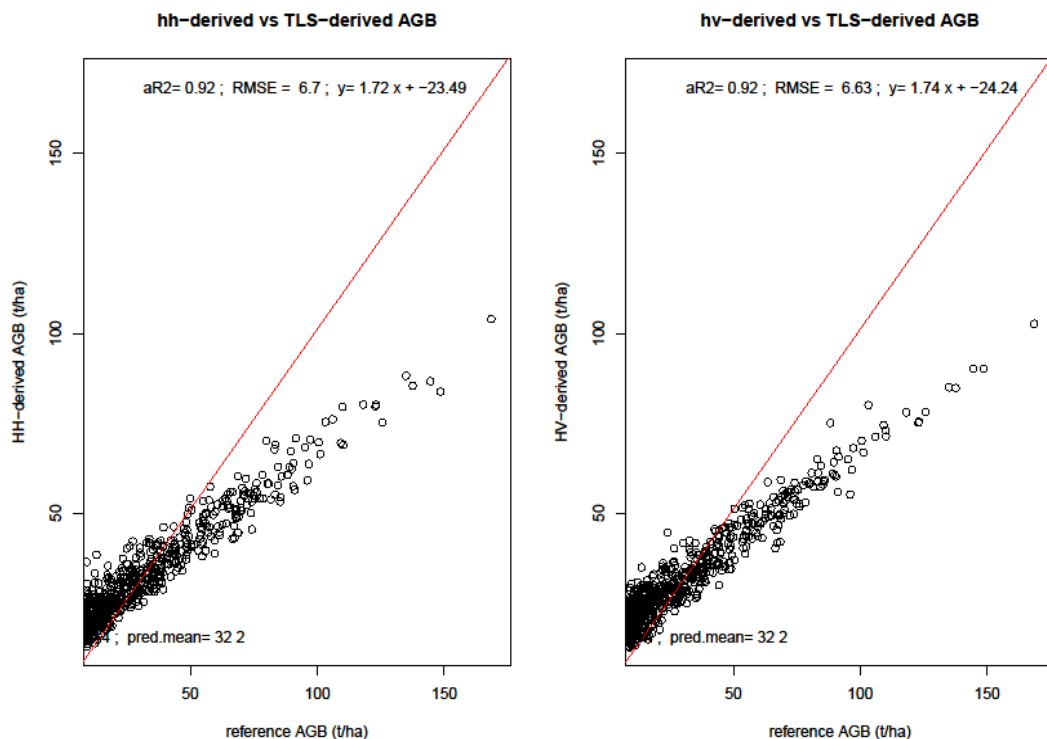


Figure 4-7. Correlation between L-band SAR-derived biomass and reference TLS-metrics derived biomass. The graphs show co- and cross polarised L-band ALOS derived AGB responses

Generally, L-band SAR underestimated AGB, with a mean AGB  $\pm \sigma$  of  $32.2 \pm 14.54$  and  $32.2 \pm 14.29$  for SAR co-polarised HH and cross-polarised HV, respectively, in comparison to TLS-metrics derived AGB. Lower AGB estimates were recorded when the polarisations for individual years combined, with 2007 and 2010 recording the lowest AGB of  $19.9 \pm 2.6$  t/ha and  $19.7 \pm 5.2$  t/ha, respectively. Figure 3-9 shows the biomass maps derived from combined datasets, different polarimetry, and individual years, using RF and linear regression models.

#### **4.4. Biomass Change Detection**

Figure 4-8 shows L-band SAR modelled AGB for the study area over the four-year period, covering dry seasons for the years 2007, 2008, 2009 and 2010. Since all the four SAR datasets were acquired during the dry season, sensor and incident angle from an ascending pass, a comparison of AGB between these years was possible with three band differencing combinations ( $t_2-t_1$ ); 2008 – 2007, 2009-2008 and 2010-2009. The temporal SAR AGB estimation for the three years yielded mean AGB ranging between the lowest in 2007 at  $19.9 \pm 2.6$  t/ha and the highest in 2009 at  $20.2 \pm 4.8$  t/ha. The study assessed the relative change in AGB within the study area over the four years of study. Generally, there was an observed slight increase in mean AGB between the years 2007 and 2009, but the overlap in the confidence intervals of the estimated AGB over this period makes the increase nonsignificant. Therefore, a relative change analysis over the four years covered by the SAR data was performed. First, biomass was reclassified with 5 t/ha interval AGB classes, followed with an assessment of the areas within the study area which experienced changes in the AGB with an increase or decrease above and below 5 t/ha AGB respectively, between the years was carried out.

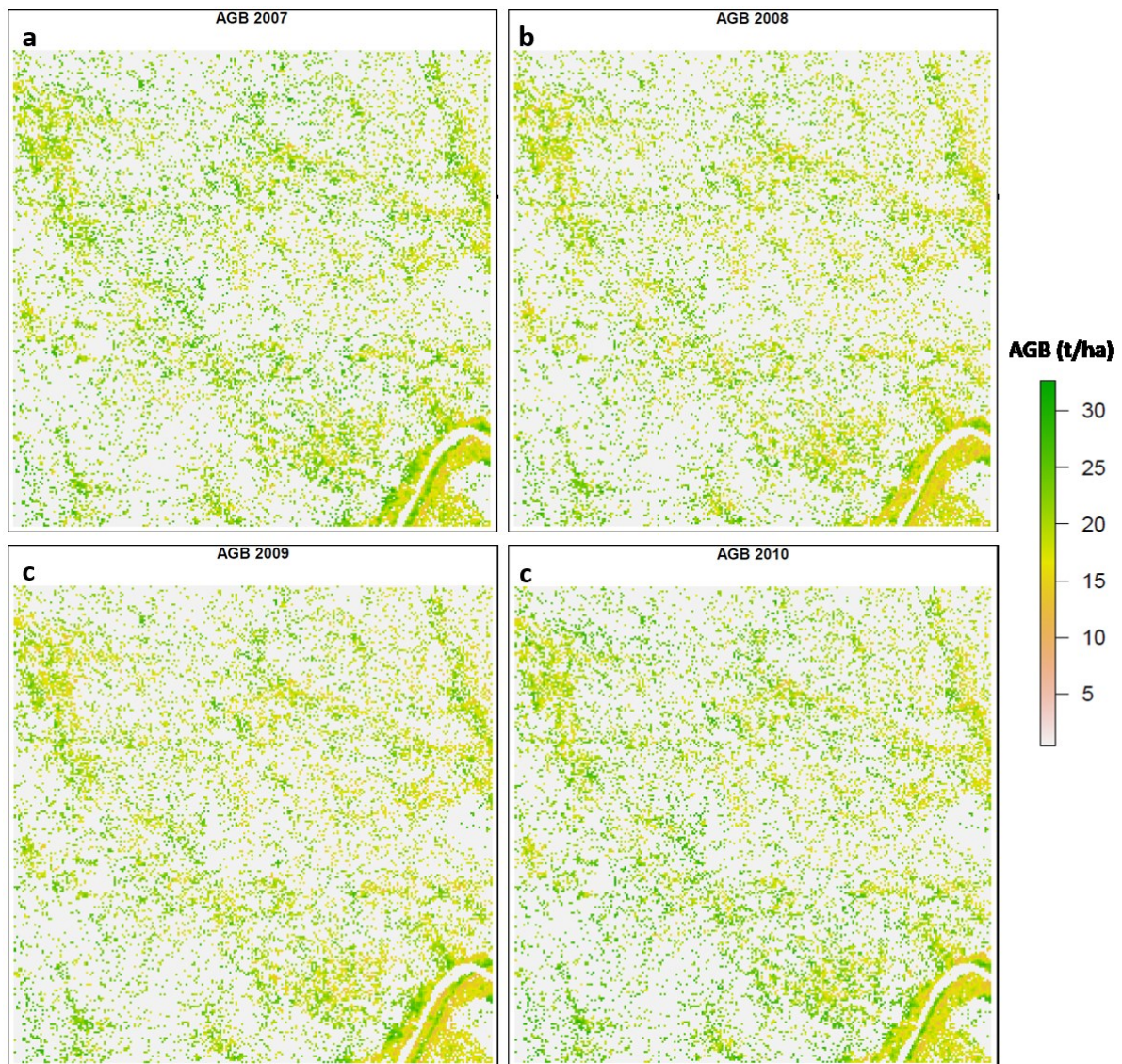


Figure 4-8. Predicted woody biomass from L-band SAR backscatter intensity (HH and HV) for the years 2007, 2008, 2009, and 2010

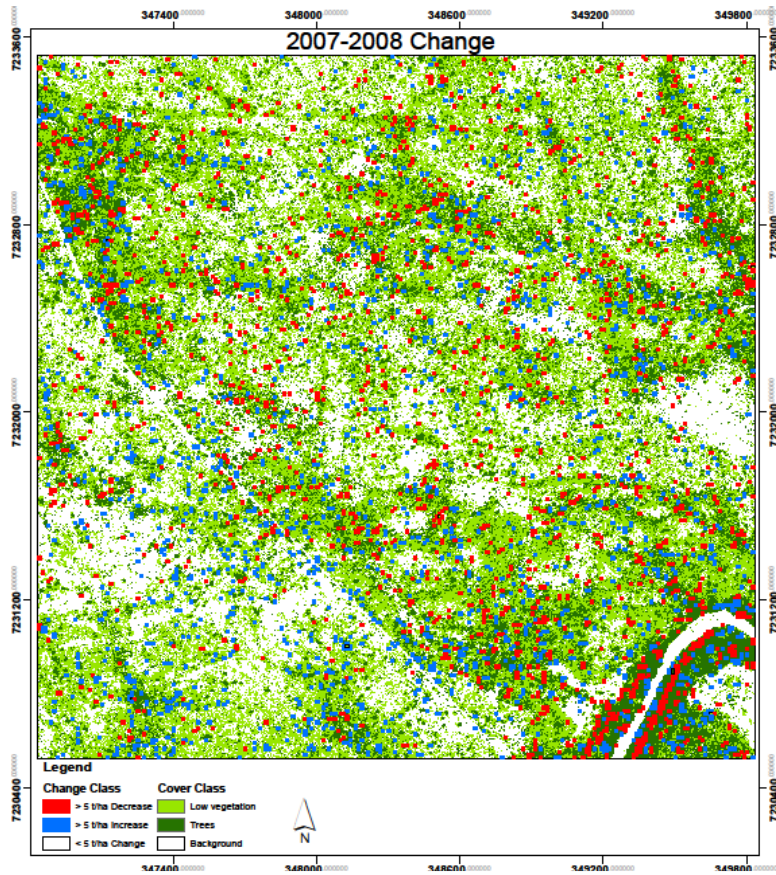
The results in Table 4-2 show an overall decrease in AGB, with 3.5% of the study area experiencing a decrease in AGB of more than 5 t/ha over the four-year period. Only 3% (27.3 ha) of the 900-ha study area showed an increase in AGB of more than 5 t/ha. Generally, biomass decreased consistently between 2007 and 2009, from 3.3% of the area with an increase >5 t/ha in 2008–2007, to 3.2% in 2009–2008, and finally, a lower 2.6% between 2010 and 2009. Conversely, the study area experienced high biomass reduction with areas experiencing >5 t/ha reduction steadily increasing from 3.2% to 3.3% and finally 4.1% for 2008–2007, 2009–2008, and 2010–2009 combinations, respectively. Over the four-year period, more than 90% of the area experienced a change in biomass of less than 5 t/ha. This constitutes areas which experienced a nonsignificant increase or decrease below the 5 t/ha threshold.

Table 0-2. Relative change in AGB in Skukuza between 2007 and 2010.

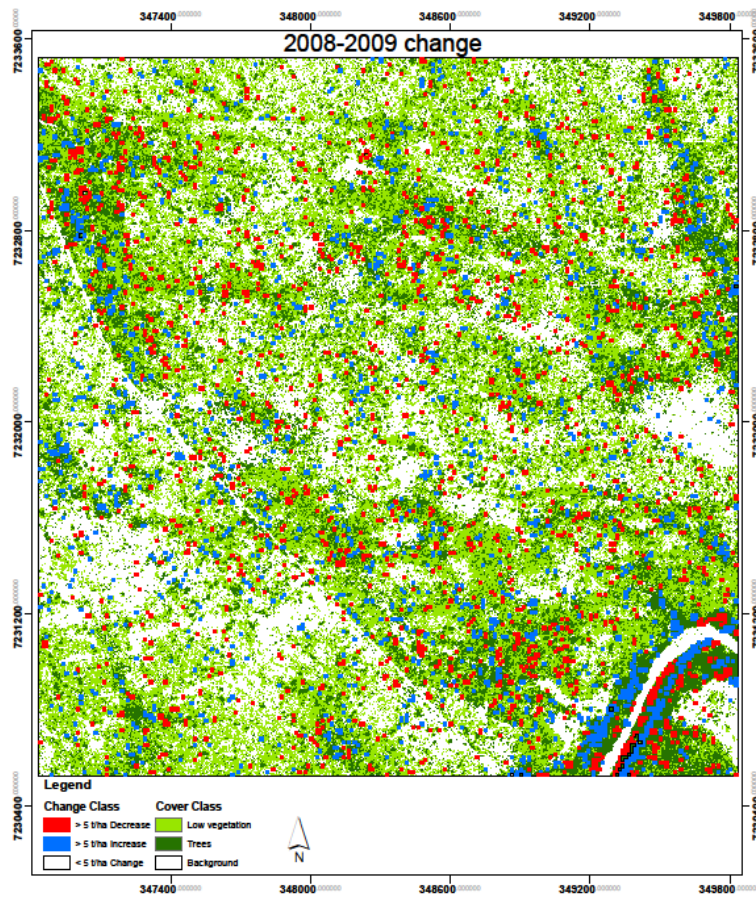
	Increase (>5 t/ha)		Decrease (>5 t/ha)		<5 t/ha	
	Area (ha)	%	Area (ha)	%	Area (ha)	%
2007–2008	29.9	3.3	28.8	3.2	841.3	93.5
2008–2009	28.9	3.2	29.9	3.3	841.2	93.5
2009–2010	23.1	2.6	37.3	4.1	839.6	93.3
Average	27.3	3.0	32.0	3.5	840.7	93.4

The cumulative change in area with >5 t/ha AGB over the four years, when summed yields a cumulative decrease in AGB within 81.9 ha (9.1%) of the study area where a cumulative increase in AGB occurred within 96 ha (10.6%) of the study area. This shows that, overall, the area with AGB above 5 t/ha was reduced for 32 ha (3.5% of the study area). From the biomass change maps in Figure 4-9, it is evident that most changes were restricted to areas around the rivers, streamlines and valleys. These areas are predominated by woody vegetation as visualized in the background land cover map in Figure 4-9. These areas are most likely to have biomass values more than 5 t/ha and changes detectable.





(a)



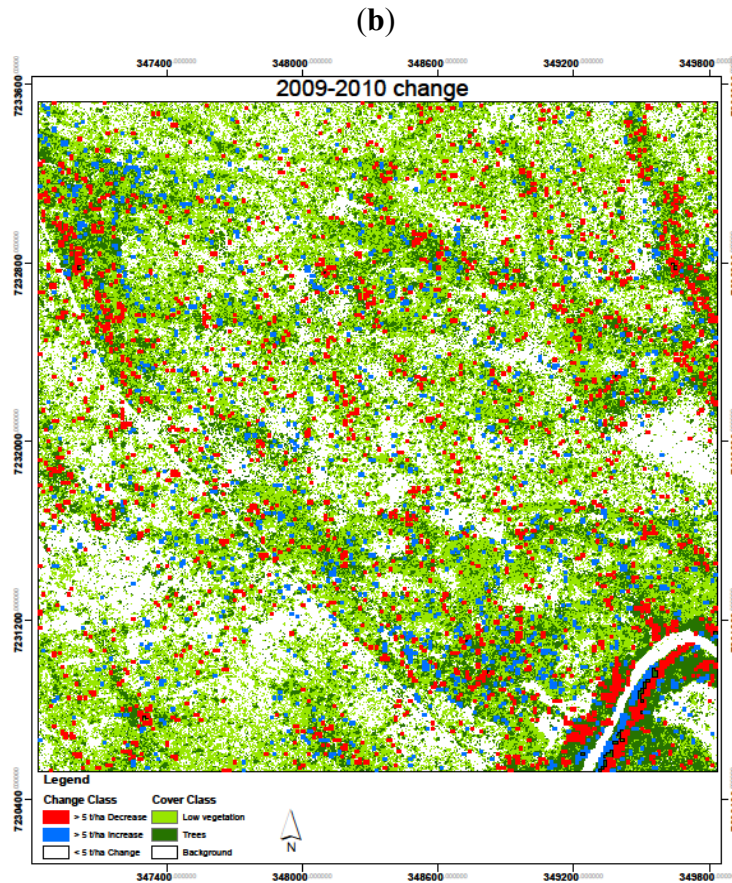


Figure 4-9. Biomass change results over the study period 2007–2010, with six change combinations with (a) 2007–2008; (b) 2008–2009; and (c) 2009–2010

## 4.5. C-band SAR interactions with savanna vegetation structure components

### 4.5.1. Interactions of C-band SAR with savanna vegetation cover

The interactions between multi-temporal C-band Sentinel-1A SAR metrics (backscatter intensity, speckle filter and seasonality) on savanna vegetation structure variables, including AGB (t/ha), CC (%) and vegetation cover classes as tree height proxy were investigated. To assess the SAR  $\sigma^0$  response to the various savanna vegetation cover classes, an intersection of every class with the 20 m SAR pixel grids made it possible to assign a dominant class for each grid. An assumption is made to the effect that despite a pixel composing multiple vegetation cover classes, the class with a higher proportion within such a pixel will contribute the most to the  $\sigma^0$  signal than the minority classes. The class with the highest proportion per pixel is referred to as the dominant class in this study. Figure 4-10 is the resultant classification from height



thresholding the TLS CHM after methods adopted in Vaughn *et al.*, (2015) and Naidoo *et al.*, (2012), and further class partitioning to compute the dominant class per SAR pixel (for example, 20 and 23 with blue borders). From Figure 4-10, the inset map and accompanying table for grid 20, background occupies some 30.6 %, small trees 1 %, medium trees 0 %, large trees 63.9 % and the shrubs 4.5 %, thus making large trees the dominant class for grid 20. Grid 23 is assigned the background class because background is the dominant class with 55.1 %, followed with medium trees at 33.3 %, and finally shrubs while small and large trees are not available in this grid. This methodology was adopted in assigning a dominant vegetation cover class to each of the pixels within the TLS footprint.

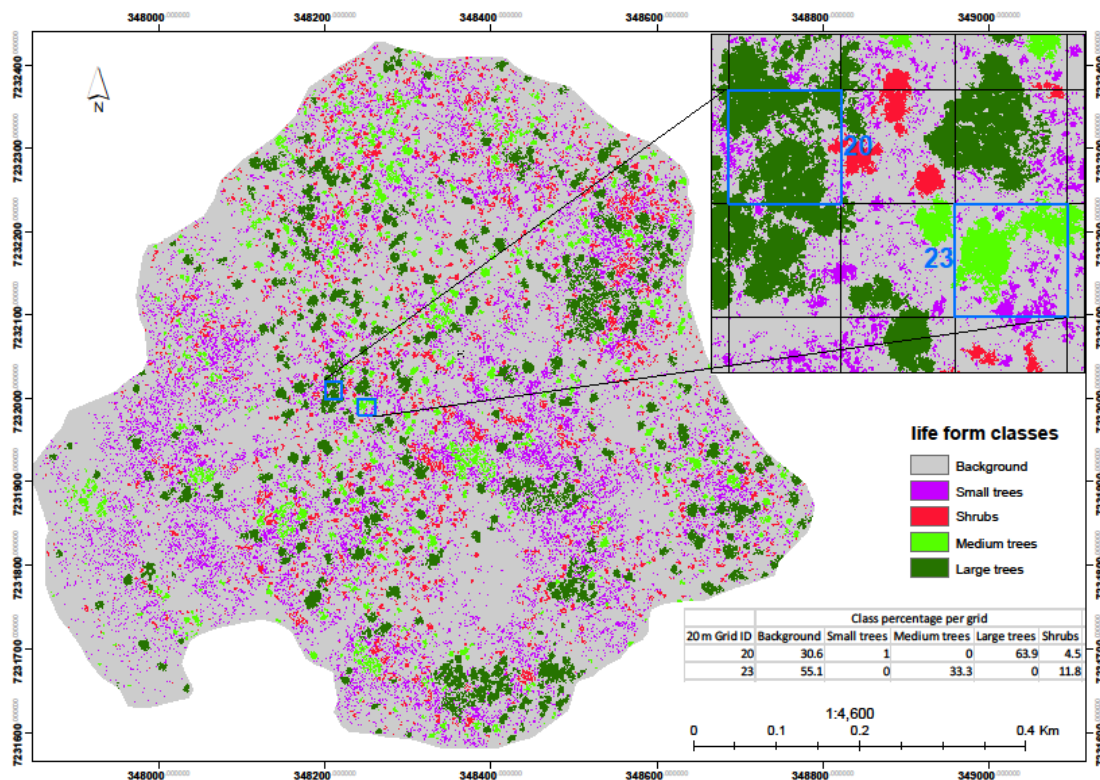


Figure 4-10. Five vegetation cover classes obtained from OBIA height thresholding the TLS CHM. Inset is the grid partition and dominant class selection.

For seasonal SAR  $\sigma^0$  response to the various structure variables, the two seasons, wet and dry are separated, with former running between November 2015 to March 2016, while the latter between May 2016 to September 2016. April and October are transition months between wet-dry and dry-wet seasons respectively and is deduced from the area's climate data analysis by Kruger *et al.*, (2002), and therefore SAR backscatter response to vegetation structure during

this period is not clear. To assess pixel-level SAR interactions with the various vegetation cover classes, the C-band SAR metrics were plotted against background over the 29 Sentinel-1 C-band SAR acquisition dates between 3.11.2015 and 28.10.2016. This period allowed assessment of seasonal response for the two polarisations (VV, VH) since it covered both dry and wet seasons. The C-band SAR metrics investigated include SAR  $\sigma^0$  and speckle filtered backscatter intensities within 3 x 3 and 5 x 5 moving windows and SAR polarisations (VV and VH).

Figure 4-11 shows the response of C-band SAR backscatter intensity (in dB) to the various vegetation classes. From the plots, VV backscatter response to all vegetation classes is higher (Figure 4-11 a) than in the VH (Figure 4-11 b) as can be seen in the backscatter coefficient ( $\sigma^0$ ) value ranges in the plots. Backscatter is higher in the VV polarization than does the VH due to depolarization of the incoming V to emitted H signal. The geometry and haphazard orientation of vegetation canopy features such as branches, twigs and trunks attenuate the signals as they bounce back and forth within the canopy “volume” and this lowers the strength/intensity of the backscattered or reflected energy back to the sensor. On the other hand, the VV does not suffer this attenuation with the signal received in the same magnitude as emitted by the sensor. However, the magnitude within which C-band backscatter is sensitive to inter-class variation is higher in the VH than in the VV. This is seen in the gap or separation between plots (inter-class dynamic ranges) in the multitemporal plots between large and small trees, high and low CC and AGB abundance classes. This inter-class separation tends to be wider/higher in the VH than it is in the VV polarization.

The  $\sigma^0$  ranges between -16 dB for small trees in the dry season (on 10.9.2016) and -10 dB for large trees in dry season (on 9.12.2015) in the VV polarisation. For the VH however, the  $\sigma^0$  range is -22 dB for small trees in both wet season (on 14.1.2016), dry season (on 10.9.2016) and -16.7 dB for large trees in the wet season on 9.12.2015. The  $\sigma^0$  response from large and medium trees is higher than from small trees in both VV and VH polarisations. The backscatter response to shrub, medium trees and background is not clear, though their response is higher than small trees but lower than large trees. These three classes seem to overlap in backscatter response because the plots cross each other at various dates, making it impossible to explain their responses individually. The difference in  $\sigma^0$  response for small and large trees is visible in both VV and VH polarisation, but more pronounced in the VH polarisation in terms of the dynamic range between the two classes. For example, after the high  $\sigma^0$  experienced on 9.12.2015, the response to large trees for the entire study period (from 21.12.2015 to

28.10.2016) ranges between -19.8 dB and -18 dB while for small trees it is from -22 dB to -20 dB (see Figure 4-11 b). VV displays two high peaked backscatter response to all cover classes on 15.11.2015 and 9.12.2015 at -10.8 dB and -10 dB respectively, while the VH response is only elevated on 9.12.2015 at -16.7 dB. On these dates, all the vegetation cover classes are displaying the same high-level backscatter response for both polarisations.

C-band SAR  $\sigma^0$  response to vegetation cover classes varies within seasons, with the plots showing high  $\sigma^0$  response in the wet season and a proportionate high dynamic range within and between classes compared to dry season for both polarisations. A closer look at the rainfall and moisture data plots for the study area during the study period in Figure 3-10 (section 3.3.6) shows that the days that experienced high backscatter response followed days of rainfall events. On 14.11.15 the area received a rainfall of 6.86 mm and on the same date the soil moisture probe had a reading of  $4.77 \text{ m}^3\text{m}^{-3}$ . The soil moisture however rose to  $7.56 \text{ m}^3\text{m}^{-3}$  on 15.11.2015. Correspondingly, this day gave a high backscatter response of  $\sim -10.8$  dB for VV. The high backscatter coefficient on 9.12.2015 for both VV and VH follows a rainfall of 20.32 mm received the previous day on 8.12.2015. The effect of this rainfall event is seen in high soil moisture of  $13.38 \text{ m}^3\text{m}^{-3}$  on 8.12.2015. On three dates of 9.3.2016 and 11.3.2016, the study area experienced rainfall events amounting to 7.59 mm and 10.16 mm respectively with an effect of rising soil moisture from 14.03 on 11.3.2016 to 15.42 on 12.3.2016. From Figure 4-11, it is worth noting that two days after, there is a corresponding increase in backscatter response on the plots on 14.3.2016. There is an interestingly high C-band SAR backscatter response to background class, which is basically soil, rocks and herbaceous layer with less than 1 m height., than small trees. Shrub and medium vegetation show an almost similar response to background class even though the high interclass dynamic range leads to overlap in backscatter response between the three classes.

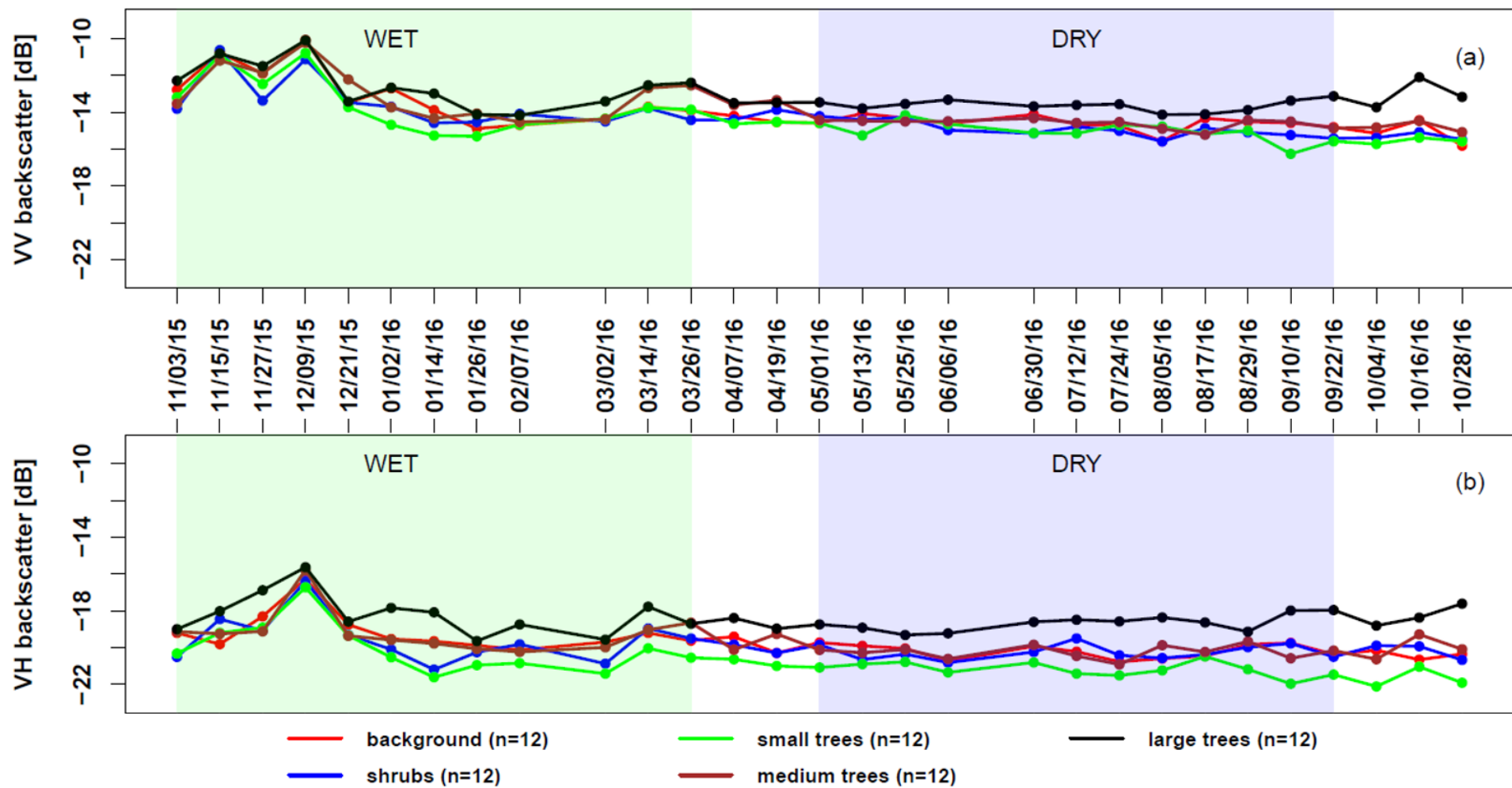


Figure 4-11. Temporal changes in C-band SAR backscatter response to the various vegetation cover classes for (a) VV - and (b) VH polarisation.

Figures 4-12 and 4-13 shows the results from application of Quegan multi-temporal speckle filter on the backscatter images used in Figure 4-11, on a 3 by 3 and 5 by 5 filter windows respectively. In each case the effects of SAR response to the vegetation cover classes was investigated for both VV and VH polarisations. The high backscatter response of the VV signal is still visible in the speckle filtered  $\sigma^0$ . From the plots, it is evident that the inter-class overlap noticed in Figure 4-11 is reduced with application of speckle filters on backscatter intensity and the gap between plots increases with an increase in filter window size from 3 by 3 to 5 by 5. Unlike the unfiltered  $\sigma^0$  images, the speckle filtered images shows a possibility of distinguishing SAR response to various cover classes even in the wet season, especially the small and large trees. Inter-class overlap between plots is reduced by lowering the within-class  $\sigma^0$  dynamic range, more so in the dry season. The extreme effects of rainfall events on backscatter causing overlap in classes is also reduced, giving a possibility to assess SAR backscatter response to individual large and small tree classes. However, same as in the non-filtered C-band SAR images, there remains overlap in SAR response to background, shrubs and medium trees for both VV and VH polarisations. The VH still displays the highest between-class  $\sigma^0$  response for small and large trees in both VV and VH, and this gap widens with an increase in speckle filter window from 3 by 3 to 5 by 5 and a move from wet to dry conditions (Figures 4-12 and 4-13).

As a summary, it can be stated that the  $\sigma^0$  response on background is more pronounced in the speckle filtered plots than in the non-filtered. As in Figure 4-11, both Figures 4-12 and 4-13 show higher backscatter response in the background than in the small trees. For speckle filtered data, backscatter response from background is higher than shrubs and small vegetation for both VV and VH signals and in some cases, both seasons.

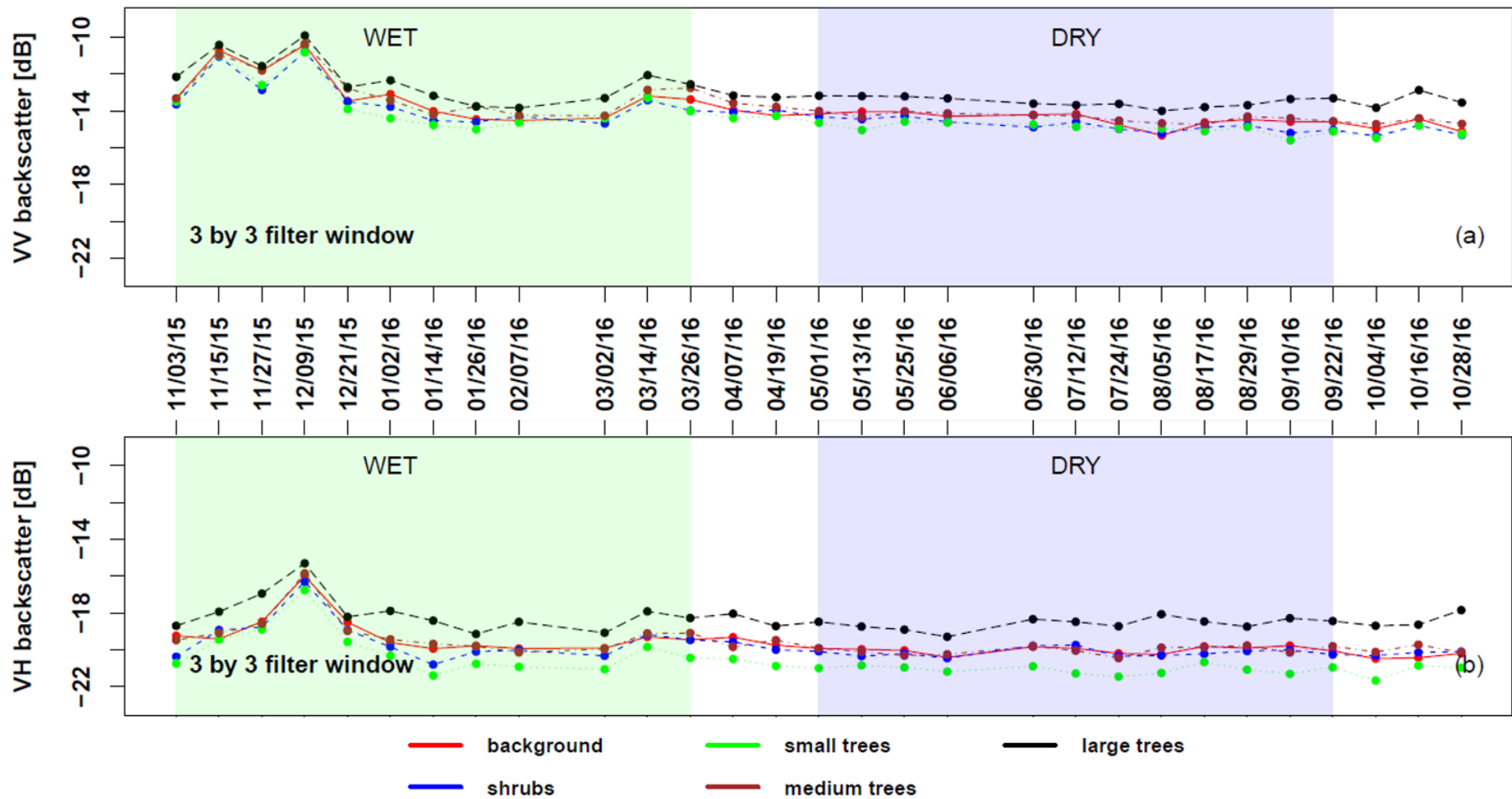


Figure 4-12. Effects of Quegan multi-temporal speckle filter on a 3 by 3 window, on the seasonal changes in C-band SAR backscatter response to the various vegetation cover classes for (a) VV - and (b) VH polarisation.

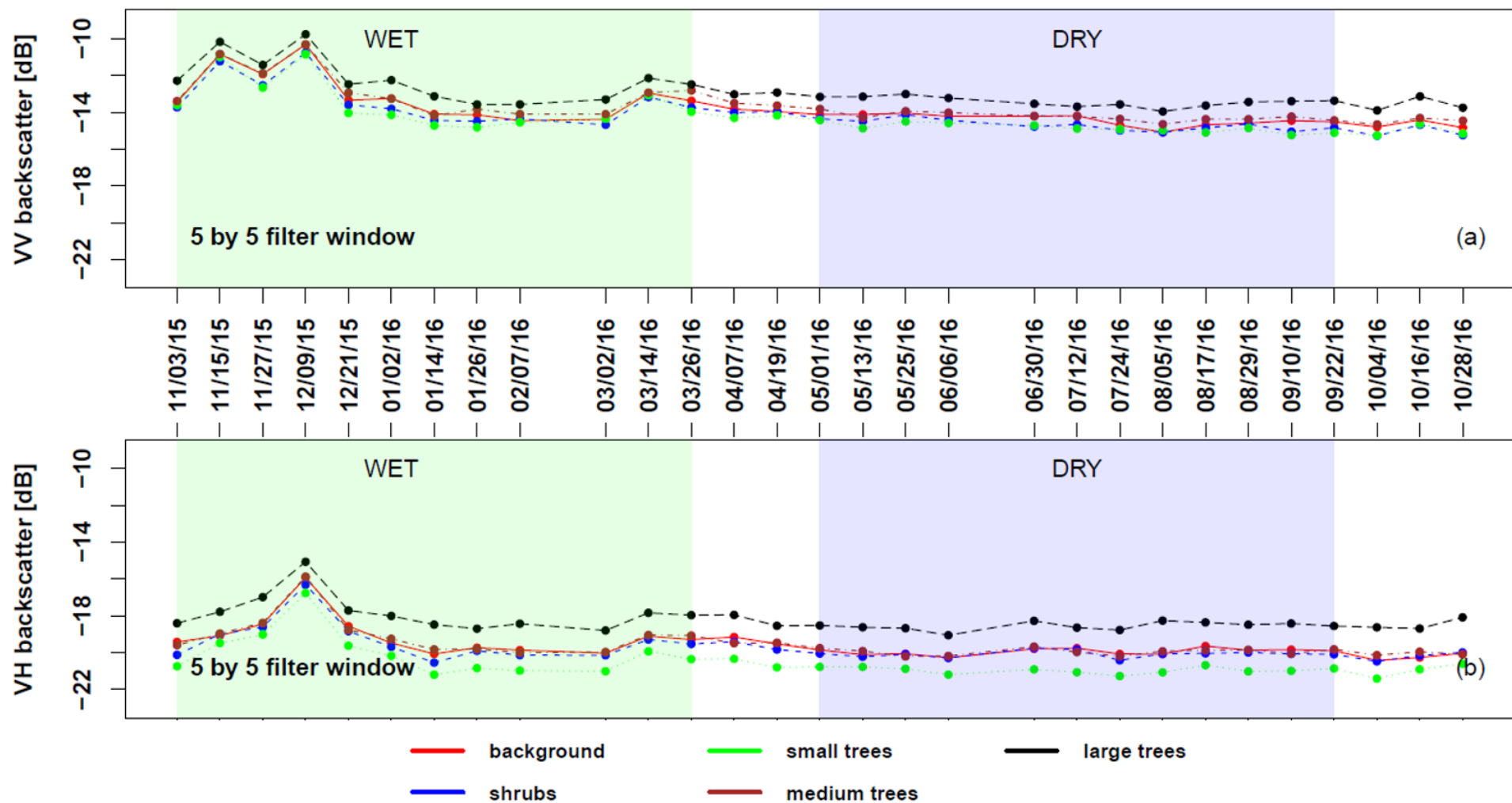


Figure 4-13. Effects of Quegan multi-temporal speckle filter on a 5 by 5 window, on the seasonal changes in C-band SAR backscatter response to the various vegetation cover classes for (a) VV - and (b) VH polarisation.

#### 4.5.2. Interactions of C-band SAR with TLS-derived CC and AGB

Figure 4-14 shows a map of TLS CHM-derived CC for 1206 grids within the TLS footprint. TLS CHM-derived CC within the study area ranges from 0.13 to 88.94 %, with a mean ( $\pm \sigma$ ) CC of  $26.34 \pm 14.55$  % (Table 4-3).

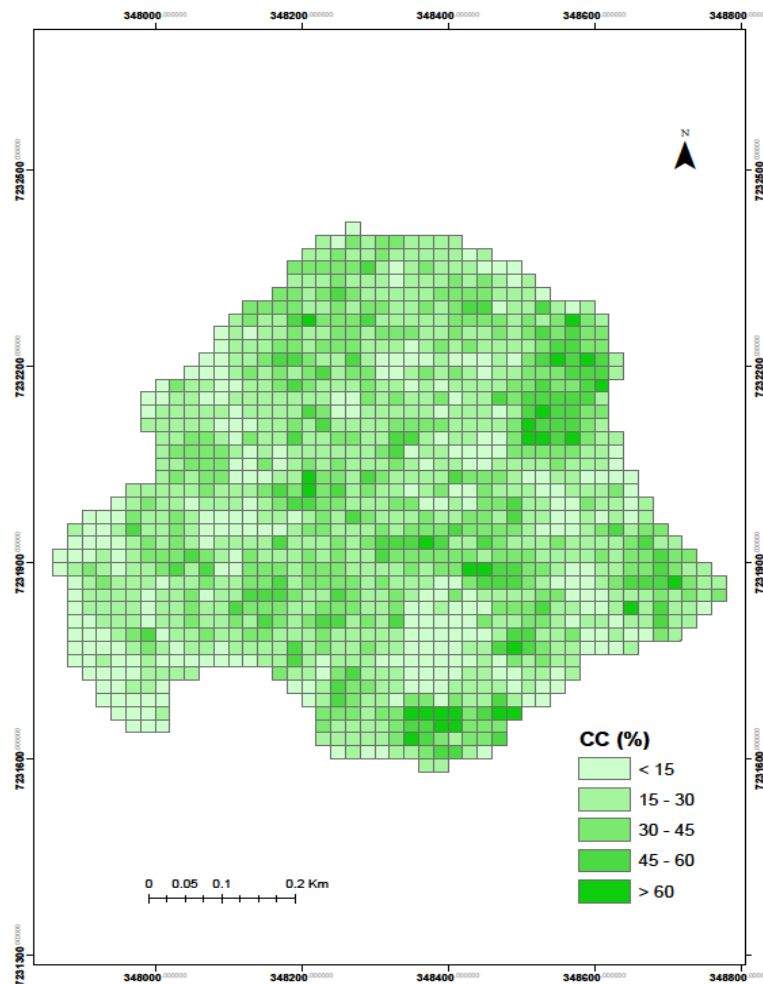


Figure 4-14. Map showing canopy cover (CC) distribution within 1206 reference plots derived from TLS CHM within the study area.

Table 0-3. Summary statistics of the TLS CHM derived canopy cover within 20 m plots in Skukuza.

TLS CHM-derived CC (%)	
No. of plots	1206
Minimum	0.128572
Maximum	88.9427
Mean	26.34342
Standard Deviation	14.55336



Both TLS-derived AGB and CC were classified into three abundance classes - low, moderate and high. To assess the SAR  $\sigma^0$  response to a dominant class, the mean of the sampled classes was computed and plotted over the 29 SAR acquisition dates, covering the period of investigation. Since abundant class partition leaves out some data points (CC and AGB values) outside the class thresholds, the mean of all CC and AGB plots was computed and included in the plots to explain the overall response and capture the behaviour of the data points outside the abundance classes. Just like in the case of vegetation cover classes, the effects of SAR polarisation (VV or VH), seasonality (wet and dry seasons) and speckle filter window (3 by 3 or 5 by 5) on multi-temporal SAR  $\sigma^0$  response to the two AGB and CC were investigated.

Figure 4-15 a and b shows  $\sigma^0$  response to CC in both VV and VH polarisations respectively. The response of the abundance classes is assessed and compared with the mean of all CC plots (black plot,  $n = 1206$ ). From the plots, it is evident that like vegetation cover classes,  $\sigma^0$  is directly proportional to CC abundance classes, with the high CC abundance class giving high  $\sigma^0$  response and low CC abundance classes showing low  $\sigma^0$  response. This is typically visible for both polarisations and seasons. The moderate CC abundance class has a SAR response like the mean backscatter response of all the CC pixels.

The plots showing backscatter response to the three CC abundance classes are shown in Figure 4-15. As observed in vegetation cover class interactions with  $\sigma^0$ , the VV signal response is higher than the VH. For VV, the overall backscatter range for high CC abundance class is between -14 dB and -10.2 dB, which reduces to -14 dB to -12.8 dB in the dry season. The highest backscatter response is experienced in the wet season on 15.11.2015 and 9.12.2015 at -10.5 dB and -10 dB respectively. The VH shows the widest gap between plots for the three CC classes (Figure 4-15 b).

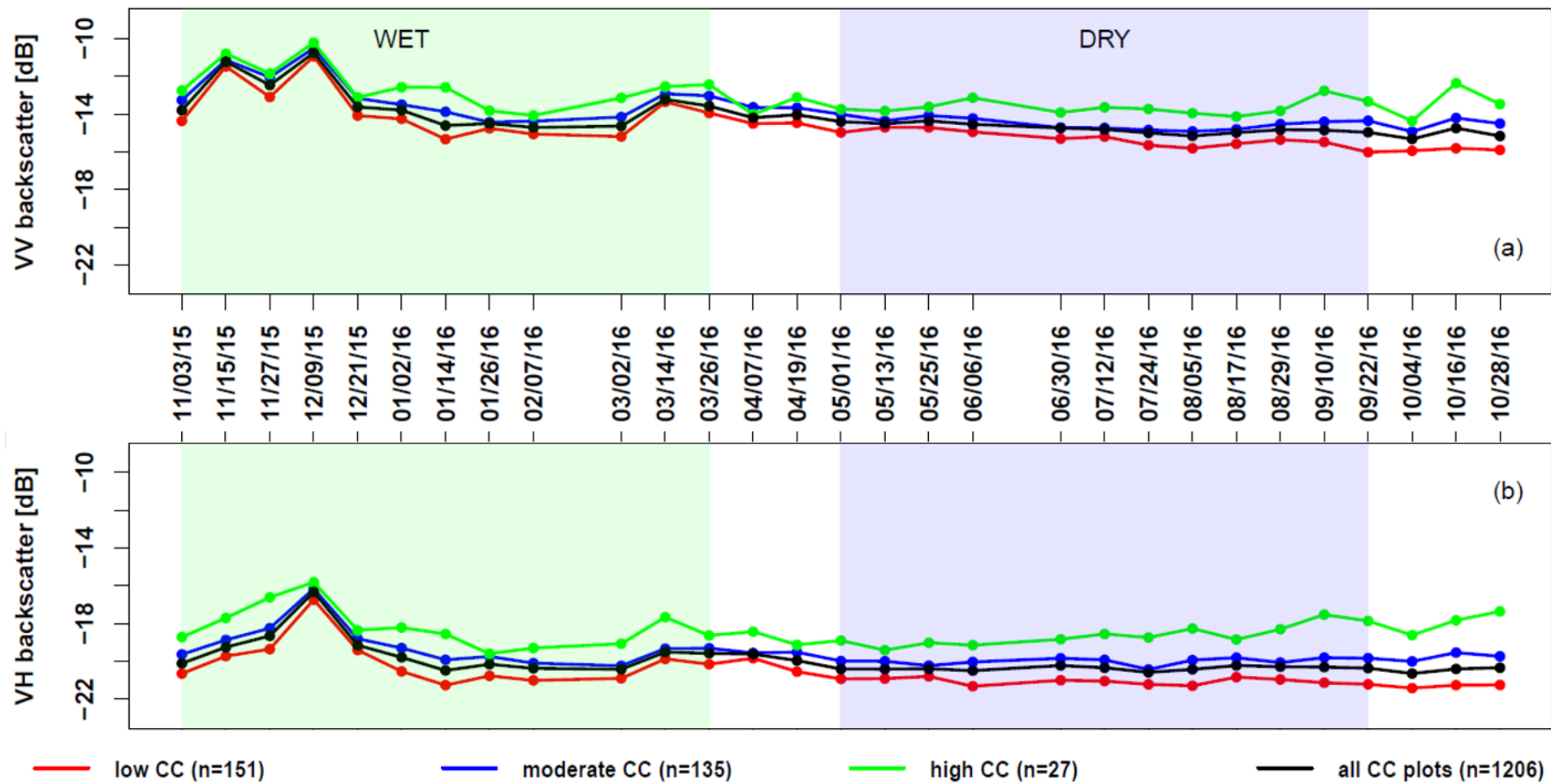


Figure 4-15. Seasonal changes in C-band SAR backscatter response to CC abundance classes for (a) VV - and (b) VH polarisation.

Like the vegetation cover classes, Quegan multi-temporal speckle filters were applied on the multi-temporal SAR backscatter values at two different moving windows, 3 by 3 and 5 by 5. The results were used to assess the effects of changes in SAR speckle filter windows on C-band SAR response to various TLS modelled CC abundance classes. Figures 4-16 and 4-17 show the plots of multi-temporal plots with changes in SAR with low, medium and high CC abundant classes.

The effects of speckle filter with 3 by 3 window in Figure 4-16 below is not so significant as the response looks like the non-filtered SAR response in Figure 4-15 above. It is however seen that in the wet season, the dates following rainfall events have different backscatter response to different CC abundant classes and not same values as in the non-filtered SAR backscatter. There is still the typical high backscatter response to high CC abundance values and low backscatter response to low CC abundance values, with the moderate CC abundance and mean CC values showing a similar SAR response. The moderate CC abundance class and mean of all CC plots are showing similar SAR  $\sigma^0$ . Also noticeable is difference in SAR polarimetric response to the abundance classes, also with speckle filtered datasets. There is high SAR sensitivity to high CC classes, followed with moderate classes (like mean CC for the study area) and the low Cc abundance class having low SAR sensitivity. The overlap in SAR response to CC abundance classes seen in the VV of Figure 4-15 (a) is no longer seen when a 3 by 3 speckle filter window is applied on the SAR backscatter images (see Figure 4-16 a).

To summarize, by increasing the speckle filter window to 5 by 5, the difference in SAR backscatter sensitivity to different CC abundant classes is clearer, for both VV and VH polarisations (Figure 4-17). In the VV, the difference between SAR sensitivity to high and low CC abundance is lower (Figure 4-17 a) compared to the VH (Figure 4-17 b). The multi-temporal plots also tend to almost flatten up in the dry season of the VH than it does in the VV polarisation. The days after rainfall events in the wet season shows high SAR  $\sigma^0$  response to all CC classes at varying degrees based on the abundance category, much higher than on the dry seasons.

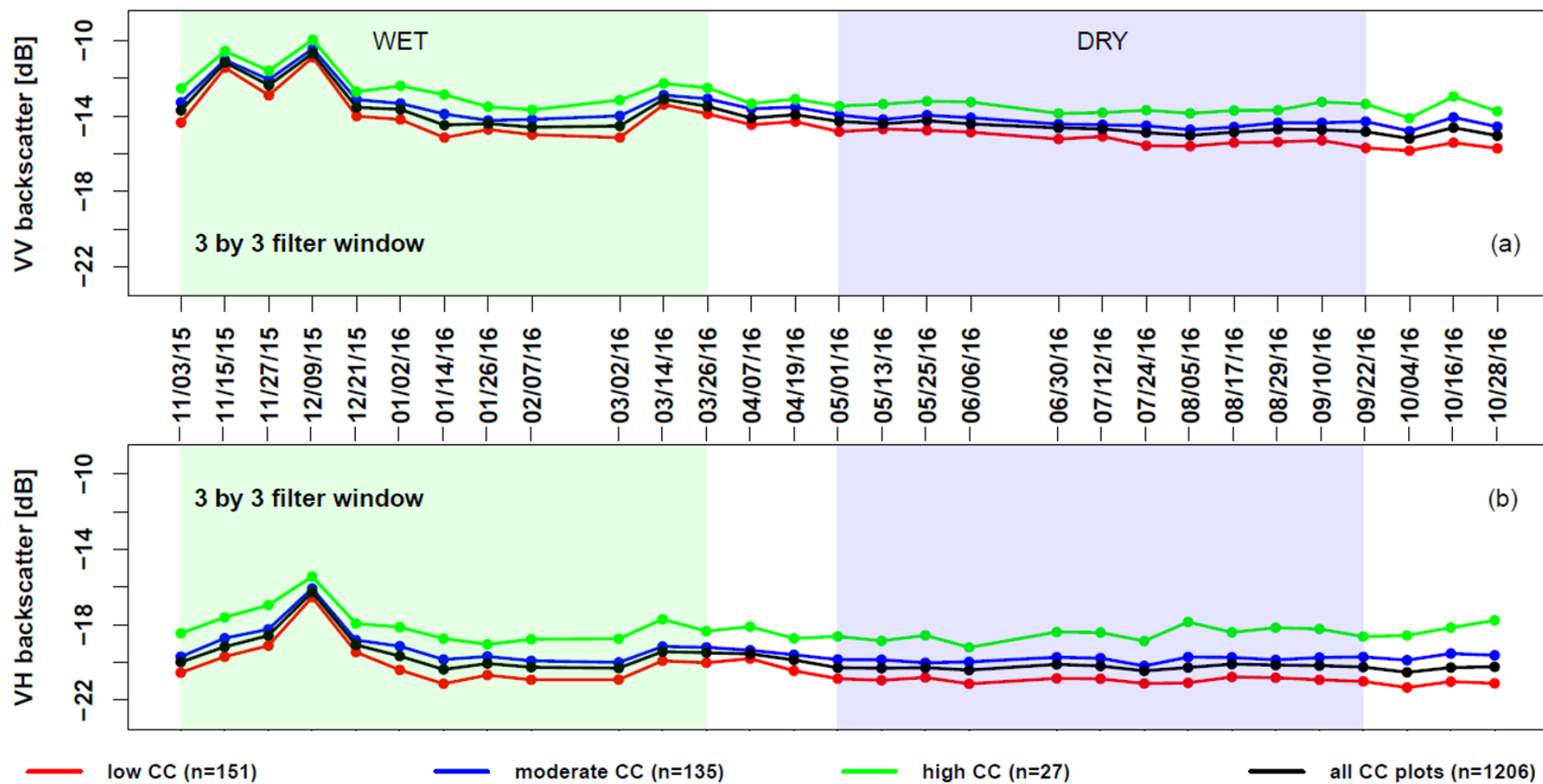


Figure 4-16. Effects of Quegan multi-temporal filter on a 3 by 3 window on the seasonal changes in C-band SAR backscatter response to CC abundance classes for (a) VV - and (b) VH polarisation.

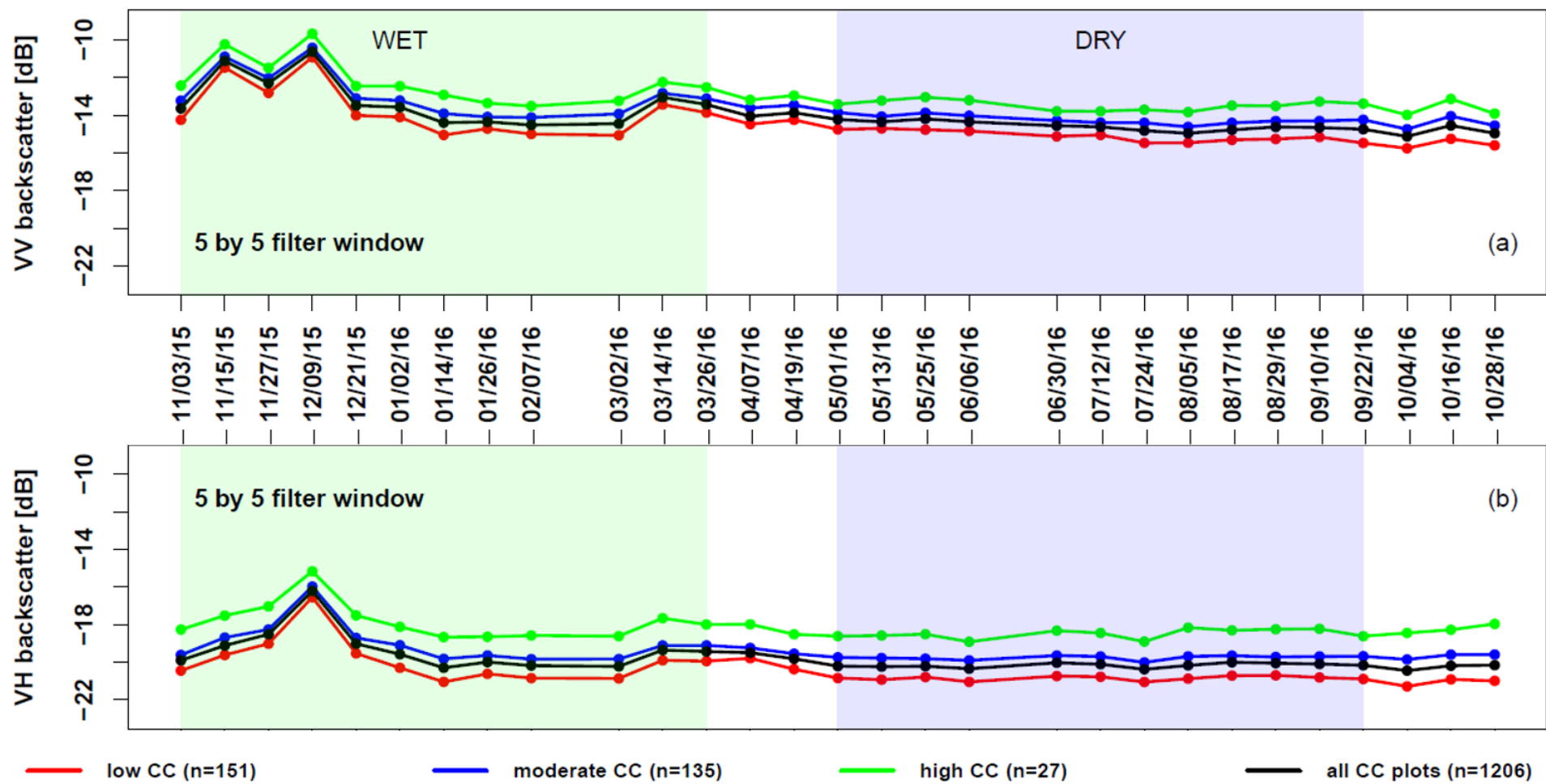


Figure 4-17. Effects of Quegan multi-temporal filter on a 5 by 5 window on the seasonal changes in C-band SAR backscatter response to CC abundance classes.

For AGB, trees with height above 5 m height were inventoried due to insufficient point clouds to reconstruct the basal diameter or trunk of tree with heights lower than 5 meter and DBH lower than 10 cm. Like CC, the AGB was also classified into abundance classes with low, medium and high. Additionally, to compensate for the AGB values outside the abundant class's thresholds, the mean AGB for the entire study area was computed and plotted alongside the abundance classes. The SAR  $\sigma^0$  response was therefore investigated against these four variables. Figure 4-18 a and b shows multi-temporal plot of C-band SAR  $\sigma^0$  response to AGB abundance classes, and the mean biomass within the study area, both for VV and VH polarisations respectively.

Typical to both vegetation cover class and CC abundance plots, the  $\sigma^0$  response to AGB abundance classes is high in the VV than the VH. For VV, the  $\sigma^0$  ranges from -14.6 dB to -9 dB, while in the case of VH, it is between -20.3 dB and -16 dB. Similar to the other vegetation structure variables,  $\sigma^0$  response is high for both VV and VH in the wet season than in the dry season. In the wet season, the  $\sigma^0$  dynamic range is high from -14.6 dB to -9 dB for VV (~ 5.6 dB difference) and from -20.3 dB to -16 dB in the VH (~ 4.3 dB). This is high compared to dry season which has a dynamic range of between -14.6 dB and -13.8 dB for VV (~ 0.8 dB), and from -20.3 dB to -19 dB for VH (~ 1.3 dB). This means there is a lot of changes in  $\sigma^0$  in the wet season than in the dry season. However, the inter-class  $\sigma^0$  response to AGB abundance classes is very low, with overlapping plots for both polarisations and seasons.

In summary, application of multi-temporal speckle filter does not improve the C-band  $\sigma^0$  response to different biomass classes as seen in Figures 4-19 and 4-20.

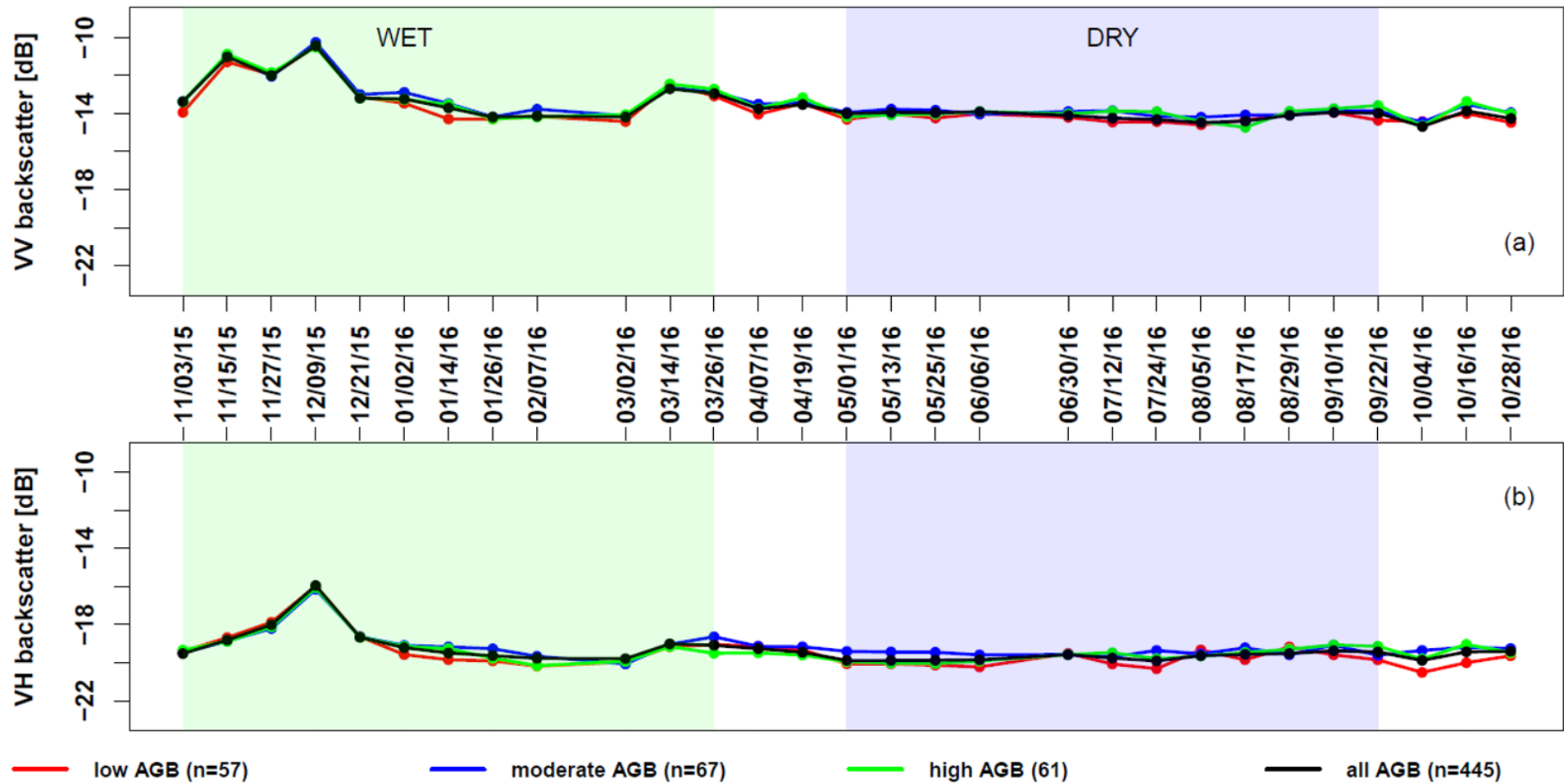


Figure 4-18. Seasonal changes in C-band SAR backscatter response to AGB abundance classes.

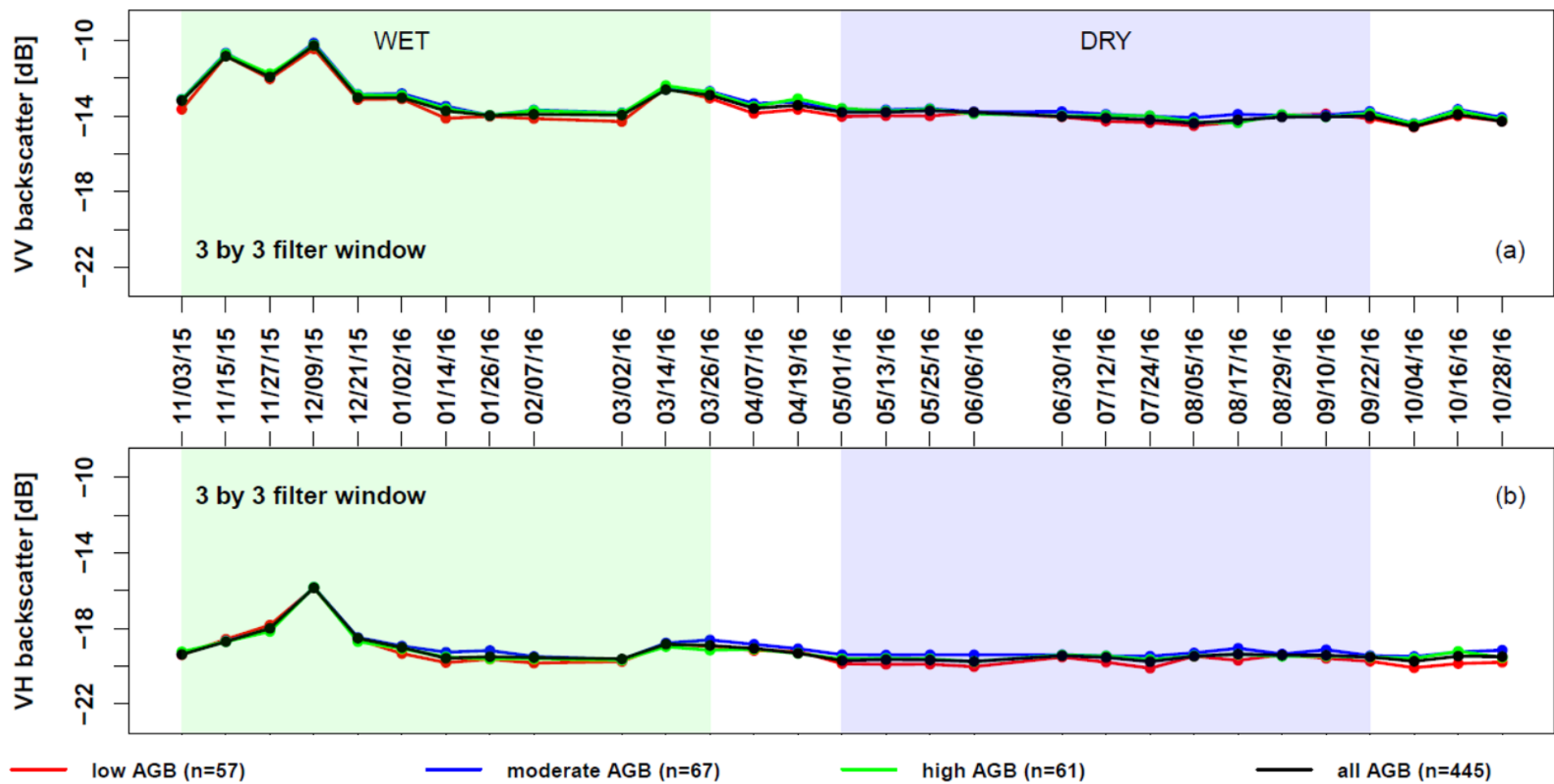


Figure 4-19. Effects of Quegan multi-temporal filter on a 3 by 3 window on the seasonal changes in C-band SAR backscatter response to AGB abundance classes.



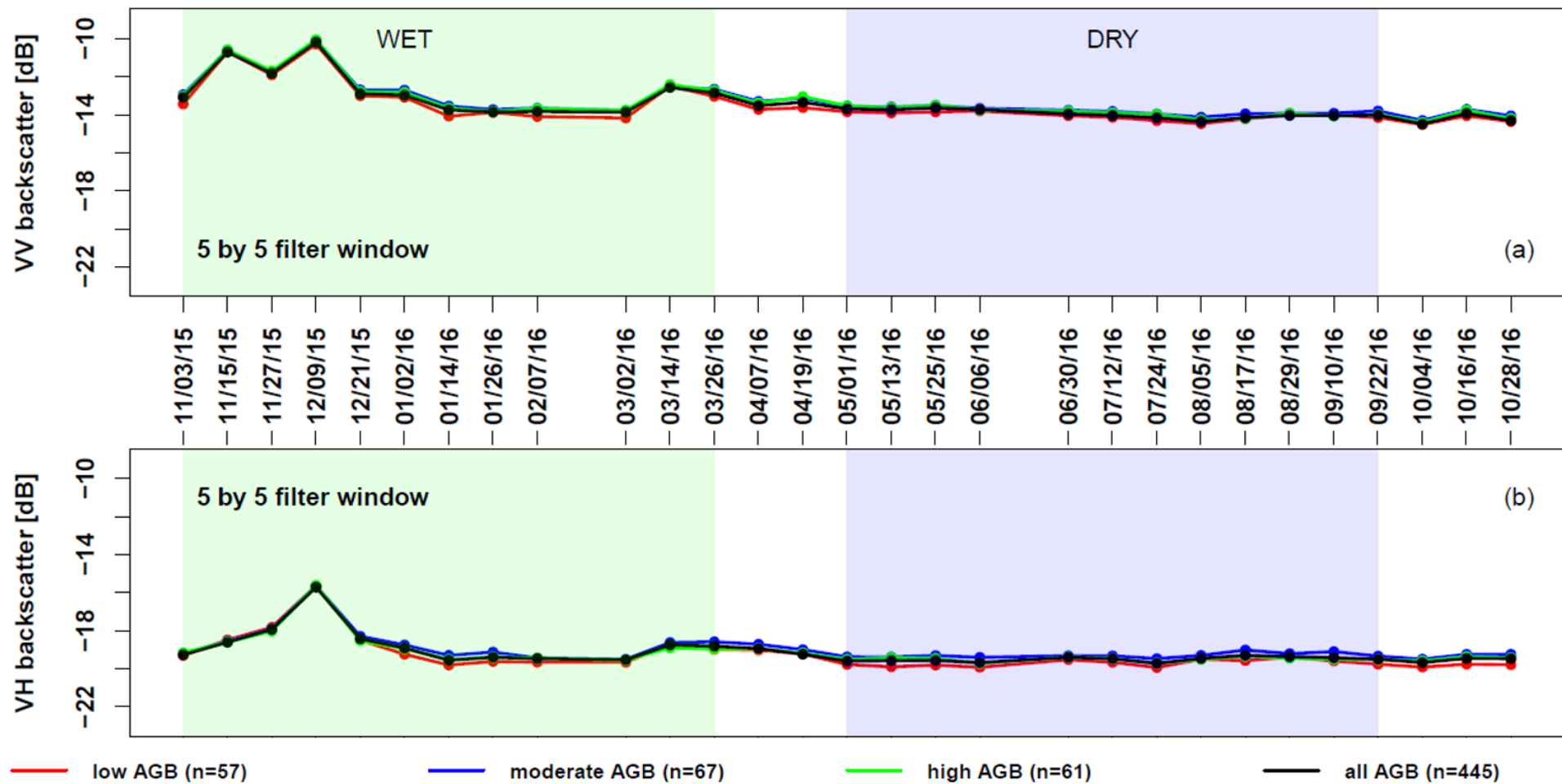


Figure 4-20. Effects of Quegan multi-temporal filter on a 5 by 5 window on the seasonal changes in C-band SAR backscatter response to AGB abundance classes.

#### 4.5.3. Summary on SAR interactions with savanna vegetation variables

Table xx below shows a summary on the interactions of Sentinel-1A SAR  $\sigma^0$  response to the various savanna vegetation structure variables, as outlined in the sections 4.5.1 and 4.5.2.

Table 0-4. Summary of interactions between SAR backscatter intensity and savanna vegetation structure variables.

<i>SAR parameter</i>	<i>Interaction with the savanna vegetation variables</i>
$\sigma^0$	<p><i>Vegetation classes:</i></p> <ul style="list-style-type: none"> <li>• High <math>\sigma^0</math> for large trees than other vegetation classes, with lowest <math>\sigma^0</math> for small trees.</li> <li>• Background class (soil and herbaceous layer) shows high <math>\sigma^0</math> response than small trees.</li> <li>• Inter-class difference in <math>\sigma^0</math> response between large and small trees more pronounced in the VH than VV.</li> <li>• High <math>\sigma^0</math> response in the wet season and an almost similar <math>\sigma^0</math> for all classes in the wet season, especially days following rainfall episodes</li> </ul> <p><i>Canopy cover:</i></p> <ul style="list-style-type: none"> <li>• High CC abundance classes give proportionate high <math>\sigma^0</math>, low CC gave low <math>\sigma^0</math> while moderate CC class gave comparable <math>\sigma^0</math> to the mean CC.</li> <li>• Wet season CC gave a higher <math>\sigma^0</math> response than in dry season, for all CC classes.</li> <li>• High inter-class <math>\sigma^0</math> response between the 3 classes achieved in the VH polarization</li> </ul> <p><i>AGB:</i></p> <ul style="list-style-type: none"> <li>• Wet season <math>\sigma^0</math> response to AGB is higher than in the dry season.</li> <li>• There is high inter- and intra-class overlap in SAR <math>\sigma^0</math> response to AGB of different abundant classes.</li> </ul>

<p>Multitemporal filter</p>	<p><i>Vegetation classes:</i></p> <ul style="list-style-type: none"> <li>• Reduced inter-class overlap in the multitemporal plots, even in the wet season.</li> <li>• Low within-class dynamic range for vegetation classes, making it possible to independently assess seasonal class response.</li> <li>• <math>\sigma^0</math> response on background is more pronounced than in non-filtered, with improvements achieved in increasing filter window size from 3 by 3 to 5 by 5.</li> </ul> <p><i>Canopy cover:</i></p> <ul style="list-style-type: none"> <li>• At 3 by 3 filter window, there is not much difference in The SAR <math>\sigma^0</math> response from unfiltered SAR data.</li> <li>• Improved inter-class <math>\sigma^0</math> response between the three CC classes is only attained at the highest filter window of 5 by 5.</li> <li>• Wet season <math>\sigma^0</math> response is comparatively higher than in the dry season.</li> </ul> <p><i>AGB:</i></p> <ul style="list-style-type: none"> <li>• Speckle filter application does not improve inter-class SAR <math>\sigma^0</math> response to all AGB abundance classes.</li> </ul>
-----------------------------	---

#### 4.6. Uncertainty and Error Analysis

In this study, there are several definite sources of uncertainty whose consideration is important towards achieving the objectives of this study. These include, among others, (i) uncertainty in plot mensuration during fieldwork, especially height measurement, (ii) uncertainties in using the field data for TLS-derived AGB for the allometric model, (iii) uncertainties in using TLS-derived AGB as reference data for AGB estimation and change detection from SAR backscatter intensity data over a small area, and (iv) uncertainties in TLS point cloud tree mensuration especially heights of fallen and multiple stems. Studies by Mitchard *et al.*, (2011) have pointed

to errors associated with field height measurement, as seen in Figure 3-15. Here, despite using TLS canopy height instead of absolute tree heights from TLS data, an underestimation of tree heights is seen, with lower field inventoried heights correlating better to the TLS canopy height than higher measured heights. This is partly because the accuracy in height measurement using a Laser rangefinder depends on the distance, and the further one moves from the tree to be inventoried, the more difficult it becomes to pinpoint the highest point of a canopy from which the measurement should be taken. There is a wide disparity in the statistics from tree inventory using the two methods. The field heights ranged between 1.5 and 12 m, while the TLS tree measurement gave a height range of 5.3 and 16.1 m. A possible solution can be achieved through repeated measurement of the same trees and by averaging the captured tree variables.

Diameter measurements are usually accurately measured and hence their accuracies are not compromised during field inventories (Adler & Synnott, 1992). Biomass model uncertainty in the study emanates from the difference in timing between acquisitions of field and TLS datasets. The former was acquired in the wet season while the latter in the dry season of the same year. There is error propagation from field-TLS biomass prediction and using the same as a reference in predicting biomass from SAR. This is visible in the results from Table 3-1 where the predictions with TLS AGB as reference yields higher RMSE values than the RMSE obtained in its prediction from field-derived biomass. Field inventoried datasets were few and therefore not representative enough as a reference in SAR based AGB model training and validation, which further motivated the use of TLS-derived AGB as the reference dataset when modelling AGB from SAR backscatter intensities.

For error analysis, the residuals ( $Residual = (Y - \hat{Y})$ ) from the fitted regression models were assessed—the difference between the reference and predicted or derived aboveground biomass. To assess the assumption of heteroscedasticity in the model residuals which should result in the model residuals being randomly distributed around zero for a range of predicted AGB, the residuals were plotted against the predicted AGB values for TLS and SAR backscatter predictors. This is also a check for systematic bias from the regression models used in predicting AGB. The residuals allowed for estimating SAR sensitivity to biomass quantity within the Lowveld savanna, because there are uncertainties in modelling AGB beyond 40 t/ha.

In TLS tree mensuration for individual tree height and DBH for AGB estimation, only those trees with height above 5 m height was measured, while the field inventory could only measure trees with heights not higher than 12 m as opposed to the highest height of 16.1 m from TLS

tree measurement (see Table 3-3). The insufficiency in point clouds to reconstruct a perfect cylindrical trunk at 1 m height for most of the trees whose heights were measured meant that these were left out in computing reference AGB from TLS-derive trees (see Figure 4-21 below). About 100 trees with heights as low as 3.4 m were left out of AGB estimation. This height threshold constitutes the shrub vegetation which contributes the bulk of woody vegetation within this biome and having left them out means that the TLS-derived AGB is overestimates and only reflects high tree biomass.

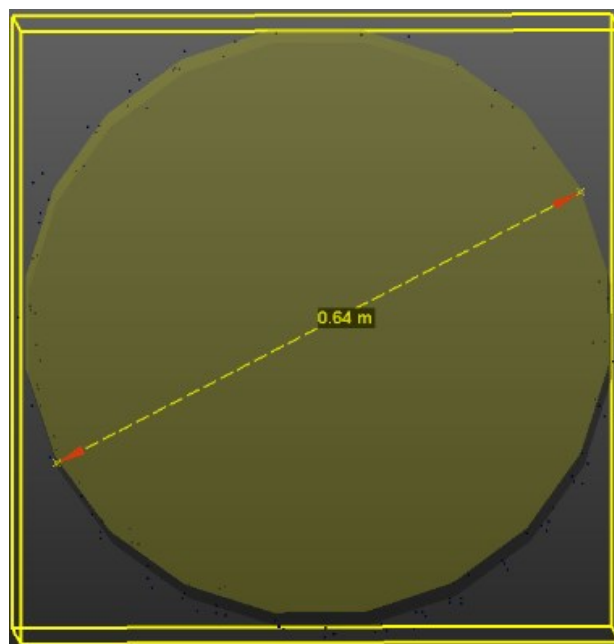


Figure 4-21. Trunk diameter measurement from TLS PCs. Reconstruction of the DBH is dependent on availability of enough points.

TLS individual tree height measurement entails estimating the distance between the lowest and the highest point cloud for every identified tree. Whereas this is more accurate compared to the use of an inclinometer in tree height measurement, sometimes these two PCs can be missed, leading to height underestimation. Savanna vegetation is made up of multiple stemmed shrubs and trees. Mensuration of these requires measuring the two stems where there are multi-stemmed trees (Figure 4-22). The ambiguity in the multi-stemmed trees within this typical savanna calls for trunk diameter measurement at heights below breast-height, with most studies recommending 1 m height (Nickless *et al.*, 2011; Mograbi *et al.*, 2015, Colgan *et al.*, 2012), while other like Colgan *et al.*, 2013 using 10 cm above the ground. Where such multiple stems branch below 1 m height, all the stems and heights are measured and averaged and assigned to

the tree. However, when branching takes place above 1 m, then one trunk is measured below the branching and assigned to the tree. In the same breadth, at 10 cm height proposed in the studies by Nickless *et al.*, (2011); Colgan *et al.*, (2012) and (2013), it is difficult to separate tree trunk point clouds from other herbaceous and other low vegetation cover classes.

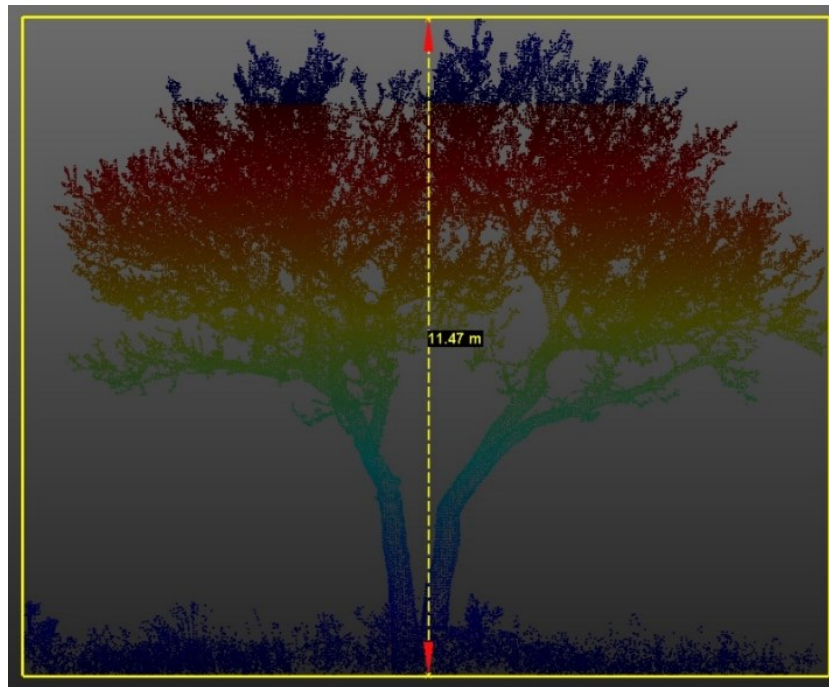


Figure 4-22. Multi-stem tree within the study area. Depending the height at which the trunks split, all must be measured, averaged and assigned to the common tree.

Dead and fallen trees make up a very high proportion of AGB and about 10% within the tropics (Condit, 2008). The latter where possible and can be identified during field inventory should be inventoried and included in the overall biomass estimation of an area. However, height measurement is not possible when the dead tree is lying vertically on the ground. For fallen trees, the height at which the tree broke, whether below or above 1 m height, further complicates such measurements. These complexities in structure and the methods deployed in measuring such fallen trees affect the final accuracy of AGB estimation within an area.

## CHAPTER 5

### 5. Discussion of results

#### 5.1. Spatial distribution of savanna vegetation structure within Skukuza

##### 5.1.1. Aboveground Biomass

The allometric computed mean AGB around Skukuza study site from 42 inventoried field plots was 31.86 t/ha with mean plot values range between 3.1 t/ha for the lowest plot value and 94.3 t/ha for the highest, which are within the range reported by earlier AGB studies within and around KNP (Nickless *et al.*, 2011; Colgan *et al.*, 2013; Mograbi *et al.*, 2015), and typical of the Lowveld savanna AGB estimates. From the 237 field inventoried trees, a high correlation between tree basal diameter or DBH and AGB was observed, making this tree variable the greatest determinant of woody biomass at both tree- and plot levels as visualised by plots in Figure 4-2. Conversely, field measured height showed little correlation with the AGB. Trees with larger DBH gave a correspondingly high biomass values irrespective of the height, while on the contrary, those with higher heights and low DBH values gave proportionately low AGB values. At plot level, high AGB values were associated with high mean DBH within a plot. This was not only observed in the field inventoried trees but also with individual tree data derived from TLS point clouds. Studies by Binot *et al.*, (1995); Luoma *et al.*, (2017); Wang *et al.*, (2019) shows that field DBH measurements suffer from fewer introduced errors as opposed to height measurement. Around 674 trees had both height and DBH measured from TLS point clouds, from which tree-level AGB was computed in kg/tree with a result showing a trend of an increase in AGB with an increase in DBH while the tree height shows clustering at lower AGB values. Figure 5-1 shows the relationship between tree-level biomass and the two variables, DBH and tree height, as computed from TLS data. As observed in the field measured data in Figure 4-2, AGB increases with an increase in tree DBH size while tree height shows little relationship with the resultant TLS modelled AGB. However, the basal diameter at plot-level does linearly correlate to the log-transformed AGB, as displayed by the residual plots in Figure 4-6. L-band SAR data was used to model AGB for the entire study area over four years using TLS modelled biomass as reference data.

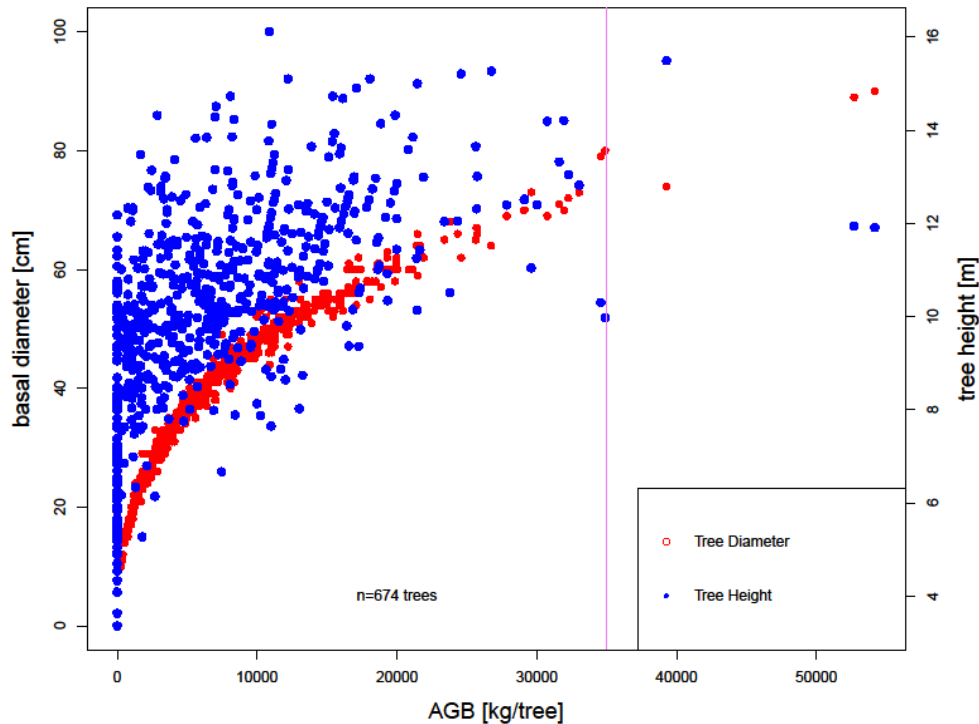


Figure 5-1. Tree-level height, diameter, and the computed AGB derived from TLS point clouds within the study area.

Despite the underestimation of woody biomass within the study area, SAR backscatter predicted spatial variations in AGB within the study area with a range from 2.9 t/ha in low vegetation areas (typically open patches with grass/shrub and bare areas), to 101.6 t/ha in areas where trees are clumped with closed canopies around rivers and stream valleys. These values are within typical biomass ranges reported previously by Nickless *et al.*, (2011) of 11.9–92.3 t/ha. Previous studies within KNP and around the study area have obtained mean AGB ranging between 20 and 35 t/ha, with some values from these studies shown in Table 5-1.

Table 0-1. Mean biomass values from various studies within and around Skukuza. \*TLS ref= TLS reference tree dataset over 20 m plots; \*\*Published and part of this dissertation.

<b>Plot size (Ha)</b>	<b>Mean AGB (t/ha)</b>	<b>Source (study)</b>
0.25	22.93	Nickless <i>et al.</i> , 2011
0.07	27	Colgan <i>et al.</i> , 2013
0.07	28.3	Colgan <i>et al.</i> , 2012
0.063	32.52	Mograbi <i>et al.</i> , 2015 <sup>3</sup>
0.09	31.86	Odipo <i>et al.</i> , 2016**
0.04	35.6	This study (TLS ref*)

<sup>3</sup> This value is based on the results from low extraction areas of Bushbuckridge, typical Lowveld with human settlement.



The spatial distribution of woody biomass around Skukuza is highly variable, and this study showed higher biomass values occurring more frequently in low-lying areas around seasonal rivers and stream valleys (Figure 4-8). From the TLS derived CHM in Figure 3-9 (c), the tallest trees around the footprint measure around 21 m height and make up mostly the riverine vegetation. These are mostly broad-leaved vegetation with large tree trunks and closed canopies thus contribute to the high AGB values typical of plots within these areas. These lowland areas have good soil foundation for larger trees because receive rich soils swept from the up-slope areas either by runoff or erosion agents are deposited downslope through colluviation. Biomass change maps and land cover overlay maps also show the likely concentration of high biomass values in these areas within the study area. It is also worth noting that these are the same areas displaying significant biomass changes of above 5 t/ha. Temporally, the areas with high biomass values within the study area also display extended vegetation greenness periods slightly beyond the start of the dry season because of moisture and water availability (Scholes *et al.*, 2001; 2002) either through their deep tap-roots which can access water under the soil layers after the onset of dry periods or through proximity to the seasonal rivers. Studies by Scholes & Walker, (1993); Levick *et al.*, (2010); Colgan *et al.*, (2012) and Baldeck *et al.*, (2014) have cited soil catena formations and associated soil and hydrological characteristics as major influences on landscape-scale vegetation structure and compositional variability. The open mid-slopes are prone to fire and herbivory especially by browsers who prefer open areas increasing their views to predators (Banks *et al.*, 1996; Sankaran *et al.*, 2005; 2014). The combination of fire and herbivory apart from low nutrient and thin soil layer because of runoff, therefore reduces woody cover development resulting to low biomass values in these regions of the study area.

TLS plot-level AGB at 20 m showed significantly higher values and large dynamic ranges compared to field inventoried and subsequently L-band SAR modelled plots (at 30 m) within the study area. This is because of two factors: (i) averaging AGB (kg/ha) from many trees within small plots and few trees over bigger plots, since the TLS could capture many large trees within each 20 m plots than was inventoried in the field over the 30 m plots, and (ii) TLS tree inventory only captured larger trees with height above 5 m and basal diameter larger than 10 cm. The resultant biomass is therefore characteristic of medium and large tree components with less low shrub components. To derive TLS canopy cover and height metrics, plot averaging was used (Colgan *et al.*, 2013), thereby degrading the spatial resolution of the TLS data from a full resolution of 0.06 m to the 20 m and 30 m plot sizes for C- and L-band SAR backscatter

responses, respectively. This method, though convenient for estimating each plot's average biomass contribution and area-wide spatial distribution, leads to errors as observed in studies by Colgan *et al.*, (2013), because intrinsic variability among individual trees within the plot are left out. Within this typical Lowveld savanna exists both multi-stemmed and single-stemmed trees, contributing biomass differently based on these tree TLS metrics, which are affected by non-linearly related biophysical variables (for example, height and basal diameter). The use of different plot sizes by different studies leads to varying mean AGB for the study area. From an analysis of a few such studies to estimate AGB in this typical biome, it is evident that inventory plot size to some extent affects mean AGB (see Table 5-1 above).

The inter-annual L-band SAR data was able to detect changes, both increases and decreases in AGB of > 5 t/ha, and the spatial extent of these changes in terms of the proportion of the study area which experienced the reported decrease or increase in biomass of this magnitude between 2007 and 2010. Previous studies on structural changes in the Lowveld savanna have showed similar decreases, with Banks *et al.*, (1996); Wessels *et al.*, (2013) and Mograbi *et al.*, (2015) associating the decreases to fuelwood and timber extractions in settlement areas close to the park. Whereas precipitation is a major limiting factor to savanna structural dynamics, biomass inclusive, studies within protected areas without anthropogenic wood extraction identify fire and herbivory as the major factors behind vegetation dynamics with similar magnitudes at local scales (Colgan *et al.*, 2012; Banks *et al.*, 1996). The former affects mainly low shrubs and herbaceous vegetation layer (grass), while the latter, especially browsers, affects mainly woody vegetation components. Given the localised scale of this study, and that mostly wooded areas have been affected by the AGB changes, it suffices to conclude that herbivory, especially by mega-herbivores like elephants, is responsible for changes in woody biomass because they push down big trees, and modify the horizontal and vertical savanna vegetation structure as would be visible in both canopy cover and height, respectively.

## **5.2. Temporal dynamics in savanna vegetation structure**

### ***5.2.1. TLS data in vegetation structure mapping***

Direct field inventory has been used for decades to obtain tree variable data for the validation of remote sensing products (FAO, 1981). These methods have however proved to be inefficient both in time and space – non-representative geographical coverage with a high possibility of

omission and commission errors during data collection process. Where data is required for allometric development for carbon stock estimation, destructive sampling for wet and dry weight measurement is preferred. However, by assessing the relationships between tree variables acquired during field inventories with TLS metrics, it is possible to predict forest structure (Niemi *et al.*, 2015; Calders *et al.*, 2015). TLS has been used in the validation of individual tree variables like height and DBH. In the current study, AGB is computed from individual tree measured height and DBH from TLS point clouds and further used in an allometry to estimate AGB with 0.04 ha plots. Individual tree DBH was manually measured from TLS point clouds by reconstructing the circumference at 1 m height, to ensure the multi-stemmed and coppicing trees are also captured since they form the bulk of woody biomass in most parts of the study site, as supported in studies by Colgan *et al.*, (2012); Naidoo *et al.*, (2015) and Main *et al.*, (2016). The DBH measurement relied upon availability of sufficient point clouds to reconstruct a complete cylindrical trunk at 1 m height. Several studies have utilised the 3-D capabilities of TLS data to reconstruct tree stem volume and DBH as seen in Wang *et al.*, (2016) who fitted point clouds at 1.3 m height to derive DBH for low vegetation for detection of shallow landslides. Herrero-Huerta *et al.*, (2017) used TLS point clouds in urban tree mapping, while Cabo *et al.*, (2018) compared tree variables derived from TLS and wearable laser scanning instruments. Most studies aimed at automating tree diameter reconstruction from TLS point clouds have adopted a similar approach. For the current study, the standard deviation (SD) for all points used in reconstructing a perfect cylindrical trunk was limited to 0.03 m, above which the trunk could not be used for subsequent allometry. The results show that most low-height vegetation comprising shrubs, could not be reconstructed with accuracy. Therefore, the lowest measured tree height and DBH were 11 cm and 5.3 m respectively (Table 3-3). This is in line with the observation made by Raunonen *et al.*, (2015) who observed that TLS point clouds could not accurately reconstruct DBH for lower trees. For the current study therefore, the TLS point clouds could not detect tree parameters from trees with height below 5 m and basal diameter below 10 cm, the majority being herbaceous and shrub vegetation. In this savanna biome, shrub vegetation makes up a higher percentage of woody vegetation, with an implication on the overall aboveground biomass (Scholes *et al.*, 2001; Colgan *et al.*, 2012; 2013). Whereas most of the field inventoried trees could not be matched with those identified in the TLS point clouds because field inventory captured more of lower vegetation than TLS, a correlation was only possible between mean plot height from field inventory and TLS canopy height. Both products are plot-averaged. According to Baronti *et al.*, (1993), biomass retrieval can be satisfactorily achieved only after a correct classification

of vegetation fields since different plant geometries produce different biomass sensitivities. For this study, AGB was derived from individual tree height and basal diameter directly from the point cloud reconstruction, while CC (%) and the five vegetation cover classes were computed from TLS-derived CHM. This also informed the classification of AGB and CC into abundant classes for further investigation with C-band SAR backscatter.

### ***5.2.2. L-band SAR sensitivity to inter-annual changes in Aboveground Biomass***

The multi-temporal L-band SAR backscatter intensity values vary within the same pixel locations within the study area. This, despite using dry season data ranging between the months of September and October over the four years of study. Using datasets from the same season is helpful in explaining the changes in biomass attributed to different change agents working in the study area concurrently at different spatial scales. These include eco-climatic variables, topography and soil (topo-edaphic), frequency of fire occurrences, and herbivory impacts within the study area. Whereas the current study never investigated the role of all these factors, their magnitude of contribution to the AGB dynamics depicted by the current change results cannot be ruled out. A study by Ryan *et al.*, (2012) suggested correction of effects of moisture to L-band SAR backscatter through recalibration of backscatter to ground data at each time step. To account for this, the L-band SAR datasets were acquired over dry season, to eliminate the effects of moisture on SAR backscatter intensity. Studies by Naidoo *et al.*, (2015) and Urbazaev *et al.*, (2015) proposed that dry season L-band SAR datasets are best suited for woody vegetation mapping for most biomes. From the inter-annual AGB maps in Figure 4-8 (a to d), there are noticeable high biomass values in the lowlands along river valleys for all years because of the presence of riverine vegetation with tree canopies. These areas apart from moisture availability during peak stream-flow in the rainy season, also store water long after the on-set of dry seasons that can be used by the trees in the absence of rainfall typical of dry seasons. The spatial distribution of trees in the study area is therefore partly attributed to fertile soil deposits from upland areas into lowland areas (Scholes *et al.*, 2001; Smit *et al.*, 2013). This corresponds to observations by Baldeck *et al.*, (2014) and Scholtz *et al.*, (2014) who cited that soil catena formations and associated soil and hydrological characteristics as major influences on landscape-scale vegetation structure and compositional variability. These topo-edaphic factors do not change much over short periods of time like four years of under the current study, as can be seen in occurrence of high AGB values in same locations within the study area.

By using multi-temporal L-band SAR data, this study detected biomass changes, both decreases and increases within the study area, by estimating the proportional area which experienced a biomass change over 5 t/ha (Table 4-2). The results from the biomass change analysis show a general reduction in biomass over the four years between 2007 and 2010. This is clearly seen in the cumulative reduction in the area that experienced a biomass increase above 5 t/ha. The areas which saw a reduction in biomass above 5 t/ha increased over the years from 28.8 ha between 2007 and 2008 to 37.3 ha between 2009 and 2010. The biomass change-maps in Figure 4-9 also shows these changes are restricted to areas with woody vegetation as opposed to mid-slopes with shrub/grassy areas. The areas with nonsignificant biomass changes (<5 t/ha) were mainly within the open areas with shrub, grass, and bare land cover classes. Without human interference in terms of woody vegetation extraction within KNP, low AGB from reduced high tree canopy is caused by mega-herbivores like elephants which when browsing top canopy knock down big trees. Studies by Asner *et al.*, (2016) investigated the effects of megafauna (African elephant) on woody vegetation between 2008 and 2014 in KNP and reported a mean biennial tree-fall rate of 12% per hectare. This destruction of the tree vertical structure can not only lead to AGB reduction of proportional magnitude but also lead to a change in land cover, with a shift from trees to either shrubs, grass or bare patches. Changes in shrub and grass classes are attributed to grazers and frequent fire episodes from high biomass, and the resultant regeneration after fire regimes and saplings from fallen trees (van Wilgen *et al.*, 2003). A reduction in woody biomass is mainly attributed to woody extraction, which in unprotected areas near settlements are caused by logging, clearance to create room for agricultural expansion and settlements among others. Mograbi *et al.*, (2015) observed a loss in woody biomass around Bushbuckridge settlement adjacent to KNP and concluded that unsustainable fuelwood extraction by settlers are the main cause of losses in tall tree height classes. Over three years, Ryan *et al.*, (2012) assessed a reduction in AGB by between 2.3 and 11.5% attributed to clearance for small-scale farming in Central Mozambique. Colgan *et al.*, (2012) assessed the effects of topography and soil on biomass distribution within South African savannas and observed that topography and precipitation had a greater influence on woody biomass distribution. The current study was carried within KNP, which has enjoyed protection from human induced woody extraction for over eight decades (Sankaran *et al.*, 2008; Scholtz *et al.*, 2014). The losses in AGB herein are therefore not attributed to anthropogenic factors such as woody products extraction.

### ***5.2.3. C-band SAR sensitivity to seasonal changes in savanna vegetation structure***

The C-band SAR backscatter and its interactions to savanna vegetation structure variables was investigated over one year, between November 2015 and October 2016, covering wet season between November 2015 and March 2016 and, dry season running between May 2016 and September 2016. April and October were left out as transition months between these two seasons, because it is assumed they could not give a clear backscatter signal response to different vegetation structure variables. To assess the response of SAR backscatter to various savanna vegetation structures, three vegetation structure components were computed within 20 m Sentinel-1 C-band SAR pixels, namely AGB (t/ha), CC (%) and vegetation cover classes. Multi-temporal SAR data was acquired over 29 dates between 2015 and 2016 and were stacked with acquisition dates as bands. From the multi-temporal stack, the predictor variables were derived including backscatter intensity and speckle filtered backscatter intensities within 3 by 3 and 5 by 5 moving windows using Quegan multi-temporal filter and the two SAR polarisations (VV and VH) against which savanna structure variables were investigated.

CC and AGB were classified into abundance classes from class sample means to ensure the variance between individual samples is reduced. The abundance classes better explain the responses given the complexity in the heterogeneous nature of the study area, where individual pixels comprise multiple scatterers with different characteristics. Savannas are mixed ecologies comprising grass, shrubs, and trees and therefore adopting an abundance classification better explains the SAR backscatter response associated with these three vegetation ecologies in the study area. This study therefore assumes that the SAR response to low abundance classes are typical of herbaceous vegetation, moderate abundance classes represent shrub vegetation response and the high abundance class is associated with a response typical of large trees within this biome. Apart from the abundance classes, the mean of all CC and AGB plots within the TLS footprint were computed, and the associated SAR backscatter response plotted alongside the abundance classes. Whereas the tree structure parameters used for TLS AGB modelling was limited by height above 5 m and basal diameter above 10 cm, the CC as a vertical vegetation above 1 m height captured all vegetation classes except herbaceous layer below 1 m height within the study area. Trunk reconstruction of trees with heights below 5 m was not possible from TLS point clouds, because this vegetation class had insufficient point clouds which could not form a perfect tree trunk at 1 m height. This observation is also made in studies by Raumonon *et al.*, (2015) who noted that low vegetation could not be reconstructed by TLS data.

Table 3-3 shows the summary statistics of inventoried tree variables and AGB distribution within Skukuza computed from field inventoried and TLS identified trees. The field survey captured trees as short as 1.5 m high with the lowest DBH of 6.4 cm. From TLS point clouds, it was only possible to identify and model trees with heights above 5.3 m with the lowest DBH being 11 cm. The difference makes up the lower vegetation classes within the study area. In this study,  $\sigma^0$  response is assessed based on the inter-class dynamic range- how far apart the temporal plots for the various (abundance) classes are separated from each other. In this way, a response can be associated with a savanna ecology. The SAR backscatter sensitivity and response is therefore how individual multi-temporal plots are far apart and hence the possibility of independent or separate assessment. The assessment was made for both the dry and wet seasons for VV and VH backscatter signal responses, respectively. These polarisations dictate which vegetation components contribute to total energy backscattered by surface targets (McNairn & Brisco, 2004).

Temporal dynamics in  $\sigma^0$  as a function of savanna vegetation structure were investigated by plotting these responses over the SAR acquisition dates, covering both dry and wet seasons. Changes in the SAR backscatter response to vegetation structure within this study area is a function of seasonal variability in moisture availability in the vegetation canopies and soil layers in the the wet season and lack of it in the dry season. The two cycles are caused by rainfall events and drought occurrence cycles, respectively (Urban *et al.*, 2018). The amount and variability of antecedent precipitation, evaporation rate from solar insolation and availability of vegetation cover affects moisture availability not only to plants but also in the soil (Reynolds, 1970). Mattia *et al.*, (2009) found a correlation between soil moisture index and antecedent precipitation index, meaning rainfall events lead to increased moisture while lack of rainfall events reduces moisture availability. Generally, vegetation structure and its water content vary in both space and time, with wet seasons exhibiting the availability of moisture on the vegetation components at all heights. In the dry season, when there is minimum water or low moisture in the plant leaves, the backscatter is low, an observation made by Costa (2002). For SAR  $\sigma^0$  interactions with vegetation components, plant water contents and the geometry of the vegetation components such as orientation of branches, stems and leaves are very important determinants (Paulo *et al.*, 2014). These orientations are responsible for the depolarisation of the incoming SAR signal in the form of VH backscatter response.

Figures 3-5 and 3-6 shows average monthly rainfall data between 1912 and 2001, and the decadal rainfall statistics with a long-term average from 1994 to 2013 respectively, for Skukuza study area (Kruger *et al.*, 2002; FAO, 2018). The two plots show the peak rainy season to be between the months of November and March and the dry season between May and September. Prior to the current study period, between October 2015 and February 2016, most parts of Southern Africa experienced drought leading to below-average rainfall caused by El Nino warming (Baudoin *et al.*, 2017; WFP, 2017; Monyela, 2017). From daily rainfall and soil moisture data obtained from the EC flux tower site for the current study period in Figure 3-10, the first rainfall event after two weeks was experienced in the study site on 14.11.2015 at 6.86 mm. On 15.11.2015 there was no rainfall event recorded but the rise in soil moisture from 4.77  $\text{m}^3\text{m}^{-3}$  the previous day to 7.56  $\text{m}^3\text{m}^{-3}$  on this date is associated with the rainfall event experienced the previous day. The rainfall event and the accompanied rise in soil moisture explains the high  $\sigma^0$  experienced around these dates as shown in Figure 3-10, especially on 15.11.2015 because the availability of moisture in both soil and vegetation canopy increased SAR signal reflectivity.

From the plots of SAR  $\sigma^0$  response to savanna vegetation structure, the VV signal response is higher than VH for all investigated variables - CC, AGB and vegetation cover classes. Both VV and VH backscatter are sensitive to savanna vegetation abundance, with the sensitivity increasing with the abundance class and the size of cover class (from small to large trees). Low abundance CC, AGB and small trees classes gave lower  $\sigma^0$  values while the high abundance classes gave proportionally high  $\sigma^0$ . The wet season shows high  $\sigma^0$  values with high between-class overlap, especially in the days within rainfall events. The overlap in SAR  $\sigma^0$  response to the various vegetation structure components makes it difficult to explain such responses because all seem to display high  $\sigma^0$  values in the wet season.

### **Vegetation cover classes**

The vegetation cover classes according to Food and Agriculture Organization's Land Cover Classification (FAO-LCC) system (Di Gregorio, 2005) comprises three natural vegetation based on height: herbaceous and graminoids (height of 0 - 3 m), shrubs (height of 3 – 5 m) and trees (height > 5 m). However, with the vertical structural complexity of the Lowveld savanna, Naidoo *et al.*, (2012) and Vaughn *et al.*, (2015) proposes, based on height thresholding, a further subdivision of these three major classes into background class (< 0.5 m) and four natural



vegetation classes: shrubs (0.5 - 2.5 m), small trees (2.5 – 5 m), medium trees (5 – 10 m) and large trees (> 10 m). With both vertical and horizontal structural complexities within a savanna ecosystem, there is a localised spatial discontinuity in vegetation classes, sometimes within a few meters. In optical remote sensing, pixels with similar digital numbers and reflectance values are clustered to represent a homogenous feature on the earth's surface (Wężyk *et al.*, 2016), with an assumption that each pixel depicts one homogenous cover type (Adam *et al.*, 2016) and the comparison between pixel data is independent of their neighbourhood. However, the backscattered signal by a SAR sensor is a results from the phase difference between the various features comprising a single pixel. In pixel-based classification, proximity and intensity measures of spatially adjacent objects are calculated only in the spectral space and do not consider the feature space relationship regarding their shape and spatial coordinates (location).

From the plots in Figure 4-11, the  $\sigma^0$  response to shrub, medium trees and background is within an almost similar dB range. C-band SAR  $\sigma^0$  response to vegetation cover classes varies within seasons, with the plots showing high  $\sigma^0$  response in the wet season and a proportionate high  $\sigma^0$  dynamic range within classes compared to dry season for both polarisations. The rainfall and moisture data in Figure 3-10 show that the dates with high  $\sigma^0$  response followed days of rainfall events. On 14.11.15 the area received a rainfall of 6.86 mm and on the same date the soil moisture probe had a reading of 4.77 m<sup>3</sup>m<sup>-3</sup>. The rise in soil moisture from 4.77 m<sup>3</sup>m<sup>-3</sup> on 14.11.2015 to 7.56 m<sup>3</sup>m<sup>-3</sup> the following day on 15.11.2015 and an accompanied observed high  $\sigma^0$  response in both the background and other cover classes points to the effects of moisture availability to SAR signal reflectivity. Correspondingly, this day gave a high backscatter response of ~ -10.8 dB for VV. The same is seen on 9.12.2015 for both VV and VH following a rainfall event of 20.32 mm on 8.12.2015 with the soil moisture rising to 13.38 m<sup>3</sup>m<sup>-3</sup> on this date.

The volumetric scattering response to background and savanna vegetation cover classes is visualised in the VH plot in Figure 4-11 b. For both seasons, the VH polarisation shows the largest  $\sigma^0$  dynamic range between large and small trees; between large trees and background, shrub and medium trees; and between small trees and background, shrub and medium trees, compared to the VV polarisation. The between- and within-class dynamic range changes with seasons. In the wet season, there is high within-class dynamism and low between-class dynamic range causing a lot of overlap between various cover classes for both VV and VH signals. In the dry season however, there is low  $\sigma^0$  within-class dynamic range as the plots seem to flatten out while the between-class dynamic range increases as the plots seem to be separated from

each other. In Figure 4-11 a, the inter-class  $\sigma^0$  dynamic range between large and small trees is negligible on days with rainfall events in the wet season. In the wet season and especially between 3.11.2015 to 26.3.2016, there are several peaks and troughs in  $\sigma^0$  response to the various cover classes on days following rainfall events and days without rainfall, respectively. This is more pronounced on 15.11.2015 and 9.12.2015 for VV and on 9.12.2015 for the VH signals. On these dates, the  $\sigma^0$  values are high and almost the same for all classes. In the wet season, the large trees recorded  $\sigma^0$  in the VV of -10 dB following the rainfall event on 14.11.2015, and this reduces to -14.2 dB on 26.1.2016 (the lowest for large trees in the wet season). This is an equivalent of 4.2 dB difference. In the dry season for the same VV polarisation however, the highest  $\sigma^0$  response to large trees is at -13 dB on 22.9.2016 and the lowest on 5.8.2016 and 17.8.2016 at -14.4 dB, translating to 1.4 dB difference. This trend in dynamism is also visible in VH polarisation and can be attributed to differences in moisture availability.

### **Canopy cover**

Seasonality is also captured by the  $\sigma^0$  response in the wet and the dry seasons. In the wet season, the high  $\sigma^0$  response peaks coincide with rainfall events in Figure 3-10 (section 3.3.6). The rainfall of 6.86 mm on 14.11.2015 can be associated with a corresponding high backscatter intensity from CC on 15.11.2015 in Figure 4-15 a. This is followed by another elevated  $\sigma^0$  value on 9.12.2015 following an observed rainfall even of 20.32 mm on 8.12.2015. There is high  $\sigma^0$  response for high CC at -12.8 dB (VV) and -16.5 dB (VH) following rainfall events experienced in the study area on 9.3.2016 and 11.3.2016 of 7.59 mm and 10.6 mm respectively. The wet season for both polarisations shows high dynamism in SAR  $\sigma^0$  especially on the dates following rainfall events. In these rainy days, the  $\sigma^0$  has the same elevated value, a phenomenon seen in both VV and VH polarisations. This is however not visible in the dry season where within-class  $\sigma^0$  dynamism is so low. The VH  $\sigma^0$  displays a high dynamic range between the various abundance classes than does the VV polarisation, with the  $\sigma^0$  range between the high CC and low CC abundance classes being the highest, followed with the range between moderate and high CC abundance classes.

The interaction between SAR  $\sigma^0$  and CC is visualised in Figure 4-15. C-band  $\sigma^0$  shows proportionality to CC abundance classes, with high CC abundance class giving a characteristic high SAR  $\sigma^0$  response, followed with moderate CC abundance class and finally low CC

abundance class with low  $\sigma^0$  response, for both VV and VH polarisations. When the mean of all CC plots is plotted (black plot), the  $\sigma^0$  response is almost equivalent to the moderate CC abundance class (blue plot). There is a difference in seasonal response to CC as seen in  $\sigma^0$  values, with the wet season showing a higher  $\sigma^0$  response than does the dry season. In the wet season, the SAR  $\sigma^0$  response to different canopy abundance classes are identical and within an almost similar  $\sigma^0$  range. This is more visible in the wet season of VV polarisation (Figure 4-15 a), where some acquisition dates show overlap in  $\sigma^0$  response to the various CC abundance classes. In the wet season, there is increased greenness accompanying development of leaves within the top canopy. This means a large canopy surface is exposed to not only the incoming C-band SAR signal but also an interception to rain-water. The accompanying increase in moisture-induced dielectric constant amplifies the  $\sigma^0$  in the wet season.

Whereas VV has high  $\sigma^0$  resulting from equal magnitude of sent and received signal intensity as opposed to VH polarisation, seasonal  $\sigma^0$  response to savanna vegetation structure is different between the two polarisations. In Figure 4-15 the  $\sigma^0$  for low abundance CC associated with shrubs and low vegetation classes can be separated from the  $\sigma^0$  for high abundance CC. Studies by Baghdadi *et al.*, (2001) to examine the potential of C-band SAR radar imagery for monitoring different wetland vegetation found out that it was in deed possible to not only detect but also separate wetland areas and other surface cover types (forests and clearing) using multi-temporal C-band SAR. This potential of C-band SAR has also been utilised by Ferrazzoli *et al.*, (1997) in discriminating herbaceous crops types even in moderate growth. For seasonal SAR  $\sigma^0$  response, and in the absence of moisture, typical of dry seasons, it should be easier to assess the SAR  $\sigma^0$  response from various abundance classes because the plots seem to flatten out with high between-class  $\sigma^0$  dynamic range causing no overlap. From the analysis of multi-temporal C-band SAR, it has been shown that the highest correlation of  $\sigma^0$  to different classes is more visible in cross polarisation, particularly VH, which is very low for low CC abundance, gradually increases with moderate CC class and increases in high CC abundance classes.

Baghdadi *et al.*, (2006) and Dubois *et al.*, (1995) have both used bare soil to develop soil moisture retrieval models. There is a high sensitivity of C-band  $\sigma^0$  to background in the current study because the SAR signal attenuation effect by vegetation components is minimised especially in the dry season. The SAR signal correlation to soil moisture availability in terms of  $\sigma^0$  signal is higher in the VV than in the VH polarisation. However, there is more inter-class sensitivity in the VH polarisation than does in the VV, as seen in the differences in backscatter values between the various cover classes – the large trees in the VH for example are distinctly

displaying high backscatter values than the small trees (Figure 4-11). There is, however, an overlap between backscatter values in the VV polarisation, making it impossible to associate  $\sigma^0$  range to a cover class. This is also visible in the VH, but for medium trees, shrubs, and background classes.

El Hajji *et al.*, (2018) assessed the penetrative ability of C- and L-band to various crop types and noted that C-band in VV polarisation can penetrate the maize canopy even when the canopy is well developed ( $NDVI > 0.7$ ) due to high-order scattering along the soil-vegetation pathway that contains a soil contribution. The high  $\sigma^0$  from soil is a sum of soil moisture and surface roughness contributions (Ulaby *et al.*, 1986), and background backscattering increases as soil roughness increases (El Hajji *et al.*, 2018). During low greenness as commonly experienced in the dry season when most leaves have fallen, the  $\sigma^0$  is dominated by direct scattering from soil. The open canopy created by deciduous trees which shed leaves allow SAR signals to reach the ground surface. For the cover classes, the  $\sigma^0$  response is low for small trees, while the background has a similar response to medium trees due to the attenuation of the direct ground scattering. A similar observation is also seen in El Hajji *et al.*, (2018) and the decrease is attributed to vertical stems and leaves that produce high absorption of the incident SAR wave associated with weak direct scattering (Mattia *et al.*, 2003; Del Frate *et al.*, 2004).

Well-developed vegetation cover classes attenuate C-band SAR signal leading to low sensitivity for high greenness values. Baghdadi *et al.*, (2015) noticed this phenomenon at peak growth season with moderate to high greenness values ( $NDVI > 0.7$ ). At the beginning of the wet season, the backscatter intensity values rise resulting from the increase in direct scattering from the vegetation canopy, an observation also made by Brown *et al.*, (2003). In this wet period, the scattering from the upper canopy elements is seen (Brown *et al.*, 2003). In the dry season however, between 1.5.2016 to 29.8.2016, there is reduced moisture resulting from lack of rainfall events and the canopy cover is reduced due to shedding of leaves typical of dry season. Here, the  $\sigma^0$  is more sensitive in the medium trees, larger trees and background (soil) due to the decrease in canopy attenuation (El Hajji *et al.*, 2018) and possibly tree trunk scattering. Sparse vegetation cover and dry season vegetation cover does not attenuate the SAR signal as observed by Moran *et al.*, (2000).

## **Aboveground biomass**

The low abundance AGB class shows exceptionally high temporal dynamics both within and between seasons. In the early wet season, the rainfall episodes following a long dry season in 2015 caused an abrupt increase in backscatter response. Since only trees with height above 5 m were inventoried from the TLS point clouds, the study assumes that shrub and small vegetation forming part of the low AGB class were left out. Therefore, the low AGB abundance class in this study falls in the lower boundary of moderate AGB abundance class. This explains the inconsistently high  $\sigma^0$  response, and the accompanying class overlap between the two for both seasons and polarisations.

Moderate AGB class constitute plots with AGB ranging between 30 and 50 t/ha. This study, and several prior studies by Colgan *et al.*, (2013); Mograbi *et al.*, (2015) and Odipo *et al.*, (2016) have cited that the mean biome AGB for this area also falls within this range. This can partly explain the high SAR  $\sigma^0$  response on the moderate AGB class than the low and high abundance classes. The results from this study further shows that SAR sensitivity to AGB increases up to about 40 t/ha and 60 t/ha in the case of C- and L-band SAR, respectively. The high AGB abundance class shows plots with AGB above 60 t/ha and the low  $\sigma^0$  response can be explained by low sensitivity of C-band SAR backscatter to AGB above 40 t/ha.

### ***5.2.4. Effects of speckle filter on C-band SAR response to savanna vegetation***

SAR resolution cells comprise many scatterers (trees, grass, shrubs) with different phases (Walker, 2000) and intensity. These elements create a random and multiplicative granular noise-like effect in a radar image, hence posing difficulties in estimating radar backscatter at the pixel level (Qiu *et al.*, 2004). The radar signal is coherent, meaning the signals are transmitted at narrow wavelength ranges (Rees, 2012; Campbell & Wynne, 2011), and the small adjacent features are pronounced or suppressed. For homogeneous ground features, the resolution contains scatterers yielding signals of the same magnitude, typical of distributed targets. Heterogeneous ground features result in different phases of each signal path as seen with point targets, leading to destructive or constructive backscattered energy with the amplitude of received signal varying randomly (Argenti *et al.*, 2013). Erroneous variations in backscatter from inhomogeneous cells increase SAR image variances (Mansourpour *et al.*, 1997), obscure image clarity, and act as a barrier for texture-based analysis. Pre-processing of the SAR data to reduce or eliminate the effects of speckle is a very crucial step before image

utilisation through multi-looking (ML). ML reduces the effects of speckle by averaging the number of independent intensity values related to the same pixel, thereby improving radar cross sectional variance (Argenti *et al.*, 2013; Moreira *et al.*, 2013). Speckle filtering significantly optimizes the ability to exploit the texture variance between neighbouring pixels in SAR imagery, and to discern spatial information of the ground scene target and land use types in forested areas, and thus enhance data interpretability and efficient image classification (Amini & Sumantyo, 2009).

Spatial speckle filters aim at estimating the noise-free radar reflectivity from the observed noisy SAR image (Argenti *et al.*, 2013; Touzi, 2002). They are executed within moving windows by averaging features in surrounding pixels, with the window size affecting effect and the larger the window, the more the effects of smaller features within a pixel are diminished, moving towards the characteristics of the dominant class within a pixel. In this study, Quegan multi-temporal filter (Quegan & Yu, 2001) was used for filtering the multi-temporal C-band SAR datasets. This filter is best suited for multi-temporal image stacks because it preserved the changes within multi-temporal data making it appropriate for forest degradation monitoring (Flores-Anderson *et al.*, 2019).

Figures 4-13 and 4-14, 4-17 and 4-18, and 4-20 and 4-21 shows the speckle filter at both 3 by 3 and 5 by 5 speckle window sizes, for vegetation cover classes, CC and AGB respectively. Validation of speckle reduction in SAR image is not an easy task because the noise-free reflectivity estimated is unknown making it difficult to compare the despeckled image and the original ground truth (Argenti *et al.*, 2013). In this study, an assessment of the effects of applied Quegan multispectral filter was done using visual inspection of the behaviour of multi-temporal backscatter plots and comparing with the original plots as suggested by Argenti *et al.*, (2013). The application of speckle filter lowered the between-class  $\sigma^0$  variations for different abundance and cover classes. Figure 4-12 and 4-14 shows that unlike the original plot in Figure 4-11, the cover class plots are more distinct and shows less variability in terms of point distribution. By averaging adjacent pixels, filtering reduces variance between SAR pixels leading to a reduced inter-class overlap.

SAR is a coherent imaging sensor and the speckle in the SAR image is caused by interference between the coherent returns from various scatterers on the surface (Goodman, 1976; Argenti *et al.*, 2013). Without speckle filtering in the wet season, the shrub vegetation responds to an increase in soil moisture following a rainfall event on 14.11.2015. This is the only instance

moisture availability after the rainfall event is seen to have affected  $\sigma^0$  response to the vegetation structure class on this date in the VV. However, with application of speckle filter within a 3 by 3 window, this backscatter response to shrub vegetation is reduced (Figure 4-12 (a)). A further enlargement of the filter window to 5 by 5 completely removes sensitivity to shrub vegetation (Figure 4-13 (a)). This is because filtering averages scatterers in the surrounding pixels and such low classes like shrubs are overshadowed by the dominant classes. For dry season, most low trees have lower response due to desiccation of the soil making shallow-rooted trees inaccessible to water, unlike medium and large trees whose roots are long and can access water deeper in the soil.

For all seasons, between-class  $\sigma^0$  dynamic range for AGB abundance classes is low, especially moderate and low AGB abundance classes. This is because the low AGB classes do not incorporate the shrub layer, hence the low classes might be the lower boundary of the moderate AGB classes. Shrub vegetation comprise the low tree class for AGB estimation and make up the bulk of savanna woody component. Therefore, leaving this component out means the lowest AGB class is left out. It is difficult to notice the effects of speckle filter for AGB classes, except the low within-class dynamic range for the abundance classes resulting from a reduction in variance; this is more visible in the VH response than VV. Having left out the lower tree trunks from the allometry AGB calculation, the speckle filter only average moderate and high vegetation classes. With an increase in speckle size from a 3 by 3 to a 5 by 5 moving window for VH, the SAR response for both high and moderate AGB is almost similar, and it becomes difficult to differentiate these two classes in both the wet and dry seasons. Conversely, in the dry season, there are some dates where the inter-classes dynamic range is high eliminating plot overlap. Low AGB classes gave the lowest SAR  $\sigma^0$  responses compared to moderate and high AGB classes.

### **5.3.Uncertainties in savanna structure mapping**

#### ***5.3.1. Tree mensuration from field and TLS***

Field data collection is time consuming, requires a lot of resources and does not cover larger areas. This limits the representativeness of the field inventoried reference tree data, which might lead to misrepresentation of the entire study area under investigation. More so, such inventories are prone to non-intentional human errors that might be introduced during data collection, apart

from a fault in the instrument used. Tree height measurement instruments such as clinometers rely on the ability of the enumerator to view the top of the canopy to triangulate the required distances for computing tree height. In most cases, and where the tree canopy is large or enumerator short, capturing the highest point of the canopy is difficult, which might lead to wrong tree height measurements. For savanna structural mapping and biomass estimation within the Lowveld savanna, studies by Scholes *et al.*, (2001); Nickless *et al.*, (2011); Colgan *et al.*, (2013) and Mograbi *et al.*, (2015) recommends tree basal diameter measurements from 1 m above the ground to capture the shrub vegetation layer which forms the bulk of the woody component and multi-stemmed trees within this typical Lowveld savanna sub-biome.

### **5.3.2. Biomass Prediction**

The error in biomass prediction varies with the method used. SAR-AGB modelling used TLS-modelled AGB as reference because the field inventory yielded fewer non-representative reference plots. The error produced in modelling AGB from TLS using field inventory data is lower than those obtained in the subsequent SAR-AGB modelling. The allometric validation error (RMSE) from TLS-CHM predictor variables are 4.77 t/ha, 2.13 t/ha and 2.32 t/ha for CC, CH, and the product of the two ( $CC \times CH$ ), respectively, making up 12.5%, 6.3%, and 6.8% of the respective predicted biomass means. The error values are reasonably small even though using the  $CC \times CH$  biomass with 7% error would lead to error propagation in subsequent predictions as highlighted in this study. The high error values reported in predicting biomass from both C- and L-band SAR backscatter are not higher than those obtained within the same area using Nickless allometry (Lefsky *et al.*, 2005; Nickless *et al.*, 2011; Colgan *et al.*, 2012) because the current study used some trees with basal diameters  $> 33$  cm. Nickless *et al.*, (2011) allometry and the resultant AGB estimates were derived from trees with basal diameters less than 33 cm. Still, predicted higher biomass values are associated with trees with larger diameters than those used in the study. As Sankaran *et al.*, (2004) notes, most allometric models lack large diameter classes and these errors associated with higher values can be explained from the deficiencies in allometries used. This explains the non-linear relationships shown in the residual errors where the prediction gets worse as the biomass gets larger above 50 t/ha in the TLS-derived AGB and 40 t/ha in the L-band SAR modelled AGB. The TLS canopy height model, when calibrated and validated by field data, produces low errors.

In this study random forest regression was used to model AGB from L-band SAR data using TLS CHM metrics (CC, CH and  $CC \cdot CH$ ). A review of many studies on the performance of RF



against other ensemble algorithms and other machine learning methods has proposed RF to outperform most of other classifiers such as the support vector machines (Akar & Güngör, 2012). With RF, it is very easy to set parameters. The algorithm is an easy to learn and use because, there is no need to prune trees and the technique uses randomization in variable (used to split the node) selection (bootstrap aggregation with sample replacement) to control diversity between tree variables in the ensemble, thereby reducing the biasness (Poona *et al.*, 2016). The information about accuracy and variable importance is also automatically generated (Horning, 2010).

Whereas RF classifiers are not prone to over-fitting (Poona *et al.*, 2016), other findings have revealed that for regression analysis, RF classifiers cannot go beyond the training data range and, the extreme values of the variables used are not accurately predicted - higher values may be underestimated while low values overestimated (Chen & Cheng, 2016; Horning, 2010). Poona *et al.*, (2016) also argues that tree building in RF is based on one feature which is selected for splitting the node and this may render the algorithm inefficient due to feature dependencies inherent in multidimensional data.

From the residual plots, the randomness in the points at lower biomass values is evidence of linearity in relationship between the TLS metrics and the field-derived biomass - shown by the scattering of residuals around the zero line. However, this linearity is visible with low biomass values up to 40 t/ha, after which the residual errors increase and become positive with canopy height (CH), and negative with both canopy cover and the product of canopy cover and height (CC and  $CC \times CH$ ). Log-transformation on the field AGB improved the randomness in the distribution of the residuals, and therefore an improvement in the linearity between log-transformed AGB and the predictors can be seen.

From the multi-temporal plots, AGB and CC abundance explain the temporal variability in the SAR backscatter response. The wet season showed high SAR backscatter intensity responses for both AGB and CC, which reduced to stable values in the dry season. From Figure 4-11, the background which comprises the herbaceous layer and bare patches display high backscatter intensity compared to shrubs and small trees. This behaviour is seen in both wet and dry seasons, though more pronounced in the dry season. Most studies have attributed this to more backscatter response from soil-lower vegetation interactions and is affected by moisture availability in the soil. Separation of backscatter response from these two layers were not

captured in this study, and so it is assumed the backscatter coefficients from the plots are cumulative for both soil and canopy interactions.

# CHAPTER 6

## 6. Summary, conclusions and outlook

### 6.1. Summary

The foregoing study achieved the following objectives:

- a) *To evaluate the potential of high-resolution terrestrial laser scanner (TLS) in extraction of savanna vegetation structure variables;*

This study developed methods through which the potential of TLS technology can be utilized as reference data necessary for mapping both vertical and horizontal savanna vegetation structure (Niemi *et al.*, 2015; Calders *et al.*, 2015) in the form of AGB, CC and vegetation cover classes within a Lowveld savanna. The TLS point clouds were processed into vegetation CHM (Khosravipour *et al.*, 2014) with the ability to model not only the terrain characteristics of the study area but also the extraction of savanna vegetation cover classes (Wang *et al.*, 2016; Huerta *et al.*, 2017; Cabo *et al.*, 2018). The proportion of CHM pixels with above 1 m height within both 20 m and 30 m SAR-pixel grids, here referred to as plots, provided the basis from which canopy height was computed, and together with CC were used to model AGB from both L-band ALOS PALSAR and C-band Sentinel-1A microwave datasets for the study area. TLS point clouds were used to reconstruct the tree variables necessary for biomass estimation; tree height and basal diameter at 1 m height. This provided a better alternative to field-based tree inventory, with the ability to measure 565 trees averaged within 445 field plots over the study area. In comparison, the field-based inventory yielded fewer trees (237) within 42 plots. The field inventory data was used for allometry-based AGB estimations within 30-m plots, and further used for TLS-based canopy height validation (Cabo *et al.*, 2018). OBIA enabled pixel-based height thresholding of TLS CHM necessary for classification of Lowveld savanna vegetation, resulting in five vegetation cover classes; background (at less than 0.5 m height), shrubs (at 0.5 – 2.5 m height), small trees (at 2.5 – 5 m height), medium trees (at 5 – 10 m height) and large trees (at over 10 m height) classes, after methodologies by FAO LUCC (Di Gregorio, 2015), Naidoo *et al.*, (2012) and Vaughn *et al.*, (2015).

b) *To estimate landscape-wide AGB and assess AGB changes over a period of four years using multi-temporal L-band SAR within a Lowveld savanna in Kruger National Park*

Field inventory was carried out during the dry season in March 2015 within the study area. The height and basal diameter variables from the inventoried trees enabled tree-level aboveground biomass calculation using Lowveld savanna biome-specific allometry. TLS CHM metrics, CC (%) and CH (m) were used to model plot level biomass over 42 inventoried plots in Skukuza, forming reference datasets for biomass estimation within the study area using L-band ALOS PALSAR backscatter intensity. Biomass regression models (CC, CH, CC.CH) enabled assessment of the potential and performance of respective TLS CHM-derived structure variables, CC & CH (Colgan *et al.*, 2012; 2013) in predicting landscape-wide AGB using the multi-temporal L-band SAR data. TLS CHM metrics increased the reference sample plots from 42 to 513 within the TLS footprint, making it representative reference for a large area AGB estimation. A product of CC x CH performed the best of the three TLS metrics, and so formed the basis for landscape-wide AGB analysis. This was performed for the years 2007, 2008, 2009 and 2010 under investigation, using L-band data acquired during the dry season (September-October). The results from model validation showed a significant linear relationship between TLS - derived predictors with field biomass,  $p < 0.05$  and adjusted  $R^2$  ranging between 0.56 for SAR to 0.93 for the TLS - derived canopy cover and height (same as in studies by Baghdadi *et al.*, 2001). The AGB change analysis between the four years under investigation showed 32 ha (3.5%) of the 900-ha experienced AGB losses above an average of 5 t/ha per annum, which can mainly be attributed to the falling of trees by mega herbivores such as elephants (Asner *et al.*, 2016). The spatial distribution of AGB within the study area is a function of topographic and soil characteristics of the area, with low AGB occurring on the high elevation areas while high AGB occurs in the lowlands, especially around river and stream valleys (Scholes *et al.*, 2001; Smit *et al.*, 2013; Baldeck *et al.*, 2014; Scholtz *et al.*, 2014). The study concludes that SAR data, especially L-band ALOS PALSAR, can be used in the detection of small changes in savanna vegetation.

c) *To assess interactions between C-band synthetic aperture radar with various savanna vegetation structure variables*

The coexistence of grass-shrub-tree within Lowveld savanna and the associated heterogeneity makes it difficult to separate the different cover patches created by these cover classes (Charles-Dominique *et al.*, 2015; Mermoz *et al.*, 2014). At pixel level, there is no single definite surface feature, rather a mixture of several features that render a single pixel impossible to interpret (Shirima *et al.*, 2011). TLS-derived vegetation structure variables like AGB (t/ha), CC (%) and vegetation cover classes produced in objective (a) above were used to assess the response of SAR metrics at pixel-level within a Lowveld savanna. Multi-temporal C-band Sentinel-1 A SAR data at 20 m resolution, enabled investigation into SAR  $\sigma^0$  response to savanna vegetation abundance and cover classes over 29 acquisition dates, covering both wet and dry seasons between November 2015 and October 2016. This study investigated the proportion of vegetation cover class and assigned a class with the highest proportion to a SAR pixel as the dominant class with an assumption that, despite a pixel comprising multiple scatterers, the dominant feature contributed the most to the  $\sigma^0$  signal. By classifying AGB and CC into low, moderate and high abundance classes through averaging the different class samples, this study assessed the  $\sigma^0$  response to these classes as proxies to the various savanna ecologies: herbaceous, shrub and tree components. The mean class values reduced inter-class variability and ensured an independent assessment of  $\sigma^0$  response to each of the abundance classes. The effects of SAR polarisation, speckle filter window, and seasonality on savanna structure parameters were investigated. The VV signal showed high sensitivity to vegetation cover classes, CC and AGB than VH, with VH showing more promise in between-class  $\sigma^0$  response. An assessment of multi-temporal C-band SAR  $\sigma^0$  response to the various vegetation structure variables within this Lowveld savanna revealed that several factors affect  $\sigma^0$  interactions with savanna vegetation: seasonality and moisture dynamics, vegetation class, soil-vegetation interactions and SAR polarisation. Wet season has low between-class dynamic range leading to an almost similar  $\sigma^0$  response between different classes, especially on the days following rainfall events. Elevated moisture levels following rainfall events increase dielectric constant of vegetation components and soil, increasing radar reflectivity which results in high  $\sigma^0$ . The open canopy within heterogeneous savanna allows for SAR signal penetration to the ground surface, resulting in cumulative backscatter response not only from the vegetation canopy but also from soil and herbaceous layer (Ulaby *et al.*, 1986; Dubois *et al.*, 1985). High  $\sigma^0$  were observed for high CC and AGB abundance classes and large trees, while low abundance classes and small trees displayed a proportionately low  $\sigma^0$  (Mattia *et al.*, 2003; Del Frate *et al.*, 2004).

## 6.2. Conclusions

Savanna vegetation structure mapping provides a basis for monitoring and assessing present and future trends of global carbon stocks within this biome. Monitoring dynamics caused by disturbances in the savannas pose a challenge because of the coexistence of grass-shrub with tree patches and the resulting heterogeneity over localized spatial scales. Remote sensing provides the best techniques for large-scale carbon stock assessment, critical for adoption of sustainable forest resources management and reporting by developing countries who are signatories to the REDD framework. Validity of remote sensing derived forest monitoring parameters such as carbon stock estimates through changes in CC and quantifying AGB dynamics are reliant on availability of high-quality calibration and validation datasets. Conventionally used field-based forest inventories are limited in the provision of validation datasets for savanna structure mapping, given the limited spatial coverage, accessibility issues, time and cost constraints and data integration problems caused by differences in sampling procedures. Assessment of intrinsic heterogeneity drivers are often left out in large-area or biome-scale studies, hence the need for a more detailed and localized assessment as adopted in the foregoing study.

This study, appreciating the importance of field inventory as a source of validation data, examined the potential of up-scaling the field inventory data with TLS data to estimate landscape-wide AGB using L-band SAR data. Despite free availability of remote sensing data for vegetation mapping, optical remote sensing data suffers from atmospheric aerosol and cloud contamination especially in the tropics resulting in inconsistency in data availability necessary for continuous vegetation monitoring initiatives. This study therefore explored the potential of freely available Sentinel-1 A SAR data by ESA under Copernicus Program. Further, C-band SAR data made it possible for assessment of savanna vegetation structure variables at pixel level. The complementarities of each of these datasets have been discussed. The field inventory and TLS datasets were used to estimate AGB at both tree and plot level, while TLS-CHM data improving the representativeness of reference data from few field inventory plots to TLS-footprint for extrapolation with L-band SAR backscatter over a wider area through regression models over the four years under investigation. The possibility of computing tree and plot biomass was explored through reconstruction of tree trunks for DBH and height measurement from TLS point clouds. The potential of TLS in AGB estimation as well as the extraction of savanna vegetation structural components like canopy cover and vegetation cover classes has

been assessed. This study has shown that it is possible to use L-band SAR data to detect biomass changes above 5 t/ha within a Lowveld savanna biome.

The availability of a small TLS footprint coupled with a few field inventoried plots over the study area should be a limiting factor in savanna vegetation structure modelling over a wider spatial coverage. This, coupled with the multi-resolution datasets used in the study, leads to a compromise in using the full potential of TLS data at high resolution. There is a possibility of exploring field biomass inventory at a tree level instead of a plot level. This, when combined with TLS data at full resolution, should go a long way in estimating canopy-level cover and height structure parameters at the tree level as opposed to the plot level.

The vegetation structure abundance in this typical Lowveld savanna explains the temporal variability in SAR backscatter response, with high abundance classes and large tree classes typical in the wet season giving higher backscatter response because of increased canopy structure parameters like leaves and branches upon which the incoming signals can interact, besides moisture effects on backscatter. Classifying savanna vegetation structure components into abundance classes reduces both between- and within-class temporal variance, making it possible for class-based analysis within a pixel and extending to the typical response from savanna heterogeneity components like herbaceous layer, shrub and trees. Moisture content not only affects the seasonal backscatter variability, but the effects are also high in the background classes (soil and herbaceous layers). This is because following a rainfall event, the soil water input through infiltration increases the soil moisture content besides other vegetation layers. This study also explored the effects of speckle suppression through the application of Quegan multi-temporal filter because of its ability to retain changes within a time series data. Whereas the savanna is composed of heterogeneous ecologies, the speckle filtering improved the inter-class SAR response to the various classes, at least to some extent.

### 6.3. Outlook

Whereas AGB change detections were possible with SAR data under outlined accuracy conditions and within the same seasons in different years, the study did not, however, look at the precise quantities of AGB losses and gains over the study duration, rather the proportion of the area that experienced a change above the threshold values of 5 t/ha. Future studies should therefore look at quantitative estimation of these changes within a typical Lowveld savanna — this should be possible under similar radar geometries (for example incident angle and pass) and seasons over multiple years. This study concentrated on the estimation of aboveground woody biomass from both C- and L-band SAR. It would be important to investigate methodologies that would capture the herbaceous biomass because this controls the heterogeneity of savannas. The high fuel load triggers frequent fires that control bush encroachment, while grass abundance controls spatial distribution of grazers within this ecosystem. The biotic and abiotic interactions within this biome and how this affects woody structure dynamics, especially climate, topography, soil, fire and herbivory are critical in altering the biome structure and so studies should be directed towards investigating the extent to which these alterations affect SAR backscatter at a case-to-case basis.

Most reviewed previous work on C-band SAR interactions with vegetation within various biomes point to the fact that co-polarised (VV and HH) parameters perform the best with AGB and CC modelling (e.g. in Wang *et al.*, 1994; Picard *et al.*, 2003). This is because of the high backscatter-vegetation parameter correlation, mainly attributed to the reception of most of the emitted V-orientation signal unlike the cross-polarised signals which are attenuated by the depolarisation effects of the ground targets. The findings of this study also tally with these previous findings. However, the between-class response to C-band SAR backscatter is best visualized in the cross-pol combination, VH. In this study, the VV despite high backscatter response for high and low abundance classes respectively, gives a minimal dynamic range between different abundance classes with the response in some dates showing overlap in backscatter signals. This makes it difficult to assess the different savanna ecologies based on vertical stratification such as height and DBH. It is known that large trees store more carbon stock than shrubs and small trees. By reclassifying the vegetation structural variables, it is possible to at least associate backscatter coefficient response to a savanna ecology, e.g. herbaceous vegetation, shrub vegetation and tree vegetation. This is only seen in the VH signal where the plots between the small tree and low abundance CC classes display plots with lower



backscatter coefficients than does large trees and high CC abundance classes, hence high backscatter dynamic ranges between classes.

Sano *et al.*, (2005) adopted a SAR-optical synergy in compensating for soil background effects on backscatter response to cerrado vegetation types in Brazil. In this study, the backscatter coefficient did not show any temporal changes between dry and wet seasons as a response to vegetation structures. By fusing optical vegetation greenness indices with backscatter variables, an improvement in cerrado classification was achieved. In studies by Gallant *et al.*, (2014) to detect wetland vegetation phenology, fusion of Landsat optical data with L-band Radarsat-2 SAR data helped in discerning wetland features from grasslands. The current study only used L- and C-band SAR backscatter parameters. It would be interesting to assess how the highlighted temporal (inter-annual and seasonal) changes in backscatter would relate to optical variables such as greenness indices. Vreugdenhil *et al.*, (2018) also showed a possibility of assessing backscatter sensitivity to vegetation through a ratio between C-band VV and VH, a method that should be tested further. This way, it should be possible to associate such changes to phenology cycles within savanna biome. There is a correlation between structural abundance and seasons. Seasonal changes affect vegetation phenology and hence the greening and browning episodes typical of wet and dry seasons, respectively. Optical derived spectral greenness indices can help explain the temporal dynamics cited in this study, a phenomenon that can be explored in vegetation phenology analysis. Of great interest should be to correlate the multi-temporal backscatter and other SAR metrics with temporal greenness indices over the study period.

There are gaps in studies to separate the effects of soil moisture on vegetation parameter interactions to SAR signals. Various studies have pointed to the need to quantify the extent to which presence of vegetation attenuates soil moisture estimations, and vice versa. Whereas these studies have assessed these effects on sparse vegetation biomes such as grasslands and farmlands with grass-like crops such as wheat and corn (Griffiths & Wooding, 1996; Picard *et al.*, 20013; McNairn & Brisco, 2004), few of them have investigated how the various savanna vegetation ecologies independently attenuate C-band SAR signal based on various moisture regimes.

Picard *et al.*, 2003 noted that VV-backscatter attenuation by the vegetation canopy increased with an increase in SAR incident angle. The current study area is relatively flat, with a slope at approximately 3 %. In this study, SAR datasets used were acquired with the same incident angles in the ascending pass for both L- and C-band. It would be of interest to assess the effects

of different SAR geometries on mapping savanna vegetation. Different vegetation species within a biome contribute differently to its carbon stock. This study did not capture species diversity and how such affects AGB values within the study area. However, there is no species-specific allometry for KNP. Based on the potential of TLS in capturing tree-level biophysical parameters non-destructively, attempts should aim at coming up with TLS-derived allometries.

## References

- Abraham J, Adolt R (2006) *Stand Heights Estimations Using Aerial Images and Laser Datasets*, Workshop on 3D RS in Forestry, Vienna, Austria. Volume 2a, pp. 24–31.
- Adam HE, Csaplovics E & Elhaja ME (2016) A comparison of pixel-based and object-based approaches for land use land cover classification in semi-arid areas, Sudan. *Earth and Environmental Science*, **37**. Doi:10.1088/1755-1315/37/1/012061.
- Adams J & Gillespie A (2006) *Remote Sensing of Landscapes with Spectral Images: A Physical Modelling Approach*. Cambridge: Cambridge University Press. Page 362 Doi: 10.1017/CBO9780511617195.
- Adler D & Synnott TJ (1992) *Permanent Sample Plot Techniques for Mixed Tropical Forest*, Tropical Forest Papers, Oxford Forestry Institute: Oxford, UK. Volume 25.
- Akar Ö & Güngör O (2012) Classification of multispectral images using Random Forest algorithm. *Journal of Geodesy & Geoinformation*, **1** (2): 105-112.
- American Society for Photogrammetry & Remote Sensing (ASPRS), (2011) *LAS Specification*, version 1.4-R6, *American Society for Photogrammetry & Remote Sensing*: Bethesda, MD, USA, Page 10.
- Amini J & Sumantyo JTS (2009) Employing a Method on SAR and Optical Images for Forest Biomass Estimation. *IEEE Transactions on Geosciences & Remote Sensing*. **47** (12). Doi: 10.1109/TGRS.2009.2034464.
- Andersen A, Cook G & Williams D (2012) Savanna burning: The ecology and economy of fire in tropical savannas. *Austral Ecology*. **37**, 633. Doi:10.1111/j.1442-9993.2012. 02410.x.
- Antonarakis AS, Saatchi SS, Chazdon RL & Moorcroft PR (2011) Using Lidar and radar measurement to constrain predictions of forest ecosystem structure and function. *Ecological Applications*. **21**, 1120–1137.

- Applied Imagery (2017) QuickTerrain Reader: Getting started. Available online: <http://appliedimagery.com/downloads/pdf/Quick%20Terrain%20Reader%20-%20Getting%20Started.pdf> . (Accessed on 27.05.2017).
- Archibald S & Scholes RJ (2007) Leaf green-up in semi-arid African savanna: separating tree and grass responses to environmental cues. *Journal of Vegetation Science*. **18**: 583-594. Doi: 10.1111/j.1654-1103.2007.tb02572.x.
- Argenti F, Lapini A, Alparone L, Bianchi T (2013) A tutorial on speckle reduction in Synthetic Aperture Radar images. *IEEE Geosciences & Remote Sensing Magazine*. **1**, 6–35.
- Asner GP, Levick SR, Kennedy-Bowdoin T, Knapp DE, Emerson R, Jacobson J, Colgan SM, & Martin RE (2008) Large-scale impacts of herbivores on the structural diversity of African savannas. *PNAS*, **106** (12): 4947-4952. Doi: 10.1073/pnas.0810637106.
- Asner GP, Vaughn N, Smit IPJ & Levick S (2016) Ecosystem-scale effects of megafauna in African savannas. *Ecography*. **39**: 240–252. Doi: 10.1111/ecog.01640.
- Asner GP, & Heidebrecht KB (2002) Spectral unmixing of vegetation, soil and dry carbon in arid regions: Comparing multispectral and hyperspectral observations. *International Journal of Remote Sensing*. **23** (19): 3939 – 3958. Doi: doi.org/10.1080/01431160110115960.
- Asner GP, Levick SR, Smit PJI (2010) Remote Sensing of Fractional Cover and Biochemistry in Savannas. in Hill, M.J & N.P Hanan (eds). *Ecosystem function in savannas: measurement and modelling at landscape to global scales*. CRC Press. Pages: 195-219.
- Baade J, & Schmallius C (2016) TanDEM-X IDEM precision and accuracy assessment based on a large assembly of differential GNSS measurements in Kruger National Park, South Africa. *ISPRS Journal of Photogrammetry & Remote Sensing*, **119**, 496–508.
- Baccini A, Friedl MA, Woodcock CE & Warbington R (2004) Forest biomass estimation over regional scales using multisource data. *Geophysical Research Letters*, **31**: L10501. Doi:10.1029/2004GL019782.

- Baccini A, Laporte N, Goetz SJ, Sun M, Dong H (2008) A first map of tropical Africa's above-ground biomass derived from satellite imagery. *Environmental Research Letters*, **3**, 045011.
- Baghdadi N, Bernier M, Gauthier R & Neeson I (2001) Evaluation of C-band SAR data for wetlands mapping. *International Journal of Remote Sensing*, **22** (1): 71–88.
- Baghdadi N, Holan N & Zribi M (2006) Soil moisture estimation using multi-incidence and multi-polarisation ASAR data. *International Journal of Remote Sensing*, **27**, 1907-1920.
- Baldeck CA, Colgan MS, Feret JB, Levick SR, Martin RE, Asner GP (2014) Landscape-scale variation in plant community composition of an African Savanna from airborne species mapping. *Ecological Applications*, **24**, 84–93.
- Banks DJ, Griffin NJ, Shackleton CM, Mavrandonis JM (1996) Wood supply and demand around two rural settlements in a semi-arid savanna. *Biomass Bioenergy*, **11**, 319–331.
- Baronti B, Del Frate F, Ferrazzoli P & Paloscia S (1993) Interpretation of Polarimetric MAC-91 data over Montespertoli Agricultural area, *Proc. of the 25<sup>th</sup> Intern. Symposium, Remote Sensing and Global Change*, Graz (Austria), 4-8 April 1993.
- Barton JM, Bristow JW & Venter FJ (1986) A summary of the Precambrian Granitoid rocks of the Kruger National Park. *Koedoe* **29**: 39-44.
- Baudoin M-A, Vogel C, Nortje K & Naik M (2017) Living with drought in South Africa: lessons learnt from the recent El Nino drought period. *International Journal of Disaster Risk Reduction*, **23**: 128-137. Doi: 10.1016/j.ijdrr.2017.05.005.
- Beer C, Reichstein M, Tomelleri E, Ciais P, Jung M, Carvalhais N, Rödenbeck C, Arain MA, Baldocchi D, Bonan GB, Bondeau A, Cescatti A, Lasslop G, Lindroth A, Lomas M, Luysseart S, Margolis H, Oleson KW, Rouspard O, Veenendaal E, Viovy N, Williams C, Woodward FI & Papale D (2010) Terrestrial gross carbon dioxide uptake: Global distribution and covariation with climate. *Science*, **329** (5993): 834-8. Doi: 10.1126/science.1184984.

- Ben-Arie JR, Hay GJ, Powers RP, Castilla G, St-Onge B (2009) Developing of a pit filling algorithm for LIDAR canopy height models. *ComputGeosci*, **35**, 1940–1949.
- Berni AJ, Kljun N, van Gorsel E, Haverd D, Leuning R, Cabello-Leblic A, Held A, Hopkinson C, Chasmer L, Youngentob K (2011) 3D spatial distribution of biophysical parameters derived from hyperspectral and lidar remote sensing. Improving the constraints in land surface modelling, in *34th International Symposium on Remote Sensing of Environment*. Sydney Australia.
- Bienert A, Scheller S, Keane E, Mullooly G, Mohan F (2006) Application of terrestrial laser scanners for the determination of forest inventory parameters In Proceedings of the *International Archives of Photogrammetry, Remote Sensing and Spatial Information Sciences*, **36**, 25–27.
- Binot J-M, Pothier D & Lebel J (1995) Comparison of relative accuracy and time requirement between the caliper, the diameter tape and an electronic tree measuring fork. *The Forestry Chronicle*, **71** (2).
- Boardman JW & Kruse FA (1994) Automated spectral analysis: A geologic example using AVIRIS data, north Grapevine Mountains, Nevada: in *Proceedings, Tenth Thematic Conference on Geologic Remote Sensing* Environmental Research Institute of Michigan, Ann Arbor, MI. Pages 407 - 418.
- Bond WJ & Archibald S (2003) Confronting complexity: Fire policy choices in South African savanna parks. *International Journal of Wildland Fire*, **12**: 381-389.
- Breiman L (2001) Random Forest. *Machine Learning*, **45**, 5–32. Doi: 10.1023/A:1010933404324.
- Breiman L, Friedman JH, Olshen RA, Stone C.I (1984) Classification and Regression Trees, Taylor & Francis: Belmont, CA, USA.
- Bright BC, Hicke JA, Hudak AT (2012) Landscape-scale analysis of aboveground carbon stocks affected by mountain pine beetles in Idaho. *Environmental Research Letters*, **7**: 045702. Doi: 10.1088/1748-9326/7/4/045702.

- Brenning A (2012) Spatial cross-validation and bootstrap for the assessment of prediction rules in remote sensing: The R package sperrorest. *IEEE International Geoscience and Remote Sensing Symposium*. Doi:10.1109/igarss.2012.6352393.
- Brown RJ (1991) Vegetation Monitoring with Multipolarisation SAR Imagery. *IEEE Geosciences & Remote Sensing Symposium*. Doi: 10.1109/IGARSS.1991.575492.
- Brown S (2002) Measuring carbon in forests: Current status and future challenges. *Environmental Pollution*, **116**, 363–372.
- Brown S (2002) Measuring carbon in forests: current status and future challenges. Winrock International, 1621 NKent Street, Suite 1200, Arlington, VA 22209, USA.
- Browning DM, Archer SR, Byrne AT (2009) Field validation of 1930s aerial photography: What are we missing? *Journal of Arid Environments*, **73**, 844–853.
- Bucksch AK (2011) Revealing the skeleton from imperfect point cloud. A doctor Dissertation presented at the Technical University Delft. ISBN: 978-3-86853-877-9.
- Cabo C, Pozo SD, Rodriguez-G P, Ordonez C & Gonzalez-A D (2018) Comparing Terrestrial Laser Scanning (TLS) and Wearable Laser Scanning (WLS) for individual tree modelling at plot level. *Remote Sensing* **10** (4), 540. Doi: 10.3390/rs10040540.
- Cai H, Zhang S & Yang X (2012) Forest Dynamics and Their Phenological Response to Climate warming in the Khingan Mountains, North-eastern China. *International Journal of Environmental Research and Public Health*, **9** (11): 3943 – 3953. Doi: 10.3390/ijerph9113943.
- Calders K, Newnham G, Burt A, Murphy S, Raunonen P, Herold M, Culvenor D, Avitabile V, Disney M, Armston J & Kaasalainen M (2015) Nondestructive estimates of aboveground biomass using terrestrial laser scanning. *Methods in Ecological Evolution*, **6**: 198–208.

- Campbell MO (2013) Biodiversity and the African Savanna: Problems of Definition and Interpretation. *Journal of Biodiversity of Endangered Species*, **1** (3): 116. Doi: 10.4172/2332-2543.1000116.
- Carlsson M (2005) Vegetation succession in savanna determined by interaction of grazing, browsing and fire, a comparison between hypotheses. Södertörns Högskola.
- Carreiras JMB, Vasconcelos MJ, Lucas RM (2012) Understanding the relationship between aboveground biomass and ALOS PALSAR in the forests of Guinea-Bissau (West Africa). *Remote Sensing of Environment*, **121**, 426–442.
- Carreiras JMB, Melo JB & Vasconcelos MJ (2013) Estimating the Above-Ground Biomass in Miombo Savanna Woodlands (Mozambique, East Africa) Using L-Band Synthetic Aperture Radar Data. *Remote Sensing*, **5** (4), 1524-1548. Doi: 10.3390/rs5041524.
- Carver K, Synthetic Aperture Radar (SAR) Earth Observation System. NASA Instrument Panel Report. Vol II. Link: <https://ntrs.nasa.gov/archive/nasa/casi.ntrs.nasa.gov/19880005902.pdf>. (Accessed on: 08.07.2018).
- Campbell J (1996) Introduction to remote sensing. New York, New York: The Guilford Press. pp.287 – 292.
- Castel T, Beaudoin A, Stach N, Stussi N, Le Toan T & Durand P (2001) Sensitivity of space-borne SAR data to forest parameters over sloping terrain theory and experiment. *International Journal of Remote Sensing*, **22**, 2351–2376.
- CCRS – Canadian Centre for Remote Sensing. Fundamentals of Remote Sensing. PDF document accessed online on 10.05.2019 at: [https://www.nrcan.gc.ca/sites/www.nrcan.gc.ca/files/earthsciences/pdf/resource/tutor/fundam/pdf/fundamentals\\_e.pdf](https://www.nrcan.gc.ca/sites/www.nrcan.gc.ca/files/earthsciences/pdf/resource/tutor/fundam/pdf/fundamentals_e.pdf).
- Chai T, Draxler RR (2014) Interactive comment on “Root mean square error (RMSE) or mean absolute error (MAE)?” *Geoscientific Model Development*, **7**: 589–590.



- Charles-Dominique T, Staver AC, Midgley GF & Bond WJ (2015) Functional differentiation of biomes in an African savanna/forest mosaic. *South African Journal of Botany*. Doi: 10.1016/j.sajb.2015.05.005.
- Chave J, Andalo C, Brown S, Cairns MA, Chambers JQ, Eramus D, Fölster H, Fromard F, Higuchi N, Kira T, Lescure JP, Nelson BW, Ogawa H, Puig H, Riera B & Yamakura T (2005) Tree allometry and improved estimation of carbon stocks and balance in tropical forests. *Oecologia*, **145** (1):87-99. Doi: 10.1007/s00442-005-0100-x.
- Chave J, Condit R, Aguilar S, Hernandez A, Lao S, Perez R (2004) Error propagation and scaling for Tropical forest biomass estimates. *Philosophical Transactions of the Royal Society*, **359**, 409–420.
- Chen L & Cheng X (2016) Classification of High-Resolution Remotely Sensed Images based on Random Forests. *Journal of Software Engineering*, **10**:318-327.
- Cho MA, Mathieu R, Asner GP, Naidoo L, van Aardt J, Ramoelo A, Debba P, Wessels K, Main R, Smit PJ, Erasmus B (2012) Mapping tree species composition in Southern African savannas using integrated airborne spectral and LiDAR system. *Remote Sensing of Environment*, **125**: 214-226. Doi: 10.1016/j.rse.2012.07.010.
- Cho MA, Skidmore AK, & Sobhan I (2009) Mapping beech (*Fagus sylvatica* L.) forest structure with airborne hyperspectral imagery. *International Journal of Applied Earth Observation and Geoinformation*, **11** (3): 201 – 211. Doi: 10.1016/j.jag.2009.01.006.
- Ciais P, Bombelli A, Williams M, Piao SL, Chave J, Ryan CM, Henry M, Brender P & Valentini R (2011) The carbon balance of Africa: synthesis of recent research studies. *Philosophical Transactions of the Royal Society. A* **369**: 1–20. Doi: 10.1098/rsta.2010.0328.
- Cifuentes-Jara M, Henry M (2013) Proceedings of the regional technical workshop on Tree Volume and Biomass Allometric Equations in South and Central America, 21 - 24 May 2013 UN-REDD MRV Report 12. Turrialba, Costa Rica. Link: <https://www.unredd.net/documents/global-programme-191/mrv-and-monitoring-296/mrv->

working-papers-meeting-reports-406/12703-wp-14-proceedings-of-the-regional-technical-workshop-on-tree-volume-and-biomass-allometric-equations-in-south-and-central-america-12703.html. (Accessed on: 08.07.2018).

Clark DA, Brown S, Kicklighter D, Chambers JQ, Thomlinson J.R, Ni J (2001) Measuring net primary production in forests: Concepts and field methods. *Ecological Applications*, **11**, 356–370.

Coetzee BJ & Werger MJA (1978) The Sudano-Zambezian Region. In: Werger MJA (eds) *Biogeography and Ecology of Southern Africa. Monographiae Biologicae*, **31**: 301 – 462. Doi: 10.1007/978-94-009-9951-0\_10.

Colgan MS, Asner GP, Levick SR, Martin RE & Chadwick OA (2012) Topo-edaphic controls over woody plant biomass in South African savannas. *Biogeosciences*, **9**: 1809–1821, 2012. Doi: 10.5194/bg-9-1809-2012.

Colgan MS, Swemmer T & Asner GP (2014) Structural relationships between form factor, wood density, and biomass in African savanna woodlands. *Trees*, **28**: 91-102. Doi: 10.1007/s00468-013-0932-7.

Colgan S.M, Asner G.P, Swemmer T (2013) Harvesting tree biomass at the stand-level to assess the accuracy of field and airborne biomass estimation in savannas. *Ecological Applications*, **5**, 1170–1184.

Colombo R, Bellingeri D, Fasolini D & Marino CM (2003) Retrieval of leaf area index in different vegetation types using high resolution satellite. *Remote Sensing of Environment*, **86** (1): 120-131. Doi: 10.1016/S0034-4257(03)00094-4.

Condit R (2008) Methods for estimating aboveground biomass of forest and replacement vegetation in the tropics. Center for Tropical Forest Science Research Manual, 73 pages.

Costa MPF (2002) Use of SAR satellites for mapping zonation of vegetation communities in the Amazon floodplain. *International Journal of Remote Sensing*, **25** (10): 1817-1835. Doi: 10.1080/0143116031000116985.

- Curran PJ (1981) Multispectral remote sensing for estimation of biomass and productivity in Plants and daylight spectrum. Academic Press, New York. Pages 65-69.
- Cutler MEJ, Boyd DS, Foody G. M. & Vetrivel A (2012) Estimating tropical forest biomass with a combination of SAR image texture and Landsat TM data. An assessment of predictions between regions. *ISPRS Journal of Photogrammetry and Remote Sensing* **70**: 66–77. Doi: 10.1016/j.isprsjprs.2012.03.011\_
- Cutler DR, Edwards TC Jr, Beard KH, Cutler A, Hess KT, Gibson J & Lawler JJ (2007) Random forest for classification in ecology. *Ecology* **88** (11): 2783-2792.
- Dassot M, Constant T & Fournier M (2011) The use of terrestrial LiDAR technology in forest science: application fields, benefits and challenges. *Annals of Forest Science*, **68** (5), 959-974. Doi: doi.org/10.1007/s13595-011-0102-2.
- Davies AB, Baldeck CA & Asner GP (2016) Termite Mounds Alter the Spatial Distribution Of African Savanna Tree Species. *Journal of Biogeography*, **43**, 301–313. Doi: 10.1111/jbi.12633.
- Di Gregorio A (2005) Land Cover Classification System: Classification concepts and user manual. Environment and natural resources series, FAO (UN). Pages 26 – 30.
- Dobson MC, Pierce L, Sarabandi K, Ulaby FT & Sharik T (1992) Preliminary analysis of ERS-1 SAR for forest ecosystem studies. *IEEE Transactions in Geosciences and Remote Sensing*, **30**:203-211.
- Duadze SEK (2004) Land use and land cover study of the savannah ecosystem in the Upper West Region (Ghana) using Remote Sensing. *Ecology and Development Series*, No16.
- Dubois PC, Van Zyl J & Engman T (1995) Measuring soil moisture with imaging radars. *IEEE Transactions on Geoscience and Remote Sensing*, **33**, 915-926.
- Earth Observation Monitor: <http://earth-observation-monitor.net>. Accessed on 08.07.2018.

Ehinger S.E (2010) Design, development and application of LiDAR data processing tools. A master Thesis presented at Idaho State University, USA.

ENVI-EXELIS:

[http://www.exelisvis.com/portals/0/pdfs/envi/Adv\\_Hyperspectral\\_Analysis.pdf](http://www.exelisvis.com/portals/0/pdfs/envi/Adv_Hyperspectral_Analysis.pdf) Accessed on 08.07.2018.

Esche SA, Franklin SE & Wulder MA (2002) Assessing cloud contamination effects on K-means unsupervised classification of Landsat data. *IEEE International Geosciences and Remote Sensing Symposium*, **6**: 3387-89. Doi: 10.1109/IGARSS.2002.1027191.

ESA (2019) Radar Course 2. Accessed online under: [https://earth.esa.int/web/guest/missions/esa-operational-eo-missions/ers/instruments/sar/applications/radar-courses/content-2/-/asset\\_publisher/qIBc6NYRXfnG/content/radar-course-2-parameters-affecting-radar-backscatter](https://earth.esa.int/web/guest/missions/esa-operational-eo-missions/ers/instruments/sar/applications/radar-courses/content-2/-/asset_publisher/qIBc6NYRXfnG/content/radar-course-2-parameters-affecting-radar-backscatter) (Accessed on 2.5.2019).

ESA (2019) User Guide: Sentinel-1 Level-1 Processing. Accessed online under: <https://sentinel.esa.int/web/sentinel/user-guides/sentinel-1-sar/product-types-processing-levels/level-1> (Accessed on 2.5.2019).

Esser, G (1984) The significance of biospheric carbon pools and fluxes for the atmospheric CO<sub>2</sub>: A proposal mode structure. *Prog Biometeorol*, **13**, 253–294.

Evans TL, Costa MPF, Tomas WM & Camilo AR (2013) A SAR fine and medium resolution approach for mapping the Brazilian Pantanal. *Geografia (Numero Especial ago.)*, **38**, 25.

Fairly I, Thomas T, Phillips M, Reeve D (2016) Terrestrial Laser Scanner Techniques for Enhancement in Understanding of Coastal Environments. In *Seafloor Mapping along Continental Shelves: Research and techniques for visualizing Benthic Environments*, Finkl CW & Makowski C (Eds). Springer, Switzerland. Pages 273-289.

- Ferrazzoli P, Paloscia S, Pampaloni P, Schiavon SS & Solimini D (1997) The potential of multifrequency polarimetric SAR in assessing agricultural and arboreous biomass. *IEEE Transactions in Geosciences & Remote Sensing*, **35**, 5-17.
- Fidelis A (2008) Fire in subtropical grasslands in Southern Brazil: effects on plant strategies and vegetation dynamics. A PhD dissertation presented at the Department of Vegetation Ecology of Technical University of München, Germany.
- Forkel M, Carvalhais N, Verbesselt J, Mahecha M, Neigh C & Reichstein M (2013) Trend change detection in NDVI time series: Effects of inter-annual variability and methodology. *Remote Sensing of Environment*, **5**: 2113-2144. Doi: 10.3390/rs5052113.
- Fravettoni R (2009) The natural fix? – The role of ecosystems in climate mitigation. UNEP/GRID-Arendal. Link: <http://www.grida.no/resources/7554>. (Accessed on 09.07.2018).
- Frost PGH, Medina E, Menaut JC, Solbrig O, Swift M & Walker B (1986) Responses of savannas to stress and disturbance. *Biology International*, **10**: 1–78.
- Fuller DO (1999) Canopy phenology of some mopane and miombo woodlands in eastern Zambia. *Global Ecology and Biogeography*, **8**: 199-209. Doi: 10.1046/j.1365-2699.1999.00130.x.
- Furley PA, Rees RM, Ryan CM & Saiz G (2008) Savanna burning and the assessment of long-term fire experiments with particular reference to Zimbabwe. *Progress in Physical Geography: Earth and Environment*, **32** (6): 611-634. Doi: 10.1177/0309133308101383.
- Furley P.A (2007) Tropical savannas and associated forests: vegetation and plant ecology. *Progress in Physical Geography*, **31**(2): 203 – 211. Doi: 10.1177/0309133307076107.
- Gagnon L, Jouan A (1997) Speckle Filtering of SAR Images - A Comparative Study between Complex-Wavelet-Based and Standard Filters. *SPIE Proceedings*, Vol3169.

- Gallant AL, Kaya SG, White L., Brisco B, Roth MF, Sandiski W & Rover J (2014) Detecting emergence, growth and senescence of wetland vegetation with polarimetric synthetic aperture radar (SAR) data. *Water*, **6**: 694-722. Doi: 10.3390/w6030694.
- GAMMA Remote Sensing AG (2008) Differential interferometry and geocoding software. In *Geocoding and Image Registration Documentation User's Guide*, Gamma, R.S, Ed, GAMMA Remote Sensing: Gümligen, Switzerland.
- Gertenbach WPD (1983) Landscapes of the Kruger National park. *Koedoe*, **26** (1): 45-58. Doi: 10.4102/koedoe.v26i1.591.
- Gesner U, Machwitz M, Conrad C, Dech S (2013) Estimating the fractional cover of growth forms and bare surface savannas. A multi resolution approach based on regression tree ensembles. *Remote Sensing of Environment*, **129**: 90-102. Doi: 10.1016/j.rse.2012.10.026.
- Gibbs HK, Brown S, O Niles J & Foley JA (2007) Monitoring and estimating tropical forest carbon stocks: making REDD a reality. *Environmental Research Letters*, **2** (4): 13. Doi: 10.1088/1748-9326/2/4/045023.
- Glenn NF, Spaete LP, Sankey TT, Derryberry DR, Hardegree SP, Mitchel JJ (2010) Errors in LiDAR-derived shrub height and crown area on a sloped terrain. *Journal of Arid Environments*, 1-6. Doi:10.1016/j.jaridenv.2010.11.005.
- Goodman JW (1976) Some fundamental properties of speckle. *Journal of Optical Society of America*, **66** (11): 1145-1150.
- Gosling CM (2014) Biotic Determinants of Heterogeneity in a South African Savanna. PhD thesis submitted to The University of Groningen, Netherlands. ISBN: 978-90-367-7518-2.
- Govender N, Trollpe WSW & van Wigen BW (2006) The effect of fire season, fire frequency, rainfall and management on fire intensity in savanna vegetation in South Africa. *Journal of Applied Ecology*, **43**: 748–758. Doi: 10.1111/j.1365-2664.2006.01184.x.

- Govender N (2003) Fire management in Kruger National park. *Fire Ecology* 1 in Arid Lands Newsletter, Arizona University. No54. Link: <https://cals.arizona.edu/oals/ALN/aln54/govender.html>. Accessed on 08.07.2018.
- Griffiths GH & Wooding MG (1996) Temporal monitoring of soil moisture using ERS-1 SAR data. *Hydrological Processes*, 10: 1127-1138.
- Guccione P, Lombardi A & Giordano R (2016) Assessment of seasonal variations of radar backscattering coefficient using Sentinel-1 data. *IEEE*. Doi: 10.1109/IGARSS.2016.7729879.
- Guerschman JP, Hill JM, Renzullo LJ, Barrett DJ, Marks SA & Botha JE (2009) Estimating Fractional cover of photosynthetic vegetation, non-photosynthetic vegetation and bare soil in the Australian tropical savanna region upscaling the EO-1 Hyperion and MODIS sensors *Remote Sensing of Environment*, **113** (5): 928-945. Doi: 0.1016/j.rse.2009.01.006.
- Haboudane D, Miller RJ, Pattey E, Zarco-Tejada JP & Strachan BI (2004) Hyperspectral vegetation indices and novel algorithms for predicting green LAI of crop canopies: Modeling and validation in the context of precision agriculture. *Remote Sensing of Environment*, **90** (3): 337-352. Doi: 0.1016/j.rse.2003.12.013.
- Hackenberg J, Wassenberg M, Spiecker H, Sun D (2015) Non-destructive method for biomass prediction combining TLS derived tree volume and wood density. *Forests*, **6**, 1274-1300. Doi: 10.3390/f6041274.
- Hamdan O, Khali AH & Mohd HI (2014) L-band ALOS PALSAR for biomass estimation of Matang Mangroves, Malaysia. *Remote Sensing of Environment*, **155**: 69-78. Doi: 10.1016/j.rse.2014.04.029.
- Hansen MC, DeFries RS, Townshend JRG, Marufu L & Sohlberg R (2002) Development of a MODIS tree cover validation dataset for Western Province, Zambia. *Remote Sensing of Environment*, **83** (1): 320-335. Doi: 10.1016/S0034-4257(02)00080-9.

- Henry M, Picard N, Trotta C, Manlay R.J, Valentini R, Bernoux M & Saint-André L (2011) Estimating tree biomass of sub-Saharan African forests: a review of available allometric equations. *Silva Fennica*, **45** (3B): 477–569.
- Herrero-Huerta M, Lindenbergh R & Rodriguez-Gonzalvez P (2018) Automatic tree parameter extraction by Mobile LiDAR system in urban context. *PLOS ONE*. Doi: 10.1371/journal.pone.0196004.
- Heritage G.L, Large ARG (2009) Laser scanning for the Environmental Sciences. Willey-Blackwell, Oxford, UK. Page 210.
- Higgins SI, Scheiter S & Sankaran M (2010) The stability of African savannas: Insights from the indirect estimation of the parameters of a dynamic model. *Ecology*, **91** (6): 1682-1692.
- Hoffmann WA, Geiger EL, Rossatto DR, Silva LCR, Lau OL, Haridasan M & Franco AC (2012) Ecological thresholds at the savanna-forest boundary: how plant traits, resources and fire govern the distribution of tropical biomes. *Ecology Letters*, **15**: 759 – 768. Doi: 10.1111/j.1461-0248.2012.01789.x.
- Holopainen M, Vastaranta M, Kankare V, Rättyä M, Vaaja M, Liang X, Yub X, Hyyppä J, Hyyppä H, Viitalad R & Kaasalainen S. (2011) Biomass Estimation of Individual Trees Using Stem and Crown Diameter TLS Measurements. *International Archives of the Photogrammetry, Remote Sensing and Spatial Information Sciences*, ISPRS Calgary 2011 Workshop, 29-31 August 2011, Calgary, Canada.
- Holopainen M, Vastaranta M, Kankare V, Hyyppä H, Vaaja M, Hyyppä J, Liang X, Litkey P, Yu X, Kaartinen H, Kukko A, Kaasalainen S, Jaakkola A (2011) The use of ALS, TLS and VLS measurements in mapping and monitoring urban trees *IEEE*. Doi: 10.1109/JURSE.2011.5764711.
- Horning N (2010) Random Forests: An algorithm for image classification and generation of continuous fields data sets. *International Conference on Geoinformatics for Spatial Infrastructure Development in Earth and Allied Sciences 2010*. American Museum of



Natural History, Center for Biodiversity and Conservation. Central Park West New York, USA.

Houghton RA & Nassikas AA (2017) Global and regional fluxes of carbon from land use and land cover change 1850-2015. *Global Biogeochemical Cycles*, **31** (3): 456-472. Doi: 10.1002/2016GB005546.

Huete AR (1988) A Soil Adjusted Vegetation Index (SAVI) (1988). *Remote Sensing of Environment*, **25** (3): 295 – 309. Doi: 10.1016/0034-4257(88)90106-X.

Hunter MO, Keller M, Victoria D & Morton DC (2013) Tree height and tropical forest biomass estimation. *Biogeosciences*, **10**: 8385 – 8399. Doi:10.5194/bg-10-8385-2013.

Hüttich C, Herold M, Wegmann M, Cord A, Strohbach B, Schmillius C, Dech S (2011) Assessing effects of temporal compositing and varying observation periods for large-area land cover mapping in semi-arid ecosystems: Implications for global monitoring. *Remote Sensing of Environment*, **115** (10): 2445-2459. Doi: 0.1016/j.rse.2011.05.005.

Intergovernmental Panel on Climate Change (IPCC) *Good Practice Guidance for Land Use, Land-Use Change and Forestry*, Glossary 1, IPCC National Greenhouse Gas Inventories Program: Hayama, Japan, 2003.

Inman-Narahari F, Giardina C, Ostertag R, Cordell S & Sack L (2009) Digital data collection in forest dynamics plots. *Methods in Ecology & Evolution*. **1** (3): 274-279. Doi: 10.1111/j.2041-210X.2010.00034.x

Isenburg, M (2016) *LAStools—Efficient Tools for LiDAR Processing*, version 111216, Rapidlasso GmbH: Gilching, Germany. Available online: <http://lastools.org> (Accessed on March, 2017).

James G, Witten D, Hastie T & Tibshirani R (2013) *An Introduction to Statistical Learning*. Springer New York. URL: <https://doi.org/10.1007%2F978-1-4614-7138-7>. Doi:10.1007/978-1-4614-7138-7.

- Jan PP, Harald J, Tore G, Bernt J & Mats R (1991) Vegetation and Forestry mapping in the Ford (UK) using combined MAESTRO SAR and Landsat TM Data. *IEEE* 697-700.
- Jaybhay J, Shastri R (2015) A Study of Speckle Noise Reduction Filters. *Signal & Image Processing*, Vol.6 (3). Doi: 10.5121/sipij.2015.6306.
- Jenkins JC, Chojnacky DC, Heath LS & Birdsey RA (2003) National-Scale Biomass Estimators for United States Tree Species. *Forest Science*, **49** (1): 12-35.
- Jin C, Xiao X, Merbold L, Arneith A, Veenendaal E, Kutsch WL (2013) Phenology and gross primary production of two dominant savanna woodland ecosystems in Southern Africa. *Remote Sensing of Environment*, **135**, 189-201. Doi: 10.1016/j.rse.2013.03.033.
- Johnson PE, Smith OM & Adams JB (1985) Quantitative analysis of planetary reflectance spectra with principal components analysis. *Journal of Geophysical Research: Solid Earth*, **90** (2): 805-810.
- Johnson PE, Smith MO & Adams JB (1992) Simple algorithms for remote determination from mineral abundances and particles sizes from reflectance spectra. *Journal of Geophysical Research*, **97** (2): 2649-2657. Doi: 10.1029/91JE02504.
- Jonckheere I, Fleck S, Nackaerts K, Muysa B, Coppin P, Weiss M, & Baret F (2004) Review of methods for in situ leaf area index determination Part I. Theories, sensors and hemispherical photography. *Agricultural and Forest Meteorology*, **121** (1-2): 19 -35. Doi: 10.1016/j.agrformet.2003.08.027.
- Joshi N, Baumann M, Ehammer A, Fensholt R, Grogan K, Hostert P, Jepsen M.R, Kuemmerle T, Meyfroidt P, Mitchard ETA, Reiche J, Ryan C.M & Waske B (2016) A review of the application of optical and radar remote sensing data fusion to land use mapping and monitoring. *Remote Sensing*, **8**, 70. Doi: 10.3390/rs8010070.
- Kandrot SM (2013) Coastal monitoring: A new approach. Department of Geography, Cork University, Ireland. *Cork University Electronic Journals*. Link: <http://research.ucc.ie/journals/chimera/2013/00/kandrot/09/en> (Accessed on 08.07.2018).

- Kankare V, Holopainen M, Vastaranta M, Puttonen E, Yu X, Hyyppä J, Vaaja M, Hyyppä H & Alho P (2013). Individual tree biomass estimation using terrestrial laser scanning. *ISPRS Journal of Photogrammetry and Remote Sensing*, **75**, 64–75. Doi: 10.1016/j.isprsjprs.2012.10.003.
- Kankare V (2015). The prediction of single- tree biomass, logging recoveries and quality attributes with laser scanning techniques. The prediction of single-tree biomass, logging recoveries and quality attributes with laser scanning techniques. Department of Forest Sciences. Faculty of Agriculture and Forestry, University of Helsinki.
- Kato A, Kajiwara K, Honda Y, Watanabe M, Enoki T, Yamaguchi Y & Kobayashi T (2014). Efficient field data collection of Tropical forest using Terrestrial Laser Scanner. *IEEE International Geoscience and Remote Sensing Symposium, IGARSS and the 35th Canadian Symposium on Remote Sensing, CSRS 2014 - Quebec City, Canada*.
- Keshava N, & Mustard JF (2002) Spectral unmixing. *IEEE Signal Processing*, **19** (1): 44–57. Doi: 10.1109/79.974727.
- Khosravipour A, Skidmore A.K, Isenburg M, Wang T, Hussin YA (2014) Generating pit-free canopy height models from airborne Lidar. *Photogrammetric Engineering & Remote Sensing*, **80**, 863–872. Doi: 10.14358/PERS.80.9.863.
- Kiker G.A, Scholtz R, Smit IPJ & Venter FJ (2014) Exploring an extensive dataset to establish woody vegetation cover and composition in Kruger National Park for the late 1980s. *Koedoe*, **56** (1). Doi: 10.4102/koedoe.v56i1.1200.
- Kong JA (1986) *Electrical Wave Theory*. Willy Publishers, New York.
- Kontoes C, Karamitsoglou I, Papoutsis I, Sifakis NI & Xofis P (2013) National Scale Operational Mapping of Burnt Areas as a Tool for the Better Understanding of Contemporary Wildfire Patterns and Regimes. *Sensors*, **13** (8): 1146 – 1166. Doi:10.3390/s130811146.

Korpella I (2004) Individual tree measurements by use of digital aerial photogrammetry. *Silva Fennica Monographs 3*, The Finnish Forest Research Institute: Helsinki, Finland.

Kruger AC, Makamo LB & Shongwe S (2002) An analysis of Skukuza climate data. *Koedoe 45* (1).

Kupidura P (2016) Comparison of Filters Dedicated to Speckle Suppression in SAR Images. *ISPRS Congres*. Doi:10.5194/isprsarchives-XLI-B7-269-2016.

Kutsch WL, Hanan N, Scholes B, McHugh I, Kubheka W, Eckhardt H, & Williams C (2008) Response of Carbon fluxes to water relations in a savanna ecosystem in South Africa. *Biogeosciences*, **5**: 1797-1808. Doi: 10.5194/bg-5-1797-2008.

Kutsch WL, Freibauer A, Brümmer C, Higgins S, Schmulius C, Thiel-Clemen T, Scholes R.J, Archibald S, Kirton A, Walker S, Midgley G, Bradshaw K, Lück W, Grant R, Twine W (2012) *Adaptive Resilience of Southern African Savannas (ARS AfricaE) Proposal Call*, German Federal Ministry of Education and Research (BMBF): Bonn, Germany. Pages 2–3.

Kutsch WL, Hanan N, Scholes B, McHugh I, Kubheka W, Eckhardt H, Williams C (2008) Response of Carbon fluxes to water relations in a savanna ecosystem in South Africa. *Biogeoscience*, **5**, 1797–1808. Doi: 10.5194/bg-5-1797-2008.

Landman M, Gaylard A, Mendela T & Kerley GIH (2014) Impact of elephant on two woody trees, *Boscia oleoides* and *Pappaea capensis*, in an arid thicket- Nama Karoo mosaic, Greater Addo Elephant National Park. *Koedoe*, **56** (1). Doi: 10.4102/koedoe.v56i1.1231.

Landscape

Toolbox:

[http://wiki.landscapetoolbox.org/doku.php/remote\\_sensing\\_methods:spectral\\_mixture\\_analysis](http://wiki.landscapetoolbox.org/doku.php/remote_sensing_methods:spectral_mixture_analysis) Accessed on 08.07.2018.

Lawrence W, Saatchi S, DeFries R, Dietz J, Rice R, Dietz LA, de Araujo SM & Alger K (1995) Utilization of SAR and Optical remote sensing data for habitat conservation in the tropical forest of Brazil. *IEEE*, **2** (95): 1480-1482.

- Lemmens M (2011). Terrestrial Laser Scanners. *Geotechnologies and the Environment* **5**, Doi: 10.1007/978-94-007-1667-4\_6.
- Le Toan T, Beaudoin A, Riom J, Guyon D (1992) Relating forest biomass to SAR data. *IEEE Transactions of Geosciences & Remote Sensing*, **30**, 403–411.
- Lefsky MA, Harding DJ, Keller M, Cohen WB, Carabajal CC, Espirito-Santo FDB, Hunter MO & Oliveria R Jr (2005) Estimates of forest canopy height and aboveground biomass using ICESat. *Geophysical Research Letters*, **32**, 1–4.
- Legendre P, & Fortin M J (1989) Spatial pattern and ecological analysis. *Vegetatio*, **80**, 107–138. URL: <https://doi.org/10.1007/bf00048036>. doi:10.1007/bf00048036.
- Levick SR & Rogers KH (2006) Lidar and Object-Based Image Analysis as Tools for Monitoring the Structural Diversity of Savanna Vegetation. *The International Archives of the Photogrammetry, Remote Sensing and Spatial Information Sciences*, **34** (XXX).
- Levick SR, Asner GP, Chadwick OA, Khomo LM, Rogers KH, Hartshorn AS, Kennedy-Bowdoin T, Knapp DE (2010) Regional insight into savanna hydrogeomorphology from termite mounds. *Nature Communications*, **1**, 1–7.
- Li S, Dragicevic S, Castro FA, Sester M, Winter S, Coltekin A, Petti, C, Jiang B, Haworth J, Stein A, et al (2016) Geospatial big data handling theory and methods: A review and research challenges. *ISPRS Journal of Photogrammetry & Remote Sensing*, **115**, 119–133.
- Liang X, Kankare V, Hyyppä J, Wang Y, Kukko A, Haggrén H, Yu X, Kaartinen H, Jaakkola A, Guan F, Holopainen M & Vastaranta M (2016) Terrestrial laser scanning in forest inventories. *ISPRS Journal of Photogrammetry and Remote Sensing* **115**: 63–77. Doi: 10.1016/j.isprsjprs.2016.01.006.
- Liaw A & Wiener M (2002) Classification and regression by random forest. *R News*, **2–3**, 18–22.

- Liew SC (2001), Electromagnetic Radiation, in "Principles of remote sensing", an online tutorial. Centre for Remote Imaging, Sensing and Processing, National University of Singapore. Accessed online on 10.05.2019 at: <https://crisp.nus.edu.sg/~research/tutorial/em.htm>.
- Lim K, Treitz P, Baldwin K, Green J (2003) Lidar remote sensing of biophysical properties of tolerant northern hardwood forests. *Canadian Journal of Remote Sensing*, **29**, 658–678.
- Litofovic R & Olthof I (2004) Accuracy assessment using sub-pixel fractional error matrices of global land cover products derived from satellite data. *Remote Sensing of Environment*, **90** (2): 153-165. Doi: 10.1016/j.rse.2003.11.016.
- Liu J, Li J, Li W, Wu J (2016) Rethinking big data: A review on the data quality and usage issues. *ISPRS Journal of Photogrammetry & Remote Sensing*, **115**, 134–142.
- Low AB & Rebelo AG (1996) Vegetation of South Africa, Lesotho and Swaziland. *Sterilitzia*. South African National Biodiversity Institute, Pretoria.
- Lucas RM, Moghaddam M, Cronin N (2004) Microwave scattering from mixed-species forests, Queensland, Australia. *IEEE Transactions on Geosciences & Remote Sensing*, **42**, 2142–2159. Doi: 10.1109/TGRS.2004.834633.
- Luoma V, Saarinen N, Wulder MA, White JC, Vastaranta M, Holopainen M & Hyypä J (2017) Assessing precision in conventional field measurements of individual tree attributes. *Forests*, **8** (38). Doi: 10.3390/f8020038.
- Magagi R, Bernier M, Bouchard MC (2002) Use of Ground Observations to Simulate the Seasonal Changes in the Backscattering Coefficient of the Subarctic Forest. *IEEE Transactions on Geosciences & Remote Sensing*, **14**. Doi: 10.1109/36.992786.
- Magarick JF (2012) Improving vegetation and background discrimination from hyperspectral imaging (HIS) and light detection and ranging (LiDAR) fusion using an added shortwave infrared (SWIR) HIS component. Master Thesis submitted to George Mason University, USA.

- Main R, Mathieu R, Kleynhans W, Wessels K, Naidoo L, Asner G.P (2016) Hyper-temporal C-band SAR for baseline woody structural assessments in deciduous savannas. *Remote Sensing*, **8**, 661. Doi: 10.3390/rs8080661.
- Malimbwi RE, Solberg B & Luoga E (1994) Estimation of Biomass and Volume In Miombo Woodland at Kitulangalo Forest Reserve, Tanzania. *Journal of Tropical Forest Science*, **7** (2): 230-242. Link: <http://www.jstor.org/stable/43581809>. Accessed on 08.07.2018.
- Maniatis D (2010) Methodologies to measure aboveground biomass in the Congo Basin Forest in a UNFCCC REDD+ context. PhD Thesis submitted to Linacre College – School of Geography and the Environment.
- Mansourpour M, Rajabi MA, Blais JAR (2006) Effects and Performance of Speckle Noise Reduction Filters on Active Radar and SAR Images. *ISPRS*, VolXXXVI-1/W41, Ankara, Turkey.
- Maraseni TN, reardon-Smith K, Griffiths G & Apan A (2016) Savanna burning methodology for fire management and emissions reduction: a critical review of influencing factors. *Carbon balance & Management*, **11**: 25. Doi: 10.1186/s13021-016-0067-4.
- Martini S, Rieke C (2015) Backscatter analysis of multi-temporal and multi-frequency SAR data in the context of flood mapping at River Saale, Germany. *Remote Sensing*, **7**, 7732-7752. Doi: 10.3390/rs/70607732.
- Mate R, Johansson T & Siteo A (2014) Biomass Equations for Tropical Forest Tree Species in Mozambique. *Forests*, **5**, 535-556. Doi:10.3390/f5030535.
- Mathieu R, Naidoo L, Cho MA, Leblon B, Main R, Wessels K, Asner GP, Buckley J, van Aardt J, Erasmus BFN, Smit IPJ (2013) Toward structural assessment of semi-arid African savannahs and woodlands: The potential of multi-temporal polarimetric RADARSAT-2 fine beam images. *Remote Sensing of Environment*, **138**: 215-231. Doi: 10.1016/j.rse.2013.07.011.

- Mattia F, Satalino G, Pauwels VRN & Loew A (2009) Soil moisture retrieval through a merging of multi-temporal L-band SAR data and hydrologic modelling. *Hydrology and Earth Systems*, **13**, 343-356.
- McNeill SJ & Belliss SE (2002) Forest Biomass Estimation in New Zealand using Full-polarisation SAR Imagery. *IEEE Geosciences & Remote Sensing Symposium*. Doi: 10.1109/IGARSS.2002.1025781.
- Md Sarker LR, Nichol J, Iz HB, Ahmad BB, Rahman AA (2013) Forest Biomass Estimation Using Texture Measurements of High Resolution Dual-Polarisation C-Band SAR Data. *IEEE Transactions on Geosciences & Remote Sensing*, **51**, 6. Doi: 10.1109/TGRS.2012.2219872.
- Merbold L, Ardö J, Arneith A, Scholes RJ, Nouvellon Y, de Grandcourt A, Archibald S, Bonnefond JM, Boulain N, Brueggemann N, Bruemmer C, Cappelaere B, Ceschia E, El-Khidir HAM, El-Tahi, BA, Falk U, Lloyd J, Kergoat L, Le Dantec V, Mougou E, Muchinda M, Mukelabai MM, Ramier D, Roupsard O, Timouk F, Veenendaal EM, & Kutsch WL (2009) Precipitation as driver of carbon fluxes in 11 African ecosystems. *Biogeosciences*, **6**, 1027-1041. Doi: 10.5194/bg-6-1027-2009.
- Mermoz S, Réjou-Méchain M, Villarda L, Le Toana T, Rossi V & Gourlet-Fleury S (2014) Decrease of L-band SAR backscatter with biomass of dense forests. Centre d' Etudes Spatiales de la BIOSphere, UMR CNRS 5126, University of Paul Sabatier, Toulouse, France.
- Mermoz S, Le Toana T, Villard V, Réjou-Méchain M & Seifert-Granzin J (2014) Biomass assessment in the Cameroon savanna using ALOS PALSAR data. *Remote Sensing of Environment*. Doi: 10.1016/j.rse.2014.01.029.
- Mishra NB, Crews KA, Miller JA & Meyer T (2015) Mapping Vegetation Morphology Types in Southern Africa Savanna Using MODIS Time-Series Metrics. A Case Study of Central Kalahari, Botswana. Department of Geography & the Environment, University of Texas, Austin, 305 E 23rd St, CLA 3.306, Austin, TX 78712, USA. Doi:10.3390/land4010197.



- Mistry J(2000) *World Savannas: Ecology and Human Use*. Pearson Education: Harlow, UK. Pages 1–25.
- Mitchard ETA, Saatchi SS, Lewis SL, Feldpausch TR, Woodhouse IH, Sonke, B, Rowland, C, Meir P (2011) Measuring biomass changes due to woody encroachment and deforestation/degradation in a forest-savanna boundary region of Central Africa using multi-temporal L-band radar backscatter. *Remote Sensing of Environment*, **115**, 2861–2873.
- Mitchard ETA, Saatchi SS, Woodhouse IH, Nangendo G, Ribeiro NS, Williams M, Ryan CM, Lewis SL, Feldpausch TR, Meir P (2009) Using satellite radar backscatter to predict above-ground woody biomass: A consistent relationship across four different Africa landscapes. *Geophysical Research Letters*, **36**, 1–6.
- Mitchell A L, Rosenqvist A & Mora B (2017) Current remote sensing approaches to monitoring forest degradation in support of countries measurement, reporting and verification (MRV) systems for REDD+. *Carbon Balance and Management*. Doi: 10.1186/s13021-017-0078-9.
- Mograbi PJ, Erasmus BF, Witkowski ETF, Asner GP, Wessels KJ, Mathieu R, Knapp DE, Martin RE, Main R (2015) Biomass increase go under cover: Woody vegetation dynamics in South African rangelands. *PLoS ONE*, *10*. Doi: 10.1371/journal.pone.0127093.
- Monyela BM (2017) A two-year long drought in summer 2014/2015 and 2015/2016 over South Africa. An MSc thesis submitted to the Department of Oceanography, University of Cape Town (April, 2017).
- Moran M, Hymer D, Qi J & Sano E (200) Soil moisture evaluation using multi-temporal synthetic aperture radar (SAR) in a semi-arid rangeland. *Agricultural & Forest Meteorology*, **105** (1/3): 69-80. Doi: 10.1016/S0168-1923(00)00189-1.
- Moses AC, Mathieu R, Asner GP, Naidoo L, van Aardt J, Ramoelo A, Debba P, Wessels K, Main R, Smit IPJ & Erasmus B (2012) Mapping tree species composition in Southern African savannas using integrated airborne spectral and LiDAR system. *Remote Sensing of Environment*, **125**, 214–226.

- Moskal LM & Zheng G (2012) Retrieving forest inventory variables with Terrestrial Laser Scanning in urban heterogeneous forest. *Remote Sensing*, **4**, 1-20. Doi: 10.3390/rs4010001.
- Mucina L & Rutherford MC (2006) The vegetation of South Africa, Lesotho and Swaziland. South African National Biodiversity Institute, Pretoria, S. Africa.
- Myburgh HC, Olivier JC, Mathieu R, Wessels K, Leblon B, Asner G & Buckley J (2011) Airborne remote sensing improves satellite-based estimates of tree structure in an African savanna. *Proceedings of the International Geosciences & Remote Sensing Symposium*.
- Naidoo L, Mathieu R, Main R, Kleynhans W, Wessels K, Asner G & Leblon B (2015) Savannah woody structure modeling and mapping using multi-frequency (X-, C- and L-band) Synthetic Aperture Radar data. *ISPRS Journal of Photogrammetry and Remote Sensing*, **105**: 234-250. Doi: 10.1016/j.isprsjprs.2015.04.007.
- Naidoo L, Cho MA, Mathieu R, & Asner G (2012) Classification of savanna tree species, in the Greater Kruger National Park region, by integrating hyperspectral and LiDAR data in a Random Forest data mining environment. *ISPRS Journal of Photogrammetry and Remote Sensing*, **69**, 167–179.
- Niemi M., Vastaranta M., Peuhkurinen J., Holopainen M. (2015). Forest inventory attribute prediction using airborne laser scanning in low-productive forestry-drained boreal peatlands. *Silva Fennica* 49:2, 1218. p. 17.
- Ngomanda A, Obiang NLE, Lebamba J, Mavouroulou QM, Gomat H, Mankou GS, Loumote J, Iponga DM, Ditsouga FK, Koumba RZ, Bobe KHB, Okouyi CM, Nyangadouma R, Lepengue N, Mbatchi B & Picard N (2013) Site-specific versus pantropical allometric equations: Which option to estimate the biomass of a moist central African forest? *Forest Ecology & Management*, **312**: 1-9. Doi: 10.1016/j.foreco.2013.10.029.
- Nguyen D.B, Clauss K, Cao S, Naeimi V, Kuenzer C, Wagner W (2015) Mapping rice seasonality in the Mekong Delta with multi-year Envisat ASAR WSM data. *Remote Sensing*, **7**, 15868-15893. Doi :10.3390/rs71215808.

- Nickless, A, Scholes, R.J, Archibald, S (2011) A method for calculating the variance and confidence intervals for tree biomass estimates obtained from allometric equations *African Journal of Science*, **107** (5/6). Doi: 10.4102/sajs.v107i5/6.356.
- Nilsson M (1996) Estimation of tree heights and stand volume using airborne Lidar system. *Remote Sensing of Environment*, **56** :1-7. Doi: 10.1016/0034-4257(95)00224-3.
- Odipo, VO, Luck W, Berger C, Schmullius C (2016) Savanna fractional cover classification using machine learning. Unpublished work.
- Odipo VO, Nickless A, Berger C, Baade J, Urbazaev M, Walther C, Schmullius C (2016) Assessment of aboveground woody biomass dynamics using terrestrial laser scanner and L-band ALOS PALSAR data in South African savanna. *Forests*, **7**, 294, Doi: 10.3390/f7120294.
- Olschofsky K, Mues V & Köhl M (2016). Operational assessment of aboveground tree volume and biomass by terrestrial laser scanning. *Computers and Electronics in Agriculture* **127**: 699–707.
- Oliver C, Quegan S (2004) *Understanding Synthetic Aperture Radar Images*, SciTech Publishing: Raleigh, NC, USA.
- Oliveras I & Malhi Y (2016) Many shades of green: the dynamic tropical forest-savanna transition zones. *Philosophical Transactions of the Royal Society*, **B371** (20150308). Doi: 10.1098/rstb.2015.0308.
- Olson D, Eric D, Eric W, Neil B, George VNP, Emma CU, Jennifer AD, Illanga E, Holly ES, John M, Colby JL, Thomas FA, Taylor R, Yumiko K, John L, Wesley WW, Prashant H, Kenneth K (2001) Terrestrial Ecoregions of the World: A New Map of Life on Earth. *Biological Sciences*, **51**: 933-938. Doi: 10.1641/0006-3568.

- Orwig DA, Boucher P, Paynter I, Saenz E, Li Z & Schaaf C (2018) The potential to characterize ecological data with terrestrial laser scanning in Harvard Forest, MA. *Interface Focus* **8**. Doi: 10.1098/rsfs.2017.0044.
- Paulo P, Giovanni M, Simoneta P & Simone S (2014) The potential of C- and L-band SAR in assessing vegetation biomass: The ERS-1 and JERS-1 experiments. ESA Earthnet online.
- Picard G, Le Toan T & Mattia F (2003) Understanding C-band radar backscatter from wheat canopy using multiple-scattering coherent model. *IEEE Transactions on Geoscience and Remote Sensing*, **41** (7). Doi: 10.1109/TGRS.2003.813353.
- Pirotti F, Guarnieri A, Vettore A (2013) Ground filtering and vegetation mapping using multi-return terrestrial laser scanning. *ISPRS Journal of Photogrammetry & Remote Sensing*, **76**: 56-63. Doi: 10.1016/j.isprsjprs.2012.08.003.
- Poona N, van Niekerk A & Ismail R (2016) Investigating the Utility of Oblique Tree-Based Ensembles for the Classification of Hyperspectral Data. *Sensors*, **16**, 1918. Doi:10.3390/s16111918.
- Prasad R, Kotwal PC, Rathore CS & Jadhav DY (2001) Information and Analysis for Sustainable Forest Management: Linking National and International Efforts in South and Southeast Asia. EC-FAO Partnership Programme (2000-2002) Tropical Forestry Budget Line B7-6201/1B/98/0531 PROJECT GCP/RAS/173/EC. Indian Institute Of Forest Management NEHRU NAGAR.
- Puttonen E, Lehtomäki M, Kaartinen H, Zhu L, Kukko A & Jaakkola A (2013). Improved Sampling for Terrestrial and Mobile Laser Scanner Point Cloud Data. *Remote Sensing*, **5**, 1754-1773. Doi:10.3390/rs5041754.
- Qi J, Chehbouni A, Huete AR, Kerr YH & Sorooshian S (1994) A Modified Soil Adjusted Vegetation Index. *Remote Sensing of Environment*, **148**: 119-126.
- Qiu F, Berglund J, Jensen JR, Thakkar P, Ren D (2004) Speckle Noise Reduction in SAR Imagery Using a Local Adaptive Median Filter. *GIScience & Remote Sensing*, **41** (3), 244-266.

- Quegan S, Yu JJ (2001) Filtering of multichannel SAR images. *IEEE Transaction of Geosciences & Remote Sensing*, **39**, 2373–2379.
- Ramoelo A, Skidmore AK, Cho MA, Schlerf M, Mathieu R & Heitkönig IMA (2012) Regional estimation of savanna grass nitrogen using the red-edge band of the spaceborne RapidEye sensor. *International Journal of Applied Earth Observation and Geoinformation*, **19**, 151–162.
- Ratnam J, Bond WJ, Fensham R.J, Hoffmann WA, Archibald S, Lehmann CER, Anderson MT, Higgins SI, Sankaran M (2011) When is a forest a savanna, and why does it matter? *Global Ecology & Biogeography*. Doi: 10.1111/j.1466-8238.2010.00634.x.
- Raumonen P, Casella E, Calders K, Murphy S, Akerblom M, Kaasalainen M (2015) Massive-scale tree modelling from TLS data. *ISPRS Annals*, **189**, 25–27.
- Rauste Y (1992) Estimation of Biomass in mixed Forests using Polarimetric SAR data. Technical Research Center of Finland. Espoo, Finland. Pages 789-791.
- Reynolds S G (1970) The gravimetric method of soil moisture determination Part III An examination of factors influencing soil moisture variability. *Journal of Hydrology*, **11**, 288-300.
- Rees WG (2011) *Physical Principles of Remote Sensing*, 2nd ed, Cambridge University Press: Cambridge, UK. Pages 109–133.
- Reinwarth B, Miller JK, Glotzbach C, Rowntree KM, Baade J (2017) Applying regularized logistic regression (RLR) for the discrimination of sediment facies in reservoirs based on composite fingerprints. *Journal of Soils Sediments*, **17**:1777-1795. Doi: 10.1007/s11368-016-1627-7.
- Reis SM, Lenza E, Gomes L, Forsthofer M, Morandi PS, Junior, BHM, Feldpausch TR & Elias F (2015) Post-fire dynamics of the woody vegetation of a savanna forest (Cerradão) in the Cerrado-Amazon transition zone. *Acta Botanica Brasílica* **29** (3): 408-416. Doi: 10.1590/0102-33062015abb0009.

- Resop JP & Hession WC (2010) Terrestrial laser scanning for monitoring streambank retreat: Comparison with traditional surveying techniques. *Journal of Hydraulic Engineering*, **136**, 794–798.
- Richardson JJ, Moskal LM, Bakker JD (2014) Terrestrial laser Scanning for vegetation sampling. *Sensors*, **14**, 20304-20319. Doi: 10.3390/s141120304.
- RIEGL VZ 1000 Data Sheet2015Available online:  
[http://www.riegl.com/uploads/tx\\_pxpriegldownloads/DataSheet\\_VZ-1000\\_2015-03-24.pdf](http://www.riegl.com/uploads/tx_pxpriegldownloads/DataSheet_VZ-1000_2015-03-24.pdf) (Accessed on 7 April 2016).
- Rouse JW, Haas RH, Schell JA & Deering DW (1973) Monitoring vegetation systems in the Great Plains with ERTS. *3rd ERTS Symposium*, NASA SP-351. Pages 309-317.
- Roy PS & Ravan AS (1996) Biomass estimation using satellite remote sensing data-An investigation on possible approaches for natural forest. *Journal of Biosciences*, **21**, No4535-561.
- Ryan CM, Hill T, Woollen E, Ghee C, Mitchard E, Cassels G, Grace J, Woodhouse IH, Williams M (2012) Quantifying small-scale deforestation and forest degradation in African woodlands using radar imagery. *Global Change Biology*, **18**, 243–257.
- Saarinen N, Kankare V, Vastaranta M, Luoma V, Pyörälä J, Tanhuanpää T, Xinlian L, Kaartinen H, Kukko A, Jaakkola A, Yu X, Holopainen M & Hyypä J (2017). Feasibility of Terrestrial laser scanning for collecting stem volume information from single trees. *ISPRS Journal of Photogrammetry and Remote Sensing* **123**: 140–158.
- Saatchi S (1996) Application of SAR remote sensing in land surface processes over Tropical region. *Simposio Brasileiro de Sensoriamento Remoto*, Annals VIII. Pages 369-374.
- Saatchi SS, Harris NL, Brown S, Lefsky M, Mitchard ETA, Salas W, Zutta BR, Buermann W, Lewis SL, Hagen S, Petrova S, White L, Silman M & Morel A (2011) Benchmark map of

forest carbon stocks in tropical regions across three continents. *Proceedings National Academy of Sciences*, **108**, 24, 9899–9904.

Saatchi SS & van Zyl JJ (1995) Estimating canopy water content in Konza Prairie grasslands using synthetic aperture radar measurements during FIFE. *Journal of Geophysical Research*, **100** (D12): 25481-25496.

Sakarya U & Demirpolat C (2017) SAR image time series analysis in vegetation classification using Global and Local information based Linear Discriminant Analysis. *IEEE*. Doi: 10.1109/SIU.2017.7960204.

Salas WA, Ducey MJ, Rignot E, Skole D (2002) Assessment of JERS-1 SAR for monitoring secondary vegetation in Amazonia: Spatial and temporal variability in backscatter across a chrono-sequence of secondary vegetation stands in Rondonia. *International Journal of Remote Sensing*, **23** (7). Doi: 10.1080/01431160110092939.

Samalca IK (2007) Estimation of Forest Biomass and its Error: A case in Kalimantan, Indonesia. GEM Master's Thesis submitted at University of Twente, Netherlands.

Sandberg G, Ulander MHL, Wallerman J, Fransson JES (2014) Measurements of Forest Biomass Change Using P-Band Synthetic Aperture Radar Backscatter. *IEEE Transaction on Geosciences & Remote Sensing*, **52** (10). Doi: 10.1109/TGRS.2013.2294684.

Sankaran M & Anderson TM (2009) Management and Restoration in African Savannas: Interactions and Feedbacks. In *New Models for Ecosystem Dynamics and Restoration*, Richard Hobbs & Kate Suding (eds). Island Press. Pages 136 – 155.

Sankaran M, Hanan NP, Scholes RJ, Ratnam J, Augustine DJ, Cade BS, Gignoux J, Higgins SI, Le Roux X, Ludwig F, Ardo J, Banyikwa F, Bronn A, Bucini G, Caylor KK, Coughenour MB, Diouf A, Ekaya W, Feral CJ, February EC, Frost PGH, Hiernaux P, Hrabar H, Metzger KL, Prins HHT, Ringrose S, Sea W, Tews J, Worden J, & Zambatis N (2005) Determinants of woody cover in African savannas. *Nature*, **438**, 846–849.

- Sankaran M, Ratnam J & Hanan NP (2007) Woody cover in African savannas The role of resources, fire and herbivory. *Global Ecology & Biogeography*. DOI: 10.1111/j.1466-8238.2007.00360.x.
- Sankaran M, Ratnam J & Hanan NP (2004) Tree-grass coexistence in savannas revisited-insights from an examination of assumptions and mechanisms invoked in existing models. *Ecological Letters*, **7**, 480-490. Doi: 10.1111/j.1461-0248.2004.00596.x.
- Sankaran M, Ratnam J & Hanan N (2008) Woody Cover in African Savannas. The Role of Resources, Fire and Herbivory. Natural Resource Ecology Laboratory, Colorado State University, Fort Collins, CO 80523-1499, USA. Blackwell Publishing Ltd. Doi: 10.1111/j.1466-8238.2007.00360.x.
- Sano EE, Ferreira LG & Heute A.R (2005) Synthetic Aperture Radar (L band) and Optical Vegetation Indices for Discriminating the Brazilian Savanna Physiognomies: A Comparative Analysis. *Earth Interactions*, **9** (15). Doi: 10.1175/EI117.1.
- Sarker MLR., Nichol J, Iz HB, Bin Ahmad B, & Rahman AA (2013) Forest Biomass Estimation Using Texture Measurements of High Resolution Dual-Polarisation C-Band SAR Data. *IEEE Transactions on Geoscience and Remote Sensing*, **51**, 6. Doi: 10.1109/TGRS.2012.2219872.
- Sarker MLR, Nichol J, Ahmad B, Busu I & Rahman AA (2012) Potential of Texture Measurements of Two-Date Dual Polarisation PALSAR data for the Improvement of Forest Biomass Estimation. *International Society for Photogrammetry and Remote Sensing*. Doi: 10.1016/j.isprsjprs.2012.03.002.
- Sawadogo L, Savadogo P, Tiveau D, Dayamba SD, Zida D, Nouvellet Y, Oden P & Guinko S (2010) Allometric prediction of above-ground biomass of eleven woody tree species in the Sudanian savanna-woodland of West Africa. Northeast Forestry University and Springer-Verlag Berlin Heidelberg. Doi: 10.1007/s11676-010-0101-4.



- Scanlon TM & Albertson JD (2004) Canopy scale measurements of CO<sub>2</sub> and water vapour exchange along a precipitation gradient in Southern Africa. *Global Change Biology*, **10**, 329-341.
- Scanlon TM, Caylor KK, Manfreda S, Levin SA & Rodriguez-Iturbe I (2005) Dynamic response of grass cover to rainfall availability: implications for function and persistence of savanna ecosystem. *Advances in Water Resources*, **28**, 291-302.
- Schlaffer S, Chini M, Dettmering D, Wagner W (2016) Mapping wetlands in Zambia using seasonal backscatter signatures derived from ENVISAT ASAR time series. *Remote Sensing*, **8**, 402. Doi:10.3390/rs8050402.
- Scholes RJ & Archer SR (1997) Tree-Grass Interactions in Savannas. *Annual Review of Ecology and Systematics*, **28**: 517-544.
- Scholes RJ & Walker BH (1993) An African Savanna: Synthesis of the Nylsvley Study. Cambridge University Press.
- Scholes RJ, Dowty PR, Caylor K, Parsons DAB, Frost, PGH & Shugart HH (2002) Trends in savanna structure and composition along an aridity gradient in the Kalahari. *Journal of Vegetation Sciences*, **13**: 419-428.
- Scholes RJ, Gureja N, Ginannecchini M, Dovie D, Wilson B, Davidson N, Piggott K, McLoughlin C, van der Velde K, Freeman A, Bradley S, Smart R, Ndala S (2001) The environmental and vegetation of the flux measurement site near Skukuza, Kruger National Park. *Koedoe*, **44**, 73–83. Doi: 10.4102/koedoe.v44i1.187.
- Scholtz R, Kiker GA, Smit IPJ, Venter FJ (2014) Identifying drivers that influence the spatial distribution of Woody Vegetation in Kruger National Park, South Africa. *Ecosphere*, **5** (6): 71. Doi: 10.1890/ES14-00034.1.
- Schratz P, Muenchow J, Iturrutxa E, Richter J & Brenning A (2018) Performance evaluation and hyperparameter tuning of statistical and machine-learning models using spatial data.

- Settle, JJ and Drake, NA(1993) Linear mixing and the estimation of ground cover proportions. *International Journal of Remote Sensing*, **14** :6, 1159-1177.
- Sheen DR, Freeman A, Kasischke ES (1989) Phase calibration of Polarimetric Radar Images. *IEEE Transactions on Geoscience and Remote Sensing*, **27**: 6, Pages 719-730.
- Shirima D, Munishi PKT, Lewis SL, Burgess ND, Marshall AR, Andrew Balmford A, Swetnam RD, & Zahabu EM (2011) Carbon Storage, Structure and Composition of Miombo, Woodlands in Tanzania's Eastern Arc Mountains. *African Journal of Ecology*, **49**, 332–342.
- Sileshi WG, Arshad MA, Kanote S & Nkunika POY (2010) Termite-induced heterogeneity in African savanna vegetation: mechanisms and patterns. *International Association for Vegetation Science*. Doi: 10.1111/j.1654-1103.2010.01197.x & 2010 .
- Simonse M, Aschoff T, Speicker H, Thies M (2003) Automatic determination of forest inventory parameters using terrestrial laser scanning. In Proceedings of the ScandLaser Scientific Workshop on Airborne Laser Scanning of Forests, Umea, Sweden, 19 September. Pages 252–258.
- Singer RB, McCord TB (1979) Mars: large scale mixing of bright and dark surface materials and implications for analysis of spectral reflectance. *Proceedings of 10th Lunar and Planetary Science Conference*, American Geophysical Union, Washington DC. Pages 1835-1848.
- Smit IPJ, Smit CF, Govender N, van der Linde M, Macfayden S (2013) Rainfall, geology and landscape position generates large-scale spatiotemporal fire pattern heterogeneity in an African savanna. *Ecography*, **36**, 447–459.
- Smit IPJ, Asner GP, Govender N, Kennedy-Bowdoin T, Knapp DE & Jacobson J (2010) Fire on the African savanna: Using Lidar. *Bulletin of the Ecological Society of America*, **91** (3): 343-346.

- Smith MO, Johnson PE & Adams JB (1985) Quantitative determination of mineral types and abundances from reflectance spectra using principal components analysis. *Journal of Geophysical Research*, **90**: 797-804.
- Sodhi NS & Ehrlich PR (2010) Conservation Biology for All. Society for Conservation Biology. Oxford University Press.
- Somers B, Asner P, Tits, L & Coppin P (2011) Endmember variability in spectral mixture analysis: A review. *Remote Sensing of Environment*, **115**: 1603-1616.
- Spaete PL, Glenn NF, Derryberry DR, Sankey TT, Mitchell JJ, Hardegree SP (2010) Vegetation and slope effects on the accuracy of LiDAR derived DEM in the Sgaebush steppe. *Remote Sensing Letters*, **2**: 4, 317-326. Doi: 10.1080/01431161.2010.515267.
- Stanley T (2013) Assessment of FARO 3D Focus Laser Scanner for forest Inventory. Bachelor's Thesis submitted at The University of Southern Queensland, Toowoomba, Australia.
- Steenkamp K, Wessels, K, Archibald S & von Maltitz G (2015) Satellite derived phenology of southern Africa for 1985-2000 and functional classification of vegetation based on phenometrics.
- Sternberg H, Kersten TH, Jahn I & Kinzel R (2004). Terrestrial 3d Laser Scanning – Data Acquisition and Object Modelling for Industrial As-Built Documentation and Architectural Applications. ISPRS International Archives of Photogrammetry, Remote Sensing and Spatial Information Sciences, Vol. XXXV: 942-947.
- Streutker DR, Glenn NF (2006) LiDAR measurement of sagebrush steppe vegetation heights. *Remote Sensing of Environment*, **102**: 135-145.
- Strobl C, Boulesteix A-L, Zeileis A & Hothorn T (2007) Bias in random forest variable importance measures: illustrations, sources and a solution. *BMC Bioinformatics*, **8**. 25. Doi: 10.1186/1471-2105-8-25.

- Strobl C, Boulesteix A-L, Kneib T, Augustin T & Zeileis A (2008) Conditional variable importance for random forests. *BMC Bioinformatics*, **9**:307. Doi: 10.1186/1471-2105-9-307.
- Stussi N, Beaudoin A, Castel T, Gigord P (1995) Radiometric correction of multiconfiguration spaceborne SAR data over hilly terrain. In Proceedings of the 1st International Workshop on Retrieval of Bio- and Geophysical Parameters from SAR Data for Land Applications. Centre National D'études Spatiales (CNES), Toulouse (France).
- Suarez CJ, Ontiveros C, Smith S & Snape S (2004) The use of airborne Lidar and aerial photography in estimation of individual tree heights in forestry. *7th AGILE Conference on GIS*. Heraklion, Greece.
- Svoray T, Shoshany M (2002) SAR-based estimation of areal aboveground biomass (AAB) of herbaceous vegetation in the semi-arid zone: a modification of the water-cloud model. *International Journal of Remote Sensing*, **23**: 19. Doi: 10.1080/01431160110115924.
- Tempfli K, Kerle N, Huurneman C & Janssen LF (2009) Principles of Remote Sensing. The International Institute for Geo-information Science and Earth Observation. Netherlands. ISBN: 978-90-6164-270-1.
- Theseira MA, Thomas G, Taylor JC, Gemmell F & Varjo J (2003) Sensitivity of mixture modelling to endmember selection. *International Journal of Remote Sensing*, **24**, 7: 1559-1575.
- Thies M, Pfeifer N, Winterhalder D & Gorge BGH (2004) Three-dimensional reconstruction of stems for assessment of taper, sweep and lean based on laser scanning of standing trees. *Scandinavian Journal of Forest Research*, **19** (6). Doi: 10.1080/02827580410019562.
- Thonicke K, Venevsky S, Sitch S & Cramer W (2001) The role of fire disturbance for global vegetation dynamics: coupling fire into a Dynamic Global Vegetation Model. *Global Ecology & Biogeography*, **10**: 661 – 677.
- Tilly NI (2015) Terrestrial Laser Scanning for Crop Monitoring-Capturing 3D Data of Plant Height for Estimating Biomass at Field Scale. Ph.D Thesis, submitted at the University of Köln, Köln, Germany.

- Tinkham WT, Hwang H, Smith AMS, Shrestha R, Falkowski MJ, Hudak AT, Link TE, Glenn NF, Marks DG (2011) A comparison of two open source LiDAR surface classification algorithms. *Remote Sensing*, **3**: 638-649. Doi: 10.3390/rs3030638.
- Torbick N, Chowdhury D, Sala W, Qi J (2017) Monitoring rice agriculture across Myanmar using time series Sentinel-1 assisted by landsat-8 and PALSAR-2. *Remote Sensing*, **9**, 119. Doi: 10.3390/rs9020119.
- Touzi, R (2002) A review of speckle filtering in the context of estimation theory. *IEEE Transactions in Geosciences & Remote Sensing*, **40** (11): 2392–2404.
- Treuhaft, R.N, Chapman, B.D, dos Santos, J.R, Goncalves, F.G, Dutra, L.V, Graca, P.M.L.A, Drake, J.B(2009) Vegetation profiles in tropical forests from multibaseline interferometric synthetic aperture radar, field and Lidar measurements. *Journal of Geophysical Research*, **114**, 1–16.
- Trimble eCognition Trainings Available online: <http://community.ecognition.com/home/training-material> (accessed on 28th May, 2017).
- Trimble, 2016 Trimble RealWorks software Version 10.2.2: System requirement, new features and changes Available online: [http://trl.trimble.com/docushare/dsweb/Get/Document-835515/Trimble\\_RealWorks\\_10.2.2\\_RELEASE-NOTES\\_ENG\\_20161205.pdf](http://trl.trimble.com/docushare/dsweb/Get/Document-835515/Trimble_RealWorks_10.2.2_RELEASE-NOTES_ENG_20161205.pdf) (Accessed on 27.05.2017).
- Urbazaev M, Thiel C, Mathieu R, Naidoo L, Levick SR, Smit IPJ, Asner PG, Schullius C (2015) Assessment of the mapping of fractional woody cover in southern African savannas using multi-temporal and polarimetric ALOS PALSAR L-band images. *Remote Sensing of Environment*, **166**, 138–153.
- Van Laar A, Akca A (2007) Forest mensuration. In van Gadow, K., Pukkala, T. & Tome, M. (eds) *Managing Forest Ecosystems*. Springer, Netherlands. ISBN: 13 978-1-4020-5990-2.

- Van Langevelde F, van de Vijver CADM, Kumar L, van der Koppel J, de Ridder N, van Andel J, Skidmore AK, Hearne JW, Stroosnijder L, Bond WJ, Prins HHT & Rietkerk M (2003) Effects of fire and herbivory on the stability of savanna ecosystems. *Ecology*, **84**, 2: 337-350.
- van Wilgen BW (2009) The evolution of fire management practices in savanna protected areas in South Africa. *South African Journal of Science*, **105**.
- van Wilgen BW, Biggs HO, Regan SP & Mare N (2000) A fire history of the savanna ecosystems in the Kruger National Park, South Africa, between 1941 and 1996. *South African Journal of Science*, **96**.
- Vaughn NR, Asner, GP, Smit IPJ & Riddel ES (2015) Multiple scales of control on the structure and spatial distribution of woody vegetation in African savanna watersheds. *PLOS One*, **10** (12). Doi: 10.1371/journal.pone.0145192.
- Venter FJ (1990) A classification of land for management purposes in the Kruger National Park. PHD Thesis presented at University of Pretoria.
- Venter FJ, Scholes RJ, & Eckhardt HC (2003) The abiotic and template its associated vegetation pattern. In Du Toit JT, Rogers KH & Biggs HC (Eds.), *The Kruger Experience: Ecology and Management of Savanna Heterogeneity*. London Island Press. Pages 83-129.
- Verbesselt J, Hyndman R, Newnham G, Culvenor D (2010) Detecting trend and seasonal changes in satellite image time series. *Remote Sensing of Environment*, **114**, 1, 106-115. Doi: 10.1016/j.rse.2009.08.014.
- Viergever KM, Woodhouse IH, Stuart N (2007) Backscatter and Interferometry for Estimating Aboveground Biomass in Tropical Savanna Woodland. *IEEE Geosciences & Remote Sensing Symposium*. Doi: 10.1109/IGARSS.2007.4423312.
- Von Maltitz GP & Scholes RJ (1995) The burning of fuelwood in South Africa. When is it sustainable? *Environmental Monitoring & Assessment* **38**, 243-251.

- Walker W (2016) Introduction to RADAR Remote Sensing for Vegetation Mapping and Monitoring. WHRC Presentation (PPT).
- Walker, BH (1985) Determinants of tropical savannas. IRL Press, Oxford. The International Union of Biological Sciences IUBS Monograph Series, No3.
- Wang B, Ono A, Muramatsu K & Fujiwara N (1999) Automated detection and removal of clouds and their shadows in Landsat TM Images. *IEEE Transactions on Information and Systems*, E82-D, 453-60.
- Wang C & Glenn FN (2008) A linear regression method for tree canopy height estimation using airborne lidar data. *Canadian Journal of Remote sensing*, **34** (3):217-227.
- Wang D, Hollaus M, Schmalz E, Wieser M, Reifeltshammer D & Pfeifer N (2016) Tree stem shapes derived from TLS data as an indicator for shallow landslides. *Procedia Earth & Planetary Science* **16**: 185-194. Doi: 10.1016/j.proeps.2016.10.020.
- Wang K, Franklin SE, Guo X, He Y & McDermid GJ (2009) Problems in remote sensing of landscapes and habitats. *Progress in Physical Geography*, **1**, 22. Doi: 10.1177/0309133309350121.
- Wang Y, Frank FW & Kasischke ES (1994) Effects of variation in soil moisture on ERS-1 SAR backscatter. *IEEE International Geoscience and Remote Sensing Symposium*. Doi:10.1109/igarss.1994.399473
- Wang Y, Kasischke ES, Melack JM, Davis FW & Christensen NJ Jr. (1994) The effects of changes in Loblolly pine biomass and soil moisture on ERS-1 SAR backscatter. *Remote Sensing of Environment*, **49**: 25-31.
- Wang Y, Lehtomäki M, Liang X, Pyärälä J, Kukko A, Jaakkola A, Liu J, Feng Z, Chen R & Hyypä J (2019) Is field-measures height as reliable as believed – A comparison study of tree height estimates from field measurement, airborne laser scanning and terrestrial laser scanning in a boreal forest. *ISPRS Journal of Photogrammetry and Remote Sensing*, **147**: 132-145. Doi: 10.1016/j.isprsjprs.2018.11.008.

- Waqar MM, Mirza FJ, Mumtaz R & Hussain E (2012) Development of new indices for extraction of Built-up area and bare soil from Landsat data. *Open Access Scientific Reports*, **1**, Issue 1.
- Warmink J (2012) Vegetation Density Measurements Using Parallel Photography and Terrestrial Laser Scanning. A Pilot Study in the Duursche en Gamerensche Waard. Master's Thesis submitted at the Department of Geography of Utrecht University, Utrecht, The Netherlands.
- Wessels KJ, Colgan MS, Erasmus BFN, Asner GP, Twine WC, Mathieu R, van Aardt, JAN, Fisher JT, Smit IPJ (2013) Unsustainable fuelwood extraction from South African savannas. *Environmental Research Letters*, **8**, 1–10. Doi: 10.1088/1748-9326/8/1/014007.
- Wężyk P, Hawryło P, Szostak M, Pierzchalski M & De Kok R (2016) Using GEOBIA and Data Fusion Approach for Land Use and Land Cover Mapping. *Quaestiones Geographicae*, **35** (1): 93–104.
- WFP - World Food Program (2017) Southern Africa Growing Season 2015-2016: A season of Regional Drought. VAM Food Security Analysis. Available online at: <https://documents.wfp.org/stellent/groups/public/documents/ena/wfp282670.pdf> (Accessed on 19.4.2019).
- White KH & Drake N (1993) Mapping the distribution and abundance of gypsum in south-central Tunisia from Landsat Thematic Mapper data. **37**. 309-325.
- White L, Brisco B, Dabboor M, Schmitt A, Pratt A (2015) A collection of SAR methodologies for monitoring wetlands. *Remote Sensing*, **7**: 7615-7645. Doi: 10.3390/rs70607615.
- Wigley BJ, Fritz H, Coetsee C & Bond WJ (2014) Herbivores shape woody plant communities in the Kruger National Park: Lessons from three long-term exclosures. *Koedoe* **56** (1). Doi: 10.4102/koedoe.v56i1.1165.
- Wijaya A, Susanti A, Liesenberg V, Wardhana W, Yanto E, Soeprijadi D, Mcfarlane C, Qomar N (2011) Leaf area index and biomass assessment over tropical peatland forest ecosystem using ALOS Palsar and ENVISAT ASAR data In Proceedings of the 5th *International*



*Workshop on Science and Applications of SAR Polarimetry and Polarimetric Interferometry* (ESRIN), Frascati, Italy, 24–28 January 2011.

Wilgen BW, Trollope WSW, Biggs HC, Potgieter ALF, Brockett BH (2003) Fire as a driver of ecosystem variability. In *The Kruger Experience: Ecology and Management of Savanna Heterogeneity*, Du Toit JT, Rogers KH, Biggs HC (Eds) Island Press. London, UK. Page 149.

Williams R, Brasington J, Vericat D, Hicks M, Labrosse F, Neal M (2011) Monitoring braided river change using Terrestrial laser Scanning and optical bathymetric mapping. In *Geomorphological Mapping: Methods and Applications*, Smith, M, Paron, P, Griffiths, J, (Eds) Vol.15:1, Oxford, UK. Pages 507-528.

Winnie JA, Cross P & Getz W (2008) Habitat quality and heterogeneity influence distribution and behavior in African buffalo (*syncerus caffer*). *Ecology*, 89, 5: 1457 – 1468.

Woodhouse IH (2006) *Introduction to Microwave Remote Sensing*, Taylor and Francis: London, UK. Pages 93–149.

Woodward FI, Lomas MR & Kelly CK (2004) Global climate and the distribution of plant biomes. *Philosophical Transactions of the Royal Society B* **359**, 1465. Doi:10.1098/rstb.2004.15251476.

Woodward FI & Lomas MR (2004) Simulating vegetation processes along the Kalahari Transect. *Global Change Biology*, 10, 383-392.

Woodward A, Hutten KM, Boetsch JR, Acker SA, Rochefort RM, Bivin MM & Kurth LL (2009) Forest vegetation monitoring protocol for National parks in the North Coast and Cascades Network: Techniques and Methods 2-A8. US Geological Survey. Link: <https://pubs.usgs.gov/tm/tm2a8/pdf/tm2a8.pdf> (accessed on 20.6.2018).

Wulder MA, Han T, White JC, Sweda T & Tsuzuki H (2007) Integrating profiling Lidar with Landsat data for regional boreal forest canopy attribute estimation and change characterization. *Remote Sensing of Environment*, **110** (1): 123-137.

Yang Y & Lin Y (2009) A novel deformable model for urban vegetation detection using LiDAR data. College of Geology, Engineering & Geomatics, Xi'an, China.

Yu X, Hyyppa J, Holopainen M, Vastaranta M (2010) Comparison of area-based and individual tree-based methods for predicting plot-level forest attributes. *Remote Sensing*, **2**, 1481-1495. Doi: 10.3390/rs2061481.

Zhang Y, Smith AM & Hill MJ (2011) Estimating fractional cover of grassland components from two satellite remote sensing sensors (Unpublished, p1-4).

## **Selbständigkeitserklärung**

Ich erkläre, dass ich die vorliegende Arbeit selbständig und unter Verwendung der angegebenen Hilfsmittel, persönlichen Mitteilung und Quellen angefertigt habe.

Jena, 26.08.2019

-----

Victor Onyango Odipo

*Erklärung gemäß § 5 Absatz 1 Nr. 3 der Promotionsordnung der Chemisch-Geowissenschaftlichen Fakultät 2014*

**Erklärung:**

Ich erkläre,

dass mir die geltende Promotionsordnung der Fakultät bekannt ist;

dass ich die Dissertation selbst angefertigt, keine Textabschnitte eines Dritten oder eigener Prüfungsarbeiten ohne Kennzeichnung übernommen und alle von mir benutzten Hilfsmittel, persönlichen Mitteilungen und Quellen in meiner Arbeit angegeben habe;

dass mich folgende Personen bei der Auswahl und Auswertung des Materials sowie bei der Herstellung des Manuskripts unterstützt haben;

dass die Hilfe eines Promotionsberaters nicht in Anspruch genommen wurde und dass Dritte weder unmittelbar noch mittelbar geldwerte Leistungen von mir für Arbeiten erhalten haben, die im Zusammenhang mit dem Inhalt der vorgelegten Dissertation stehen;

dass ich die Dissertation noch nicht als Prüfungsarbeit für eine staatliche oder andere wissenschaftliche Prüfung eingereicht habe;

dass ich nicht die gleiche, eine in wesentlichen Teilen ähnliche oder eine andere Abhandlung bei einer anderen Hochschule als Dissertation eingereicht habe.

Ort, Datum, Unterschrift